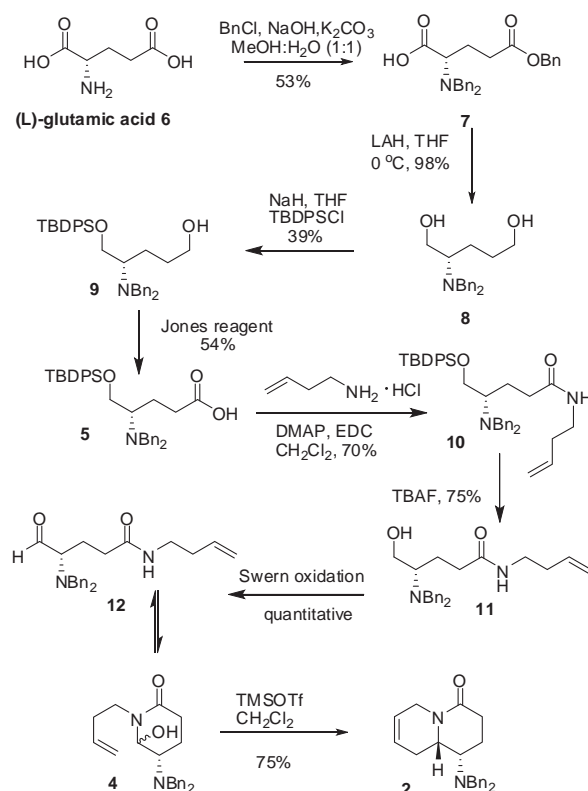


Scheme 1. Retrosynthetic Analysis of Epiquinamide

Our synthesis commenced with the benzylation of (L)-glutamic acid (**6**) to provide dibenzylamino benzoate **7** in moderate yield. Treatment of acid/ester **7** with lithium aluminum hydride gave diol **8** in quantitative yield and subsequent treatment with TBDPSCI afforded monosilyl ether **9** with silyl protection selectively on the more hindered side in 39% yield. Oxidation of alcohol **9** with Jones reagent produced carboxylic acid **5** in 54% yield. Coupling of acid **5** and 3-butenylamine hydrochloride in the presence of DMAP and EDC proceeded smoothly to give amide **10**. Deprotection of the silyl ether with TBAF gave amide alcohol **11**. Swern oxidation of the hydroxyl group then afforded aldehyde **12**. The aldehyde was in equilibrium with hydroxylactam **4** and its reaction with TMSOTf resulted in *in situ* generation of *N*-acyliminium ion. Cyclization of this intermediate gave bicyclic lactam **2**. The protected amino quinolizidinone framework of this compound is equipped for the completion of the total synthesis of epiquinamide with further steps of functional group conversions.

4. Conclusions

A synthesis of 5-dibenzylamino quinolizidinone is herein reported. This key intermediate in our synthetic approach toward epiquinamide was synthesized in 8 steps from (L)-glutamic acid. The key reaction was *N*-acyliminium ion cyclization. The completion of total synthesis of epiquinamide from this advanced intermediate required a few more steps of lactam carbonyl reduction, *N*-benzyl hydrogenolysis/C=C bond hydrogenation, and *N*-acetylation. The completion of the total synthesis will be reported in due course.



Scheme 2. Synthesis of Dibenzylamino Quinolizidinone **2**

Acknowledgements

Financial supports are provided by the Faculty of Science, Silpakorn University and the Thailand Research Fund. Scholarship for Chitlada Hemmara from the Department of Chemistry is gratefully acknowledged.

References

- [1] Fitch, R. W.; Sturgeon, G. ; Patel, S. R.; Spande, T. F.; Garraffo, H. M.; Daly, J. W.; Blaauw, R. H. *J. Nat. Prod.* **2009**, *72*, 243-247
- [2] Suyama, T. L.; Gerwick, W. H. *Org. Lett.* **2006**, *8*, 4541-4543.
- [3] Ghosh, H.; Shashidhar, J. *Tetrahedron Lett.* **2009**, *50*, 1177-1179.
- [4] Wijdeven, M.; Botman, P. N. M.; Wijtman, R.; Shoemaker, H. E.; Rutjes, F. P. J. T.; Blaauw, R. H. *Org. Lett.*, **2005**, *7*, 4005-4007.
- [5] Kuntiyong, P.; Akkarasamiyo, S.; Eksinitkun, G. *Chem. Lett.* **2006**, *35*, 1008-1008.
- [6] Kuntiyong, P.; Akkarasamiyo, S.; Piboonsrinakara, N.; Hemmara, C.; Songthammawat, P. *Tetrahedron*, **2011**, *67*, 8034-8040.
- [7] Fun, H. K.; Kuntiyong, P.; Tuntiwachwuttikul, P.; Chantapromma, S. *Acta Cryst. E.* **2011**, *E67*, o113-o114.

SYNTHESIS OF REVERSE CAPSIATE ANALOGUES: ENHANCEMENT OF CAPSIATE STABILITY

Arpon Pongkasetkam¹, Nuntavan Bunyapraphatsara², Uthai Wichai^{1,*}

¹Department of Chemistry, Faculty of Science, Naresuan University, Phitsanulok, 65000 Thailand

²Department of Pharmacognosy, Faculty of Pharmacy, Mahidol University, Bangkok, 10400 Thailand

*E-mail: uthaiw@nu.ac.th, Tel. +66 55 96 3433, Fax. +66 55 96 3401

Abstract: Capsiate (1) is a chemical analogue of capsaicin and belongs to capsinoid family. Both capsaicin and capsiate were composed of hydrophilic aromatic ring well known as vanilloid region and hydrophobic long chain fatty acid through an amide bond and ester bond, respectively. The potential clinical use of its analgesic and peripheral anti-inflammatory effects has attracted much attention and prompted investigation into the relationship between the structure of capsiate analogues and their agonist activities. Structural design to enhance binding interaction with TRPV1 receptor becomes the main point of both anti-inflammatory and anti-pain. Replacement of the amide bond in capsaicin with the ester bond in the capsiate resulted in a non-pungent property making it possible to utilize capsiate as food and drugs. Although capsiate has played an important role similarly to capsaicin through non-pungent and non-toxicity properties, on the other hand, it is unstable and easily decomposed. Consequently, improvement the stability of capsiate (1) was initially conducted by modification of capsiate (1) to reverse capsiate analogue, alteration of ester bond position, via esterification reaction. Reverse capsiate analogue, (*E*)-oct-5-enyl 2-(4-hydroxy-3-methoxy phenyl) acetate (2), was prepared as a model structure for preliminary observation of its stability comparing with capsiate. The reverse capsiate analogue was easily prepared via esterification reaction of homovanillic acid and (*Z*)-oct-5-en-1-ol by using *N,N'*-dicyclohexylcarbodiimide (DCC), and 4-dimethylamino pyridine (DMAP), and 1-hydroxybenzotriazole (HOBt) then followed with isomerization. It was found that reverse analogue (2) was successfully prepared in 72% yields and it was more stable than capsiate at ambient environment and was easily purified by conventional chromatographic procedure. The more stable reverse capsiate analogues will be employed as one of alternative tool to validate the binding mechanism between capsiate and TRPV1 receptor. The valuable binding information of capsiate will be further employed for designing of the capsiate analogues that contain specific desired activities in the future.

1. Introduction

Capsinoid, an analogue of capsaicinoids, was composed of capsiate, dihydrocapsiate and norhydrocapsiate. In 1998, capsinoids was first isolated by Kobata and co-workers [1] from a sweet pepper named "CH-19 sweet" with an exceptionally physical property that was totally different from capsaicinoids. Usually, capsaicinoids are high pungency and exhibit a significant burning sensation; however, capsinoids show slightly pungent and almost no sign of burning sensation when exposed to skin.

With such drastic diverse physical properties between capsinoids and capsaicinoids, several researches proposed that this might contribute from their minor different in their molecular structures.

The molecular structure of capsinoids and capsaicinoids were almost identical. Both of capsinoids and capsaicinoids were composed of a hydrophilic ring which well known as vanilloid region (A-region) and a lipophilic carbon chain on the other (C-region).[2-5] The only difference was that capsinoids use an ester bond linkage (region B) to connect A-region and B-region together while capsaicinoids use an amide bond. (Figure 1)

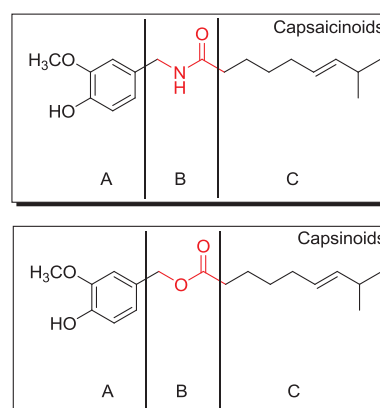


Figure 1 Structure of Capsaicinoids and Capsinoids

With such excellent physical properties that mentioned above, several researches were concentrated on how their activities would be as well as how to implement them for pharmaceutical applications. Since then, several biological activities were disclosed. For example, it has a wide range of biological effects on the cardiovascular, nervous, and respiratory systems and anti-obesity.[6-8] Some capsinoid analogues were useful as an analgesic drug and anti-inflammatory property.[9]

Although capsinoids has played an important role similarly to capsaicinoids with more advantages in term of non-pungent and non-toxicity; on the other hand, they were highly unstable and easily decomposed when exposed under the light and high temperature over a short periods of time.[10] Consequently, it would be very difficult to apply capsinoids in several applications especially pharmaceutical applications due to capsinoids would decompose instantly after exposure to water and all

protic solvents which make capsinoids become less practical for using as drugs.

In this investigation, we modified capsiate (**1**) to reverse analogue, (*E*)-oct-5-enyl 2-(4-hydroxy-3-methoxy phenyl) acetate (**2**) (Figure 2), alteration of ester bond position, via esterification reaction and studied the stability of both **1** and **2** in protic solvent system in order to evaluate the possible use as a novel anti-inflammatory and anti-pain agents.

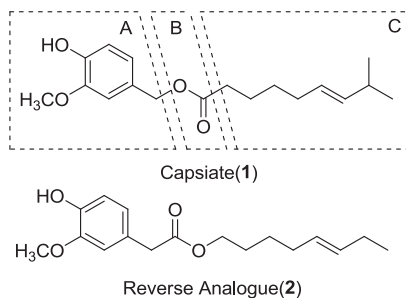


Figure 2 Structure of capsiate (**1**) and reverse analogue (**2**)

2. Materials and Methods

2.1 Chemicals and reagents

All of chemical reagent were purchased from Fluka Co., Ltd., Merck Co., Ltd., Acros Co., Ltd., Aldrich Co., Ltd., Chemprep Co., Ltd. and Lab Scan Co., Ltd., solvent for reactions were AR grade and anhydrous CH_2Cl_2 were dried over activated 3\AA molecular sieves ($\text{H}_2\text{O} \leq 0.01\%$) using as solvent was purchased from Merck.

For esterification synthesis, coupling agents were obtained from commercial source and used without purification. IUPAC name *N,N'*-Dicyclohexylcarbodiimide (DCC) 98%, 4-Dimethylaminopyridine (DMAP) 98%, 1-Hydroxybenzotriazole (HOBt) 98%. Chemical substances, Homovanillic acid 98% and (*Z*)-oct-5-en-1-ol 98%, were purchased from Sigma-Aldrich Co., Ltd. Deuterated solvent for NMR characterization, Chloroform- d (CDCl_3) was purchased from Aldrich Co., Ltd., respectively.

HPLC grade Methanol for HPLC experiments, obtained from Lab Scan, were filtered through Nylon membrane before use. DI water was obtained from ultrapure water system with ELGA (England).

2.2 Apparatus

All glassware was oven dried. The progress of reactions was monitored by thin layer chromatography (TLC) (Merck D.C. silica gel 60 F_{254} 0.2 mm-pre-coated aluminium plates). Visualization of TLC plates was accomplished using either UV light (254 nm), stained by Phosphomolybdic acid solution. Evaporation of solvents was performed on Büchi Rotavapor R-114 with a water aspirator model B-480 or a Refco Vacubrand pump. The weight of all chemical substances was determined on Sartorius electrical balance. Column chromatography was

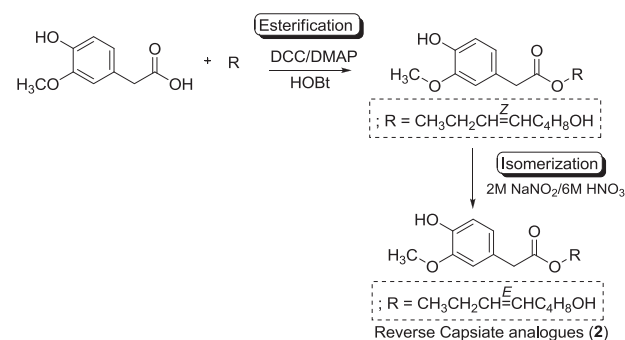
performed on silica gel having 60-200 μm for column chromatography.

^1H -NMR and ^{13}C -NMR spectra were recorded on a Bruker NMR spectrometer operating at 400 MHz for ^1H -NMR and 100 MHz for ^{13}C -NMR in appropriate deuterated solvents. Chemical shifts (δ) are reported in part per million (ppm) relative to either tetramethylsilane (TMS) or the residual protonated solvent signal as a reference.

HPLC chromatograms were recorded on Agilent 1100 series, HPLC system composed of a G1311A Quat Pump and G1315A DAD HPLC System, controller system equipped with gradient pump and Agilent 1100 series photodiode array detector. A VertiSep UPS C18 HPLC column, 4.6 x 250 mm, 5 μm . was used for the stability test. Peak monitoring and data processing were performed on the base Empower software.

2.3 Synthesis of reverse analogue **2**

The synthetic procedures of reverse capsiate analogue can be prepared via esterification reaction [11] between homovanillic acid and unsaturated primary alcohol using coupling reagents DCC, DMAP and HOBt (scheme 1)



Scheme 1 Synthesis of reverse analogue **2**

(*E*)-oct-5-enyl 2-(4-hydroxy-3-methoxy phenyl) acetate (**2**), started with stirred solution of homovanillic acid 0.274 mmol and 1-hydroxybenzotriazole (HOBt) 0.549 mmol in anhydrous dichloromethane 3 mL then slowly added *N,N'*-dicyclohexylcarbodiimide (DCC) 0.549 mmol by dropwise over 20 minutes after that added the solution of *Z*-5-octen-1-ol 0.549 mmol and 4-dimethylaminopyridine (DMAP) 0.549 mmol in anhydrous dichloromethane 3 mL at 0°C under N_2 atmosphere then added into reaction and stirred reaction for 24 hours. The precipitate of DCU was filtered and washed with dichloromethane then work up with brine solution extracted with diethyl ether 10 mL for 3 times after that evaporated and purification by Column chromatography silica gel (AcOEt/hexane) gave the *Z* isomer as a colorless liquid oil.

Next, isomerization of (*Z*)-oct-5-enyl 2-(4-hydroxy-3-methoxy phenyl)acetate [12,13], a quantity of 1.33 mmol of this compound was reacted with 2M NaNO_2 and 6M HNO_3 , the mixture reaction was submitted to vigorous stirring, and was heated to 70°C

for 1.5 hours. Then, the reaction mixture was left to cool. Once cooled, the reaction was stopped with about 10 mL of ethyl ether, after purification of the mixture, whitish colorless oil was obtained that corresponded to (*E*)-oct-5-enyl 2-(4-hydroxy-3-methoxy phenyl)acetate give 72% yields, $^1\text{H-NMR}$ (400 MHz, CDCl_3) δ_{H} 6.842 (*d*, $J=8$ Hz, 1H), 6.796 (*s*, 1H) and 6.749 (*d*, $J=9.6$ Hz, 1H), OH show at 5.581 (*s*, 1H) *trans* double bond of this structure show at 5.370 (*q*, $J=10.8$, 1H) and 5.267 (*q*, $J=10.8$, 1H), O-CH₂ (ester bond) show at 4.076 (*t*, $J=13.2$ Hz, 2H) O-CH₃ show peak at 3.866 (*s*, 3H), -CH₂ bond with carbonyl position show peak at 3.521 (*s*, 2H), CH₂ next to double bond show peak at 2.021 (*m*, 4H), -CH₂ alkane chain show peak at 1.618 (*m*, 2H), 1.377 (*m*, 2H) and 0.938 (*m*, 3H), $^{13}\text{C-NMR}$ (100 MHz, CDCl_3) δ_{C} 172.1, 146.6, 144.8, 132.3, 128.6, 126.0, 122.2, 114.5, 111.8, 64.9, 56.0, 41.1, 28.2, 26.7, 26.1, 20.6, 14.4.

2.3 Stability of capsitae (1) and reverse analogues 2 in protic solvent

Capsitae 1.10 mmol in methanol and reverse analogues 2, (*E*)-oct-5-enyl 2-(4-hydroxy-3-methoxy phenyl)acetate 1.10 mmol in methanol and ethanol were kept at room temperature. An aliquot of the each samples were taken at adequate time. After that, the amount of capsitae and reverse analogue 2 had been monitored by HPLC technique.

HPLC was carried out under the following conditions: column, VertiSep UPS C18 HPLC column, 4.6 x 250 mm, 5 μm ; mobile phase solvent, 80% methanol in H₂O; flow rate, 0.5 mL/min; detection DAD UV, 280 nm.

3. Results and Discussion

3.1 Synthesis of reverse analogue 2

Reverse analogue 2 was readily prepared via coupling reaction using HOBt and DCC as coupling agents and the yield of reverse analogue 2 was 72%. To confirm the ester linkage formation of 2, $^{13}\text{C-NMR}$ spectroscopy was utilized and the peak at 172.1 ppm was observed which clearly indicated that homovanillic acid was converted to ester group. Additionally, $^1\text{H-NMR}$ was also employed to reconfirm the presence of reverse analogue 2 and it was found that both aromatic proton with chemical shift at 6.84, 6.79, and 6.74 ppm and hydrocarbon proton residue at 5.37 and 5.26 ppm (*trans* double bond moiety) were also observed.

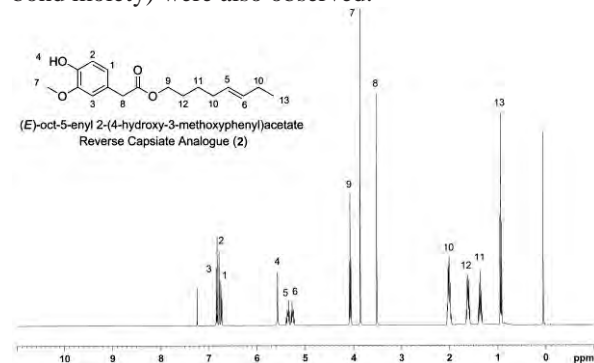


Figure 3 $^1\text{H-NMR}$ spectrum of reverse analogue 2

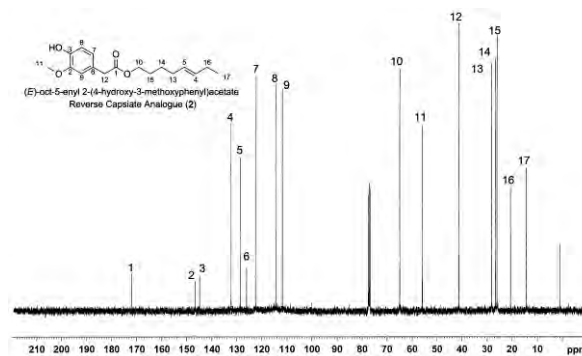


Figure 4 $^{13}\text{C-NMR}$ spectrum of reverse analogue 2

3.2 Stability of reverse analogue 2 in protic solvents

Having 2 in hand, stability of the reverse analogue 2 was investigated by compare with capsitae. Previous reports mentioned that capsitae was unstable in the presence of protic solvent and this disadvantage make capsitae is less likely attractive as drugs due to complicated steps during drug formulation. To evaluate the stability of reverse analogue 2, both of capsitae and reverse analogue 2 were dissolved in protic solvent and were sampling then were injected to HPLC to monitor the decreased amount of both capsitae and reverse analogue 2

From figure 5, it was found that capsitae was gradually decomposed over period of times and the half-life period was approximately 45 hours. It was totally degraded after 70 hours. The decomposition of capsitae was possibly originating from the destruction of ester bond via quinone methide pathways.[14] On the other hand, reverse analogue 2 showed no sign of degradation even at more than 70 hours and 2 was also stable in both methanol and ethanol system. This result showed that alteration of ester linkage was significantly hindered the destruction of reverse analogues from *p*-quinone methide degradation. More details of this incident are currently investigating.

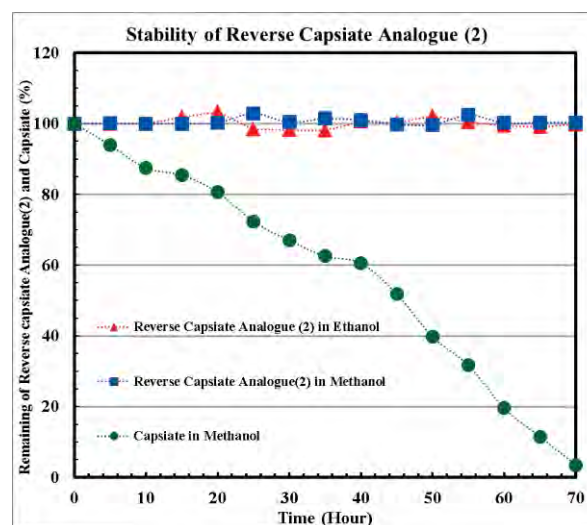


Figure 5 Change in reverse analogue (2) with time in methanol (■) and ethanol (▲) at 25 °C (●) capsitae in methanol.

4. Conclusions

In this study, it showed that reverse analogue **2** was easily synthesized and was also stable in both methanol and ethanol. Moreover, the reverse analogue **2** was more stable than capsiate. Next, the stable reverse analogue **2** will be employed as one of alternative tool to validate the binding mechanism between capsiate and TRPV1 receptor and the valuable binding information of capsiate will be further used for designing of the more potent capsiate analogues that contain specific desired activities in the future.

Acknowledgements

We would like to thank Center of Excellence for Innovation in Chemistry (PERCH-CIC), Thailand Research Fund (TRF) RDG5320030, Science Lab Centre (SLC) and Department of Chemistry, Faculty of Science, Naresuan University for financial support.

References

- [1] K. Kobata, T. Todo, S. Yazawa, K. Iwai, T. Watanabe, *J. Agri. Food Chem.* **46** (1998) 1695-1697.
- [2] C. S. J. Walpole, R. Wrigglesworth, S. Bevan, E. A. Campbell, A. Dray, I. F. James, M. N. Perkins; D. J. Reid J. Winter, *J. Med. Chem.* **36** (1993) 2362-2372.
- [3] C. S. J. Walpole, R. Wrigglesworth, S. Bevan, E. A. Campbell, A. Dray, I. F. James, M. N. Perkins, D. J. Reid, J. Winter, K. J. Masdin, *J. Med. Chem.* **36** (1993) 2373-2380.
- [4] C. S. J. Walpole, R. Wrigglesworth, S. Bevan, E. A. Campbell, A. Dray, I. F. James, M. N. Perkins, D. J. Reid, J. Winter, K. J. Masdin, *J. Med. Chem.* **36** (1993) 2381-2389.
- [5] M. Hosseini, D. J. Maddalena, I. Spence, *J. Chem. Inf. Comput. Sci.* **37** (1997) 1129-1137.
- [6] G. Klopman and J. Li, *J. Comput. Aided. Mol. Des.* **9** (1995) 283-294.
- [7] R. M. Virus and G. F. Gebhart, *Life Sci.* **25** (1979) 1273-1284.
- [8] J. N. Wood, J. Winter, I. F. James, H. P. Rang, J. Yeats, S. Bevan, *J. Neurosci.* **8** (1988) 3208-3220.
- [9] J. Winter, S. Bevan, E. A. Campbell, *British Journal of Anaesthesia* **75** (1995) 157-168.
- [10] K. Sutoh, K. Kobata, T. Watanabe, *J. Agric. Food. Chem.* **49** (2001) 4026-4030.
- [11] Md. C. Sheikh, S. Takagi, T. Yoshimura, H. Morita, *Tetrahedron* **66** (2010) 7272-7278.
- [12] H. Kaga, M. Miura, K. Orito, *J. Org. Chem.* **54** (1989) 3477-3478.
- [13] F. B. Gerardo, M. G. Molinillo, R. M. Varela, M. Palma, A. M. Francisco, C.G. Barroso, *J. Agric. Food Chem.* **58** (2010) 3342-3349.
- [14] A. Amino and et. Al., *US patent A10020738* (2007)

STABILITY STUDY OF CAPSIATE AND ITS ANALOGUE

Parintorn Eiamsa-ard¹, Uthai Wichai^{1*}

¹Department of Chemistry and Center of Excellence for Innovation in Chemistry, Faculty of Science, Naresuan University, Phitsanulok 65000, Thailand.

*E-mail: uthaiw@nu.ac.th, Tel. +66 55 96 3433, Fax. +66 55 96 3401

Abstract: Capsaicin is the high potential natural pain relief agent that found in *Capsicum annuum* fruits via interacts to transient receptor potential cation channel, subfamily V member 1 (TRPV1) with the 3 main forces H-bonding, steric fit and π - π stacking. Forasmuch, the very strong pungency and burning sensation make capsaicin become less attractive to use as drugs. Interestingly, capsiate or (*E*)-4-hydroxy-3-methoxybenzyl 8-methylnon-6-enoate, the natural analogue of capsaicin that obtained from *Capsicum annuum* cv. CH-19 Sweet fruits, is the non-pungent substance. Despite the difference of structure, it was found that capsiate still interacted with TRPV1 in the gut. Due to lacking of pungency and burning sensation, it clearly makes capsiate become a very interesting substance for substitution on capsaicin to provide effective pain reduction in human. The modification of capsiate by means of enhance π - π stacking interaction could provide the highly interaction with TRPV1 receptor. Therefore, designed capsiate analogue underwent by replacement of -OCH₃ on aromatic with the highly electron withdrawing group to promote dipole moment that is -NO₂ group without disturbing -OH. The synthesis of capsiate and nitro-capsiate were successes by Mitsunobu reaction with yield of 72% and 65%, respectively. Next, the stability of capsiate and nitro-capsiate in protic solvent were investigated. From HPLC chromatogram, it was found that both capsiate and nitro-capsiate were unstable in protic solvent. Especially, nitro-capsiate was decomposed 2 times faster than the capsiate. From the results, it's shown that replacement of -NO₂ group could possibly accelerate the decomposition through the para-quinonemethide intermediate. Such a highly unstable behavior of nitro-capsiate hindered itself as a potential pain relief agent. Therefore, further alteration of nitro-capsiate will be explored in order to render the rapid decomposition while maintaining high π - π stacking interaction.

1. Introduction

Capsaicin (1), the most active ingredient of capsaicinoid group, usually exhibits in *Capsicum annuum*. Capsaicinoids are consisting of two functional groups. One is vanilly amine and the other is fatty acid containing either long chain alkyl or alkenyl groups and both functional groups are connected together via amide bond.[1] Generally, capsaicinoids are widely used as food additives, antioxidant supplementary,[2] antimicrobial drug,[3] anti-inflammatory drug[4] and especially antipain agent.[5] The pain relief mechanism of capsaicin is involved with transient receptor potential cation

channel, subfamily V member 1 (TRPV1) on noniceptive C-fibre to rapidly increase substance P (SP) and calcitonin gene-related peptide (CGRP) in a short period of time. After that, SP and CGRP will simultaneously replace the pain receptor resulting pain relief.[6] However, the very strong pungency and burning sensation make capsaicin become less attractive to use as drugs.

Recently, the non-pungency isostere compound of capsaicin named capsiate (2) was isolated from *Capsicum annuum* cv. CH-19 Sweet. Interestingly, the chemical structure of capsiate is similar to capsaicin except the linkage between vanilly alcohol and fatty acid which is connected by ester bond. Having such a different linkage, they still exhibit almost similar properties with capsaicin such as solubility, biosynthesis pathway and metabolic pathway.[8] Lacking of pungency while still maintaining activity as similar as capsaicin makes capsiate become a very interesting substance for substitution on capsaicin to provide more effective pain reduction in human. Surprisingly, the binding mechanism between capsiate and TRPV1 receptor has not yet been clear even though capsiate was isolated since 20 years ago. However, many researchers have been demonstrated that mechanism of both capsaicin and capsiate should have somewhat similar manner.[9] From the previous reports, it was established that capsaicin and TRPV1 receptor interacted by three difference forces (figure 1); hydrogen bonding interaction at position 1, 3 and 4, π - π stacking interaction of the aromatic part at position 2, and finally a steric fit interaction of the long chain fatty acid at position 5.[10]

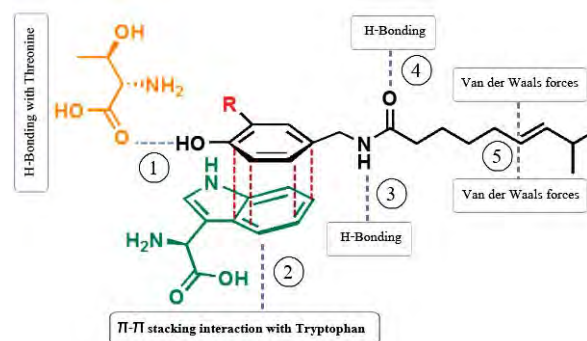


Figure 1. Binding interaction between capsaicin and TRPV 1 receptor

In the case of capsiate, it lacks of hydrogen bonding at position 3. Therefore, increasing of π - π stacking interaction of aromatic region should be one appropriate choice to enhance the binding affinity of capsiate and TRPV1 receptor.

Under this investigation, we designed capsiate analogue via replacement of $-\text{OCH}_3$ on aromatic with the highly electron withdrawing group to promote dipole moment that is $-\text{NO}_2$ group (**3**) and studied the stability in the polar protic solvent system.

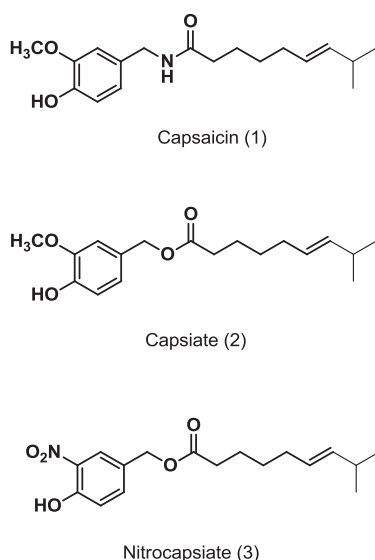


Figure 2. Chemical structures of capsaicin (**1**), capsiate (**2**) and nitrocapsiate (**3**)

2. Materials and Methods

2.1 Chemicals

All commercially available chemicals were purchased from Fluka Co., Ltd, Merck Co., Ltd, Acros Co., Ltd, Aldrich Co., Ltd, Chempep Co., Ltd and Lab Scan Co., Ltd, Thai can biotech Co., Ltd. and all chemicals were used without purification unless otherwise stated. Commercial grade solvents for column chromatography were distilled prior to use.

Solvent for reactions were AR grade and were used without purification. HPLC grade methanol for HPLC experiments, obtained from Lab Scan, was filtered through 0.45 μm Nylon membrane before use. DI water was obtained from ultrapure water system with ELGA (England).

For capsiate and analogue synthesis, anhydrous DMF and THF ($\text{H}_2\text{O} \leq 0.01\%$ dried over activated 3Å molecular sieves) using as solvent was purchased from Merck. Isomerization and coupling agents were obtained from commercial source and used without purification, IUPAC name 95% 4-(hydroxymethyl)-2-methoxyphenol, 99% triphenyl phosphine, 37% hydrochloric acid, 65% nitric acid, 98% diethyl azodicarboxylate (DIAD).

Deuterated solvent for NMR characterization, Chloroform- d (CDCl_3) and Deuterium (D_2O) were purchased from Aldrich.

2.2 Apparatus

All glasswares were oven dried. The progress of reactions were monitored by thin layer chromatography (TLC) (Merck D.C. silica gel 60 F_{254} 0.2 mm pre-coated aluminium plates). Visualization of TLC plates was accomplished by using either UV light (254 nm), or staining by *p*-anisaldehyde and phosphomolybdic acid solution. Evaporation of solvents was performed on Büchi Rotavapor R-114 with a water aspirator model B-480 or a Refco Vacubrand pump. The weight of all chemical substances was determined on Sartorius electrical balance. Column chromatography was performed on silica gel having 60-200 μm for column chromatography.

^1H -NMR spectra were recorded on a Bruker NMR spectrometer operating at 400 MHz in appropriate deuterated solvents. Chemical shifts (δ) are reported in part per million (ppm) relative to either tetramethylsilane (TMS) or the residual protonated solvent signal as a reference.

HPLC chromatograms were recorded on Agilent 1100 series, HPLC system composed of a G1311A Quat Pump and G1315A DAD HPLC System, controller system equipped with gradient pump and Agilent 1100 series photodiode array detector. A VertiSep UPS C18 HPLC column, 4.6 x 250 mm, 5 μm . was used for the isolation of E/Z isomers. Peak monitoring and data processing were performed on the base Empower software.

2.3 Synthesis of capsiate and analogue

(*E*)-4-hydroxy-3-methoxybenzyl-8-methylnon-6-enoate (**2**). 4-(hydroxymethyl)-2-methoxyphenol (0.176 mmol), a mixture of 1:6 (*Z*) and (*E*)-8-methyl-6-nonenic acid (0.212 mmol) and triphenylphosphine (0.353 mmol) were dissolved in 3 mL of dry THF, stirred at 0 $^\circ\text{C}$ for 0.5 hour. After that, DIAD (0.353 mmol) was added dropwise to the solution. The mixture was stirred for 24 hour at room temperature, the reaction followed by TLC (30% EtOAc in Hexane). The solution was removed THF with N_2 purged and rapidly purified by silica gel column chromatography under the conditions of 30% EtOAc in Hexane. The eluent gave colourless oil (38.8 mg, 72% yield). The structure was confirmed by ^1H NMR 400 MHz (CDCl_3) δ_{H} 0.92 ppm (d, $j = 4$ Hz, 6H), δ_{H} 1.31 ppm (m, 2H), δ_{H} 1.59 ppm (m, 2H), δ_{H} 1.98 ppm (m, 2H), δ_{H} 2.19 ppm (m, 1H), δ_{H} 2.24 ppm (m, 2H), δ_{H} 3.90 ppm (s, 3H), δ_{H} 5.02 ppm (s, 2H), δ_{H} 5.30 ppm (m, 2H), δ_{H} 5.62 ppm (s, 1H), δ_{H} 6.88 ppm (m, 3H).

(*E*)-4-hydroxy-3-nitrobenzyl 8-methylnon-6-enoate (**3**). 4-(hydroxymethyl)-2-nitrophenol (0.176 mmol), a mixture of 1:6 (*Z*) and (*E*)-8-methyl-6-nonenic acid (0.212 mmol) and triphenylphosphine (0.353 mmol) was dissolved in 3 mL of dry THF, stirred at 0 $^\circ\text{C}$ for 0.5 hour. After that, DIAD (0.353 mmol) was added dropwise to the solution. The mixture was stirred for 24 hour at room temperature, the reaction followed by TLC (30% EtOAc in Hexane). The solution was

removed THF with N_2 purged and rapidly purified by silica gel column chromatography under the conditions of 30% EtOAc in Hexane. The eluent gave colourless oil (36.7 mg, 65% yield). The structure was confirmed by 1H NMR 400 MHz ($CDCl_3$) δ_H 0.96 ppm (d, $j = 4$ Hz, 6H), δ_H 1.38 ppm (m, 2H), δ_H 1.60 ppm (m, 2H), δ_H 1.99 ppm (m, 2H), δ_H 2.20 ppm (m, 1H), δ_H 2.35 ppm (m, 2H), δ_H 5.06 ppm (s, 2H), δ_H 5.30 ppm (m, 2H), δ_H 7.14 ppm (d, $j = 8$, 1H), δ_H 7.58 ppm (d, $j = 6$ Hz, 1H), δ_H 8.12 ppm (s, 1H), δ_H 10.59 ppm (s, 1H).

2.4 Stability of capsiate and nitro-capsiate in polar protic solvent.

Capsiate (1.1 mmol) and nitro-capsiate (1.1 mmol) was dissolved in methanol solution (80% methanol in water). Immediately after the preparation, the sample was kept at 25 °C. An aliquot of the sample (5 μ l) was taken at adequate time to analyse by HPLC for 50 hours. HPLC was carried out under the following conditions: column, VertiSep UPS C18, 4.6 x 250 mm, 5 μ m, solvent, 80% methanol in water with 0.05 % glacial acetic acid, flow rate 0.5 mL/min for capsiate and 0.4 mL/min for nitro-capsiate, detection UV 280 nm.

3. Results and Discussion

3.1 Synthesis of capsiate and its analogue

Capsiate and nitro-capsiate were successfully synthesized via Mitsunobu esterification with highly yield. The chemical structures of both compounds were proved by 1H NMR (figure 3), confirmed with the chemical shift of $-OCH_3$ group at 3.90 ppm in capsiate, the shielding of aromatic protons in nitro-capsiate and proton on $-OH$ group that disappeared in capsiate, whereas appeared in nitro-capsiate due to the electron withdrawing effect of $-NO_2$ group at 10.59 ppm.

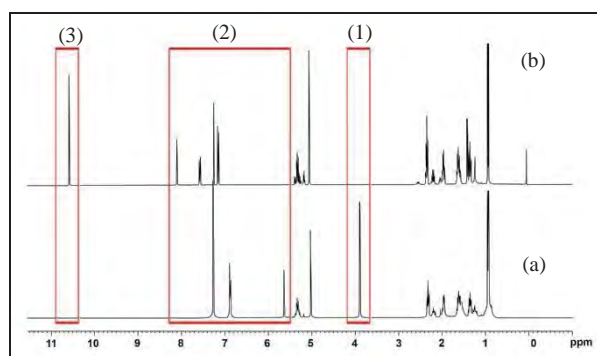


Figure 3. 1H NMR spectrum, (a) capsiate, (b) nitro-capsiate. (1) shows the chemical shift of 1H on $-OCH_3$ group in capsiate, (2) shows the shielding of aromatic 1H and (3) shows 1H of $-OH$ group in nitro-capsiate.

3.2 Stability of capsiate and its analogue

Due to the capsiate and nitro-capsiate was designed base on a potential anti-pain drug, the stability in cell solution (buffer pH 7.4) or polar protic solvent become the most important property. Therefore, the stability of

both compounds was investigated, 80% Methanol in water was used as a polar protic solvent to study.

The stability of capsiate was determined by reverse phase HPLC (C-18) in the condition of 80 % methanol in water with 0.005 % of glacial acetic acid, the flow rate was elucidated for separated (Z) and (E)-isomers, and the optimum is 0.5 ml/min. The chromatogram of capsiate shown the separation of (Z)-isomer, the retention time at 28.34 min and (E)-isomer, the retention time at 29.40 min at the ratio 1: 6 of (Z) : (E)-isomer (figure 4).

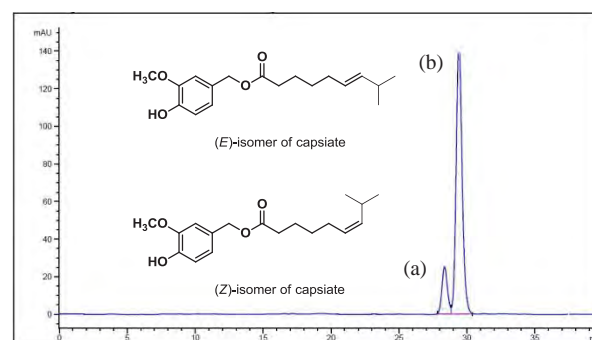


Figure 4. Chromatogram of capsiate, (a) (Z)-isomer capsiate and (b) (E)-isomer capsiate.

For the determination of the stability of nitro-capsiate, the same method of capsiate was carried out. The flow rate was elucidated for separated (Z) and (E)-isomers, and the optimum is 0.4 ml/min. Figure 4 shows the chromatogram of nitro-capsiate, (Z) and (E)-isomers, the retention time of (Z)-isomer is 166.74 min and (E)-isomer is 173.93 min at the ratio 1: 6 of (Z) : (E)-isomer.

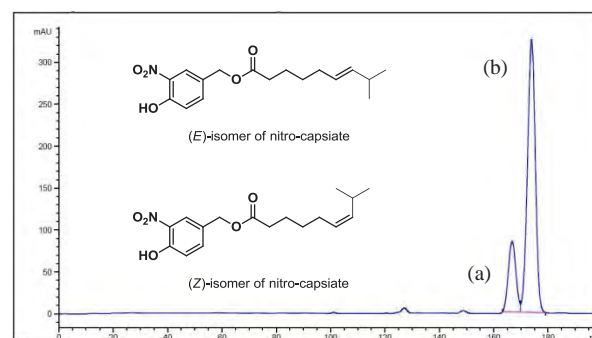


Figure 5. Chromatogram of nitro-capsiate. (a) (Z)-isomer nitro-capsiate and, (b) (E)-isomer nitro-capsiate.

Figure 6 shows percent remaining of capsiate and nitro-capsiate that obtained from peak area of (E)-isomer of both compounds with time in polar protic solvent (80% methanol in H_2O with 0.005 % of glacial acetic acid) at 25 °C. In the period of 0-5 hours, capsiate and nitro-capsiate show no significant differential but after 5 hours, it was clearly that nitro-capsiate start degrading faster than capsiate and completely decomposed at 50 hours whereas capsiate

still remaining 40 %. The half-life of capsiate is approximately 46 hours but nitro-capsiate is 20 hours.

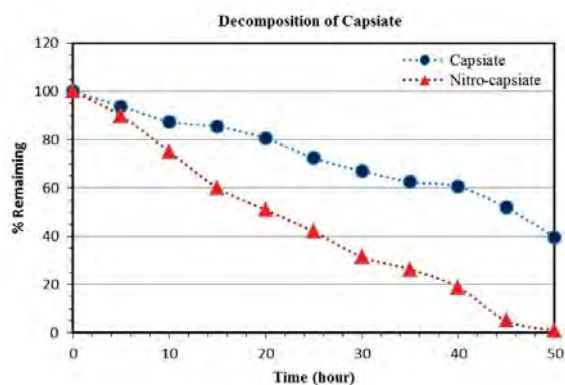
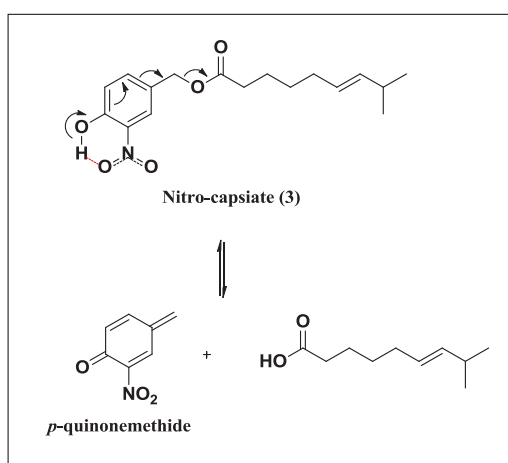


Figure 6. The stability of capsiate and nitro-capsiate in 80% methanol in H₂O

As the results, capsiate is more stable in polar protic solvent than nitro-capsiate. It suggested that the highly dipole moment of -NO₂ group induced the intra molecular H-bonding between O atom on -NO₂ group and H atom of -HO group and makes H-O bond become weakly leading to rapid decomposition of nitro-capsiate through the *p*-quinonemethide intermediate (scheme 1).



Scheme 1. The propose of decomposition pathway of nitro-capsiate through *p*-quinonemethide intermediate.

4. Conclusions

Nitro-capsiate is the analogue that designs to promote π - π stacking interaction for enhancement the binding affinity to TRPV1 receptor. However, the highly unstable behavior of nitro-capsiate hindered itself as a potential pain relief agent. Therefore, further alteration of nitro-capsiate will be explored in order to render the rapid decomposition via *p*-quinonemethide process while maintaining high π - π stacking interaction.

Acknowledgements

We would like to thank Center of Excellence for Innovation in Chemistry (PERCH-CIC), Thailand Research Fund (TRF) RDG5320030, Science Lab Centre (SLC) and Department of Chemistry, Faculty of Science, Naresuan University for financial support.

References

- [1] K. Kobata, T. Todo, S. Yazawa, K. Iwai and T. Watanabe, *J. Agri. Food Chem.* **46** (1998) 2563–2570.
- [2] D. E. Henderson and A. M. Slickman, *J. Agri. Food Chem.* **47** (1999) 2563–2570.
- [3] M. Careaga, E. Fernández, L. Dorantes, L. Mota, M. E. Jaramillo, H. Hernandez-Sanchez, *Int. J. Food Microbiol.* **83** (2003) 331–335.
- [4] G. C Morris, S. J. Gibson, R. D. Helme, *Pain.* **63** (1995) 93–101.
- [5] C. S. Kim, T. Kawada, B. S. Kim, I. S. Han, S. Y. Choe, T. Kurata, R. Yu, *Cellular Signalling.* **15** (2003) 299–306.
- [6] M. J. Caterina, D. Julius, *Annu. Rev. Neurosci.* **24** (2001) 487–517.
- [7] K. Kobata, T. Todo, S. Yazawa, K. Iwai and T. Watanabe, *J. Agri. Food Chem.* **46** (1998) 1695–1697.
- [8] Y. J. Surh, H. S. Ahn, K. C. Kim, J. B. Park, W. Y. Sohn, S. Lee, *Life Sci.* **16** (1995) 305–311.
- [9] S. Yazawa, N. Tatsuo, T. Watanabe, T. Fushiki, K. Kobata, M. Imai, Y. Setoguchi, S. Hashizume, US Patent 6, 333, 421 B1 December 18(2001).
- [10] K. Orito, M. Miura, H. Kaga, *J. Org. Chem.* **54** (1989) 2477–2478.
- [11] J. Szolcsanyi, A. Jancso-Gabor, *Arzneim.-Forsch. (Drug Res.* **25** (1975) 1877–18.

BIOTRANSFORMATION OF CYPERENOIC ACID BY *CURVULARIA LUNATA* NRRL 2178

Ruthaiwan Kongcharoen¹, Ratchanaporn Chokchaisiri², Oratai Sukcharoen³
and Apichart Suksamrarn^{1*}

¹Department of Chemistry and Center of Excellence for Innovation in Chemistry, Faculty of Science, Ramkhamhaeng University, Bangkok 10240, Thailand

²Division of Chemistry, School of Science, Phayao University, Phayao 56000, Thailand

³Department of Biotechnology, Faculty of Science, Ramkhamhaeng University, Bangkok 10240, Thailand

E-mail: s_apichart@ru.ac.th, Tel. +66 23191900

Abstract: Cyperenoic acid (**1**) is the major sesquiterpene from the roots of *Croton crassifolius*. Biotransformation of this compound by the fungus *Curvularia lunata* NRRL 2178 produced three new metabolites, (4*S*)-4-hydroxycyperenoic acid (**2**), 12-hydroxycyperenoic acid (**3**) and (8*R*)-4-hydroxycyperenoic acid (**4**). The isolated metabolites were characterized by spectroscopic (IR, NMR and MS) means.

1. Introduction

Croton crassifolius (family Euphorbiaceae) is a monoecious undershrub, up to 30–50 cm tall. It is a medicinal plant that grows in hilly countries with a moderately dry climate, and is widely distributed in south-east Asia and south China [1]. As part of our investigation of medicinal plants on the roots of *Croton crassifolius*, we have isolated cyperenoic acid (**1**), the sesquiterpene previously isolated from other *Croton* species [2].

Biotransformation is a useful tool to modify the structures of natural products. Microbial transformation has such advantages over chemical synthesis as high stereo- and regio-selectivity [3]. We were interested in microbial transformation of compound **1** by a fungus which possesses a broad specificity in the substrate. In the present study, *Curvularia lunata* NRRL 2178 was used to metabolize the sesquiterpene.

2. Materials and Methods

2.1 General experimental procedures

Optical rotation was measured on a JASCO-1020 polarimeter. ¹H and ¹³C NMR spectra were recorded on a Bruker AVANCE 400 spectrometer. Mass spectra were obtained on a Finnigan LC-Q mass spectrometer. Column chromatography and TLC were carried out using Merck silica gel 60 (<0.063 mm) and precoated silica gel 60 F₂₅₄ plates, respectively. Spots on TLC were detected under UV light and by spraying with anisaldehyde-H₂SO₄ reagent followed by heating.

2.2 Microorganism

Curvularia lunata (strain no. 2178) was obtained from NRRL (Illinois, USA). Stock culture of the

fungus was maintained on potato dextrose agar slant. It was stored at 4 °C and subcultured monthly at 30 °C.

2.3 Incubation experiments

Erlenmeyer flask (250 mL), each containing 100 mL of liquid medium consisting of 0.1% peptone, 0.1% yeast extract, 0.1% beef extract, and 0.5% glucose were inoculated with freshly obtained *C. lunata* cultured from the agar slant on a rotary shaker at 180 rpm. After cultivation at ambient temperature for 2 days, the substrate solution (5 mg in 1 mL DMSO : Tween 80, 100:5) was added to each flask, and the incubation continued for 3 days. Culture control consisted of fermentation blank in which *C. lunata* was grown under identical condition but without substrate.

2.4 Biotransformation of cyperenoic acid (**1**)

Compound **1** (20×5 mg) was fed to *C. lunata* NRRL 2178 in Erlenmeyer flasks (20×250 mL), each containing 100 ml of the same medium as outlined above. After 3 days the culture was filtered, the mycelium was washed with EtOAc, and the broth was extracted with EtOAc (3×100 mL). The organic phase was washed with water, dried over anhydrous Na₂SO₄, and concentrated *in vacuo*. The crude extract (191.3 mg) was subjected to column chromatography eluting with *n*-hexane–EtOAc (60:40) to give **2** (6.1 mg, based on the unrecovered starting material) **3** (4.8 mg), **4** (15.8 mg) and the starting material **1** (71.8 mg).

2.4.1 Cyperenoic acid (**1**)

Colorless needles; [α]_D²⁹ -16.5° (*c* 0.39, CHCl₃); ¹H NMR (CDCl₃, 400 MHz): δ 0.85 (s, 3H, H-13), 0.88 (d, *J* = 6.4 Hz, 3H, H-11), 1.01 (s, 3H, H-12), 1.15 (ddt, *J* = 14.0, 12.8, 7.2 Hz, 1H, H-5 β), 1.53 (m, 1H, H-5 α), 1.40, 1.91 (m, 2H, H-6 α , H-6 β), 1.57 (ddd, *J* = 13.2, 7.6, 0.8 Hz, 1H, H-3 α), 1.78 (dt, *J* = 13.2, 10.0 Hz, H-3 β), 2.09 (m, 1H, H-4), 2.27, 2.75 (m, 2H, H-8 α , H-8 β), 2.72, 2.82 (m, 2H, H-2); ¹³C NMR (CDCl₃, 100 MHz): 123.1 (C-1), 36.3 (C-2), 25.7 (C-

3), 68.2 (C-3a), 36.0 (C-4), 27.9 (C-5), 26.9 (C-6), 48.2 (C-7), 31.3 (C-8), 173.1 (C-8a), 41.7 (C-9), 170.7 (C-10), 18.0 (C-11), 19.3 (C-12), 26.2 (C-13).; ESMS (+ve): 235 [M+H]⁺.

2.4.2 (4S)-4-Hydroxycyperenoic acid (2)

Colorless amorphous solid; $[\alpha]_D^{29}$ 21.2° (*c* 0.61, CHCl₃); IR: ν_{\max} 3424, 2925, 1677, 1101, 754 cm⁻¹; ¹H NMR (CDCl₃, 400 MHz): δ 0.79 (s, 3H, H-13), 1.17 (s, 3H, H-11), 1.23 (s, 3H, H-12), 1.77, 1.81 (m, 2H, H-3 α , H-3 β), 1.38, 2.10 (m, 2H, H-6 α , H-6 β), 1.53 (dd, *J* = 15.0, 6.0 Hz, 1H, H-5 α), 1.65 (m, 1H, H-5 β), 1.98 (m, 1H, H-7), 2.27, (br d, *J* = 19.4 Hz, 1H, H-8 α), 2.72 (dd, *J* = 19.4, 6.8 Hz, 1H, H-8 β), 2.82 (m, 1H, H-2); ¹³C NMR (CDCl₃, 100 MHz): 123.7 (C-1), 36.8 (C-2), 22.8 (C-3), 76.9 (C-3a), 71.3 (C-4), 33.6 (C-5), 24.7 (C-6), 47.8 (C-7), 30.1 (C-8), 172.6 (C-8a), 42.3 (C-9), 170.1 (C-10), 28.6 (C-11), 22.0 (C-12), 27.6 (C-13); HMBC correlation: H-2 (C-1, C-8a), H-3 (C-1, C-2, C-3a, C-4 C-8a, C-9), H-5 α (C-3a, C-4, C-6, C-7, C-11), H-5 β (C-3a, C-6, C-11), H-6 α (C-5, C-7, C-9), H-6 β (C-5, C-7, C-8, C-9), H-7 (C-4, C-5, C-8), H-8 α (C-1, C-6, C-7, C-8a, C-9), H-8 β (C-1, C-6, C-8a), H-11(C-3a, C-4, C-5), H-12 (C-4, C-7, C-9, C-13), H-13(C-4, C-7, C-9, C-12); ESMS (-ve): 249 [M-H]⁻.

2.4.3 12-Hydroxycyperenoic acid (3)

Colorless amorphous solid; $[\alpha]_D^{29}$ -9.7° (*c* 0.48, CHCl₃); IR: ν_{\max} 3358, 2929, 1678, 1202, 763 cm⁻¹; ¹H NMR (CDCl₃, 400 MHz): 0.86 (d, *J* = 6.4 Hz, 3H, H-11), 0.93 (s, 3H, H-13), 1.37, 1.81 (m, 2H, H-6 α , H-6 β), 1.61, 1.83 (m, 2H, H-3 α , H-3 β), 1.57 (m, 2H, H-5), 2.07 (m, 1H, H-4), 2.16 (m, 1H, H-7), 2.27 (m, 2H, H-2), 2.25, 2.77 (m, 2H, H-8 α , H-8 β), 3.78, 3.86 (each d, *J* = 10.9 Hz, 1H each, H-12a, H-12b); ¹³C NMR (CDCl₃, 100 MHz): 123.4 (C-1), 36.6 (C-2), 26.3 (C-3), 67.4 (C-3a), 35.6 (C-4), 27.8 (C-5), 27.1 (C-6), 45.3 (C-7), 31.2 (C-8), 171.5 (C-8a), 46.0 (C-9), 169.7 (C-10), 17.9 (C-11), 65.3 (C-12), 20.5 (C-13); HMBC correlation: H-2 (C-1, C-3a, C-8a), H-3 α (C-1, C-4, C-8a), H-3 β (C-3a, C-4), H-4 (C-5, C-8a, C-9, C-11), H-5 (C-3a, C-4, C-7), H-6 α (C-5), H-6 β (C-5, C-8), H-7 (C-5), H-8 α (C-8a), H-8 β (C-8a, C-9), H-11(C-4, C-5, C-9), H-12 (C-7, C-9, C-13), H-13(C-7, C-9, C-12); ESMS (-ve): 249 [M-H]⁻.

2.4.4 (8R)-8-Hydroxycyperenoic acid (4)

White amorphous solid; $[\alpha]_D^{29}$ -12.1° (*c* 0.66, CHCl₃); IR: ν_{\max} 3502, 2923, 1655, 1282, 763 cm⁻¹; ¹H NMR (CDCl₃, 400 MHz): δ 0.79 (s, 3H, H-13), 0.85 (d, *J* = 6.4 Hz, 3H, H-11), 1.21 (s, 3H, H-12), 1.37, 1.55 (m, 2H, H-5 α , H-5 β), 1.56, 1.73 (m, 2H, H-3 α , H-3 β), 2.06 (m, 1H, H-7), 2.30 (m, 1H, H-4), 2.44 (br d, *J* = 19.8 Hz, 1H, H-6 α), 2.69 (m, 1H, H-6 β), 2.66, 2.77 (m, 2H, H-2 α , H-2 β), 3.91 (t-like, *W*_{1/2} = 17.7 Hz, 1H, H-8); ¹³C NMR (CDCl₃, 100 MHz): 124.4 (C-1), 36.3 (C-2), 25.5 (C-3), 67.7 (C-3a), 33.6

(C-4), 36.5 (C-5), 31.3 (C-6), 54.1 (C-7), 73.1 (C-8), 169.9 (C-8a), 41.4 (C-9), 168.8 (C-10), 17.6 (C-11), 20.7 (C-12), 27.1 (C-13); HMBC correlation: H-2 (C-1, C-3, C-3a, C-8a), H-3 α (C-1, C-4, C-8a), H-3 β (C-2, C-3a, C-4, C-9), H-4 (C-3a, C-5, C-6, C-8a, C-9, C-11), H-5 α (C-4, C-11), H-5 β (C-3a, C-4, C-7), H-6 (C-8, C-8a, C-9), H-7 (C-3a, C-5, C-6, C-8, C-8a, C-13), H-8 (C-4, C-7, C-9), H-11(C-3a, C-4, C-5), H-12 (C-3a, C-7, C-9, C-13), H-13(C-3a, C-7, C-9, C-12); ESMS (+ve): 251 [M+H]⁺.

3. Results and Discussion

The biotransformation of cyperenoic acid (1) to the metabolites (2-4) is shown below.

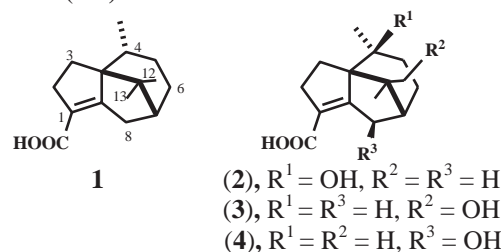


Figure 1. Structures of cyperenoic acid **1** and metabolites **2-4**.

Cyperenoic acid (1) was converted into three new metabolites (2-4) by *C. lunata* NRRL 2178 (Figure 1). Their structures were determined by spectroscopic techniques.

Compound **2** was obtained as colorless amorphous solid. The IR spectrum indicated the presence of hydroxy (3429 cm⁻¹) and carboxylic carbonyl (1677 cm⁻¹) groups. The electrospray mass spectrum (ESMS) showed the [M-H]⁻ peak at *m/z* 249, corresponding to the molecular formula of C₁₅H₂₂O₃. The ¹H-NMR features (CDCl₃) of **2** were similar to those of **1**, 4 α ,9,9-trimethyl-2,4,5,6,7 α ,8-hexahydro-3H-3a [4], with the exception of the difference in the absence of chemical shift of proton multiplet at δ 2.09 (H-4), and the downfield shift of C-4 (δ 71.3) instead of δ 36.0 for compound **1**. The HMBC correlations between H-11 and C-3a (δ 76.9), C-4 (δ 71.3) and C-5 (δ 33.6), and the HMBC correlations between H-5 and C-3a (δ 76.9), C-4 (δ 71.3), C-6 (δ 24.7) and C-11(δ 28.6) suggested that compound **2** was hydroxylated at C-4 position. The β -orientation of the 4-OH group was established by NOESY experiment. Thus, 11-Me showed cross peak with H-2. Compound **2** is thus (4S)-4-hydroxycyperenoic acid.

Compound **3** was obtained as colorless amorphous solid. The IR spectrum indicated the presence of similar functionalities as those of compound **2**. The ESMS showed the [M-H]⁻ peak at *m/z* 249, corresponding to the molecular formula of C₁₅H₂₂O₃. The ¹H-NMR (CDCl₃) spectral features were similar to those of **1**. The significant difference was the presence of a hydroxymethylene signal at δ 3.78 and 3.86 (1H each, d, *J* = 10.9 Hz) assignable to H-12. The HMBC correlations between H-12 and C-7 (δ 45.3), C-9 (δ 46.0) and C-13 (δ 20.5). The evidence that

hydroxylation has taken place at the 12-Me group was from the presence of cross peak between H-12 and H-4 and H-6 β in the NOESY spectrum. On the basis of the above evidence, the structure of the metabolite **3** was established as 12-hydroxycyperenoic acid.

Compound **4** was obtained as white amorphous solid. The IR spectrum revealed similar absorption bands as those of the above metabolites. The ESMS showed the [M+H]⁺ peak at m/z 251, corresponding to the molecular formula of C₁₅H₂₂O₃. The ¹H-NMR spectral (CDCl₃) of **4** was found to be similar to those of **1**. The significant difference was the presence of a carbinol proton signal at δ 3.91 assignable to H-8. In the ¹³C NMR data, the signal at δ 31.3 (C-8) was shifted downfield to δ 71.3. The COSY correlation between H-8 (3.91) and H-7 (δ 2.06) and the HMBC correlations between H-8 and C-6 (δ 31.3), C-7 (δ 54.1) and C-9 (δ 41.4) confirmed the location of H-8. These results indicated that **4** is an 8-hydroxyl analogue of **1**. The β -orientation of the 8-OH group was established by NOE experiments. Thus, irradiating the H-8 signal caused enhancements of the H-5 α and the H-6 α signals. Irradiation of the H-5 α signal caused enhancement of the H-8 signal. The absolute configuration at C-8 was also established as *R* by the modified Mosher's method. Compound **4** was therefore concluded to be (8*R*)-4-hydroxycyperenoic acid.

4. Conclusions

Biotransformation of cyperenoic acid (**1**) by *C. lunata* NRRL 2178 gave three new metabolites, compounds **2-4**. Compound **4** was found to be the major metabolite. Bioconversion by this fungal strain indicated that hydroxylation at C-4, C-12 and C-8 has occurred to yield compounds **2**, **3**, and **4**, respectively.

Acknowledgements

This work was supported by The Thailand Research Fund (TRF). Support from the Center of Excellence for Innovation in Chemistry (PERCH-CIC), Office of the Higher Education Commission, Ministry of Education is gratefully acknowledged.

References

- [1] J. Zhao, F. Fang, L. Yu, G. Wang and L. Yang, *J. Ethnopharmacol.* **142** (2012) 367-373.
- [2] S. Boonyaratavej and S. Roengsumran, *J. Nat. Prod.* **51** (1998) 769-770.
- [3] X. C. Ma, J. Zheng and D. A. Guo, *Chem. Eng. Microb. Technol.* **40** (2007) 1013-1019.
- [4] L. Boonyarathanakornkit, C. T. Che, H. S. Fong and N. R. Farnsworth, *Planta med.* **54** (1988) 61-63.

SYNTHESIS AND CYTOTOXICITY EVALUATION OF 9,13-DISUBSTITUTED BERBERINE DERIVATIVES

Chalueomchai Jampadang, Duangkhae Srikun, Mayuso Kuno, Pornpimol Lertsopapun, Pornpimol Wongsuwan, Siritron Samosorn*

Department of Chemistry, Faculty of Science, Srinakharinwirot University, Bangkok, 10110 Thailand

* Author for correspondence; E-Mail: siritron@swu.ac.th, Tel. +66 26495907, Fax. +66 22592097

Abstract: Berberine, a naturally occurring isoquinoline alkaloid widely spread in many medicinal plant families such as Berberidaceae and Papaveraceae, has been shown to suppress the growth of breast, lung and tongue cancer cells. Introduction of various substituents into the 9 and 13 positions of berberine has been reported to have better anticancer activities than berberine. In this study, a series of 9,13-disubstituted berberine derivatives was synthesized and evaluated for cytotoxic activities against human cancer cell lines. The key synthetic precursor was the phenol betaine derived from berberine. Subsequently *O*-alkylation of the betaine with alkyl bromide gave 9,13-disubstituted berberine derivatives in moderate yields. A novel compound, 9-propyloxy-13-pentyloxyberberine was shown to be more active than berberine 2- and 19-fold against KB-oral cavity cancer and MCF-7 breast cancer cell lines, respectively.

1. Introduction

Berberine (**1**), an isoquinoline alkaloid, is isolated from Chinese and Thai medicinal plants in the families of Berberidaceae, Menispermaceae, Papaveraceae, Rutaceae and others. Berberine showed remarkable antiproliferative activities against various human cancer cell lines [1,2] leading to much attraction in this molecule as a lead compound for the development of anticancer agents. Studies on structure modifications of berberine at C-9 and C-13 have been reported. Introduction of a side chain with a terminal amino group at the 9-position could significantly improve interactions of the derivatives with G-quadruplex DNA, resulting in inhibitory effects on telomerase in cancer cells leading to stop extension of DNA chain length [3,4]. Substitution of alkyl, alkoxy and aryloxy groups at the 13-position has been reported to have better anticancer activities than the parent berberine [5-9]. Cytotoxicity screening of anticancer agents synthesized in our laboratory revealed that 13-*n*-propyloxyberberine (**5a**) and 13-*n*-pentyloxyberberine (**5d**) were highly active against NCI-H187 small cell lung cancer and KB-oral cavity cancer cell lines with the IC₅₀ of 0.002, 0.0003 and 0.33, 0.004 µg/mL, respectively [6] (Table 1). These results showed that alkoxy substituent at the 13-position might be important for the anticancer activities. In particular, the size of *n*-propyloxy and *n*-pentyloxy groups might be appropriate to fit in the binding pockets of NCI-H187-small cell lung cancer and KB-oral cavity cancer. Therefore, in this study we designed and synthesized 9,13-disubstituted berberine derivatives which retained the *n*-propyloxy and *n*-pentyloxy groups at the 13-position and introduced ethoxy and *n*-propyloxy groups at the 9-position of berberine to evaluate for their cytotoxic activities.

2. Materials and Methods

2.1. Chemistry

Berberine (chloride salt) and all alkylating agents were purchased from Sigma-Aldrich Chemical Co., and were used as supplied. Melting points were obtained using a Griffin melting point apparatus and are uncorrected. Thin layer chromatography (TLC) on aluminum backed sheets of Merck Silica Gel 60 F254 plates were used to follow the progress of chemical reactions. Compounds were detected by examination under UV light. Column chromatography was performed under medium pressure on silica gel 60 (230–400 mesh). All solvent proportions were vol/vol. NMR spectra were obtained on a Bruker AVANCE 300 FT-NMR spectrometer, where proton (¹H) and carbon (¹³C) spectra were obtained at 300 MHz and 75 MHz, respectively. Spectra were recorded in CDCl₃ (unless otherwise indicated) and were referenced to the residual non-deuterated solvent signal. Superscript letters refer to interchangeable chemical shift assignments. Low resolution electrospray ionization mass spectra, ESI-MS, were obtained with a Thermo Finnigan LC-Q mass spectrometer. Compounds for testing were >95% pure on the basis of TLC and ¹H NMR analysis.

2.1.1. Berberubine (**2**) [10]

A yellow suspension of berberine chloride (0.25 g, 0.67 mmol) in dimethyl formamide (DMF, 1 mL) in a sealed tube was heated at 150°C for 2h. The resulting red solution was cooled to room temperature and then concentrated. The residue was crystallized from 5% HCl in EtOH. The crystals were filtered, washed with cold EtOH and dried to give berberubine (**2**) (0.18 g, 76 %) as a red solid. ¹H NMR (CD₃OD/CDCl₃, 300 MHz): δ 9.29 (s, 1H, 8-H), 8.01 (s, 1H, 13-H), 7.55 (d, 1H, *J* = 8.4 Hz, 11-H), 7.43 (s, 1H, 14-H), 6.96 (d, 1H, *J* = 8.1 Hz, 12-H), 6.84 (s, 1H, 4-H), 6.03 (s, 2H, OCH₂O), 4.62 (t, 2H, *J* = 6.0 Hz, 5-H), 3.88 (s, 3H, 10-OCH₃), 3.12 (t, 2H, *J* = 6.0 Hz, 6-H); ESI-MS: *m/z* 322.2 (M)⁺.

2.1.2. General procedure for the preparation of **1a-b**

A suspension of the berberubine **2** (1.4 mmol), K₂CO₃ (1.4 mmol), and 1-bromoethane or 1-bromopropane (3 mmol) in dry CH₃CN (5 mL) was heated at 65 °C for 3 h under a nitrogen atmosphere. The reaction mixture was then concentrated and the residue was chromatographed on silica gel (4% MeOH in DCM) to give **1a-b**.

2.1.2.1. 2,3-Methylenedioxy-9-ethoxy-10-methoxy berberine bromide (**1a**) [10]

Yellow solid: 0.37 g (61%). ^1H NMR ($\text{CD}_3\text{OD}/\text{CDCl}_3$): δ 9.56 (s, 1H, 8-H), 8.30 (s, 1H, 13-H), 7.79 (d, 1H, $J = 8.0$ Hz, 11-H)^a, 7.79 (d, 1H, $J = 8.0$ Hz, 12-H)^a, 7.31 (s, 1H, 14-H)^b, 6.71 (s, 1H, 4-H)^b, 5.95 (s, 2H, 2-H), 4.82 (t, 2H, $J = 5.9$ Hz, 6-H), 4.36 (q, 2H, $J = 6.9$ Hz, OCH_2), 3.93 (s, 3H, 10- OCH_3), 3.11 (t, 2H, $J = 6.3$ Hz, 5-H), 1.37 (t, 3H, $J = 7.0$ Hz, CH_3); ESI-MS: m/z 350.2 (M)⁺.

2.1.2.2. 2,3-Methylenedioxy-9-*n*-propyloxy-10-methoxyberberine bromide (**1b**)

Yellow solid: 0.14 g (58%). ^1H NMR ($\text{DMSO}-d_6$): δ 9.75 (s, 1H, 8-H), 8.94 (s, 1H, 13-H), 8.19 (d, 1H, $J = 9.1$ Hz, 11-H)^a, 7.98 (d, 1H, $J = 9.1$ Hz, 12-H)^a, 7.79 (s, 1H, 14-H)^b, 7.08 (s, 1H, 4-H)^b, 6.16 (s, 2H, 2-H), 4.95 (t, 2H, $J = 5.9$ Hz, 6-H), 4.24 (t, 2H, $J = 6.8$ Hz, OCH_2), 4.04 (s, 3H, 10- OCH_3), 3.20 (t, 2H, $J = 6.0$ Hz, 5-H), 1.84-1.92 (m, 2H, CH_2), 1.04 (t, 3H, $J = 7.4$ Hz, CH_3). ^{13}C NMR ($\text{DMSO}-d_6$): δ 150.4 (C-3a)^a, 149.8 (C-10), 147.6 (C-14a)^a, 145.2 (C-8), 142.9 (C-9), 137.4 (C-13a), 133.0 (C-12a), 130.7 (C-4a), 126.7 (C-11), 123.2 (C-12), 121.6 (C-8a), 120.4 (C-13), 120.1 (C-13b), 108.37 (C-4)^b, 105.4 (C-14)^b, 102.0 (C-2), 75.8 (OCH_2), 57.0 (OCH_3), 55.3 (C-6), 26.3 (C-5), 22.8 (CH_2), 10.2 (CH_3). ESI-MS: m/z 364.2 (M)⁺.

2.1.3. General procedure for the preparation of **3a-b**

To a suspension of **1a** or **1b** (4.6 mmol) in acetone (50 mL), was added 30% aqueous sodium hydroxide until pH 11. The mixture was heated at 65 °C for 30 min. The reaction mixture was concentrated and then poured into ice water (200 mL). The precipitate was filtered and dried to give a yellow solid which was then dissolved in acetone (20 mL) and slowly added a solution of KMnO_4 (370 mg in H_2O 33 mL) at -10 °C. After vigorous stirring for 3 h, the reaction mixture was filtered to remove a brown solid and washed with H_2O . The filtrate was evaporated and then added MeOH (2 mL) and conc. HCl (2 mL). The yellow suspension was heated at reflux for 12 h. The mixture was concentrated and chromatographed on silica gel (2 % MeOH in DCM) to give **3a** or **3b**.

2.1.3.1. 2,3-Methylenedioxy-9-ethoxy-10-methoxy-13-hydroxyberberine chloride (**3a**)

Orange-yellow solid 0.57 g (28%). ^1H NMR (CDCl_3): δ 8.89 (s, 1H, 14-H)^a, 8.27 (d, 1H, $J = 9.0$ Hz, 12-H)^b, 7.71 (s, 1H, 8-H), 7.30 (d, 1H, $J = 9.0$ Hz, 11-H)^b, 6.57 (s, 1H, 4-H)^a, 5.90 (s, 2H, 2-H), 4.43 (t, 2H, $J = 6.0$ Hz, 6-H), 4.20 (q, 2H, $J = 6.9$ Hz, OCH_2), 3.93 (s, 3H, 10- OCH_3), 2.97 (t, 2H, $J = 6.0$ Hz, 5-H), 1.39 (t, 3H, $J = 7.0$ Hz, CH_3). ^{13}C NMR (CDCl_3): δ 166.0 (C-13), 150.3 (C-10), 146.3 (C-14a)^a, 146.1 (C-3a)^a, 141.2 (C-9), 130.9 (C-8a)^b, 126.4 (C-4a), 124.2 (C-13b), 124.0 (C-12a)^b, 123.8 (C-13a), 121.9 (C-12)^c, 117.4 (C-11)^c, 117.2 (C-8), 108.8 (C-14)^d, 106.8 (C-4)^d, 101.0 (C-2), 69.3 (OCH_2), 57.5 (C-6), 56.4 (OCH_3), 28.6 (C-5), 15.7 (CH_3). ESI-MS: m/z 366.4 (M)⁺.

2.1.3.2. 2,3-Methylenedioxy-9-*n*-propyloxy-10-methoxy-13-hydroxyberberine chloride (**3b**)

Orange-yellow solid 0.12 g (22%). ^1H NMR ($\text{DMSO}-d_6$): δ 8.89 (s, 1H, 14-H)^a, 8.06 (d, 1H, $J = 9.0$ Hz, 12-H)^b, 7.97 (s, 1H, 8-H), 7.50 (d, 1H, $J = 9.0$ Hz, 11-H)^a, 6.87 (s, 1H, 4-H)^a, 6.03 (s, 2H, 2-H), 4.61 (t, 2H, $J =$

6.0 Hz, 6-H), 4.05 (t, 2H, $J = 6.8$ Hz, OCH_2), 3.99 (s, 3H, 10- OCH_3), 2.97 (t, 2H, $J = 5.9$ Hz, 5-H), 1.70-1.78 (m, 2H, CH_2), 1.01 (t, 3H, $J = 7.5$ Hz, CH_3). ^{13}C NMR (CDCl_3): δ 165.1 (C-13), 150.2 (C-10), 145.3 (C-14a)^a, 145.2 (C-3a)^a, 141.4 (C-9), 130.2 (C-8a)^b, 127.3 (C-4a), 123.9 (C-13b), 123.7 (C-12a)^b, 122.2 (C-13a), 121.1 (C-12)^c, 117.6 (C-11)^c, 117.2 (C-8), 107.9 (C-14)^d, 107.2 (C-4)^d, 100.8 (C-2), 75.4 (OCH_2), 56.4 (C-6), 56.3 (OCH_3), 27.6 (C-5), 22.8 (CH_2), 10.2 (CH_3). ESI-MS: m/z 380.4 (M)⁺.

2.1.4. General procedure for the preparation of **5b-c** and **5e-f**

A yellow suspension of **3a** or **3b** (0.49 mmol) in 5% NaOH (20 mL) was extracted with DCM (3 x 20 mL). A combined organic layer was washed with H_2O and dried with anhydrous Na_2SO_4 , and then evaporated and dried to yield **4a-b** as a yellow solid. A solution of the phenolbetaine **4a-b** (1 mmol) and the 1-bromopropane or 1-bromopentane (2 mmol) in dry CH_3CN (2 mL) was heated at 65 °C for 12h under a nitrogen atmosphere. The reaction mixture was concentrated and then was chromatographed on silica gel (2% MeOH in DCM) to give the desired products **5b-c** and **5e-f**.

2.1.4.1. 2,3-Methylenedioxy-9-ethoxy-10-methoxy-13-*n*-propyloxyberberine bromide (**5b**)

Yellow solid 0.12 g (46%). ^1H NMR ($\text{CDCl}_3/\text{CD}_3\text{OD}$): δ 9.90 (s, 1H, 8-H), 7.95 (d, 1H, $J = 9.0$ Hz, 11-H)^a, 7.89 (s, 1H, 14-H), 7.79 (d, 1H, $J = 9.0$ Hz, 12-H)^a, 6.83 (s, 1H, 4-H)^b, 6.04 (s, 2H, 2-H), 5.06 (t, 2H, $J = 5.6$ Hz, 6-H), 4.50 (q, 2H, $J = 6.9$ Hz, 9- OCH_2), 4.02 (s, 3H, 10- OCH_3), 3.76 (t, 2H, $J = 6.6$ Hz, 13- OCH_2), 3.22 (t, 2H, $J = 6.0$ Hz, 5-H), 1.78-1.85 (m, 2H, CH_2), 1.53 (t, 3H, $J = 6.9$ Hz, CH_3), 1.05 (t, 3H, $J = 7.5$ Hz, CH_3). ^{13}C NMR ($\text{CDCl}_3/\text{CD}_3\text{OD}$): δ 151.1 (C-13)^a, 150.5 (C-10), 150.0 (C-3a)^a, 147.0 (C-14a)^a, 144.0 (C-9), 142.6 (C-8), 132.1 (C-4a), 131.0 (C-8a), 130.0 (C-12a), 125.3 (C-12), 123.0 (C-13a), 117.7 (C-13b), 116.5 (C-11), 108.4 (C-4)^b, 108.3 (C-14)^b, 102.0 (C-2), 75.7 (OCH_2 -13), 71.2 (OCH_2 -9), 57.2 (C-6), 56.2 (OCH_3), 28.1 (C-5), 23.4 (CH_2), 15.7 (CH_3 -9), 10.4 (CH_3 -13). ESI-MS: m/z 408.3 (M)⁺.

2.1.4.2. 2,3-Methylenedioxy-9,13-di-*n*-propyloxy-10-methoxyberberine bromide (**5c**)

Yellow solid 198 mg (41%). ^1H NMR ($\text{CDCl}_3/\text{CD}_3\text{OD}$): δ 10.18 (s, 1H, 8-H), 7.96 (d, 1H, $J = 9.0$ Hz, 11-H)^a, 7.92 (s, 1H, 14-H)^b, 7.79 (d, 1H, $J = 9.0$ Hz, 12-H)^a, 6.82 (s, 1H, 4-H)^b, 6.07 (s, 2H, 2-H), 5.26 (t, 2H, $J = 5.9$ Hz, 6-H), 4.47 (t, 2H, $J = 6.9$ Hz, 9- OCH_2), 4.04 (s, 3H, 10- OCH_3), 3.78 (t, 2H, $J = 6.5$ Hz, 13- OCH_2), 3.30 (t, 2H, $J = 5.7$ Hz, 5-H), 2.02-2.10 (m, 2H, CH_2), 1.81-1.88 (m, 2H, CH_2), 1.10 (t, 3H, $J = 7.5$ Hz, CH_3), 1.07 (t, 3H, $J = 7.5$ Hz, CH_3). ^{13}C NMR ($\text{CDCl}_3/\text{CD}_3\text{OD}$): δ 151.3 (C-10), 150.6 (C-13), 149.9 (C-3a)^a, 147.5 (C-14a)^a, 146.0 (C-9), 143.3 (C-8), 132.3 (C-4a), 130.8 (C-8a)^b, 129.9 (C-12a)^b, 125.3 (C-12), 123.2 (C-13a), 118.5 (C-13b), 117.5 (C-11), 108.4 (C-4, C-14), 102.0 (C-2), 77.2 (OCH_2 -13), 77.1 (OCH_2 -9), 57.2 (C-6), 57.1 (OCH_3), 28.3 (C-5), 23.6 (CH_2), 23.5 (CH_2), 10.5 (CH_3 -9), 10.3 (CH_3 -13). ESI-MS: m/z 422.5 (M)⁺.

2.1.4.3. 2,3-Methylenedioxy-9-ethoxy-10-methoxy-13-*n*-pentyloxyberberine bromide (**5e**)

Yellow solid 0.12 g (42%). ¹H NMR (CDCl₃/CD₃OD): δ 10.23 (s, 1H, 8-H), 7.95 (d, 1H, *J* = 9.0 Hz, 11-H)^a, 7.92 (s, 1H, 14-H)^b, 7.79 (d, 1H, *J* = 9.0 Hz, 12-H)^a, 6.83 (s, 1H, 4-H)^b, 6.07 (s, 2H, 2-H), 5.27 (t, 2H, *J* = 5.6 Hz, 6-H), 4.60 (q, 2H, *J* = 6.9 Hz, 9-OCH₂), 4.05 (s, 3H, 10-OCH₃), 3.80 (t, 2H, *J* = 6.5 Hz, 13-OCH₂), 3.29 (t, 2H, *J* = 6.0 Hz, 5-H), 1.70-1.82 (m, 2H, CH₂), 1.60 (t, 3H, *J* = 6.9 Hz, CH₃), 1.40-1.50 (m, 2H, CH₂), 1.30-1.40 (m, 2H, CH₂), 0.93 (t, 3H, *J* = 7.2 Hz, CH₃). ¹³C NMR (CDCl₃/CD₃OD): δ 151.5 (C-10), 150.7 (C-13), 149.5 (C-3a)^a, 147.5 (C-14a)^a, 145.0 (C-9), 143.4 (C-8), 132.2 (C-4a), 131.0 (C-8a)^b, 130.0 (C-12a)^b, 125.2 (C-12), 123.0 (C-13a), 119.0 (C-13b), 117.6 (C-11), 108.4 (C-4, C-14), 102.0 (C-2), 75.8 (OCH₂-13), 71.6 (OCH₂-9), 57.2 (C-6), 57.0 (OCH₃), 29.8 (CH₂), 28.2 (C-5), 28.1 (CH₂), 22.4 (CH₂), 16.0 (CH₃-9), 13.9 (CH₃-13). ESI-MS: *m/z* 436.3 (M)⁺.

2.1.4.4. 2,3-Methylenedioxy-9-*n*-propyloxy-10-methoxy-13-*n*-pentyloxyberberine bromide (**5c**)

Yellow solid 0.2 g (39%). ¹H NMR (CDCl₃/CD₃OD): δ 10.16 (s, 1H, 8-H), 7.94 (d, 1H, *J* = 9.3 Hz, 11-H)^a, 7.91 (s, 1H, 14-H)^b, 7.79 (d, 1H, *J* = 9.3 Hz, 12-H)^a, 6.82 (s, 1H, 4-H)^b, 6.06 (s, 2H, 2-H), 5.26 (t, 2H, *J* = 6.6 Hz, 6-H), 4.47 (t, 2H, *J* = 6.9 Hz, 9-OCH₂), 4.04 (s, 3H, 10-OCH₃), 3.80 (t, 2H, *J* = 6.5 Hz, 13-OCH₂), 3.30 (t, 2H, *J* = 5.7 Hz, 5-H), 2.05 (q, 2H, *J* = 7.2 Hz, 5-H), 1.70-1.90 (m, 2H, CH₂), 1.30-1.50 (m, 4H, CH₂), 1.10 (t, 3H, *J* = 7.5 Hz, CH₃), 0.92 (t, 3H, *J* = 7.2 Hz, CH₃). ¹³C NMR (CDCl₃/CD₃OD): δ 151.2 (C-10), 150.7 (C-13), 149.8 (C-3a)^a, 147.4 (C-14a)^a, 145.5 (C-9), 143.1 (C-8), 132.2 (C-4a), 130.8 (C-8a)^b, 129.9 (C-12a)^b, 125.3 (C-12), 123.0 (C-13a), 118.5 (C-13b), 117.5 (C-11), 108.4 (C-4, C-14), 102.0 (C-2), 77.2 (OCH₂-9), 75.8 (OCH₂-13), 57.2 (C-6), 57.0 (OCH₃), 29.8 (CH₂), 28.2 (C-5), 28.0 (CH₂), 23.6 (CH₂), 22.4 (CH₂), 13.9 (CH₃-13), 10.3 (CH₃-9). ESI-MS: *m/z* 450.2 (M)⁺.

2.2 Biological Assay

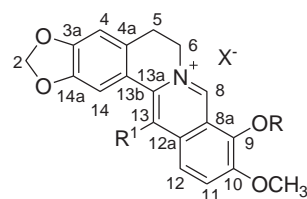
2.2.1 Cancer cell growth inhibition [11]

Resazurin microplate assay (REMA) was performed using the method described by Brien et al. Cells at a logarithmic growth phase are harvested and diluted to 2.2 x 10⁴ cells/mL for KB, 3.3 x 10⁴ cells/mL for MCF-7, and NCI-H187, in fresh medium. Successively, 5 µL of test sample diluted in 5% DMSO and 45 µL of cell suspension were added to 384-well plates then incubated at 37 °C in 5% CO₂ incubator. After the incubation period (3 days for KB and MCF-7, and 5 days for NCI-H187), 12.5 µL of 62.5 µg/mL resazurin solution was added to each well, and the plates were then incubated at 37 °C for 4 h. Fluorescence signal was measured using SpectraMax M5 multi-detection microplate reader (Molecular Devices, USA) at the excitation and emission wavelengths of 530 nm and 590 nm.

2.2.2 Cytotoxicity against primate cell line [12]

The Green fluorescent protein-expressing Vero cell line was generated in National Center for Genetic Engineering and Biotechnology (BIOTEC) by stably transfecting the African green monkey kidney cell line (Vero, ATCC CCL-81), with pEGFP-N1 plasmid (Clontech). The cell line was maintained in minimal essential medium supplemented with 10% heat-inactivated fetal bovine serum, 2 mM L-glutamine, 1 mM sodium pyruvate, 1.5 g/L sodium bicarbonate and 0.8 mg/mL geneticin, at 37 °C in a humidified incubator with 5% CO₂. The assay was carried out by adding 45 µL of cell suspension at 3.3 x 10⁴ cells/mL to each well of 384-well plates containing 5 µL of test compounds previously diluted in 0.5% DMSO, and then incubating for 4 days in 37 °C incubator with 5% CO₂. Fluorescence signals were measured by using SpectraMax M5 microplate reader (Molecular Devices, USA) in the bottom reading mode with excitation and emission wavelengths of 485 and 535 nm.

Table 1: *In vitro* cytotoxic activity of compounds **1**, **3** and **5** against NCI-H187 small cell lung cancer, KB-oral cavity cancer, MCF7 breast cancer, and Vero cell lines



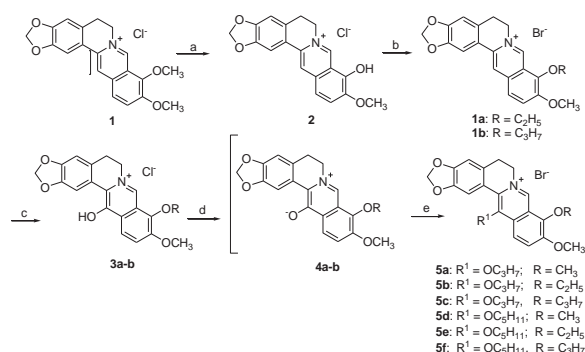
Com -pd	R ¹	R	Cytotoxicity IC ₅₀ (µg/mL)			
			NCI-H187	KB	MCF7	Vero cells
1	H	CH ₃	0.16	1.63	37.9	>50
1a	H	C ₂ H ₅	0.38	5.41	2.19	>50
1b	H	C ₃ H ₇	0.27	2.26	1.40	>50
3a	OH	C ₂ H ₅	>50	>50	34.22	>50
3b	OH	C ₃ H ₇	19.05	>50	>50	>50
5a^a	OC ₃ H ₇	CH ₃	0.002	0.33	40.26	27.02
5b	OC ₃ H ₇	C ₂ H ₅	4.19	6.69	>50	>50
5c	OC ₃ H ₇	C ₃ H ₇	1.83	6.56	>50	20.22
5d^a	OC ₅ H ₁₁	CH ₃	0.0003	0.004	7.51	3.50
5e	OC ₅ H ₁₁	C ₂ H ₅	0.26	2.39	1.09	2.22
5f	OC ₅ H ₁₁	C ₃ H ₇	0.67	0.89	1.98	2.48
Elipticine	-	-	0.684	0.448	>50	0.829
Doxorubicin	-	-	0.035	0.249	0.573	not tested

^a Values are retrieved from Samosorn et al [6].

3. Results and Discussion

Six novel 9,13-disubstituted berberine derivatives (**3a-b**, **5b-c** and **5e-f**) were synthesized from berberine (**1**) as shown in scheme 1. Synthesis of compounds **5b-c** and **5e-f** was started from demethylation of **1** in DMF at 150 °C in sealed tube to give berberubine (**2**)

in a good yield and subsequently alkylation with ethyl bromide or *n*-propyl bromide to give compounds **1a** and **1b** in yields of 58% and 61%, respectively. Treatment of **1a-b** with acetone and sodium hydroxide gave an unstable 8-acetonyldihydro intermediate which was then oxidized straightaway with potassium permanganate to give **3a-b** in yields of 22-28%. Deprotonation of **3a-b** with aqueous sodium hydroxide gave the key intermediate phenol betaine **4a-b** and then *O*-alkylation of the betaine immediately with appropriate alkyl bromide accomplished the desired products **5b-c** and **5e-f** in yields of 39-46%. [13].



Scheme 1. Reagents and conditions: (a) i: 150 °C, DMF, 3 h; ii: 5% HCl in EtOH; (b) K_2CO_3 , CH_3CH_2Br or $CH_3CH_2CH_2Br$, CH_3CN , 65 °C, 3 h; (c) i: 30% NaOH, CH_3COCH_3 , 30 min.; ii: $KMnO_4$, CH_3COCH_3 , -10 °C, 3 h; iii: 5% HCl in EtOH (d) 5% NaOH, CH_2Cl_2 ; (e) $CH_3CH_2CH_2Br$ or $CH_3CH_2CH_2CH_2CH_2Br$, CH_3CN , 65 °C, overnight.

Compounds **1-3** and **5** were evaluated for their *in vitro* cytotoxic activities against three human cancer cell lines and one primate normal cell line including KB (epidermoid carcinoma of oral cavity cell line, ATCC CCL-17), MCF-7 (breast adenocarcinoma cell line, ATCC HTB-22), NCI-H187 (small cell lung carcinoma cell line, ATCC CRL-5804), and Vero (normal African green monkey kidney cell line, ATCC CCL-81). Doxorubicin and Elicipticine were used as positive controls. Cytotoxicity results were summarized in Table 1. The concentration of each compound required to inhibit 50% cell growth was expressed as IC_{50} value. The results showed that replacement of methoxyl group at the 9-position of **1** by ethoxyl and *n*-propyloxy groups to give compounds **1a-b** with no substitution on C-13 exhibited better cytotoxic activities against MCF7 than the parent berberine 17- and 27-folds, respectively, and also low toxicity to Vero cell line. Introduction of a hydroxyl group into the 13-position of **1a** and **1b** to afford compounds **3a-b** led to completely loss of the activity against all tested cell lines. Substitution of hydroxyl group at the 13-position of **1a** and **1b** with *n*-propyloxy and *n*-pentyloxy groups gave compounds **5b-c** and **5e-f**. Compounds **5b-c** with *n*-propyloxy on the 13-position showed less potent than their leads **5a**, whereas compounds **5e-f** with *n*-pentyloxy at the 13-position exhibited 4-7 folds greater activities against the MCF7 than their lead **5d**, 19-35 folds better than the parent **1**, and over 25-46 folds more potent than Elicipticine anticancer agent. It seemed that introducing

of lipophilic group with appropriate size at the 9- and 13-positions might be beneficial for cytotoxic activities against only MCF7 but not for NCI-H187, KB, and Vero cell lines.

4. Conclusions

In conclusion, six new 9,13-disubstituted berberine derivatives were synthesized and evaluated for their cytotoxic activities against three human cancer cell lines and one primate normal cell line. Structure activity relationship analysis revealed that introduction of lipophilic group at the 9-position could improve cytotoxic activity against MCF7 breast cancer cell line. Substitution of a hydroxyl group at the 13-position of 9-*O*-alkyl berberine derivatives diminished cytotoxic activities against all cell lines tested. *n*-Pentyloxy group at the 13-position might be crucial for the cytotoxicity [6]. Therefore replacement of methoxyl at the 9-position by ethoxyl and *n*-propyloxy groups, especially ethoxyl group, improved the activity against MCF7 cell line. Compound **5e** showed the best activity of all the synthesized compounds against MCF7 with the IC_{50} value of 1.09 $\mu g/mL$. These data could provide useful information for designing berberine derivatives in the future.

Acknowledgements

We thank Science Faculty Grant, Srinakharinwirot University (027/2555) and The Thailand Research Fund (MRG5380085) for support, and are also grateful to Prof. Apichart Suksamrarn and Ms. Kanyarat Chanchang, Ramkhamhaeng University for recording the mass spectra.

References

- [1] Y. T. Ho, C. C. Lu, J. S. Yang, J. H. Chiang, T. C. Li, *Anticancer Res* **29** (2009), 4063-4070.
- [2] M. A. James, H. Fu, Y. Liu, D. R. Chen, M. You, *Mol Carcinogen* **50** (2011), 1-7.
- [3] W.-J. Zhang, T.-M. Ou, Y.-J. Lu, Y.-Y. Huang, W.-B. Wu, Z.-S. Huang, J.-L. Zhou, K.-Y. Wong, L.-Q. Gu, *Bioorg. Med. Chem.* **15** (2007), 5493-5501.
- [4] Y. Ma, T.-M. Ou, J.-H. Tan, J.-Q. Hou, S.-L. Huang, L.-Q. Gu, Z.-S. Huang, *Bioorg. Med. Chem. Lett.* **19** (2009), 3414-3417.
- [5] K. Gornall, S. Samosorn, J. Talib, J. B. Bremner, J. Beck, **21** (2007), 1759-1766.
- [6] S. Samosorn, B. Tanwirat, A. Suksamrarn, *Thai Patent Application Number 1101002293* (27 September 2011).
- [7] S. Samosorn, *Thai Petty Patent Application Number 1103000985* (16 September 2011).
- [8] K. C. Gornall, S. Samosorn, B. Tanwirat, A. Suksamrarn, J. B. Bremner, M. J. Kelso, J. L. Beck, *ChemComm* **46** (2010), 6602-6604.
- [9] B. Debipreeta, H. Maidul, B. Franco, D. A. Rosaria, L. Paolo, K. G. Suresh, *J. Phys. Chem. B* **116** (2012), 2314-24.
- [10] K. Iwasa, M. Kamigauchi, M. Ueki, M. Taniguchi, *Eur. J. Med. Chem.* **31** (1996), 469-478.
- [11] J. O. Brien, I. Wilson, T. Orton, F. Pognan, *Eur J Biochem* **267** (2000), 5421-5426.

- [12] L. Hunt, M. Jordan, M. De Jesus, F. M. Wurm,
Biotechnol and Bioeng **65** (1999), 201-205.
- [13] K. Iwasa, H. Nanba, D.-U. Lee, S.-I. Kang, *Planta Med.*
64 (1998), 748-751.

CHOLINESTERASE INHIBITORS FROM THE LEAVES AND ROOTS OF *CITRUS HYSTRIX* DC.

Setthakorn Niamthiang, Pattara Sawasdee *

* Natural Products Research Unit, Department of Chemistry, Faculty of Science, Chulalongkorn University, Bangkok, 10330, Thailand

* Corresponding Author : pattara.T@chula.ac.th, Tel. +66 22 187624

Abstract: Preliminary screening indicated that the extracts from the leaves and roots of *Citrus hystrix* showed potent anti-cholinesterase activity. Therefore, it is of interest to further examine the active compounds from these extracts. Three compounds were isolated from the leaf extract and one compound was obtained from the root extract. Their structures were elucidated by NMR spectroscopy as hesperidin, neohesperidin, oxypeucedanin hydrate and limonin. Neohesperidin showed the highest activity against acetylcholinesterase with the IC_{50} value of 0.16 mM, whereas oxypeucedanin hydrate has the highest inhibition toward butyrylcholinesterase with the IC_{50} value of 0.26 mM. Moreover, this is the first report regarding the isolation of limonin from *C. hystrix*.

1. Introduction

Alzheimer's disease (AD) is the most common neurodegenerative disease, characterized by progressive memory loss, decline in language skills and hallucinations [1]. Several factors such as low levels of acetylcholine (ACh), beta amyloid protein deposits, tau protein aggregation, oxidative stress, and inflammation are thought to play important roles in the pathophysiology of AD [2]. The cholinergic hypothesis correlated with cholinergic deficits such as reduced synaptic acetylcholine synthesis and choline acetyltransferase activity by cholinesterases [3]. Two types of cholinesterase enzymes, acetylcholinesterase (AChE) and butyrylcholinesterase (BChE), terminate the impulse transmission by rapid hydrolysis of acetylcholine [4]. In the treatment of AD, there are four FDA-approved drugs (tacrine, donepezil, galantamine and rivastigmine) that improve symptoms by inhibiting AChE to increase and prolong the availability of acetylcholine [2]. But BChE might play the same role as AChE by increasing levels of BChE in AD patients [5]. So, therapeutic drugs that serve as inhibitors of either AChE or BChE could provide additional benefits in AD.

Citrus hystrix DC. (Rutaceae), called Makruut in Thai, is used in traditional cuisines and remedies such as headaches and sore throats [6]. Many active compounds were isolated from this plant such as glycerolglycolipids, tannins, furanocoumarins and flavonoids [7-10]. They showed a variety of pharmaceutical effect such as anti-tumor, anti-viral, and anti-oxidant activities [11]. Recently, furanocoumarins, isolated from *C. hystrix* fruit peels, showed potent anti-butyrylcholinesterase activity [12].

In this study, the preliminary screening test was found that the extracts of leaves and roots of this plant showed interesting anti-cholinesterase activity. Thus, the anti-cholinesterase compounds from *Citrus hystrix* were isolated and evaluated their anti-acetyl- and butyrylcholinesterase activities.

2. Materials and Methods

2.1 General Experiment Procedures

The 1H -NMR spectra (at 400 MHz) and ^{13}C -NMR spectra (at 100 MHz) were recorded on a Bruker or a Varian with tetramethylsilane as an internal standard. To isolate and purify active compounds, silica gel 60 (particle size: 0.063-0.200 mm, Merck), Sephadex LH-20 (Amersham Pharmacia Biotech), and thin layer chromatography precoated silica gel (silica gel 60 F₂₅₄, Merck) were used. The spots on plate were detected under UV light. Acetylthiocholine iodide (ATCI), *S*-butyrylthiocholine iodide (BTCl), 5,5'-dithiobis-[2-nitrobenzoic acid] (DTNB), acetylcholinesterase (AChE) from electric eel, butyrylcholinesterase (BChE) from equine serum, and eserine were purchased from Sigma company. All solvent were distilled prior to use.

2.2 Plant Material

The leaves and roots of *C. hystrix* were collected in May 2012 from Chonburi Province, Thailand and identified by Assoc. Prof. Nijisiri Ruangrunsi, Faculty of Pharmaceutical Sciences, Chulalongkorn University. A voucher specimen (No. NPRU 0002) has been deposited in the Natural Products Research Unit, Department of Chemistry, Faculty of Science, Chulalongkorn University, Thailand.

2.3 Extraction and Isolation

The dried leaves of *C. hystrix* (0.8 kg) were ground and extracted with methanol at room temperature. The extract solution was concentrated under reduced pressure, and further subsequently partitioned with hexane, dichloromethane and *n*-butanol yielding hexane (17 g), dichloromethane (6 g), and *n*-butanol (9 g) extracts, respectively. The butanolic extract (8 g) was subjected to a silica gel column chromatography with a gradient system of hexane-EtOAc and EtOAc-MeOH to give 7 fractions. Fraction 2 was further separated by a silica gel column chromatography using

a gradient system of hexane-EtOAc and EtOAc-MeOH to obtain 6 fractions (2.1-2.6). Subfraction 2.2 was re-chromatographed on a silica gel column with a gradient system of hexane-EtOAc and EtOAc-MeOH to obtain 6 fractions (2.2.1-2.2.6). Subfraction 2.2.3 was purified by a sephadex LH-20 column eluting with MeOH to give hesperidin (5.4 mg). Subfraction 2.2.4 was also purified by a sephadex LH-20 column eluting with MeOH to yield neohesperidin (40.6 mg).

A portion of CH₂Cl₂ extract (5 g) was subjected to a silica gel column with a gradient system of hexane-EtOAc and EtOAc-MeOH to obtain 3 fractions. Fraction 2 was chromatographed on a silica gel column using a gradient system of hexane-EtOAc and EtOAc-MeOH to give 6 fractions (2.1-2.6). Subfraction 2.4 was further fractionated using a silica gel column eluting with a gradient system of hexane-EtOAc to yield 6 fractions (2.4.1-2.4.6). Subfraction 2.4.3 was purified with a silica gel column using a gradient system of hexane-EtOAc to give oxypeucedin hydrate (30.3 mg).

The dried roots of *C. hystris* (1.9 kg) were ground and extracted with EtOAc at room temperature. After remove solvent under reduced pressure, 20 g of the EtOAc was obtained. This extract was further fractionated by a silica gel vacuum column chromatography with a gradient system of hexane-EtOAc and EtOAc-MeOH to obtain 5 fractions. Limonin (250.2 mg) was afforded after recrystallization from fraction 4 with EtOAc at room temperature.

The structure of these isolated compound were fully elucidated on the spectral data (¹H-NMR and ¹³C-NMR) and by comparison with published data [13-16].

Hesperidin: ¹H-NMR (CD₃OD, 400 MHz) δ(ppm): 6.85 (3H, m, H-2', 5', 6'), 6.11 (2H, brs, H-8, 6), 5.32 (1H, dd, *J* = 12.0, 2.8 Hz, H-2), 4.85 (1H, d, *J* = 7.2 Hz, glucosyl H-1'), 4.60 (1H, d, *J* = 0.8 Hz, rhamnosyl, H-1''), 3.78 (3H, s, OMe-4'), 3.20-3.60 (9H, m, rhamnoglucosyl protons), 3.04 (1H, dd, *J* = 16.4, 12.8 Hz, H-3b), 2.70 (1H, dd, *J* = 17.0, 3.0 Hz, H-3a), 1.10 (3H, d, *J* = 6.4 Hz, rhamnosyl CH₃); ¹³C-NMR (DMSO-*d*₆, 100 MHz) δ(ppm): 196.9 (C-4), 165.0 (C-7), 162.9 (C-5), 162.4 (C-9), 147.9 (C-4'), 146.3 (C-3'), 130.7 (C-1'), 118.0 (C-6'), 114.0 (C-2v), 112.0 (C-5'), 103.3 (C-10), 100.4 (C-1''), 99.4 (C-1'), 96.4 (C-6), 95.5 (C-8), 78.3 (C-2), 76.1 (C-5'), 75.4 (C-3'), 72.9 (C-5''), 72.0 (C-2''), 70.6 (C-4''), 70.2 (C-2'), 69.6 (C-3''), 68.2 (C-4'), 65.9 (C-6'), 55.6 (C-4'-OCH₃), 41.9 (C-3) 17.6 (C-CH₃). [13-14]

Neohesperidin: ¹H-NMR (CD₃OD, 400MHz) δ(ppm): 6.86 (3H, m, H-2', 5', 6'), 6.10 (1H, d, *J* = 2.0 Hz, H-8), 6.06 (1H, d, *J* = 2.4 Hz, H-6), 5.28 (1H, dd, *J* = 12.2, 2.8 Hz, H-2), 5.16 (1H, d, *J* = 1.2 Hz, rhamnosyl, H-1''), 5.01 (1H, d, *J* = 7.6 Hz, glucosyl H-1'), 3.78 (3H, s, OMe-4'), 3.20-3.60 (9H, m, rhamnoglucosyl protons), 3.04 (1H, dd, *J* = 17.2, 12.4 Hz, H-3b), 2.69 (1H, dd, *J* = 17.0, 3.0 Hz, H-3a), 1.20 (3H, d, *J* = 6.0 Hz, rhamnosyl CH₃); ¹³C-NMR (DMSO-*d*₆, 100 MHz) δ(ppm): 196.9 (C-4), 164.7 (C-7), 162.8 (C-5), 162.5 (C-9), 148.0 (C-4'), 146.4 (C-3'), 130.8 (C-1'), 117.9 (C-6'), 114.0 (C-2'), 112.0 (C-

5'), 103.3 (C-10), 100.4 (C-1''), 97.4 (C-1'), 96.2 (C-6), 95.1 (C-8), 78.4 (C-2), 77.0 (C-5'), 76.8 (C-3'), 76.2 (C-5''), 71.8 (C-2''), 70.4 (C-4''), 70.3 (C-2'), 69.5 (C-3''), 68.3 (C-4'), 60.0 (C-6'), 55.6 (C-4'-OCH₃), 42.0 (C-3), 17.9 (C-CH₃). [13-14]

Oxypeucedanin hydrate: ¹H-NMR (CDCl₃, 400 MHz) δ(ppm): 8.17 (1H, d, *J* = 10.0 Hz, H-4), 7.60 (1H, d, *J* = 1.2 Hz, H-10), 7.17 (1H, s, H-8), 6.98 (1H, m, H-11), 6.29 (1H, d, *J* = 9.6 Hz, H-3), 4.53 (1H, dd, *J* = 9.6, 2.4 Hz, H-1'a), 4.44 (1H, dd, *J* = 9.2, 8.4 Hz, H-1'b), 3.91 (1H, dd, *J* = 7.4, 2.6 Hz, H-2'), 1.36 (3H, s, H-4'), 1.31 (3H, s, H-5'); ¹³C-NMR (CDCl₃, 100 MHz) δ(ppm): 161.0 (C-2), 158.1 (C-7), 152.6 (C-5), 148.5 (C-8a), 145.3 (C-10), 138.9 (C-4), 114.3 (C-6), 113.1 (C-3), 107.4 (C-4a), 104.7 (C-11), 94.8 (C-8), 76.5 (C-2'), 74.5 (C-1'), 71.6 (C-3'), 26.6 (C-4'), 25.2 (C-5'). [15]

Limonin: ¹H-NMR (CDCl₃, 400 MHz) δ(ppm): 7.40 (1H, m, H-21), 7.39 (1H, m, H-23), 6.33 (1H, brs, H-22), 5.46 (1H, s, H-17), 4.75 (1H, d, *J* = 12.8 Hz, H-19a), 4.45 (1H, d, *J* = 13.2 Hz, H-19b), 4.02 (2H, brs, H-1, 15), 2.96 (1H, dd, *J* = 16.8, 3.6 Hz, H-2a), 2.85 (1H, dd, *J* = 15.2, 15.2 Hz, H-6a), 2.67 (1H, d, *J* = 16.8 Hz, H-2b), 2.54 (1H, dd, *J* = 12.4, 2.4 Hz, H-9), 2.45 (1H, dd, *J* = 14.4, 2.8 Hz, H-6b), 2.22 (1H, dd, *J* = 15.6, 2.8 Hz, H-5), 1.80 (2H, m, H-11), 1.50 (2H, m, H-12), 1.28 (3H, s, H-28), 1.17 (6H, s, H-18, 29), 1.06 (3H, s, H-30); ¹³C-NMR (CDCl₃, 100 MHz) δ(ppm): 206 (C-7), 169.0 (C-3), 166.6 (C-16), 143.2 (C-23), 141.1 (C-21), 120.0 (C-20), 109.6 (C-22), 80.3 (C-4), 79.1 (C-1), 77.8 (C-17), 65.7 (C-14), 65.3 (C-19), 60.5 (C-5), 53.9 (C-15), 51.3 (C-8), 48.1 (C-9), 46.0 (C-10), 38.0 (C-13), 36.4 (C-6), 35.6 (C-2), 30.8 (C-28), 30.2 (C-12), 21.4 (C-18), 20.7 (C-29), 18.9 (C-11), 17.6 (C-30). [16]

2.4 Cholinesterase Inhibition Assay

The assay was measured by the modified method of Ellman et al. [17] and Ingkaninan et al. [18]. In the 96-well plates, 50 μL of buffer A (50 mM Tris-HCl, pH 8.0), 25 μL of 1.5 mM ATCI (or BTCl) in MilliQ water, 25 μL of sample (1mg/mL) in buffer A, 125 μL of 3 mM DTNB in buffer C (50 mM Tris-HCl, pH 8.0, containing 0.1 M NaCl and 0.02 M MgCl₂·6H₂O), and 25 μL of 1.0 U/mL of enzyme were added and the absorbance was measured the formation of yellow 5-thio-2-nitrobenzoate anion as a result of the reaction of DTNB with thiocholine released by the enzymatic hydrolysis of ATCI (or BTCl) at a wavelength of 415 for 2 min at 5 sec intervals. Each experiment was done in triplicate. The IC₅₀ value was calculated using software package Prism (version 5.01).

3. Results and Discussion

The leaf and root extracts of *C. hystris* were fractionated and isolated pure compounds by chromatography techniques. Two flavanone glycosides namely hesperidin, and neohesperidin, and one furanocoumarin namely oxypeucedanin hydrate were isolated from the butanolic and dichloromethane extracts of *C. hystris* leaves, respectively. The ethyl

acetate extract of *C. hystrix* roots gave one limonoid namely limonin. Limonin was isolated for the first time from *C. hystrix* roots. The chemical structures of all isolated compounds were shown in Figure 1.

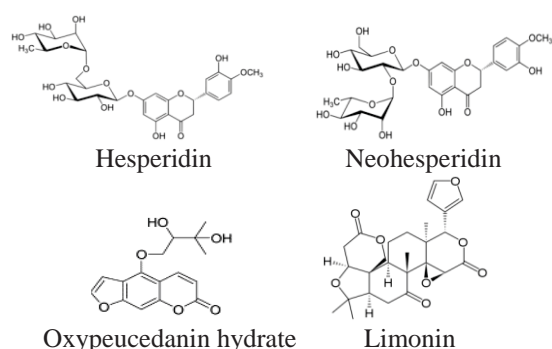


Figure 1. The isolated compounds from *Citrus hystrix*.

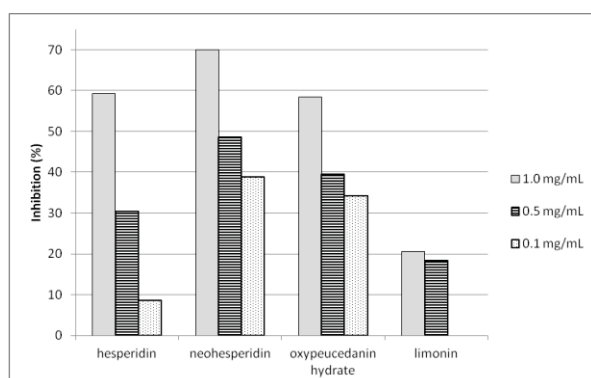


Figure 2. The AChE inhibitory activity of isolated compounds.

All isolated compounds were further evaluated their AChE and BChE inhibitory activities. The results (Figures 2 and 3) indicated that these isolated compounds inhibited both enzymes in dose-dependent manners. Limonin showed low activities against both enzymes. Neohesperidin and oxypeucedanin hydrate showed the highest inhibition towards AChE and BChE, respectively. According to low solubility under assay condition of all isolated compounds, only neohesperidin and oxypeucedanin hydrate were further determined for the IC_{50} values and comparing with those values of standard compound (eserine). The IC_{50} value of neohesperidin towards AChE was 0.16 mM, and that of oxypeucedanin hydrate toward BChE was 0.26 mM. These values were quite high comparing with those of eserine which were 0.73 and 2.54 μ M of AChE and BChE, respectively. Although, isolated compounds from *C. hystrix* showed low to medium anti-cholinesterase activities comparing to eserine, but they were purified from natural plant which is safe for health. Moreover, previous reports indicated that neohesperidin and hesperidin showed the anti-oxidant, anti-viral, anti-allergic, anti-tyrosinase, and anti-bacterial activities [19-23]. Oxypeucedanin hydrate possessed anti-fungal, anti-proliferative, anti-microbial, anti-oxidant, and GABA-transaminase inhibitory activities [24-28]. Thus, these compounds

should be useful for the potential treatment of AD and other diseases, or use as supplement dietary.

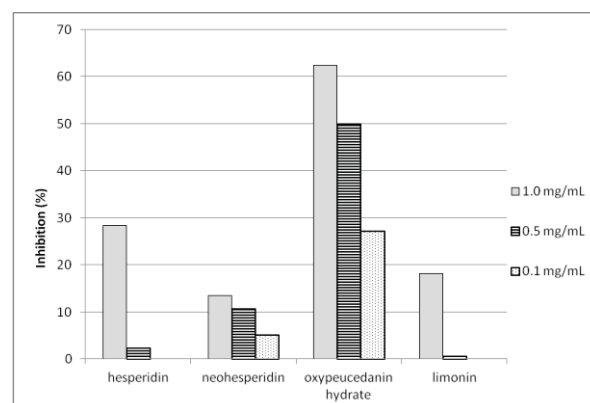


Figure 3. The BChE inhibitory activity of isolated compounds.

4. Conclusions

In summary, hesperidin, neohesperidin and oxypeucedanin hydrate were isolated from the *Citrus hystrix* leaves and limonin obtained from roots of this plant. Limonin was reported for the first time from this plant. All isolated compounds show low to medium anti-cholinesterase activity towards AChE and BChE. The highest active compounds were neohesperidin and oxypeucedanin with the IC_{50} values of 0.16 mM toward AChE, and 0.26 mM toward BChE, respectively.

Acknowledgements

This work was financially supported by the Special Task Force for Activating Research (STAR) from the Centenary Academic Development Project, Chulalongkorn. ST is also grateful to the 90th Anniversary of Chulalongkorn University Fund (Ratchadaphiseksomphot Endowment Fund) for a research fellowship.

References

- [1] M. Goedert and M.G. Spillantini, *Science* **314** (2006) 777-781.
- [2] D.K. Lahiri, M.R. Farlow, N.H. Greig and K. Sambamurti, *Drug Dev. Res.* **56** (2002) 267-281.
- [3] P.T. Francis, A.M. Palmer, M. Snape and G.K. Wilcock, *J. Neurol. Neurosurg. Psychiatry* **66** (1999) 137-147.
- [4] G. Silverstrelli, A. Lanari, L. Parnetti, O. Tomassoni and F. Amenta, *Mech. Ageing Dev.* **127** (2006) 148-157.
- [5] S. Darvesh, D.A. Hopkins and C. Geula, *Nat. Rev. Neurosci.* **4** (2003) 131-138.
- [6] S. Elliott and J. Brimacombe, *J. Ethnopharmacol.* **19** (1987) 285-317.
- [7] A. Murakami, S. Jiawajinda, S. Koshimizu and H. Ohigashi, *Cancer Lett.* **95** (1995) 139-146.
- [8] H. Fortina, C. Vigora, F.L. Dévéhata, V. Robina, B.L. Bossé, J. Boustiea and M. Amorosa, *Fitoterapia* **73** (2002) 346-350.

- [9] A. Murakami, G. Gao, O.K. Kim, M. Omura, M Yano, C. Ito, H. Furukawa, S. Jiwajinda, K. Koshimizu and H. Ohigashi, *J. Agric. Food Chem.* **47** (1999) 333-339.
- [10] K.H. Miean and S. Mohamed, *J. Agric Food Chem.* **49** (2001) 3106-3112.
- [11] K. Ogawa, A. Kawasaki, T. Yoshida, H. Nesumi, M. Nakano, Y. Ikoma and M. Yano, *J. Agric. Food Chem.* **48** (2000) 1763-1769.
- [12] J. Youkwan, S. Sutthivaiyakit and P. Sutthivaiyakit, *J. Nat. Prod.* **73** (2010) 1879-1883.
- [13] F. Maltese, C. Erkelens, F.V.D. Kooy, Y.H. Choi and R. Verpoorte, *Food Chem.* **116** (2009) 575- 579.
- [14] D.Hamdani, M.Z. Elreadi, A. Tahrani, F. Herrmann, D. Kaufmann, N. Farrag, A. El-Shazly and M. Wink, *Food Chem.* **127** (2011) 394-403.
- [15] S. Harkar, T.K. Razdan and E.S. Waight, *Phytochemistry* **23** (1984) 419-426.
- [16] Y.D. Min, H.C. Kwon, M.C. Yang, K.H. Lee, S.U. Choi and K.R. Lee, *Arch. Pharm. Res.* **30** (2007) 58-63.
- [17] G.L. Ellman, K.D. Courtney, V. Andres and R.M. Featherstone, *Biochem. Pharmacol.* **7** (1961) 88-95.
- [18] K. Ingkaninan, P. Temkitthawon, K. Chuenchom, T. Yuyaem and W. Thongnoi, *J. Ethnopharmacol.* **89** (2003) 261-264.
- [19] J. Suarez, M.D. Herrera and E. Marhuenda, *Phytomedicine* **5** (1998) 469-473.
- [20] D.H. Kim, M.J. Song, E.H. Bae and M.J. Han, *Biol. Pharm. Bull.* **23** (2000) 356-358.
- [21] K. Itoh, M. Masuda, S. Naruto, K. Murata and H. Matsuda, *J. Nat. Med.* **63** (2009) 443-450.
- [22] K. Itoh, N. Hirata, M. Masuda, S. Naruto, K. Murata, K. Wakabayashi and H. Matsuda, *Biol. Pharm. Bull.* **32** (2009) 410-415.
- [23] C.G. Alapont, R.G. Domenech, J. Gálvez, M.J. Ros, S. Wolski and M.D. Gracia, *Bioorg. Med. Chem. Lett.* **10** (2000) 2033-2036.
- [24] A. Marston and K. Hostettmann, *J. Nat. Prod.* **58** (1995) 128-130.
- [25] Y.K. Kim, Y.S. Kim and S. Y. Ryu, *Phytother. Res.* **21** (2007) 288-290.
- [26] M.D.J. Dongfack, M.C. Lallemand, V. Kuete, C.D. Mbazon, J.D. Wansi, H.T. Dufat, S. Michel and J. Wandji, *Chem. Pharm. Bull.* **60** (2012) 1072-1075.
- [27] X.L. Piao, I.H. Park, S.H. Baek, H.Y. Kim, M.K. Park and J.H. Park, *J. Ethnopharmacol.* **93** (2004) 243-246.
- [28] S.Y. Choi, E.M. Ahn, M.C. Song, D.W. Kim, J.H. Kang, O.S. Kwon, T.C. Kang and N.I. Baek, *Phytother. Res.* **19** (2005) 839-845.

CHEMICAL CONSTITUENTS FROM THE BRANCHES OF *PARAMERIA BARBATA*

Suphaluck Limpanawisut, Kanok-on Rayanil*

Department of Chemistry, Faculty of Science, Silpakorn University, Sanamchandra Palace Campus,
Nakorn Pathom, Thailand 73000

* Author for correspondence; E-Mail: kanok-on@su.ac.th, Tel. +66-34-255797

Abstract: Plants from the *Parameria* genus (Apocynaceae) have been used as traditional medicines in Indonesia such as antiulcer and antidiarrhea drugs. To date, only *Parameria laevigata* from this genus has been investigated, leading to the isolation of proanthocyanidins which were isolated as dimeric, trimeric and tetrameric forms. The present study, the first phytochemical investigation of the ethanolic extract of branches of *Parameria barbata*, led to the successful isolation of five compounds including friedelin (1), β -sitosterol glucoside (2) and lupeol esters (3-5). The structures were elucidated by spectroscopic analysis, as well as comparison with literature data.

1. Introduction

The apocynaceae comprises more than 150 genus and 1700 species [1]. Some plants in this family have been used as traditional medicine in several countries in Asia, for example, to treat cough and asthma in China [2], and as antidiarrhea, antiulcer and wound-healing agents in Indonesia [3]. They are also used to treat meningitis and fractures in China, Thailand and Burma [4]. Apocynaceous plants are important sources of the terpenoids and indole alkaloids. Several indole alkaloids showed significant activity against several cancer cell lines [2, 4].

Parameria barbata is a woody vine found in Thailand. The plant showed inhibitory activity against NO release from macrophages and antioxidant activity [5]. In the present work, we describe the first isolation of five compounds from the branches of *Parameria barbata*, which were identified as friedelin (1), β -sitosterol glucoside (2) and lupeol esters (3-5).

2. Materials and Methods

2.1 Plant material

The branches of *P. barbata* were collected in January 2011 from Bangkok, Thailand and were identified by Dr. Piya Chalermglin of the Thailand Institute of Scientific and Technological Research. A voucher specimen (SS614/272) was deposited at the Department of Chemistry, Faculty of Science, Silpakorn University, Sanamchandra Palace Campus, Nakorn Pathom, Thailand.

2.2 General Experimental Procedures

Melting points were determined by a Kofler hot stage apparatus and are uncorrected. Optical rotations

were measured on a JASCO P-1010 polarimeter. Infrared spectra (IR) were recorded on a Perkin Elmer GX-FT-IR spectrophotometer. ^1H , ^{13}C , COSY, HMQC and HMBC were recorded in CDCl_3 solutions on a Bruker AVANCE 300 (300 MHz for ^1H -NMR and 75 MHz for ^{13}C -NMR) spectrometer. Chemical shifts are in δ (ppm) with tetramethylsilane (TMS) as an internal standard.

2.2 Extraction and Isolation

The dried branches of *P. barbata* (2.58 kg) were extracted with EtOH at room temperature to give the EtOH extract (217.11 g) which was diluted in water and extracted with hexane, EtOAc and *n*-BuOH, respectively. Each solvent was evaporated under reduced pressure to yield respectively the hexane extract (21.85 g), the EtOAc extract (19.59 g) and the *n*-BuOH extract (19.20 g). The hexane extract was chromatographed over a silica gel column, eluted with a hexane/EtOAc mixture gradient to give sixty-five fractions. Fraction 1 was further separated by silica gel column chromatography using hexane/benzene (10:1) to give subfractions A-D and then subfraction B was purified by prep. TLC using hexane/benzene (10:1) to give an unseparable mixture of lupeol esters **3-5** (56.2 mg). Fraction 5 (34.5 mg) was recrystallized with EtOH to afford friedelin **1** (14.5 mg). The recrystallization of fraction 57-59 in EtOH yielded β -sitosterol glucoside **2** (82.7 mg).

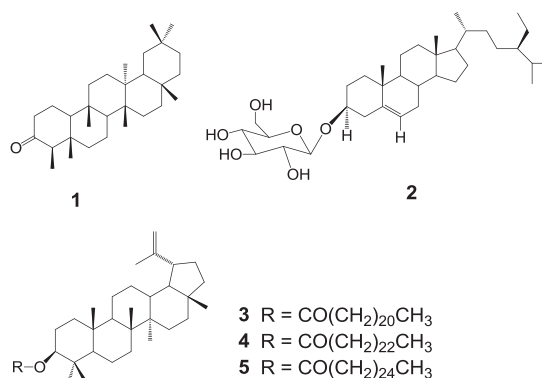


Figure 1. Structure of compounds **1-5** from *P. barbata*

3. Results and Discussion

The hexane extract was purified by silica gel column chromatography and prep. TLC to give five known compounds: friedelin (1), β -sitosterol glucoside (2) and lupeol esters (3-5). The structures of these compounds were elucidated by a combination of 1D and 2D-NMR spectra as well as by comparison with literature data.

Friedelin (1): colorless, crystalline solid; mp 242-244 °C (lit. 260-263 °C); $[\alpha]_D$ -15.1 (c = 0.0522, CHCl_3); IR ν_{max} cm^{-1} : 2919, 2847, 1714, 1454, 1388; ^1H and ^{13}C -NMR data were consistent with literature values [6].

β -sitosterol glucoside (2): white solid; mp 160-162 °C (lit. 160-163 °C); $[\alpha]_D$ -15.1 (c = 0.0329, CHCl_3); IR ν_{max} cm^{-1} : 3368, 2931, 1462, 1367, 1022; ^1H and ^{13}C -NMR data were consistent with literature values [7].

Lupeol esters (3-5): white solid; mp 63-65 °C (lit. 53-57 °C); $[\alpha]_D$ +19.4 (c = 0.0416, CHCl_3); IR ν_{max} cm^{-1} : 2920, 2849, 1728, 1467, 1380, 1171, 1113, 977, 882; MS m/z 771.6947, 799.7221, 827.7469 $[\text{M}+\text{Na}]^+$ (calcd for $\text{C}_{52}\text{H}_{92}\text{O}_2$ 748.7097, $\text{C}_{54}\text{H}_{96}\text{O}_2$ 776.7410, $\text{C}_{56}\text{H}_{100}\text{O}_2$ 804.7723); ^1H and ^{13}C -NMR data were consistent with literature values [8].

4. Conclusions

The phytochemical investigation of *Parameria barbata* led to the isolation of friedelin (1), β -sitosterol glucoside (2) and lupeol esters (3-5) for the first time from the genus *Parameria* and they have been shown to have significant biological activities. Friedelin showed soybean lipoxygenase (SBL) inhibitory [9], anti-inflammatory [10], antibacterial and anticandidal activities [11]. β -sitosterol glucoside had potent mosquitocidal activity against adult *Aedes aegypti* [12] and also spasmolytic activity [13]. The lupeol ester was reported as an antihepatotoxic agent [14].

Acknowledgements

The authors are grateful to the Department of Chemistry, Faculty of Science, Silpakorn University for financial support.

References

- [1] T. Aniszewski, Alkaloid Chemistry, Biological Significance, Applications, 2007 pp. 13-16.
- [2] L.-S. Gan, S.-P. Yang, Y. Wu, J. Ding, J.-M. Yue, Terpenoid indole alkaloids from *Winchia calophylla*, *J. Nat. Prod.*, **69** (2006) 18-22.
- [3] K. Kamiya, C. Watanabe, H. Endang, M. Umar, T. Satake, Studies on the constituents of bark of *Parameria laevigata* Moldenke, *Chem. Pharm. Bull.*, **49** (2001) 551-557.
- [4] T. Feng, X.-H. Cai, Y.-P. Liu, Y. Li, Y.-Y. Wang, X.-D. Luo, Melodininines A-G, monoterpenoid indole alkaloids from *Melodinus henryi*, *J. Nat. Prod.*, **73** (2010) 22-26.
- [5] E.-M. Choi, J.-K. Hwang, Screening of Indonesian medicinal plants for inhibitor activity on nitric oxide

- production of RAW264.7 cells and antioxidant activity, *Fitoterapia* **76** (2005) 194-203.
- [6] J. Klass, W.F. Tinto, Friedelane triterpenoids from *Perzassa Compta*: complete ^1H and ^{13}C assignments by 2D NMR spectroscopy, *J. Nat. Prod.*, **55** (1992) 1626-1630.
 - [7] J. Sakakibara, T. Kaiya, H. Fukuda, T. Ohki, 6 β -hydroxyursolic acid and other triterpenoids of *Enkianthus cernuus*, *Phytochemistry*, **22** (1983) 2553-2555.
 - [8] H. Tomosaka, H. Koshino, T. Tajika, S. Omata, Lupeol esters from the twig bark of Japanese pear (*Pyrus serotina* Rehd.) cv. Shinko, *Biosci. Biotechnol. Biochem.*, **65** (2001) 1198-1201.
 - [9] R. Kumaria, A. Meyyappanb, P. Selvamani, J. Mukherjeeb, P. Jaisankar, Lipoxygenase inhibitory activity of crude bark extracts and isolated compounds from *Commiphora berryi*, *J. Ethnopharmacol.*, **138** (2011) 256-259.
 - [10] M. Shimizu, T. Tomoo, Constituents and anti-inflammatory effect of Aoki, *Aucuba japonica* Thunb., *Biol. Pharm. Bull.*, **17** (1994) 665-667.
 - [11] V. Kuete, J.R. Nguemaving, V.e.P. Benga, A.G.B. Azebaze, F.o.-X. Etoa, M.e. Meyer, B. Bodod, A.E. Nkengfack, Antimicrobial activity of the methanolic extracts and compounds from *Vismia laurentii* De Wild (Guttiferae), *J. Ethnopharmacol.*, **109** (2007) 372-379.
 - [12] E. Amin, M.M. Radwan, S.S. El-Hawary, M.M. Fathy, R. Mohammed, J.J. Becnel, I. Khan, Potent Insecticidal Secondary Metabolites from the Medicinal Plant *Acanthus montanus*, *Rec. Nat. Prod.*, **6** (2012) 301-305.
 - [13] M.M. Al-Oqail, A.J. Al-Rehaily, W.H.B. Hassan, T.A. Ibrahim, M.S. Ahmad, S.S. Ebada, P. Proksch, New flavonol glycosides from *Barbeya oleoides* Schweinfurth, *Food Chemistry*, **132** (2012) 2081-2088.
 - [14] C.-N. Lin, W.-P. Tom, Antihepatotoxic principles of *Sambucus formosana*, *Planta Med.*, **54** (1988) 223-224.

SYNTHESES OF PIPERAZINE-2,5-DIONE DERIVATIVES

Cholthicha Prempre, Kanok-on Rayanil*

Department of Chemistry, Faculty of Science, Silpakorn University, Nakorn Pathom 73000, Thailand

* Author for correspondence; E-Mail: kanok-on@su.ac.th, Tel. +66 34255797

Abstract: The piperazine-2,5-dione moiety is an active functionality in several drugs and natural products. Pharmaceutical studies of several piperazine-2,5-dione derivatives have shown that they possess anti-inflammatory activity. Herein we report the syntheses of piperazine-2,5-dione derivatives by varying the C-3 benzene substituents in order to evaluate their biological activities. The syntheses of piperazine-2,5-dione derivatives were completed in four steps with 59% overall yield from glycine anhydride using the aldol condensation reaction as a key step.

1. Introduction

Piperazine-2,5-dione derivatives continue to be attractive synthetic targets for organic chemists since many natural products containing piperazine-2,5-dione in their structures have been shown to have a wide range of biological activities. Plinabulin, a synthetic analog of a natural product isolated from *Aspergillus* sp., has been evaluated as an anti-cancer drug in Phase II clinical trials in four countries [1,2]. XR5118, a synthetic compound based on a natural product lead, inhibits plasminogen activator inhibitors-1 with an IC_{50} value of 0.2 μ M [3] (Figure 1.). Albonoursin, isolated from an actinomycete strain, *Micromonospora* sp. IM 2670 [4], shows strong inhibition on the growth of transplantable solid tumors in mice (Figure 1). In addition, piperazine-2,5-dione derivatives have also been reported as potential therapeutic agents with antibiotic and anti-cancer activities [5]. According to the literature, most of the piperazine-2,5-dione natural products have been isolated from culture filtrates of *Streptomyces* species [6,7], including lansa A-D, which were isolated in our laboratory from *Streptomyces* sp. SUC1, an endophyte on the aerial roots of *Ficus benjamina*. Pharmaceutical studies of the isolates revealed that lansa D showed significant anti-inflammatory activity [8]. In this paper, we describe syntheses of lansa D derivatives by varying the C-3 benzene substituents in order to evaluate their anti-inflammatory activity (Figure 1).

2. Materials and methods

2.1 General methods

All melting points were measured with a Kofler hot stage apparatus and are uncorrected. Infrared spectra were recorded on a Perkin Elmer GX FT-IR spectrophotometer. 1H -NMR and ^{13}C -NMR spectra were obtained on a Bruker AVANCE (300 MHz) spectrometers, with tetramethylsilane (TMS) as an internal standard.

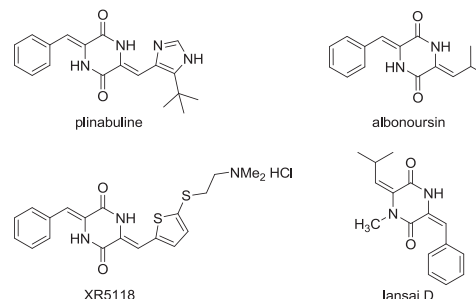


Figure 1. Structure of piperazine-2,5-dione derivatives

2.2 Chemistry

1,4-Diacetylpiperazine-2,5-dione (2) [3,9]. A mixture of glycine anhydride (10.20 g, 89.40 mmol) in acetic anhydride (44.97 ml) was stirred under reflux for 7 hours. The acetic anhydride was removed by azeotropic distillation with methanol and toluene under reduced pressure. The residue was crystallized from ethyl acetate-ether to yield **2** as a colorless solid (91%), mp 98-100 °C. IR (KBr) cm^{-1} : 1727, 1705, 1364, 1265, 1185. 1H NMR ($CDCl_3$) δ : 2.58 (6H, s, 2xAc), 4.60 (4H, s, 2xCH₂). ^{13}C NMR ($CDCl_3$) δ : 26.8, 47.2, 165.9, 170.8.

4-Acetyl-6-isobutylidene-piperazine-2,5-dione (3) [9-11]. Compound **2** (5.19 g, 26.19 mmol) was dissolved in DMF (61.76 ml) under argon. To this solution was added dropwise isobutylaldehyde (11.47 ml) and 0.5 N potassium *tert*-butoxide (3.46 g, 30.86 mmol) in *tert*-butanol (61.76 ml) over 20 minutes at 0 °C. After the pale yellow solution had been stirred at room temperature for 6 hours, it was neutralized with 30% acetic acid and poured into water. The product was extracted with CH_2Cl_2 , dried over anhydrous sodium sulfate, and concentrated in vacuum to give a crude yellow syrup, which was purified on a column of silica gel (hexane-ethyl acetate 2:1) to yield **3** as colorless crystals (99%), mp 151-153 °C. IR (KBr) cm^{-1} : 3192, 1687, 1650, 1635, 1360, 1142. 1H NMR ($CDCl_3$) δ : 1.10 (6H, d, J = 6.6 Hz, 2xCH₃), 2.60 (3H, s, N-Ac), 2.80 (1H, m, CH-Me₂), 4.42 (2H, s, CH₂), 6.18 (1H, d, J = 10.2 Hz, CH), 9.81 (1H, s, N-H). ^{13}C NMR ($CDCl_3$) δ : 22.0, 25.8, 27.1, 46.0, 132.0, 124.6, 160.3, 164.7, 172.7.

1-Methyl-4-acetyl-6-isobutylidene-piperazine-2,5-dione (4) [12]. To a suspension of 60% sodium hydride (1.21 g, 30.21 mmol) in dry DMF (143.70 ml) was added a solution of compound **3** (5.28 g, 25.14 mmol) in dry DMF (25.20 ml) with stirring at 0 °C. Stirring was continued at this temperature for 30 min and methyl iodide (3.14 ml, 50.34 mmol) was added

dropwise, and the solution was stirred for 2 hours at 0 °C, then kept at room temperature overnight, neutralized with 30% acetic acid, poured into ice-water, and then extracted with CH₂Cl₂. Usual work-up of the extract gave a crude syrup which was purified on a column of silica gel (hexane-ethyl acetate 2:1) to yield **4** as a colorless syrup (84%), IR (neat) cm⁻¹: 2968, 1709, 1639, 1429, 1357, 1279, 1202, 1139. ¹H NMR (CDCl₃) δ: 1.15 (6H, d, *J* = 6.6 Hz, 2xCH₃), 2.57 (3H, s, N-Ac), 2.80 (1H, m, CH-Me₂), 3.27 (3H, s, N-CH₃), 4.39 (2H, s, CH₂), 6.16 (1H, d, *J* = 10.5 Hz, CH). ¹³C NMR (CDCl₃) δ: 23.0, 26.6, 27.1, 34.9, 45.7, 131.1, 137.0, 164.0, 164.8, 171.5.

1-Methyl-3-benzylidene-6-isobutylidene-piperazine-2,5-dione (5a) [13]. Compound **4** (0.82 g, 3.66 mmol) was dissolved in DMF (7.32 ml) under argon. To this solution was added dropwise benzaldehyde (0.37 ml, 3.66 mmol) and 0.5 N potassium *tert*-butoxide (0.62 g, 5.49 mmol) in *tert*-butanol (10.98 ml) over 20 minutes at 0 °C. After the pale yellow solution had been stirred at room temperature for 6 hours, it was neutralized with 30% acetic acid and poured into water. The product was extracted with CH₂Cl₂, dried over anhydrous sodium sulfate, and concentrated in vacuum to give a crude syrup, which was purified on a column of silica gel (hexane-ethyl acetate 2:1) to yield **5a** as a white solid (42%), mp 131-133 °C. IR (KBr) cm⁻¹: 3170, 3027, 2966, 1688, 1620, 1402, 1366, 1098. ¹H NMR (CDCl₃) δ: 1.12 (6H, d, *J* = 6.6 Hz, 2xCH₃), 2.95 (1H, m, CH-Me₂), 3.43 (3H, s, N-CH₃), 6.06 (1H, d, *J* = 11.1 Hz, CH), 7.01 (1H, s, CH), 7.42 (5H, m, Ph-H), 8.19 (1H, br s, N-H). ¹³C NMR (CDCl₃) δ: 23.1, 27.4, 35.6, 116.6, 125.9, 127.5, 128.5, 129.4, 131.7, 132.9, 133.1, 159.1, 159.8.

1-Methyl-3-(2-methoxy-3,4-methylenedioxybenzylidene)-6-isobutylidene-piperazine-2,5-dione (6). By the same procedure used to prepare compound **5**, compound **6** was obtained in 29% yield as a yellow solid, mp 141-143 °C. IR (KBr) cm⁻¹: 3343, 2965, 1689, 1619, 1470, 1392, 1350, 1077, 1050. ¹H NMR (CDCl₃) δ: 1.12 (6H, d, *J* = 6.6 Hz, 2xCH₃), 2.94 (1H, m, CH-Me₂), 3.42 (3H, s, N-CH₃), 4.02 (3H, s, OCH₃), 6.09 (1H, d, *J* = 13.8 Hz, CH), 6.07 (2H, s, OCH₂O), 6.60 (1H, d, *J* = 7.8 Hz, CH), 6.80 (1H, d, *J* = 13.5 Hz, CH), 6.91 (1H, s, CH), 8.61 (1H, br s, N-H). ¹³C NMR (CDCl₃) δ: 23.1, 27.3, 35.5, 60.4, 101.6, 103.9, 113.7, 119.7, 124.5, 128.9, 131.1, 140.8, 150.1, 159.5.

1-Methyl-3-(4-benzoyloxy-3-methoxybenzylidene)-6-isobutylidene-piperazine-2,5-dione (7). By the same procedure used to prepare compound **5**, compound **7** was obtained in 36% yield as a yellow solid, mp 146-147 °C. IR (KBr) cm⁻¹: 3247, 2972, 1689, 1632, 1516, 1351, 1142, 1035. ¹H NMR (CDCl₃) δ: 1.13 (6H, d, *J* = 6.6 Hz, 2xCH₃), 2.94 (1H, m, CH-Me₂), 3.42 (3H, s, N-CH₃), 3.89 (3H, s, OCH₃), 5.17 (2H, s, CH₂), 6.06 (1H, d, *J* = 11.1 Hz, CH), 6.89 (1H, d, *J* = 9.6 Hz, CH), 6.93 (1H, d, *J* = 9.6 Hz, CH), 6.94 (1H, s, CH), 7.34 (5H, m, Ph-H), 8.07 (1H, br s, N-H). ¹³C NMR (CDCl₃) δ: 23.1, 27.4, 35.5, 56.1, 70.9, 112.5, 114.2, 116.5, 120.9, 124.9, 126.2, 126.9,

128.0, 128.6, 128.7, 131.5, 136.6, 148.6, 150.2, 159.3, 159.7.

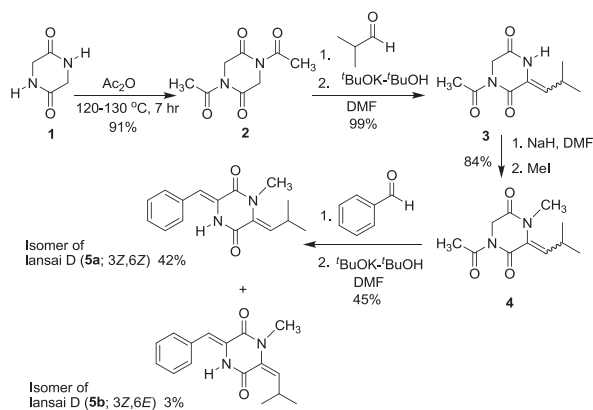
1-Methyl-3-(2-bromo-5,6-dimethoxybenzylidene)-6-isobutylidene-piperazine-2,5-dione (8). By the same procedure used to prepare compound **5**, compound **8** was obtained in 31% yield as a yellow syrup. IR (KBr) cm⁻¹: 3269, 2966, 1687, 1632, 1468, 1391, 1361, 1297, 1081, 1003. ¹H NMR (CDCl₃) δ: 1.12 (6H, d, *J* = 6.6 Hz, 2xCH₃), 2.94 (1H, m, CH-Me₂), 3.45 (3H, s, N-CH₃), 3.76 (3H, s, OCH₃), 3.89 (3H, s, OCH₃), 6.06 (1H, d, *J* = 11.4 Hz, CH), 6.83 (1H, d, *J* = 8.7 Hz, CH), 6.95 (1H, s, CH), 7.36 (1H, d, *J* = 8.7 Hz, CH), 8.41 (1H, br s, N-H). ¹³C NMR (CDCl₃) δ: 23.0, 27.4, 35.6, 56.1, 61.5, 112.6, 113.5, 115.2, 127.1, 127.8, 131.8, 146.6, 152.6, 159.2, 159.5.

1-Methyl-3-(3-bromo-5,6-dimethoxybenzylidene)-6-isobutylidene-piperazine-2,5-dione (9). By the same procedure used to prepare compound **5**, compound **9** was obtained in 39% yield as a yellow solid syrup. IR (KBr) cm⁻¹: 3227, 2966, 1686, 1630, 1478, 1392, 1352, 1302, 1270, 1230, 1105, 993. ¹H NMR (CDCl₃) δ: 1.13 (6H, d, *J* = 6.6 Hz, 2xCH₃), 2.95 (1H, m, CH-Me₂), 3.44 (3H, s, N-CH₃), 3.78 (3H, s, OCH₃), 3.89 (3H, s, OCH₃), 6.05 (1H, d, *J* = 11.1 Hz, CH), 6.82 (1H, s, CH), 7.03 (2H, d, *J* = 9.9 Hz, 2xCH), 9.04 (1H, br s, N-H). ¹³C NMR (CDCl₃) δ: 23.1, 27.3, 35.5, 56.2, 61.3, 111.3, 116.7, 117.0, 124.9, 127.5, 129.1, 131.5, 145.3, 153.8, 159.0, 159.4.

1-Methyl-3-(2-bromo-4,5-methylenedioxybenzylidene)-6-isobutylidene-piperazine-2,5-dione (10). By the same procedure used to prepare compound **5**, compound **10** was obtained in 35% yield as a yellow syrup. IR (KBr) cm⁻¹: 3193, 2967, 1683, 1628, 1479, 1392, 1354, 1243, 1151, 1120, 1093, 1038. ¹H NMR (CDCl₃) δ: 1.13 (6H, d, *J* = 6.6 Hz, 2xCH₃), 2.96 (1H, m, CH-Me₂), 3.43 (3H, s, N-CH₃), 6.07 (1H, d, *J* = 9.0 Hz, CH), 6.04 (2H, s, OCH₂O), 6.85 (1H, s, CH), 6.93 (1H, s, CH), 7.08 (1H, s, CH), 8.27 (1H, br s, N-H). ¹³C NMR (CDCl₃) δ: 23.1, 27.4, 35.5, 102.4, 108.8, 113.6, 116.0, 126.1, 126.5, 128.4, 131.7, 147.7, 148.7, 158.6, 159.7.

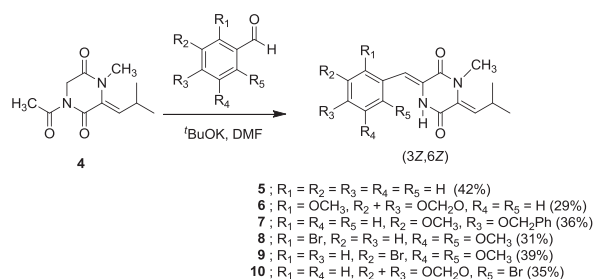
3. Results and Discussion

The syntheses of piperazine-2,5-dione derivatives were carried out with the condensation of glycine anhydride (**1**) and acetic anhydride to afford 1,4-diacetylpiperazine-2,5-dione (**2**, 91% yield). Condensation of **2** with isobutylaldehyde gave 4-acetyl-6-isobutylidene-piperazine-2,5-dione (**3**, 99% yield). Methylation of **3** with iodomethane provided 1-methyl-4-acetyl-6-isobutylidene-piperazine-2,5-dione (**4**) in 84% yield. Finally, the aldol condensation of **4** with benzaldehyde furnished the piperazine-2,5-dione derivatives (**5a** and **5b**) in 45% yield (Scheme 1.).



Scheme 1.

A number lansai D derivatives with different aryl groups on C-3 (**6-10**) were prepared in a similar manner using different aromatic aldehydes (Scheme 2).



Scheme 2.

4. Conclusions

The first syntheses of the lansai D derivatives (**6-10**) were prepared in four steps from glycine anhydride by using the aldol condensation reaction as a key step. The synthetic molecules will be evaluated for anti-inflammatory activity. Further results will be reported in due course.

Acknowledgements

Financial supports provided by the Department of Chemistry, Faculty of Science, Silpakorn University are gratefully acknowledged.

References

- [1] Y. Yamazaki, M. Sumikura, K. Hidaka, H. Yasui, Y. Kiso, F. Yakushiji and Y. Hayashi, *Bioorg. Med. Chem. Lett.* **18** (2010) 3169-3174.
- [2] B. Nicholson, G. K. Lloyd, B. R. Miller, M. A. Palladino, Y. Kiso, Y. Hayashi and S. T. C. Neuteboom, *Anti-Cancer Drugs*, **17** (2006) 25-31.
- [3] A. Folks, M. Roe, S. Sohal, J. Golec, R. Faint, T. Brooks and P. Charlton, *Bioorg. Med. Chem. Lett.* **11** (2001) 2589-2592.
- [4] H. Wang, S. Yeo, J. Xu, X. Xu, H. He, F. Ronca, E. Anthony, T. Wang, V. Yu and M. Sim, *J. Nat. Prod.* **65** (2002) 721-724.
- [5] W. Loughlin, R. Marshall R, A. Carreiro and K. Elson, *Bioorg. Med. Chem. Lett.* **10** (2000) 91-94.

- [6] C. Gallina and A. Liberatori, *Tetrahedron* **30** (1974) 667-673.
- [7] D. Villemain and A. Alloum, *Synthetic Commun.* **20** (1990) 3325-3331.
- [8] P. Tuntiwachwuttikul, T. Taechowisan and S. Thadaniti, *Tetrahedron* **64** (2008) 7583-7586.
- [9] A. Kubo, N. Saito, H. Yamato and Y. Kawakami, *Chem. Pharm. Bull.* **35** (1987) 2525-2532.
- [10] C. Shin, Y. Yonezawa and H. Ohno, *Agric. Biol. Chem.* **51** (1987) 2033-2034.
- [11] M. Yamaura, T. Suzuki, H. Hashimoto, J. Yoshimura, T. Okamoto and C. Shin, *Bull. Chem. Soc. Jpn.* **58** (1985) 1413-1420.
- [12] K. Hari, R. Santhapuram, A. Datta, E. Oliver, I. Gunda and J. Georg, *J. Org. Chem.* **73** (2008) 4705-4708.
- [13] S. Shin, *Jpn. Kokai Tokkyo Koho* (1989) JP 01013075 A 19890117.

CHOLINESTERASE INHIBITORS FROM FRUITS OF THAI BITTER GOURD *MOMORDICA CHARANTIA* L.

Wichuta Kuanhut, Pattara Sawasdee*

Natural Products Research Unit, Department of Chemistry, Faculty of Science, Chulalongkorn University, Bangkok, 10330 Thailand

* Author for correspondence; E-Mail: pattara.T@chula.ac.th, Tel. +66 22187624, Fax. +66 22 187598

Abstract: *Momordica charantia* L. or Thai bitter gourd is an edible plant and a folk medicine in Asia. Extracts of this plant have been widely reported to possess anti-cancer, anti-oxidant, anti-HIV and antidiabetic activities. However, there are no reports presented the cholinesterase inhibitory activity of this plant. The present study was to investigate the chemical constituents of the fruits of Thai bitter gourd with fractionating bio-assay guided. The dichloromethane extract led to the isolation of four cucurbitane-type triterpenes (23*E*)-5 β ,19-epoxy-19-methoxycucurbita-6,23,25-trien-3 β -ol (1), charantadiol A (2), (23*E*)-5 β ,19-epoxycucurbita-6,23-diene-3 β ,25-diol (3) and 5 β ,19-epoxy-25-methoxycucurbita-6,23-diene-3 β ,19-diol (4). In addition, momordicoside K (5) was obtained from the butanolic extract. Compounds 3 and 4 showed the most potent acetylcholinesterase and butyrylcholinesterase inhibitory activities. The minimal amount of compound 4 to inhibit acetylcholinesterase and butyrylcholinesterase was 0.125 and 0.0313 μ g, respectively, whereas that of compound 3 to inhibit both enzymes was 0.0625 μ g by TLC-bioautographic method.

1. Introduction

Momordica charantia L. or Thai bitter gourd, belonging to Cucurbitaceae family, is an edible plant and a folk medicine in Asia. Extracts of this plant have been reported to possess anti-cancer, anti-oxidant, anti-diabetic, anti-inflammatory, anti-viral and cholesterol lowering effects [1]. Phytochemical studies of fruits and seeds of *M. charantia* have resulted in the isolation of triterpenes, proteins, steroids, glycosides, saponins and alkaloids [2]. Charantin, a sterol glucoside mixture, is isolated from immature fruits and have significant anti-diabetic property [3]. Moreover, MRK29 proteins isolated from the ripe fruit and seeds possess a human immunodeficiency virus (HIV) inhibitory activity [4]. Triterpenoid kuguacin J induces apoptosis on a cancer cell line such as a human cervical carcinoma and an androgen-dependent human prostate cancer cell lines [5-6]. In addition, phenolic compounds show potential antioxidant activity [7] and several triterpenoid glycosides inhibit moderate α -glucosidase enzyme [8]. However, there are no reports presented the cholinesterase inhibitory activity of this plant.

Our interest in this plant was raised when preliminary anti-cholinesterase screening of *M. charantia* extract by the TLC-autobiography assay showed high activities against acetylcholinesterase (AChE) and butyrylcholinesterase (BChE). These

enzymes hydrolyze acetylcholine which is cholinergic neurotransmission in the brain. One causal Alzheimer's disease (AD) is the decline of acetylcholine levels that take the poor cognitive performance in patients. Therefore, one therapeutic approach of them is the using of cholinesterase inhibitors for the increasing of the acetylcholine level in the brain [9]. Herein, the present study was to investigate the constituents of *M. charantia* fruits and determine their anti-cholinesterase activity.

2. Materials and Methods

2.1 Materials and reagents

The fruits of *M. charantia* were collected from Phetchaburi Province, Thailand, in January, 2011 and identified by Assoc. Prof. Nijisiri Ruangrunsi, Faculty of Pharmaceutical Sciences, Chulalongkorn University. A voucher specimen (No. NPRU 0003) has been deposited in the Natural Products Research Unit, Department of Chemistry, Faculty of Science, Chulalongkorn University, Thailand.

Acetylthiocholine iodide (ATCI), butyrylthiocholine iodide (BTCI), 5,5'-dithiobis(2-nitrobenzoic acid) (DTNB), acetylcholinesterase (AChE) from electric eels (type VI-S, EC 3.1.1.7), butyrylcholinesterase (BChE) from horse serum (EC 3.1.1.8) and eserine (standard compound) were obtained from Sigma-Aldrich Co.Ltd.

2.2 Extraction and isolation

The air-dried fruits of *M. charantia* (2.5 kg) were extracted three times with MeOH and then concentrated in vacuo to give MeOH extract. This extract was partitioned subsequently with *n*-hexane, CH₂Cl₂ and saturated BuOH to yield *n*-hexane (18.8 g), CH₂Cl₂ (102.9 g) and BuOH (54.7 g) extracts, respectively.

A portion of CH₂Cl₂ extract (83.9 g) was subjected to a silica gel column using an increasingly polarity of *n*-hexane and EtOAc followed by EtOAc and MeOH, respectively, to give eight fractions (MD1–MD8). Fraction MD2 was separated by using a silica gel column and eluted with a gradient system of *n*-hexane-EtOAc and then EtOAc-MeOH to give six sub-fractions (MD2.1-MD2.6). Recrystallization of fraction MD2.1 using MeOH afforded (23*E*)-5 β ,19-

epoxy-19-methoxycucurbita-6,23,25-trien-3 β -ol (**1**, 45.5 mg). Fraction MD2.3 was further isolated by using a silica gel column using a mixture system of *n*-hexane:acetone (9:1) as eluent to afford charantadiol A (**2**, 31.7 mg). In the same way, (23*E*)-5 β ,19-epoxycucurbita-6,23-diene-3 β ,25-diol (**3**, 96.2 mg) and 5 β ,19-epoxy-25-methoxy-cucurbita-6,23-diene-3 β ,19-diol (**4**, 145.3 mg) were successively obtained from fraction MD2.4.

The BuOH extract (53.5 g) was subjected to a Diaion HP-20 column and eluted with H₂O, MeOH and acetone, respectively. The MeOH residue (53.5 g) was applied to vacuum silica gel column chromatography (VCC) and eluted with a stepwise gradient of *n*-hexane-EtOAc and then EtOAc-MeOH to give seven fractions (MB1-MB7). Fraction MB1 was further fractionated by a silica gel column a stepwise system of CH₂Cl₂:acetone (50:1, 20:1, 15:1, 5:1) and CH₂Cl₂:acetone:H₂O (1:5:0.5) to afford six sub-fractions (MB1.1-MB1.6). Fraction MB1.4 was further separated on a Sephadex LH-20 column using 50% of CHCl₃ in MeOH as eluent and then submitted to purify over a silica gel column eluting with a gradient system of CH₂Cl₂:acetone to obtain momordicoside K (**5**, 28.5 mg).

(23*E*)-5 β ,19-epoxy-19-methoxycucurbita-6,23,25-trien-3 β -ol (**1**) : ¹H NMR (CDCl₃, 400 MHz) δ 6.12 (1H, d, *J* = 15.6 Hz, H-24), 5.99 (1H, dd, *J* = 9.6, 1.6 Hz, H-6), 5.64 (1H, br d, *J* = 15.2 Hz, H-23), 5.63 (1H, dd, *J* = 9.2, 2.8 Hz, H-7), 4.86 (2H, s, H-26), 4.65 (1H, s, H-19), 3.44 (3H, s, 19-OCH₃), 3.41 (1H, br s, H-3), 2.89 (1H, br s, H-8), 2.40 (1H, t, *J* = 8.4 Hz, H-10), 1.83 (3H, s, H-27), 1.33-2.22 (methine and methylene protons), 1.22 (3H, s, H-29), 0.89 (3H, d, *J* = 6.4 Hz, H-21), 0.87 (3H, s, H-18), 0.85 (6H, s, H-28 and H-30) ; ¹³C NMR (CDCl₃, 100 MHz) δ 142.2 (C-25), 134.2 (C-24), 132.8 (C-7), 131.0 (C-6), 129.3 (C-23), 114.1 (C-26), 112.1 (C-19), 86.8 (C-5), 76.2 (C-3), 58.2 (19-OCH₃), 50.3 (C-17), 48.3 (C-14), 48.0 (C-9), 45.1 (C-13), 41.7 (C-8), 40.5 (C-10), 39.8 (C-22), 37.3 (C-4), 36.6 (C-20), 33.5 (C-15), 30.6 (C-12), 28.1 (C-16), 27.2 (C-2), 24.1 (C-28), 23.2 (C-11), 20.5 (C-29), 19.8 (C-30), 18.8 (C-21), 18.7 (C-27), 17.4 (C-1), 14.7 (C-18) [10].

Charantadiol A (**2**) : ¹H NMR (CDCl₃, 400 MHz) δ 6.12 (1H, d, *J* = 16.4, H-24), 6.09 (1H, dd, *J* = 2.0, 10.4 Hz, H-6), 5.61 (1H, dd, *J* = 8.4, 15.6 Hz, H-23), 5.56 (1H, dd, *J* = 3.6, 9.6 Hz, H-7), 5.30 (1H, s, H-19), 4.86 (2H, s, H-26), 3.41 (1H, br s, H-3), 2.84 (1H, br s, H-8), 2.47 (1H, t, *J* = 8.8 Hz, H-10), 1.83 (3H, s, H-27), 1.23-2.29 (methine and methylene protons), 1.21 (3H, s, H-29), 0.90 (3H, d, *J* = 6.4 Hz, H-21), 0.89 (3H, s, H-28), 0.88 (3H, s, H-18), 0.85 (3H, s, H-30) ; ¹³C NMR (CDCl₃, 100 MHz) δ 142.2 (C-25), 134.2 (C-24), 133.0 (C-6), 130.4 (C-7), 129.2 (C-23), 114.1 (C-26), 107.5 (C-19), 86.6 (C-5), 76.3 (C-3), 50.4 (C-8), 50.3 (C-17), 49.7 (C-9), 48.1 (C-14), 45.2 (C-13), 39.8 (C-22), 38.0 (C-10), 37.2 (C-4), 36.6 (C-20), 33.5 (C-15), 28.1 (C-16), 27.9 (C-12), 24.4 (C-11), 24.0 (C-28), 21.6 (C-2), 20.6 (C-29), 20.0 (C-30), 18.8 (C-21), 18.7 (C-27), 17.0 (C-1), 15.0 (C-18) [11].

(23*E*)-5 β ,19-epoxycucurbita-6,23-diene-3 β ,25-diol (**3**) : ¹H NMR (CDCl₃, 400 MHz) δ 6.03 (1H, dd, *J* = 1.6, 9.6 Hz, H-6), 5.63 (1H, dd, *J* = 3.6, 9.6 Hz, H-7), 5.59 (2H, m, H-23 and H-24), 4.01 (1H, br s, 3-OH), 3.66 and 3.51 (2H, d, *J* = 8.4 Hz, H-19), 3.40 (1H, br s, H-3), 2.33 (1H, br s, H-8), 2.27 (1H, dd, *J* = 6.8, 11.2, H-10), 1.35-2.19 (methine and methylene protons), 1.31 (6H, s, H-26 and H-27), 1.19 s (3H, s, H-28), 0.89 (3H, s, H-29), 0.88 (3H, d, *J* = 6.8 Hz, H-21), 0.86 (6H, s, H-18 and H-30) ; ¹³C NMR (CDCl₃, 100 MHz) δ 139.6 (C-24), 131.8 (C-6), 131.5 (C-7), 125.2 (C-23), 87.5 (C-5), 79.9 (C-19), 76.2 (C-3), 70.7 (C-25), 52.0 (C-8), 50.0 (C-17), 48.6 (C-14), 45.5 (C-13), 45.3 (C-9), 39.1 (C-22), 38.9 (C-10), 37.2 (C-4), 36.2 (C-20), 33.2 (C-15), 30.8 (C-12), 30.0 (C-26), 29.9 (C-27), 28.0 (C-16), 27.4 (C-2), 24.6 (C-29), 23.6 (C-11), 20.5 (C-28), 20.0 (C-30), 18.6 (C-21), 17.6 (C-1), 14.9 (C-18) [12].

5 β ,19-epoxy-25-methoxy-cucurbita-6,23-diene-3 β ,19-diol (**4**) : ¹H NMR (CDCl₃, 400 MHz) δ 6.08 (1H, d, *J* = 10.0 Hz, H-6), 5.66 (1H, dd, *J* = 3.2, 9.6 Hz, H-7), 5.50 (1H, m, H-23), 5.40 (1H, d, *J* = 15.6 Hz, H-24), 5.13 (1H, s, H-19), 3.79 (1H, s, 19-OH), 3.40 (1H, br s, H-3), 3.15 (3H, s, 25-OMe), 2.84 (1H, br s, H-8), 2.46 (1H, br t, *J* = 8.8, H-10), 1.31-2.22 (methine and methylene protons), 1.25 (3H, s, H-26 and H-27), 1.21 (3H, s, H-28), 0.89 (3H, s, H-29), 0.86 (3H, s, H-18), 0.85 (3H, s, H-30) ; ¹³C NMR (CDCl₃, 100 MHz) δ 136.9 (C-24), 132.8 (C-6), 132.4 (C-7), 128.3 (C-23), 105.4 (C-19), 86.6 (C-5), 76.1 (C-3), 74.9 (C-25), 50.2 (25-OCH₃), 50.0 (C-17), 48.6 (C-14), 48.1 (C-9), 45.1 (C-13), 41.4 (C-8), 40.6 (C-10), 39.4 (C-12), 37.2 (C-4), 36.1 (C-20), 33.6 (C-15), 30.5 (C-11), 27.9, (C-16), 27.2 (C-22), 26.1 (C-27), 25.8 (C-26), 24.0 (C-29), 23.1 (C-2), 20.4 (C-28), 19.7 (C-30), 18.7 (C-21), 17.3 (C-1), 14.7 (C-18) [13].

Momordicoside K (**5**) : ¹H NMR (CDCl₃, 400 MHz) δ 9.74 (1H, s, H-19), 5.86 (1H, d, *J* = 5.2 Hz, H-6), 5.43 (1H, m, H-23), 5.31 (1H, d, *J* = 15.6 Hz, H-24), 4.17 d (1H, d, *J* = 7.6, H-1'), 3.92 d (1H, d, *J* = 5.2, H-7), 3.76 (2H, m, H-6'), 3.50 (1H, br s, H-3), 3.41 (1H, dd, *J* = 9.2, 8.8, H-4'), 3.34 (1H, dd, *J* = 9.2, 8.8, H-5'), 3.18 (1H, d, *J* = 9.2, H-3'), 3.15 (1H, d, *J* = 8, H-2'), 3.07 (3H, s, 25-OCH₃), 2.44 (1H, m, H-10), 1.99 s (1H, s, H-8), 1.22-2.44 (methine and methylene protons), 1.18 (9H, s, H-26, H-27 and H-29), 0.98 (3H, s, H-28), 0.84 s (6H, s, H-18 and H-21), 0.68 s (3H, s, H-30) ; ¹³C NMR (CDCl₃, 100 MHz) δ 210.1 (C-19), 146.9 (C-5), 136.8 (C-24), 128.6 (C-23), 122.5 (C-6), 101.7 (C-1'), 75.9 (C-3, C-3'), 76.3 (C-5'), 75.2 (C-25), 73.4 (C-7, C-2'), 69.8 (C-4'), 61.8 (C-6'), 50.3 (25-OCH₃), 50.0 (C-9), 49.4 (C-17), 47.3 (C-14), 46.4 (C-8), 45.6 (C-13), 41.6 (C-4), 39.4 (C-22), 36.1 (C-20), 35.8 (C-10), 34.8 (C-15), 28.9 (C-2), 28.5 (C-12), 27.4 (C-16), 27.1 (C-28), 26.1 (C-27), 25.8 (C-26), 25.3 (C-29), 22.4 (C-11), 21.0 (C-1), 18.8 (C-21), 18.2 (C-30), 14.9 (C-18) [14].

2.3 TLC-bioautographic cholinesterase inhibitory method

The cholinesterase inhibitory activities of all isolated compounds were evaluated by the TLC-autobiography assay based on Ellman's method with modifications [15].

Each tested compound was dissolved in MeOH to prepare a concentration of 100, 50, 25, 12.5, 6.25, 3.13, 1.56, 0.78, 0.39 and 0.20 $\mu\text{g/mL}$. Ten microliters of each concentration were spotted on a silica gel TLC plate and left to dry at room temperature for 3 hours. After dry, the amount of compounds in each spot was 1, 0.5, 0.25, 0.125, 0.0625, 0.0313, 0.0156, 0.0078, 0.0039 and 0.0020 μg , respectively. Eserine was used as standard control.

Then, the dried TLC plates were sprayed with a reagent mixture (1:1) of 5 mM substrate (ATCI or BTCI) and 5 mM DTNB in 50mM Tris-HCl, pH 8 (buffer A). They were allowed to dry for 5 min and then sprayed with a 3 U/ml of enzyme (AChE or BChE) in buffer A. The clear spot with yellow background indicated inhibition activity. The lowest concentration at which clear spot is observed within 15 min after spraying enzyme.

3. Results and Discussion

Four compounds (**1-4**) were isolated from the dichloromethane extract together with one compound (**5**) from the butanolic extract of *M. charantia*. All of them were identified based on NMR spectroscopic data and compared with the literature values [10-14]. The chemical structures of these isolated compounds were shown in Figure 1.

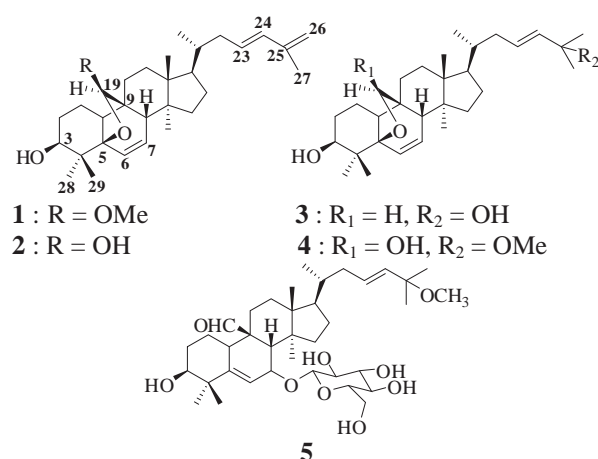


Figure 1. Chemical structures of compounds **1-5**

All isolated compounds were further evaluated *in vitro* AChE and BChE inhibitory activities. According to their low aqueous solubility, microplate assay cannot use to determine their activities. Thus, in this report, TLC-autobiography assay was used to determine cholinesterase inhibition and the minimal inhibitory amount (MIA) was reported. The results of activity tests were shown in Figures 2 and 3. After spraying enzyme on TLC plate, the inhibition spots (white circles) were observed within 15 minutes. However, some inhibition spots showed white ring

instead of white circle. Thus, in this study, MIA was defined as the lowest concentration that showed more than 50% white area in a circle. The MIA of each compound was tabulated in Table 1. Compounds **3** and **4** showed higher cholinesterase inhibitory activities than others. The absence of exo-double bond at C-25 and C-26 of compounds **3** and **4** seem to be increase inhibition comparing with the presence of this group in compounds **1** and **2**. The highest active compound for inhibition AChE and BChE was compound **3** (MIA = 0.0625 μg) and **4** (0.0313 μg), respectively. However, both compounds were less potent than standard drug eserine.

Of the several natural compounds previously found to inhibit ChE, the most significant inhibition is alkaloids but they might have significant side effects in clinical use [16]. Therefore, the search for other classes of ChE inhibitors in a nature such as terpenoids, is a great interesting. Previous publications have reported that lanostane-type triterpenes (*G. lucidum*) [17] and pentacyclic triterpenes (*C. erinacea*) [18] exhibited moderate cholinesterase-inhibitory properties. However, cucurbitane-type triterpenes have not been reported to exhibit cholinesterase-inhibitory properties. Thus, this is the first report of anti-cholinesterase activity of cucurbitane-type triterpenes from *M. charantia*. Our researching outcome suggests that *M. charantia* and its triterpene components might be a new choice for the treatment and prevention of AD and also other neurodegenerative disorders.

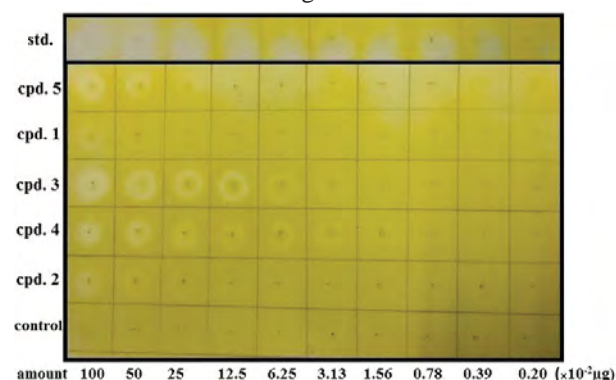


Figure 2. The AChE inhibitory activity of compounds by TLC-autobiography assay.

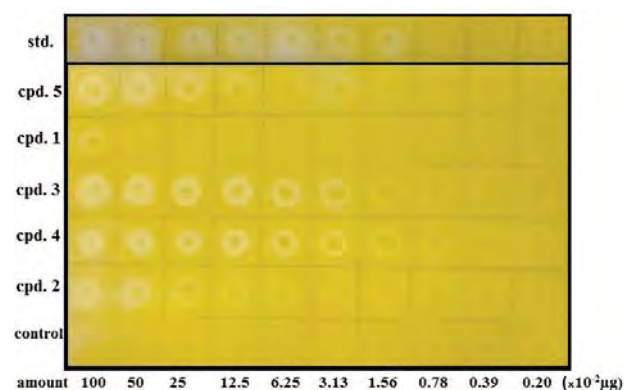


Figure 3. The BChE inhibitory activity of compounds by TLC-autobiography assay.

Table 1: The minimal inhibitory amount of tested compounds in TLC-autobiography assay.

Compound	The minimal inhibitory amount ($\times 10^{-2}$ μ g)	
	AChE	BChE
1	100	100
2	50	50
3	6.25	6.25
4	12.5	3.13
5	50	25
Eserine	< 0.02	1.56

4. Conclusions

In this research, the extracts of *M. charantia* fruits were isolated to give four cucurbitane-type triterpenoids (**1-4**) and one glycoside (**5**). Compounds **3** and **4** showed the most potent cholinesterase inhibitory activities by TLC-bioautographic method. The MIA of compound **3** towards either AChE or BChE was 0.0625 μ g. And those of compound **4** were 0.125 and 0.0313 μ g, respectively. This is the first anti-cholinesterase inhibitory study of cucurbitane-type triterpenes isolated from natural plants.

Acknowledgements

This study was supported by the Higher Education Research Promotion and National Research University Project of Thailand, the Office of the Higher Education Commission (FW645A), Chulalongkorn University.

References

- [1] J.K. Grover and S.P. Yadav, *J. Ethnopharmacol.* **93** (2004) 123–132.
- [2] A. Raman and C. Lau, *Phytomedicine* **2** (1996) 349–362.
- [3] M.B. Krawinkel and G.B. Krawinkel, *Nutr. Rev.* **64** (2006) 331–337.
- [4] W. Jiratchariyakul, C. Wiwat, M. Vongsakul, A. Somanabandhu, W. Leelamanit, I. Fujii, N. Suwannaroj and Y. Ebizuka, *Planta Med.* **67** (2001) 350–353.
- [5] P. Pitchakarn, S. Ohnuma, K. Pintha, W. Pompimon, S. Ambudkar and P. Limtrakul, *J. Nutr. Biochem.* **23** (2012), 76–84.
- [6] P. Pitchakarn, S. Suzuki, K. Ogawa, W. Pompimon, S. Takahashi, M. Asamoto, P. Limtrakul and T. Shirai, *Cancer Lett.* **306** (2011) 142–150.
- [7] J. Kubola and S. Siriamornpun, *Food Chem.* **110** (2008) 881–890.
- [8] N.X. Nhiem, P.V. Kiem, C.V. Minh, N.K. Ban, N.X. Cuong, N.H. Tung, L.M. Ha, D.T. Ha, B.H. Tai, T.H. Quang, T.M. Ngoc, Y.I. Kwon, H.D. Jang and Y.H. Kim, *Chem. Pharm. Bull.* **58** (2010) 720–724.
- [9] J. Grutzendler, J.C. Morris, *Drugs* **61** (2001) 41–52.
- [10] Y. Kimura, T. Akihisa, N. Yuasa, M. Ukiya, T. Suzuki, M. Toriyama, S. Motohashi and H. Tokuda, *J. Nat. Prod.* **68** (2005) 807–809.
- [11] Y. Zhang, J. Cui, H. Piao and Y. Zhao, *Chin. Tradit. Herb Drugs* **40** (2009) 509–512.

- [12] C.I. Chang, C.R. Chen, Y.W. Liao, H.L. Cheng, Y.C. Chen and C.H. Chou, *J. Nat. Prod.* **69** (2006) 1168–1171.
- [13] D.A. Mulholland, V. Sewram, R. Osborne, K.H. Pegel, and J.D. Connolly, *Phytochemistry* **45** (1997) 391–396.
- [14] H. Okabe, Y. Miyahara, T. Yamauchi, *Chem. Pharm. Bull.* **30** (1982), 4334–4340.
- [15] S.M. Salah and A.K. Jäger, *J. Ethnopharmacol.* **97** (2005) 45–149.
- [16] V. Schulz, *Phytomedicine* **10** (2003) 74–79.
- [17] I. Lee, B. Ahn, J. Choi, M. Hattori, B. Min and K. Bae, *Bioorg. Med. Chem. Lett.* **21** (2011) 6603–6607.
- [18] M.S.V. Gurovic, M.J. Castro, V. Richmond, M.B. Faraoni, M.S. Maier and A.P. Murray, *Planta Med.* **76** (2010) 607–610.

SYNTHESIS OF POLY(PHENYLENEETHYNYLENE)S FROM THE COST EFFECTIVE CALCIUM CARBIDE AS ACETYLENE SURROGATE

Nopparat Thavornsin¹, Mongkol Sukwattanasinitt², Sumrit Wacharasindhu^{2*}

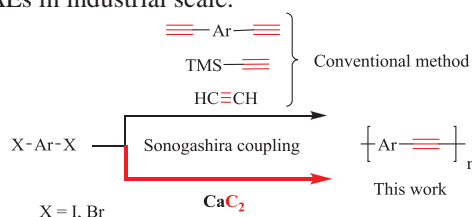
¹Program of Petrochemical and Polymer Science, ²Organic Synthesis Research Unit, Department of Chemistry, Faculty of Science, Chulalongkorn University, Bangkok 10330, Thailand.

* Author for correspondence; E-mail: sumrit.w@chula.ac.th, Tel. +66 22187634, Fax. +66 22187598

Abstract: A convenient and cost-effective synthetic method for poly(phenyleneethynylene)s (PPEs) has been discovered. PPEs are synthesized via the efficient Pd-catalyzed cross coupling reaction between diiodoarene and inexpensive calcium carbide as an acetylene source. Catalyst loading 0.05 mol% are sufficient to afford complete conversion of starting materials. Yields of the resulting PPE are in between 70 to 85% with the polydispersity index varying from 2.0 to 2.4 and high degree of polymerization ranging from 35 to 130.

1. Introduction

poly(phenyleneethynylene)s (PPEs) are an important class of conjugated polymers displaying attractive photophysical properties in absorption and emission. Thus, they find a broad use in sensor application and display technologies¹. Classically, PPEs are easily synthesized by two general methods. The first one is the alkyne metathesis which is powerful to form PPEs in good yield and high molecular weight. However, it requires high reaction temperature, high pressure and expensive catalyst while the second one is the Sonogashira cross-coupling reaction which is the most efficient method because of its mild reaction condition and remarkable functional group tolerance². The reaction involves the coupling of dihaloarenes to acetylene source such as diethynylarenes, protected acetylenes and acetylene gas³ (Scheme 1) which have several disadvantages such as multiple step synthesis and high cost material. Although, acetylene gas is appreciably more economical but the major drawback of acetylene gas is its high flammability and its complicated instrument set up. Recently, calcium carbide (CaC₂) has been used as an acetylene sources for synthesis of small acetylenic molecules⁴ since its easy to handle and its negligible price. Thus we interest to synthesis of PPEs using calcium carbide as starting material in the present of commercially available reagents under mild condition. The resulting PPEs are of similar or better quality in term of purity with other reported acetylene sources. This methodology could find potential use for the synthesis of PAEs in industrial scale.



Scheme 1. Synthetic method for PPEs

2. Results and discussion

2.1 Initial observation

Firstly, we screened Pd catalyst system by using typical PPE polymerization condition using THF/TEA as solvent for the coupling of iodobenzene. This would give us the quick idea of catalyst system. Therefore, 4-iodotoluene and calcium carbide were subjected to sonogashira coupling using various Pd sources such as Palladium acetate (Pd(OAc)₂), Bis (triphenylphosphine) palladium(II) dichloride (PdCl₂(PPh₃)₂) and Tetrakis(triphenylphosphine)Palladium (Pd(PPh₃)₄) (Table 1). We found that both PdCl₂(PPh₃)₂ and Pd(PPh₃)₄ gave low yield of diphenyl ethyne (34 and 43% yield respectively) and recovery stating material. In contrast, Pd(OAc)₂ were sufficient to afford complete conversion of starting materials 4-iodotoluene into the desired diphenyl ethyne 77% yield. (Table 1)

Table 1. Initial observation^a

Pd-catalyst	Yield (%)
PdCl ₂ (PPh ₃) ₂	34
Pd(PPh ₃) ₄	43
Pd(OAc) ₂	77

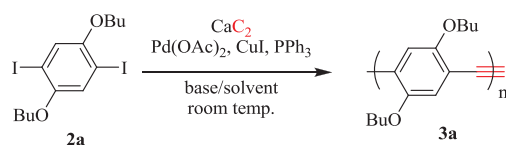
2.2 Reaction condition screening

Following the initial observation, we selected Pd(OAc)₂ as catalyst and CuI, PPh₃ as co-catalyst based on above results. Firstly, we are interested in synthesizing a simple PPE such as poly(1,4-dibutoxy-*p*-phenyleneethynylene) which have been reported in several literatures⁵ in order to compare with our report in term of yield and molecular weight. Therefore, the reaction optimization studies, including various amount of catalyst, type of bases and solvents were first screened (Table 2).

We began our study by coupling reaction between 1,4-dibutoxy-2,5-diiodobezene (**2a**) with calcium carbide via Sonogashira coupling reaction and the average molecular weight of result PPEs were characterized by gel permeation using polystyrene as standard after single precipitation with MeOH. In a preliminary experiment, the amount of Pd(OAc)₂ were

screened and found that 1% of Pd(OAc)₂ loading is insufficient for complete conversion of the starting materials, it produced oligomer with low molecular weight along with recovery starting diiodo compound. Hence, it could not be reprecipitated in MeOH/DCM (entry 1). However, this could be improved by increasing amount of Pd(OAc)₂ up to 5% mol. The orange solid of PPE **3a** were isolated in 84% yield without remaining starting material (entry 2). A second set of experiments were run in order to determine the best solvent and base system (entries 2-7). In the case of TEA as base (entries 2-4), we screened type of solvent and found that MeCN gave the highest yield of polymer. However, degree of polymerization remained low (DP_n = 13) in comparison with THF (DP_n = 20). This is due to the poor solubility of starting material in MeCN. Next, type of base was screened (entries 2, 5-7). It indicated that inorganic base is inefficient causing incomplete conversion of starting material (entries 6, 7) while DBU was the most effective base giving satisfactory yield of yellow-orange solid of PPE **3a** (71%) along with the highest degree of polymerization (DP_n = 36) and polydispersity (M_w/M_n = 2.3) (entry 5). Therefore, we selected THF and DBU as the best solvent and base.

Table 2. Synthesis of dibutoxy-PPEs from calcium carbide via sonogashira coupling reaction^a



entry	% mol of Pd	Base/solvent	Yield ^b (%)	DP _n ^c	M _w /M _n
1	1	TEA /THF	N.A.	-	-
2	5	TEA/THF	84	20	2.3
3	5	TEA/MeCN	90	13	2.1
4	5	TEA/DMF	N.A	-	-
5	5	DBU/THF	71	36	2.3
6	5	K ₂ CO ₃ /THF	N.A	-	-
7	5	Cs ₂ CO ₃ /THF	N.A	-	-
8 ^d	5	DBU/MeCN /THF	100	17	2.3

^aUnless noted, CaC₂ (6 equiv), Pd(OAc)₂ (0.05 equiv), PPh₃ (0.10 equiv), CuI (0.10 equiv), Base:solvent (1:2) was stirred at room temperature for 20 h under nitrogen atmosphere.

^bReprecipitation by MeOH.

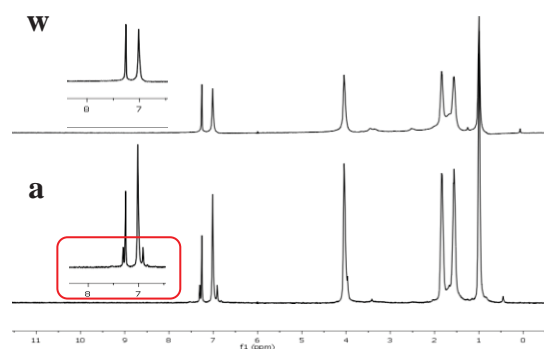
^cCharacterized by gel permeation chromatography using PS as reference.

^dTMS-acetylene were used instead of CaC₂

2.3 Comparison ¹H NMR of calcium carbide method with the conventional method (TMS-acetylene)

At the end of above section, we used the TMS-acetylene (Table 2, entry 8) as acetylene surrogate in order to compare with our method, calcium carbide.

The ¹H NMR of PPE from the optimized condition (entry 5) was compared with PPE from which was synthesized from Sonogashira TMS-acetylene which is prepared (entry 8) by following the reported literature⁵. As seen in ¹H NMR spectra (Scheme 2), we found that PPE from TMS-acetylene experiment displayed small peaks in the aromatic region suggesting the possibility of end group formation, while PPE from our optimized condition no end group and diyne signal presented (entry 5). We therefore suggested that PPE derived from calcium carbide had high molecular weight and quality. This result is in corresponding with GPC data showing lower molecular weight (DP_n = 17) of the polymer comparing with PPE from CaC₂ (DP_n = 36). The reason why PPE from CaC₂ have higher molecule weight with no diyne defect or end-group formation is perhaps due to the slow release of acetylene gas from hydrolysis of calcium carbide. The proton source from the hydrolysis process came from the small amount of H₂O in undried solvent and HI which is derived from Sonogashira coupling process.



Scheme 2. ¹H NMR spectra of PPE of 3a from TMS acetylene (a) and calcium carbide (w)

3. Conclusion

In conclusion, we have successfully developed a cost-effective synthesis method for poly(phenyleneethynylene)s with high molecular weight and high quality by using calcium carbide and diiodoarenes as starting materials via a Pd-catalyzed coupling reaction. The fact that calcium carbide is primary chemical feed stock for petrochemical industry, this process will allow the large scale synthesis of high quality-PPE in polymer process industry.

4. Experimentals

4.1 Materials

All reagents were purchased from Sigma-Aldrich, Fluka® (Switzerland) or Merck® (Germany) and used without further purification. Analytical thin-layer chromatography (TLC) was performed on Kieselgel F-254 pre-coated plastic TLC plates from EM Science. Visualization was performed with a 254 nm ultraviolet lamp. Gel column chromatography was carried out with silica gel (60, 230-400 mesh) from ICN Silitech. The ¹H and ¹³C NMR spectra were recorded on a Varian 400 or Bruker 400 in CDCl₃. All polymer

solutions were filtered through 0.45 μm syringe filters prior to use. Polymer molecular weights were determined at 25 $^{\circ}\text{C}$ on a HP series 1100 GPC system in THF at 1.0 mL/min (3mg/mL sample concentrations) equipped with a diode array detector (254 nm and 450 nm) and a refractive index detector. Polymer molecular weights are reported relative to polystyrene standards.

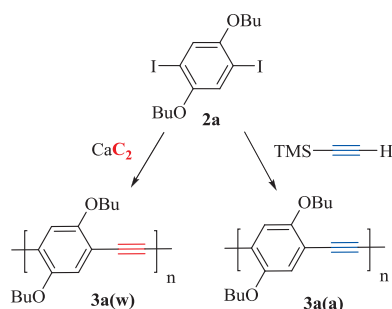
4.2 Synthesis

1,4-bis(butoxy)benzene (1a)

To a stirred suspension of KOH (4.58 g, 81.72 mmol) and hydroquinone (2.00 g, 18.16 mmol) in DMF (15 mL) was added dropwise *n*-butyl bromide (9.95 g, 72.64 mmol). The mixture was stirred at room temperature for overnight. The mixture was poured into 300 mL of cool water and the organic layer was filtered, washed with cool water many times, and dried over a steam bath to afford 8.82 g (18.16 mmol, 76%) of **1a** as a light brown solid: ^1H NMR (400 MHz, CDCl_3) δ ppm 6.82 (s, 4H), 3.92-3.89 (t, 4H), 1.77-1.70 (m, 4H), 1.52-1.43 (m, 4H), 0.98-0.94 (t, 6H). ^{13}C NMR (101 MHz, CDCl_3) δ ppm 153.7, 115.9, 68.9, 32.0, 19.7, 14.3.

1,4-dibutoxy-2,5-diiodobenzene (2a)

To a stirred of **1a** (4.00 g, 17.99 mmol) in MeOH (30 mL) at temperature below 15 $^{\circ}\text{C}$ was added dropwise iodine(I) chloride (12.76 g, 78.61 mmol) and the mixture was stirred reflux for 4 h. The mixture was extracted three times with CH_2Cl_2 . The combined extract was washed with aqueous $\text{Na}_2\text{S}_2\text{O}_3$, water, and brine, dried over anhydrous Na_2SO_4 , concentrated *in vacuo* and purified by column chromatography to provide product to afford 6.25 g (17.99 mmol, 74%) of **2a** as a white solid. ^1H NMR (400 MHz, CDCl_3) δ ppm 7.17 (s, 2H), 3.95-3.92 (t, 4H), 1.82-1.75 (m, 4H), 1.58-1.49 (m, 4H), 1.00-0.96 (t, 6H). ^{13}C NMR (101 MHz, CDCl_3) δ ppm 153.2, 123.2, 86.6, 70.4, 31.6, 19.6, 14.1.



Scheme 3. Diagram for synthesized of **3a(w)**, **3a(a)**.

Synthesis of poly(1,4-dibutoxy-*p*-phenyleneethynylene) (**3a(w)**) via Pd-catalyzed coupling reaction of calcium carbide with **2a**

A 100 mL round bottom flask with a magnetic stirrer bar was charged with **2a** (150 mg, 0.31 mmol), palladium(II)acetate (3.37 mg, 0.015 mmol), copper iodide (5.90 mg, 0.031 mmol), triphenylphosphine (8.13 mg, 0.031 mmol), calcium carbide (119.22 mg, 1.86 mmol) and DBU (2 mL) in THF (4 mL). The

reactions were carried out under positive pressure of N_2 filled in rubber balloons. The mixture was stirred at room temperature for 20 hours. The solution was then filtrated with cotton wool by methylene chloride as eluent, concentrated to a small volume and precipitated by dropping the solution into 150 mL of methanol. The precipitate that formed was collected by centrifuge, washed repeatedly with methanol and evaporated under vacuum to afford 53.48 mg (0.22 mmol, 71%) of **3a(w)** as a orange-yellow solid. $M_w = 20168$, $M_w/M_n = 2.30$, $\text{DP}_n = 36$, ^1H NMR (400 MHz, CDCl_3) δ ppm 7.02 (s, 2H), 4.05 (br, 4H), 1.84 (br, 4H), 1.66 – 1.49 (m, 4H), 1.01-0.98 (t, 6H). (Scheme 2).

Synthesis of poly(1,4-dibutoxy-*p*-phenyleneethynylene) (**3a(a)**) via Pd-catalyzed coupling reaction of trimethylsilylacetylene with **2a**

Synthesized following the reported literature⁶. A 100 mL round bottom flask with a magnetic stirrer bar was charged with **2a** (150 mg, 0.31 mmol), tetrakis(triphenylphosphine)palladium (17.34 mg, 0.015 mmol), copper iodide (5.90 mg, 0.031 mmol), trimethylsilylacetylene (36.53 mg, 0.37 mmol) and DBU (2 mL) in mixture solvent of MeCN (3 mL), THF (2 mL). The reaction was carried out under positive pressure of N_2 filled in rubber balloons. The mixture was stirred at room temperature for 3 days. The mixture was then purified according to **3a(w)** to afford 75.64 mg (0.31 mmol, 100%) of **3a(a)** as a green-yellow solid. $M_w = 9765$, $M_w/M_n = 2.30$, $\text{DP}_n = 17$, ^1H NMR (400 MHz, CDCl_3) δ ppm 7.02 (br, 1H), 6.91 (br, 1H), 4.04 (br, 4H), 1.84 (br, 4H), 1.56 (br, 4H), 1.00 (br, 6H) (Scheme 2).

Acknowledgements

This study is financially supported by the Thailand Research Fund (TRF-RSA5480004) and National Nanotechnology Center (NANOTEC), NSTDA (NN-B-22-FN9-10-52-06), Center for Petroleum, Petrochemicals and Advanced Materials, Chulalongkorn University. This work is part of the Project for Establishment of Comprehensive Center for Innovative Food, Health Products and Agriculture supported by the Thai Government Stimulus Package 2 (TKK2555, SP2), Asahi Glass Foundation, and also the National Research University Project of CHE (AM1006A). Thesis Scholarships for Students No. 1/2556 Second Semester Academic Year 2555, Fiscal Year 2556, Graduate School, Chulalongkorn University.

References

- [1] Wang, Y., Park, J. S., Leech, J. P., Miao, S., Bunz, U. H. F., *Macromolecules* **40** (2007) 1843.
- [2] Veller, B. V., Swager, T. M., *Design and synthesis of conjugated polymers* (eds Leclerc, M. and Morin, J. F.), Wiley-VCH Verlag GmbH (2010) 175-176.
- [3] Wilson, J. N., Waybright, S. M., McAlpine, K., Bunz, U. H. F., *Macromolecules* **35** (2002) 3799-3800.

- [4] Chuentragool. P., Vongnam. K., Rashatasakhon. P., Sukwattanasinitt. M., Wacharasindhu. S., *Tetrahedron* 67 (2011) 8177-8182.
- [5] a) Giardina. G., Rosi. P., Ricci. A., Sterzo. C. L., *Journal of Polymer Science: Part A: Polymer Chemistry*, **38** (2000) 2603–2621., b) Pizzoferrato. R., Berliocchi. M., Carlo. A. D., Lugli. P., Venanzi. M., Micozzi. A., *Macromolecules* **36** (2003) 2215-2223., c) Shinar. J., Swanson. L. S., Lu. F., Ding. Y., *United State Patent*, Patent NO. 5,334,539.
- [6] Khan. A., Müller. S., Hecht. S., *Chem. Commun.* (2005) 584-586.

SYNTHESIS OF GLUCOPYRANOSYL-1,4-DIHYDROPYRIDINE AS A NEW FLUORESCENT SENSOR TO DETECT PROTEINS

Oran Pinrat¹, Mongkol Sukwattanasinitt² and Anawat Ajavakom^{2*}

¹Program of Petrochemistry and Polymer Science, Faculty of Science, Chulalongkorn University, Bangkok 10330, Thailand

²Center for Petroleum, Petrochemicals and Advanced Materials, Department of Chemistry, Faculty of Science, Chulalongkorn University, Bangkok 10330, Thailand

*E-mail: anawat77@hotmail.com

Abstract: Glucosamine (GlcNH) is an abundant compound in Thailand, particularly from two marine crustaceans: shrimp and crab. The new way to utilize GlcNH has to be developed; otherwise this resource will be wasted millions ton a year. Glucopyranosyl-1,4-Dihydropyridine **3** (Glc-DHP) has been synthesized as a new fluorescent biosensor. Primary amine **1** was obtained from D-glucosamine hydrochloride (GlcNHCl) as the starting material by using the reported synthetic procedure.¹ Subsequent addition reaction of the primary amine **1** and ethyl propiolate in DCM under refluxing temperature for 3 days was carried out to produce β -amino acrylate **2**. Because β -amino acrylate **2** has both nucleophilic and electrophilic sites, the cyclotrimerization (3 eq.) of the β -amino acrylate to 1,4-Dihydropyridine **3** (DHP) was observed smoothly in the presence of TiCl₄.² By possessing fluorescence property, this Glc-DHP **3** was used as fluorescent biosensor for the detection of proteins; e.g. BSA, hemoglobin, papain, etc. The fluorescence signal of Glc-DHP **3** was selectively and completely quenched by hemoglobin.

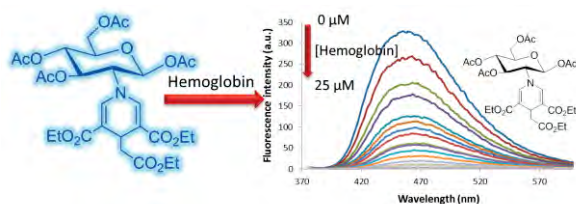
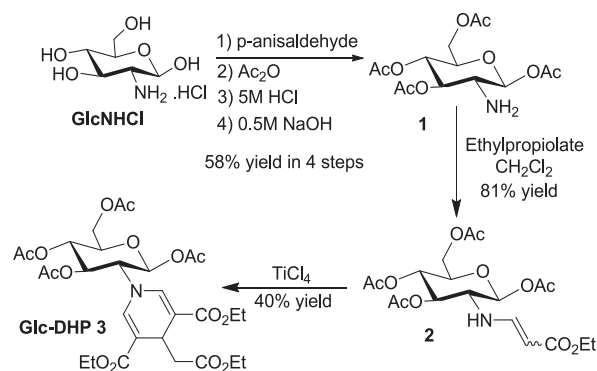


Figure 1. Structure of heme protein.

GlcNHCl, easily synthesized from GlcNH by HCl treatment, was initially treated with *p*-anisaldehyde for the protection of NH₂ unit, then acetylation, removal of the *p*-methoxybenzylidene protecting group with HCl in acetone and neutralized by 0.5M NaOH to obtain primary amine **1** in 58% yield over 4 steps.¹ Glucopyranosyl-1,4-Dihydropyridine (Glc-DHP **3**) was synthesized via cyclotrimerization of the β -amino acrylate **2**, obtained from the reaction of amine **1** with ethyl propiolate, in the presence of TiCl₄ (Scheme 1). The structure of Glc-DHP **3** was confirmed by ¹H NMR, ¹³C NMR. The Glc-DHP **3** gave strong blue light emission (450 nm) under black light. The strong emission of Glc-DHP **3** was used as sensor for the detection of proteins such as BSA, hemoglobin, papain, etc. Interestingly, the fluorescence signal of Glc-DHP **3** was selectively and completely quenched by hemoglobin.

1. Introduction

For the last 2-3 decades, heme proteins, metalloproteins containing the heme prosthetic group, either covalently or non-covalently bound to the protein, have been extensively studied, due to their capacities to undergo reduction and oxidation at the iron heme^{3,4}. Some of these proteins are electron carriers (cytochrome c, catalase), others are involved in catalysis (e.g. peroxidase, cytochrome oxidase) and in active membrane transport or in oxygen transport (e.g. hemoglobin, myoglobin, cytoglobin). Hemoglobin is a protein in red blood cells that transports oxygen throughout the body. The most common hemoglobin, tetramer consisting of four subunits non-covalently bound (Figure 1), is normally tested for the diagnosis of the diseases such as anemia, leukemia.^{5,6} Among the current methods for proteins



Scheme 1. Synthesis of Glc-DHP **3**.

2. Materials and Methods

2.1 General

Chemicals and materials: ethyl propiolate and TiCl_4 were purchased from Sigma-Aldrich and Fluka. Dichloromethane (CH_2Cl_2) was dried over CaH_2 and distilled prior to use. Thin layer chromatography (TLC) was carried out using Merck 60 F254 plates with a thickness of 0.25 mm. Column chromatography was performed on Merck silica gel 60 (70-230 mesh).

Analytical Instruments: Absorption spectra were measured by a Varian Cary 50 UV-Vis spectrophotometer. Fluorescence spectra were performed on a Varian Cary Eclipse spectrofluorometer. The ^1H and ^{13}C NMR spectra were collected on a 400 MHz NMR spectrometer (Mercury 400, Varian) and 100 MHz NMR spectrometer (NETZSCH DSC 204 F1), respectively.

2.2 Preparation of 1,3,4,6-tetra-*O*-acetyl- β -D-glucosamine **1**.

Primary amine **1** was prepared from GlcNHCl according to the reference method¹ in 58% yield over 4 steps. The structure was confirmed in good agreement with literally reported information.

2.3 Preparation of ethyl β -amino acrylate **2**.

To the solution of primary amine **1** (1 g, 1 equiv) in CH_2Cl_2 25 mL, ethyl propiolate (5 equiv) was slowly added and the reaction mixture was stirred under refluxing temperature for 3 days. The mixture was evaporated in vacuo and condensed residue was purified by column chromatography ($\text{EtOAc/Hexane}=30/70$) to provide the ethyl β -amino acrylate **2** (81% yield) as a pale yellow oil. ^1H NMR (400 Hz, CDCl_3) δ 7.65 (1H, *NH*), 6.47 (1H, =*CHN*), 5.56 (1H, *H-1*), 5.27 (1H, *H-3*), 5.05 (1H, *H-4*), 4.46 (1H, *CH=CHN*), 4.30 (1H, *H-6*), 4.21 (1H, *H-6'*), 4.08 (2H, OCH_2CH_3), 3.74 (1H, *H-5*), 3.21 (1H, *H-2*), 1.89-2.12 (12H, 4OAc), 1.18 (3H, OCH_2CH_3).

2.4 Preparation of 1,3,4,6-tetra-*O*-acetyl- β -D-glucosaminyl-1,4-dihydropyridine (Glc-DHP **3**).

To the solution of ethyl β -amino acrylate **2** (1 equiv) in dry CH_2Cl_2 25 mL in an ice bath, TiCl_4 (0.3 equiv) was added rapidly and the reaction mixture was stirred overnight at room temperature under nitrogen atmosphere. After the solution was quenched with distilled deionized water (25 mL) was added and the mixture was extracted with CH_2Cl_2 (25 mL). The organic portions were combined and neutralized by addition of 10% w/v NaHCO_3 solution. The organic phase was washed with deionized water (3x25 mL), dried over MgSO_4 , and evaporated under reduced pressure. The crude product was purified by column chromatography ($\text{EtOAc/Hexane}=20/80$) to provide the 1,3,4,6-tetra-*O*-acetyl- β -D-glucosaminyl-1,4-dihydropyridine **3** (40% yield) as a pale yellow oil.


^1H NMR (400 Hz, CDCl_3) δ 7.05 (2H, *CH=C*), 5.76 (1H, *H-1*), 5.31 (1H, *H-3*), 5.12 (1H, *H-4*), 4.30 (1H, *H-6*), 4.23-4.06 (5H, DHP- $\text{CO}_2\text{CH}_2\text{CH}_3$ and $\text{CHCH}_2\text{CO}_2\text{Et}$), 4.03 (1H, *H-6'*), 3.85 (1H, *H-5*), 3.74

(2H, $\text{CH}_2\text{CO}_2\text{CH}_2\text{CH}_3$), 3.46 (1H, *H-2*), 2.45 (2H, $\text{CH}_2\text{CO}_2\text{Et}$), 1.89-2.12 (12H, 4OAc), 1.23 (6H, DHP- $\text{CO}_2\text{CH}_2\text{CH}_3$), 1.11 (3H, $\text{CH}_2\text{CO}_2\text{CH}_2\text{CH}_3$).

3. Results and Discussion

The chemosensor behavior was investigated by the fluorescence measurement in aqueous solution (1 μM) upon excitation at 360 nm (Table 1). The molar absorption coefficient of Glc-DHP **3** was $6,900 \text{ M}^{-1} \text{ cm}^{-1}$. Glc-DHP **3** exhibited an emission peak at 450 nm with fluorescent quantum efficiency (Φ_f) of 0.29.

Table 1: Photophysical property of Glc-DHP **3** in aqueous solution.

Absorption		Emission		Appearance (2 μM) under black light
λ_{max} (nm)	ϵ $\text{M}^{-1} \cdot \text{cm}^{-1}$	λ_{max} (nm)	Φ_f	
360	6,900	450	0.29	

The fluorescent responses of Glc-DHP **3** (1 μM) towards proteins (BSA, lysozyme, papain, histone, α -casein, carbonic anhydrase, α -lactalbumin, β -lactalbumin, lectin (50 μM) and hemoglobin (25 μM)) were evaluated in aqueous solutions (Figure 2). Upon the addition of the proteins into a solution of DHP **3**, only hemoglobin caused a significant fluorescence quenching effect.

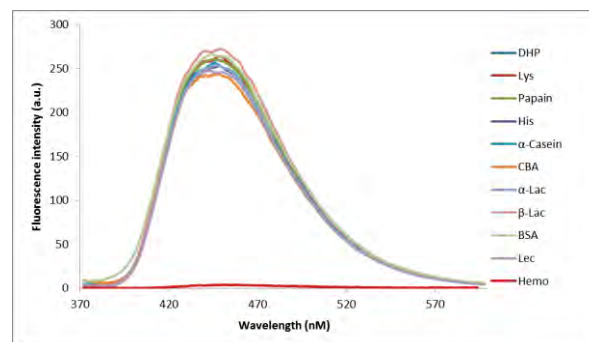


Figure 2. Fluorescence quenching profile of DHP **3** (1 μM), after addition of each protein (50 μM) (only hemoglobin 25 μM) in aqueous solution ($\lambda_{\text{ex}} = 360 \text{ nm}$).

Thus, we carried out the fluorescence titrations of the aqueous solution of DHP **3** (1 μM) with hemoglobin. Upon addition of incremental amount of 1 μM of hemoglobin to the solution of DHP **3** in aqueous solution, the quenching in fluorescence emission was observed at the concentration as low as 25 equiv (Figure 3). As shown in the spectra, with increase of hemoglobin concentration from 0 to 5 μM , the fluorescent signal was rapidly decreased. However, at a higher concentration of hemoglobin (from 6 to 25 μM), the fluorescence signal was gradually dropped and was completely quenched at 25 μM .

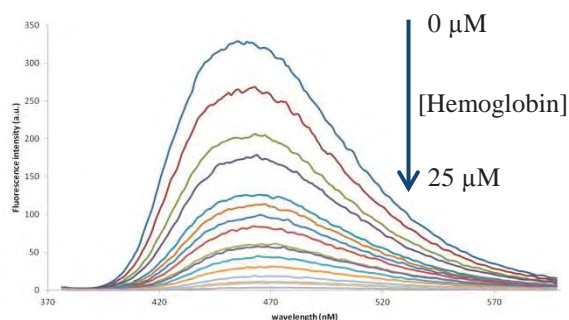


Figure 3. Fluorescence change of DHP **3** (1 μM) with the addition of hemoglobin (0 to 25 equiv) in aqueous solution ($\lambda_{\text{ex}} = 360 \text{ nm}$).

The emission response to hemoglobin was also investigated by using Stern-Volmer relationship and linear plot (inset Figure 4) with a Stern-Volmer constant of $424,000 \text{ M}^{-1}$ at the concentration of hemoglobin was below $7 \mu\text{M}$.

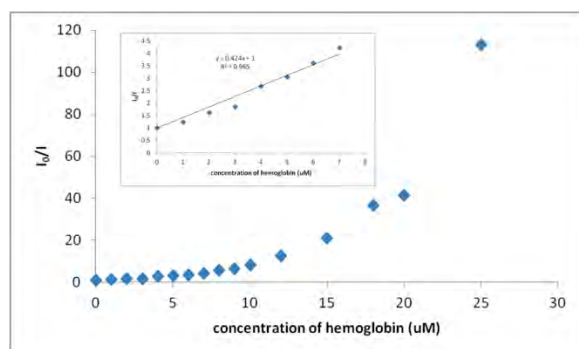


Figure 4. Stern-Volmer plot in response to hemoglobin. Inset: Stern-Volmer plot obtained at lower concentration of hemoglobin ($7 \mu\text{M}$).

The change in fluorescence spectra of Glc-DHP **3** with the addition of hemoglobin was presumably due to the corporation (interaction) with metal (Fe^{2+}) within the hemoglobin. As future work, in order to confirm this hypothesis, we will investigate with other metalloproteins such as myoglobin, cytochrome c as Fe^{2+} complexes and chlorophyll as other metal complexes.

4. Conclusions

In summary, we have reported a new fluorescent Glc-DHP **3** which can be used as selective biosensor for hemoglobin in aqueous solution. The decrease of fluorescence signal was proportional to the hemoglobin concentration with high quenching efficiency ($K_{\text{SV}} = 424,000 \text{ M}^{-1}$).

Reference

- [1] H. Myszka, D. Bednarczyk, M. Najder and W. Kacac, *Carbohydrate Research* **338** (2003) 133-141.
- [2] T. Sirijindalert, K. Hansuthirakul, P. Rashatasakhon, M. Sukwattanasinitt and A. Ajavakom, *Tetrahedron* **66** (2010) 5161-5167.
- [3] Y. M. Lvov, Z. Lu, J. B. Shenkmann, X. Zu, J. F. Rusling, *J. Am. Chem. Soc.* **120** (1998) 4073-4080.
- [4] D.L. Nelson, M. M. Cox, *Lehninger Principles of Biochemistry*, fifth ed., W. H. Freeman, USA, 2008.
- [5] Y. Wu, S. Hu, *Microchim. Acta* **159** (2007) 1-17.
- [6] M. Barsan, E. Pinto, C. Brett, *Electrochimica Acta* **55** (2010) 6358-6366.

Keywords; glucosamine, fluorescent biosensor, 1,4-dihydropyridine, hemoglobin

DIPHENYLACETYLENE DERIVATIVES WITH DICYANO PERIPHERIES FOR NAKED EYES DETECTION OF CN⁻ ION

Nakorn Niamnont^{1*}, Choladda Srisuwannaket¹, Jay S. Siegel², Mongkol Sukwattanasinitt³

¹ Department of Chemistry, Faculty of Science, King Mongkut's University of Technology Thonburi, Bangkok, 10400 Thailand

² Organic Chemistry Institute, University of Zurich, Winterthurerstrasse, Zurich, 8057 Switzerland

³ Department of Chemistry, Faculty of Science, Chulalongkorn University, Bangkok, 10330 Thailand

*E-Mail: Nakorn.nia@kmutt.ac.th, Tel. +66 24708970, Fax. +66 24708843

Abstract: Phenyleneethyne fluorophores (F1) with dicyano receptor as cyanide probe was successfully synthesized by the sonogashira coupling. The probe displayed apparent colour changes from deep red to colourless and turned on green fluorescent emission via the reducing intramolecular charge transfer (ICT) process. With the aid of the UV-vis and fluorescent spectrometer, the detection limit could be as low as 2.0 μ M. Additionally, ¹H-NMR titration confirmed that CN⁻ as electrophile attacked at alpha carbon of the probe. The fluorophore possessed high selectivity for cyanide with respect to other common anions. Additionally, fluorophores could serve as practical colorimetric probe for on-site measurements.

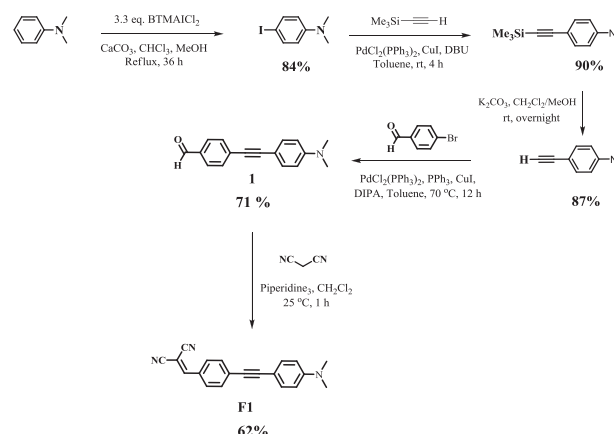
1. Introduction

Cyanide is very toxic to human even at low contamination that can cause death. Cyanide can strongly inhibit the process of cellular respiration when entering into human blood system by interacting with a heme unit in the active site of cytochrome aa3 [1]. However, it remains widely used (1.5 million tons per year) and its poisoning may occur in particular industry such as in metal trades, mining, electroplating, jewellery manufacturing, and X-ray film recovery [2]. In nature, cassava, cyanogenic algae, bacteria and fungi can produce and release cyanide compounds that sometime cause food and water contamination [3]. Water-soluble potassium and sodium cyanide salts have been known to be ones of the most lethal chemical reagents and even used as poisoning materials [4-5]. The maximum concentration of cyanide allowed in drinking water by the WHO manual is 2.7 μ M [6]. Significantly, the detection of cyanide ion under biologically relevant aqueous solution is thus vital for safety management and sensors for food and agriculture such as Thai tapioca starch industry. Recent development of fluorescence turn-on sensors based on nucleophile with addition of cyanide has encouraged much interest due to its high sensitivity and selectivity [6, 7].

Thus, it is reasonable to develop novel conjugated fluorophores (CF)-based chemodosimetric sensors for cyanide detection, which will exhibit both the high sensitivity of CF-based sensors and the high selectivity of chemodosimetric sensors. To our surprise, this desirable combination of these sensing

properties has not been mentioned at all for the reaction-based *N,N'*-dimethyl-phenyleneethyne containing dicyano receptor.

In this work, we designed and synthesized a novel conjugated fluorophore (F1) containing dicyano-vinyl unit to be a highly selective and sensitive cyanide sensor. Its design is based on the consideration that the dicyanovinyl group can act as a selective cyanide reactive unit for the nucleophilic addition reaction. This is due to an efficient fluorescence turn-on sensor for cyanide ion [10].



Scheme 1. The Synthetic Scheme of F1.

2. Materials and Methods

2.1 Analytical instruments

The melting points of all products were acquired from a melting point apparatus (Electrothermal 9100, Fisher Scientific, USA). Mass spectra were recorded on a microflex MALDI-TOF mass spectrometer (Bruker Daltonics) using doubly recrystallized α -cyano-4-hydroxy cinnamic acid (CCA) as a matrix. The HRMS spectra were measured on an electrospray ionization mass spectrometer (microTOF, Bruker Daltonics). ¹H-NMR and ¹³C-NMR spectras were acquired from sample solution in CDCl₃ and acetone-d₆, on Varian Mercury NMR spectrometer (Varian, USA) at 400 MHz and 100 MHz and Bruker AV-500 NMR Spectrometer at 500 MHz and 125 MHz respectively. The UV-visible absorption spectra were

obtained from a Varian Cary 50 UV-vis spectrophotometer (Varian, USA). The fluorescence emission spectra were recorded on a Varian Cary Eclipse spectrofluorometer (Varian, USA) and Hitachi model F-2500 fluorometer.

Preparation of 4-iodo-*N,N*-dimethylaniline. A mixture of *N,N*-dimethylaniline (6.0 g, 50 mmol) in chloroform (100 mL) and methanol (50 mL) was added with BTMAICl₂ (18.08 g, 52 mmol) and CaCO₃ (16.45 g, 0.15 mmol). After the reaction mixture was refluxed for 36 h, 20% Na₂S₂O₃ solution was added to the mixture until the mixture became light yellow. The mixture was filtered and the filtrate was extracted with dichloromethane (3 × 50 mL). The combined organic phase was washed with water (2 × 100 mL) and dried over anhydrous MgSO₄. The solution was concentrated and the residue was precipitated in methanol/CH₂Cl₂. 4-Iodo-*N,N*-dimethyl-aniline was obtained in a form of purple solid (10.37 g, 84%). mp: 91-93°C; ¹H NMR (CDCl₃, 400 MHz): δ (ppm) 7.46 (d, *J* = 5.6 Hz, 2H), 6.49 (d, *J* = 5.6 Hz, 2H), 2.92 (s, 6 H); ¹³C NMR (CDCl₃, 100 MHz): δ (ppm) 137.5, 114.7, 40.4.

Preparation of *N,N*-dimethyl-4-((trimethylsilyl)ethynyl)aniline. A mixture of 4-iodo-*N,N*-dimethyl-aniline (2.51 g, 10 mmol), PdCl₂(PPh₃)₂ (0.35 g, 0.5 mmol), CuI (0.08 g, 0.5 mmol) and trimethylsilyl-acetylene (1.08 g, 11 mmol) in toluene (10 mL) was added with DBU (1 mL) and the mixture was stirred at room temperature for 4 h. The reaction mixture was then filtered and the solid was washed with toluene (3 × 15 mL). The filtrate was evaporated and the residue was eluted through a silica gel column by gradient solvents starting from pure hexane to dichloromethane/hexane (1/3) as an eluent to afford *N,N*-dimethyl-4-((trimethyl-silyl)ethynyl)aniline as a yellow solid (2.17 g, 90% yield). mp: 88-89°C; ¹H NMR (CDCl₃, 400 MHz): δ (ppm) 7.11(d, *J* = 7.2 Hz, 2H), 6.35 (d, *J* = 7.2 Hz, 2H), 2.72 (s, 6H), 0.01 (s, 9H); ¹³C NMR (CDCl₃, 100 MHz): δ (ppm) 149.9, 132.9, 111.3, 109.6, 106.3, 90.9, 39.9, 0.01.[8]

Preparation of 4-ethynyl-*N,N*-dimethylaniline. A mixture of *N,N*-dimethyl-4-((trimethylsilyl)ethynyl)-aniline (1.00 g, 4.6 mmol) and K₂CO₃ (0.059 g, 0.43 mmol) in dichloromethane (15 mL) and methanol (15 mL) was stirred at room temperature for 12 h. Next addition of water, the organic layer was separated and the aqueous phase was extracted with dichloromethane (2 × 50 mL) and was then dried over anhydrous MgSO₄. The filtrate was evaporated and the residue was eluted through a silica gel column by gradient solvents starting from pure hexane to dichloromethane/hexane (1/3) as an eluent to afford 4-ethynyl-*N,N*-dimethylaniline as a brown-yellow solid (0.60 g, 87% yield). mp: 67-69°C; ¹H NMR (CDCl₃, 400 MHz): δ (ppm) 7.37 (d, *J* = 8.8 Hz, 2H), 6.62 (d, *J* = 8.8 Hz, 2H), 2.07 (s, 7H); ¹³C NMR (CDCl₃, 100 MHz): δ (ppm) 150.4, 133.2, 111.7, 108.7, 84.9, 74.9, 40.

Preparation of 1. A mixture of 4-ethynyl-*N,N*-dimethylaniline (146.0 mg, 1.0 mmol), 4-Bromoben-

zaldehyde (190 mg, 1.1 mmol), PdCl₂(PPh₃)₂ (35.0 mg, 0.05 mmol), CuI (9.5 mg, 0.05 mmol) in THF (5 mL) was added with isopropylamine (1 mL) and the mixture was stirred at 70 °C for 15 h. The reaction mixture was then evaporated and the residue was eluted through a silica gel column by gradient from pure hexane to hexane/CH₂Cl₂ (1:2, v/v) as an eluent to afford 1 as a yellow solid. (176.2 mg, 71% yield). mp: 150-152°C; ¹H NMR (CDCl₃, 500 MHz): δ (ppm) 10.02 (s, 1H), 7.85 (d, 2H, *J* = 8.2 Hz), 7.63 (d, 2H, *J* = 8.2 Hz), 7.45 (d, 2H, *J* = 8.4 Hz), 6.75 (d, 2H, *J* = 8.4 Hz), 3.03 (s, 6H). MS-ES+ *m/z*, Calcd for C₁₇H₁₅NO, calcd 249.307, found 249.345.

Preparation of F1. Piperidine (0.2 mL) was added to a solution of compound 1 (99.2 mg, 0.39 mmol) in CH₂Cl₂ (20 mL) and then malononitrile (55 mg, 0.72 mmol) was added, and the reaction mixture was stirred for 1 h at 25 °C. The reaction mixture was then evaporated and the residue was purified by using column chromatography with 4/1 CH₂Cl₂/hexane to give compound F1 as a dark red solid was obtained (72.4 mg, 62 %). mp: 125-127 °C; ¹H NMR (500 MHz, Acetone-d₆): δ (ppm) 8.20 (s, 1H), 7.95 (d, 2H, *J* = 8.8 Hz), 7.60 (d, *J* = 8.8 Hz, 2H), 7.34 (d, *J* = 8.8 Hz, 2H), 6.68 (d, *J* = 8.8, 2H), 3.06 (s, 6 H) ppm. ¹³C NMR (500 MHz, Acetone-d₆): δ (ppm) 161.5, 151.9, 132.4, 131.6, 131.5, 130.8, 129.5, 114.2, 113.1, 111.7, 108.5, 99.0, 88.7, 82.6, 40.2 ppm. APCI-MS *m/z*, Calcd for C₂₀H₁₆N₃ calcd. 297.3532; found 297.3598.

2.2 Photophysical property study

The spectroscopic studies were conducted on solutions of F1 prepared from a 50 μM stock solution of F1 in water/THF (40:60, v/v) solution [9]. The UV-visible absorption spectra were recorded from the solution sample in a quartz cuvette with 10 mm optical path length at ambient temperature. The emission spectra were recorded from the solution sample in a 10 mm quartz cuvette at ambient temperature using an excitation wavelength at 345 nm.

Preparation of solutions of anions, one millimole of inorganic salt (NaOAc, NaNO₂, NaNO₃, NaF, NaCl, NaBr, NaI, NaHSO₄, NaH₂PO₄, KSCN, and NaCN) was dissolved in water/THF (40:60, v/v) solution (20 mL) to afford 1 × 10⁻¹ mol/L aqueous solution. The stock solutions were diluted to desired concentrations with water/THF (40:60, v/v) when needed.

Preparation of solutions for selectivity study between F1 and 11 anions, a solution of F1 (1 μM) was prepared in water/THF (40:60, v/v). Then 1.0 mL of the solution of F1 was placed in a quartz cell and the UV-vis absorption spectrum was recorded. The NaCN aqueous media was introduced in portions and the absorption and fluorescent changes were recorded at room temperature each time.

3. Results and Discussion

The F1 synthesis and its structural characterization, the compound F1 synthetic scheme was depicted in Scheme 1. It was easily seen that the target compound was prepared conveniently through the sonogashira

and general condensation reaction between **1** and malononitrile. The results achieved in high yields. Its structure was confirmed by ^1H NMR, ^{13}C NMR, and MS spectroscopic data. The synthetic route and purification were simple.

Compound **F1** displayed good solubility in common organic solvents, such as CH_2Cl_2 , EtOAc, THF, etc. Its structure was characterized by spectroscopic methods. Compound **F1** was orange-red color in water/THF (40:60, v/v) and showed two distinct absorption bands at 345 and 440 nm. The former attributed to the π - π^* transition and the latter presented an intramolecular charge transfer (ICT) transition.

To study the selectivity of **F1** for cyanide detection, other different 11 anions (OAc^- , NO_2^- , NO_3^- , F^- , Cl^- , Br^- , I^- , HSO_4^- , H_2PO_4^- , SCN^- , and CN^-) were also tested. Solutions were allowed to equilibrate for 15 min before taking the measurement. Figure 1 clearly showed that only cyanide ion changed the absorption signal, absorption bands diminished, while new band at 345 nm, showed up. The change of the color could be observed clearly by naked eyes.

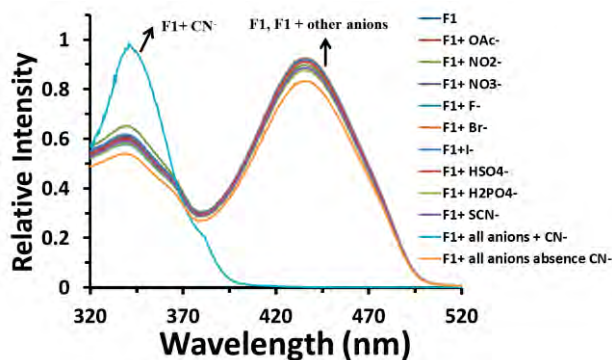


Figure 1. Absorption spectra of **F1** (2×10^{-5} M) in water/THF 40:60, v/v) solution with and without anions OAc^- , NO_2^- , NO_3^- , F^- , Cl^- , Br^- , I^- , HSO_4^- , H_2PO_4^- , and SCN^- (20 equiv each). The absorption spectra of **F1** (2×10^{-5} M) changed upon the addition of CN^- anion (3 eq.).

The fluorescence signal of **F1** ($1 \mu\text{M}$) was monitored by titration in a mixed solution of 40:60 (v/v) water/THF upon excitation at 360 nm. The addition of 20 eq. of eleven anions abovementioned showed that no significant change was observed at the absorption spectra. To study the selectivity of **F1** for cyanide detection (3 eq.), Figure 2(a) showed that only cyanide ion could enhance the fluorescent signal. Unlike other ions tested, **F1** probe demonstrated high selectivity of cyanide ion. The interference test was also conducted by adding cyanide and other anions into the **F1** solution. The results proved that the **F1** probe still could detect cyanide ion in the mixture solution as shown in Figure 2(b).

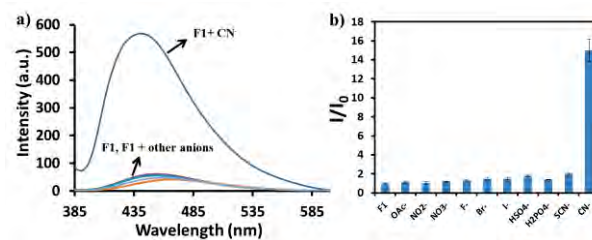


Figure 2. (a) Fluorescence spectra of **F1** and **F1** + each 10 anions (b) Histograms of I/I_0 obtained from the corresponding fluorescence spectra. ($\lambda_{\text{ex}} = 360$ nm; Medium = water/THF (40:60, v/v); [**F1**] = $1 \mu\text{M}$; [9 other anion] = $20 \mu\text{M}$, [CN^-] = $3 \mu\text{M}$).

The degree of the fluorescence intensity change ($(I - I_0)/I_0 \times 100$) was plotted against the cyanide concentration in the range of 0- $40 \mu\text{M}$. It presented a linear line (Figure 3). The plot also gave the detection limit (at $3 \times \text{noise}$) of cyanide ion as $2.0 \mu\text{M}$ or 40 ppb. This is below the concentration limit of $2.7 \mu\text{M}$ allowed to be presented in drinking water by WHO guideline.

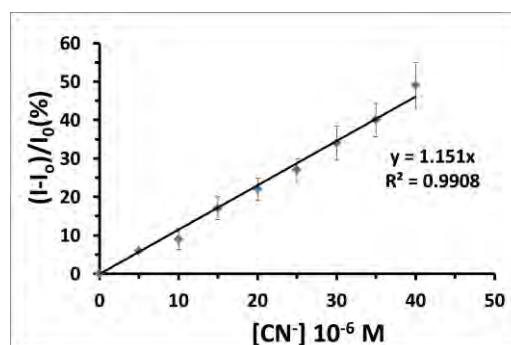


Figure 3. A plot of the fluorescence intensity change ($(I - I_0)/I_0 \times 100$) of **F1** vs $[\text{CN}^-]$. ($\lambda_{\text{ex}} = 360$ nm; $\lambda_{\text{em}} = 445$ nm; Medium = water/THF (40:60, v/v); [**F1**] = $1 \mu\text{M}$; 15 min).

The interaction of **F1** with cyanide anion exhibited the changes in ^1H NMR experiments. Figure 4 showed the ^1H NMR spectra of **F1** upon the addition of sodium cyanide in Acetone- d_6 solution. The addition of cyanide resulted in a slow reduction of the vinylic proton signal H(e) at 8.20 ppm and finally disappeared with addition of 1 eq. of cyanide. However, a new signal appeared at 4.32 ppm, which corresponded to the H(e') proton. Thus, the results were consistent with the proposed mechanism that cyanide was added to the α position of dicyanoethylene group. Meanwhile, the shield shift of two sets of aromatic proton (Ha & Hb, Hc & Hd) were observed. Ha & Hb presented a strong shield shift at the ortho and meta position due to its close proximity to the ethylene group. In contrast, Hc & Hd showed slightly shield shift due to its long distance of cyanohydrin group. After the cyanide anion was added to the vinyl group, the electron density of **F1** increased

- [9] Y. D. Lin, Y. S. Peng, W. Su, C. H. Tu, C.H. Sun and T. J. Chow, *Tetrahedron* **68** (2012) 2523-2526.

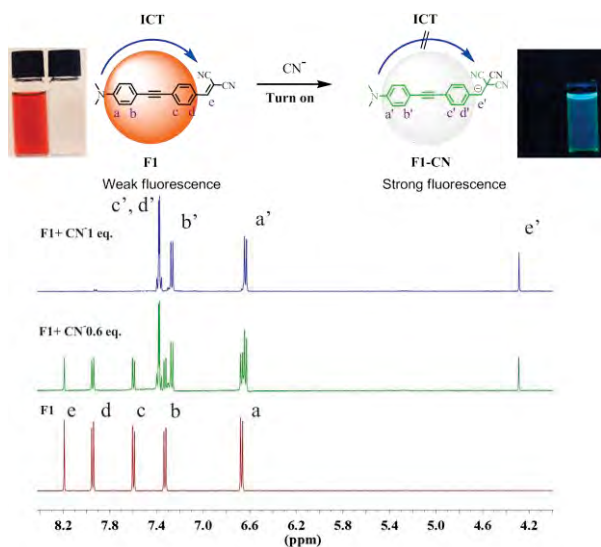


Figure 4. ^1H NMR spectral changes of **F1** in Acetone- d_6 upon the addition of CN^- anion.

4. Conclusions

In summary, we synthesized a novel fluorophore containing dicyano as a selective probe for CN^- by using sonogashira reaction. The **F1** displayed the highest selective cyanide detection via naked eyes and a fluorescent “turned on” in water media. The method showed a linear range of cyanide concentration in micromolar unit. The results exhibited the detection limit of $2.0\ \mu\text{M}$, which was lower than the CN^- contaminated allowance in drinking water determined by WHO guideline.

Acknowledgements

This work was supported by Faculty of Science, King Mongkut's University of Technology Thonburi, Bangkok, Organic Chemistry Institute, University of Zurich, Zurich, Switzerland and KMUTT Research Fund.

References

- [1] C. Young, L. Tidwell, C. Anderson, *Cyanide: Social, Industrial, and Economic Aspects*; Minerals, Metals, and Materials Society: Warrendale, 2001.
- [2] Vetter, J., *Toxicol.* **38** (2000) 11–36.
- [3] T. F. Cumming., *Occupational Medicine*. **54** (2004). 82-85.
- [4] Guidelines for drinking-water quality; 3rd ed.; World Health Organization: Geneva, 2004. Also available at http://www.who.int/water_sanitation_health/dwq/guidelines/en
- [5] Bhattacharya, R. and Flora, S. J. S. In *Handbook of Toxicology of Chemical Warfare Agents*. pp 255-270. Gupta, R. C., Ed.; Academic Press: Boston (2009).
- [6] J. Yoshino, M. Kano, and T. Kawashima, *J. Org. Chem.* **74** (2009) 7496-7503.
- [7] L. Peng, M. Wang, G. Zhang, D. Zhang and D. Zhu, *Org. Lett.* **11** (2009) 1943–1946.
- [8] N. Niamnont, W. Siripornnoppakhun, P. Rashatasakhon and M. Sukwattanasinitt, *Org. Lett.* **13** (2009) 2768-2771.

CHEMICAL CONSTITUENTS AND ANTICANCER ACTIVITIES FROM *CAESALPINIA SAPPAN* L

PhakinManosri, BordinChitkul*

Department of Chemistry and Center of Excellence for Innovation in Chemistry, Faculty of Science, Ramkhamhaeng University, Bangkok, 10240 Thailand

*E-mail: b_chitkul@ru.ac.th, +66-2-3191900

Abstract: 3,10-di-O-Methylbrazilin, a new derivative of brazilin, was isolated from *Caesalpiniasappan* heartwoods, together with four known compounds identified as protosappanin A, 3-deoxysappanchalcone, 3-deoxysappanone B and brazilin. These isolated compounds were tested for inhibitory activity against KB-Oral cavity cancer and NCI-H187-small cell lung cancer. 3-Deoxysappanone B exhibited anticancer activity against KB-Oral cavity cancer with IC_{50} 3.74 μ g/ml whereas brazilin exhibited anticancer activity against NCI-H187-small cell lung cancer with IC_{50} 4.20 μ g/ml.

1. Introduction

*Caesalpineasappan*L, known locally as “Phang” in Thai, is found in China, India, Burma, Thailand, Indonesia, Vietnam and South India. The tree is cultivated in the gardens, 6-9m in height. The leaves are compound with 8-12 pairs of oblong leaflets and small prickles. Flowers are yellow in terminal and auxiliary pinnacles, fruits are woody pods. Wood is orange-red, hard and very heavy [1-2].

The heartwood has been used in Chinese traditional medicine as analgesic and anti-inflammatory agent. The small core of heartwood produces a dark red solution in water and is being used as herbal drinking water [3-4]. Its various biological activities include antioxidant activity, anti-bacteria activity, anti-arthritis activity, and anti-acne agent [5-7].

Anticancer agents in this plant have been reported to possess DNA strand-nicking ability [8]. In the preceding papers, we report the isolation and elucidation of five compounds and inhibitory activity against KB-Oral cavity cancer and NCI-H187-small cell lung cancer.

2. Materials and Methods

2.1 Plant materials

The heartwoods of *Caesalpineasappan* L were collected in Karnjanaburi province, Thailand in December 2010.

2.2 General experimental procedures

The IR spectra were obtained using a Perkin-Elmer FT-IR spectrum 400 spectrometer (ATR). The 1H and ^{13}C NMR spectra were recorded with a Bruker AVANCE 400 MHz spectrometer. Mass spectra

obtained by Electrospray mass spectra (ESMS) were determined on Finnigan LC-Q mass spectrometers.

2.3 Anticancer activity

The anticancer activities of the pure compounds of heartwood from *Caesalpineasappan*L were determined by Resazurin Microplate assay (REMA) using KB-Oral cavity cancer (Oral Cavity cancer, ATCC CCL-17) and NCI-H187-Small cell lung cancer (Human small cell lung carcinoma, ATCC CRL-5804). This assay was performed using the method described by previous report [9]. The compounds were first diluted to 50 μ g/ml in 0.5% DMSO and then subjected to a doubling series of dilutions. Cells at the logarithmic growth phase were harvested and diluted to 7×10^4 cells/ml for KB and 9×10^4 cells/ml for MCF-7 and NCI-H187, in fresh medium. Successively, 5 μ l of each sample solution and 45 μ l cell suspensions were added to 96-well plates, incubated at 37°C in 5% CO_2 in an incubator. After the incubation period (3 days for KB and MCF-7 and 5 days for NCI-H187), 12.5 μ l resazurin solutions (62.5 μ g/ml) were added to each well, and the plates were then incubated at 37°C for 4 h. The fluorescence was measured using a SpectraMax M5 multi-detection microplate reader (Molecular Devices, USA) at excitation and emission wavelengths of 530 and 590 nm. The percentage inhibition of cell growth (%) was calculated as $[1 - (FUT/FUC)] \times 100$ where FUT and FUC are the mean fluorescent units from treated and untreated conditions, respectively. The IC_{50} values were derived from the dose-response curves using the SOFTMax Pro software. Ellipticine and doxorubicin were used as positive controls and 0.5% DMSO was used as a negative control.

2.5 Extraction and isolation

The air-dried ground heartwoods (2.5 kg) of *Caesalpineasappan*L were successively extracted at room temperature with ethanol (3×6 L, each 5 days). The crude extracts were evaporated under reduced pressure to afford brownish ethanol (300.74 g). The crude ethanol extract was extracted with EtOAc and water, and the organic portions were evaporated under reduced pressure to afford a reddish EtOAc extract (175.68 g). The residue was further purified by column chromatography (CC) on silica gel using hexane as eluent and increasing polar with EtOAc to give nine

fractions (C1-C9). Fraction C2 (30.83 g) was further purified by CC with EtOAc-hexane (30:70) to give 5(35.5 mg). Fraction C1 (3.12 g) was subjected to CC with EtOAc-hexane (30:70) to afford nine fractions (C4a-C4i). Subfraction C4b (86.7 mg) was separated by CC with EtOAc-hexane (40:60) to give 2 (26.3 mg). Subfractions C4d (65.3 mg) was purified by CC with EtOAc-hexane (40:60) to give 3 (36.5 mg). Fraction C5 (7.3 g) was recrystallized from EtOAc and hexane to give 1 (2.14 g). Fraction C5 (6.93 g) was purified by CC with EtOAc-hexane (60:40) to give 4 (3.24 g).

2.5.1. protosappanin A (1)

White solid; R_f = 0.61 (60:40, Hexane-Ethyl acetate); m.p. 110-122 °C; Negative-ion ES-MS m/z (rel. int.%): 269.2 [M+H]⁻ (100). ¹H NMR (400 MHz, DMSO-*d*₆): δ_H 10.23 (1H, s, 3-OH), 9.48 (1H, s, 10-H), 9.46 (1H, s, 11-H), 7.57 (1H, d, *J* = 8.6 Hz, 1-H), 7.18 (1H, d, *J* = 8.6 Hz, 2-H), 7.15 (1H, s, 9-H), 7.14 (1H, s, 12-H), 7.13 (1H, s, 4-H), 4.97 (2H, s, 6-CH₂), 3.81 (2H, s, 8-CH₂). ¹³C NMR (100 MHz, DMSO-*d*₆): δ_C 205.8 (C-7), 158.6 (C-4a), 157.7 (C-3), 144.8 (C-11), 144.6 (C-10), 129.9 (C-1, 1a), 125.4 (C-8a), 123.2 (C-12a), 117.1 (C-9), 116.9 (C-12), 112.6 (C-2), 108.3 (C-4), 77.9 (C-6) and 48.3 (C-8). The data were identified by comparison of its ¹H-NMR and ¹³C NMR data reported for this compound [10].

2.5.2. 3-deoxysappanalcone (2)

Orange solid; R_f = 0.66 (50:50, Hexane-Ethyl acetate); m.p. 98-102 °C; Negative-ion ES-MS m/z (rel. int.%): 269.7 [M+H]⁻ (100). ¹H NMR (400 MHz, DMSO-*d*₆): δ_H 10.23 (1H, s, 13-OH), 9.99 (1H, s, 3-OH), 3.82 (3H, s, 5-OCH₃), 7.50 (2H, d, *J* = 8.4 Hz, 11-H, 15-H), 7.49 (1H, d, *J* = 8.4 Hz, 1-H), 7.45 (1H, d, *J* = 16.0 Hz, 8-H), 7.34 (1H, d, *J* = 16.0 Hz, 9-H), 6.80 (2H, d, *J* = 8.4 Hz, 12-H, 14-H), 6.48 (1H, d, *J* = 1.6 Hz, 4-H), 6.43 (1H, dd, *J* = 1.6, 8.4 Hz, 2-H). ¹³C NMR (100 MHz, DMSO-*d*₆): δ_C 188.9 (C-7), 162.5 (C-3), 160.3 (C-5), 159.5 (C-13), 141.5 (C-8), 141.3 (C-1), 130.1 (C-11, 15), 125.9 (C-10), 123.9 (C-9), 120.2 (C-6), 116.3 (C-4, C-12, C-14) and 55.6 (OCH₃ at C-5). The data were identified by comparison of its ¹H-NMR and ¹³C NMR data reported for this compound [11].

2.5.2.3-deoxysappanone B (3)

Colorless powder; R_f = 0.45 (45:55, Hexane-Ethyl acetate); m.p. 105-108 °C; Negative-ion ES-MS m/z (rel. int.%): 285.7 [M+H]⁻ (100). ¹H NMR (400 MHz, DMSO-*d*₆): δ_H 11.08 (1H, s, 7-OH), 9.30 (1H, s, 4'-OH), 9.23 (1H, s, 3'-OH), 8.15 (1H, d, *J* = 8.4 Hz, 5-H), 7.18 (1H, d, *J* = 7.6 Hz, 5'-H), 7.10 (1H, s, 2'-H), 7.00 (1H, d, *J* = 8.4 Hz, 6-H), 6.97 (1H, d, *J* = 7.6 Hz, 6'-H), 6.81 (1H, s, 8-H), 4.78 (1H, dd, *J* = 8.0, 4.0 Hz, 2-Hb), 4.58 (1H, dd, *J* = 8.0, 4.0 Hz, 2-Ha), 3.41 (1H, dd, *J* = 14.0, 10.0 Hz, 9-Hb), 3.29 (2H, m, 3-H), 2.97 (1H, dd, *J* = 14.0, 10.0 Hz, 9-Hb), ¹³C NMR (100 MHz, DMSO-*d*₆): δ_C 191.5 (C-4), 164.4 (C-7), 163.0 (C-8a), 145.1 (C-4'), 143.6 (C-3'), 129.1 (C-4a), 128.8 (C-5), 119.6 (C-6'), 116.5 (C-2'), 115.5 (C-5'), 113.1 (C-1'),

110.6 (C-6), 102.2 (C-8), 69.4 (C-2), 46.5 (C-3) and 31.2 (C-9). The data were identified by comparison of its ¹H-NMR and ¹³C NMR data reported for this compound [12].

2.5.3 brazilin (4)

Reddish-pale; R_f = 0.50 (40:60, Hexane-Ethyl acetate); Negative-ion ES-MS m/z (rel. int.%): 285.6 [M+H]⁻ (100). ¹H NMR (400 MHz, DMSO-*d*₆): δ_H 9.80 (1H, s, 3-OH), 9.18 (1H, s, 9-OH), 9.15 (1H, s, 10-OH), 7.65 (1H, d, *J* = 8.4 Hz, 1-H), 7.15 (1H, s, 8-H), 7.06 (1H, s, 11-H), 6.93 (1H, d, *J* = 8.4 Hz, 2-H), 6.73 (1H, s, 4-H), 4.36 (1H, s, 12-H), 4.35 (1H, d, *J* = 11.2 Hz, 6-Ha), 4.08 (1H, d, *J* = 11.2 Hz, 6-Hb), 3.39 (1H, d, *J* = 16.0 Hz, 7-Ha), 3.21 (1H, d, *J* = 16.0 Hz, 7-Hb). ¹³C NMR (100 MHz, DMSO-*d*₆): δ_C 156.5 (C-4a), 154.1 (C-3), 144.3 (C-10), 144.0 (C-9), 135.6 (C-11a), 130.9 (C-1), 129.8 (C-7a), 144.4 (C-1a), 112.1 (C-8), 111.7 (C-11), 108.8 (C-2), 102.8 (C-4), 76.4 (C-6), 69.6 (C-6a) and 49.6 (C-12). The data were identified by comparison of its ¹H-NMR and ¹³C NMR data reported for this compound [13].

2.5.3 3,10-di-O-methylbrazilin (5)

Pale yellow; R_f = 0.65 (75:25, Hexane-Ethyl acetate); Negative-ion ES-MS m/z (rel. int.%): 297.3 [M+H]⁻ (100). ¹H NMR (400 MHz, DMSO-*d*₆): δ_H 6.95 (1H, d, *J* = 8.0 Hz, 1-H), 6.78 (1H, d, *J* = 8.0 Hz, 11-H), 6.67 (1H, d, *J* = 2.0 Hz, 4-H), 6.55 (1H, dd, *J* = 2.0 Hz, 8-H), 6.81 (1H, s, 4-H), 6.73 (1H, d, *J* = 8.0, 2.0 Hz, 10-H), 6.41 (1H, d, *J* = 8.0, 2.0 Hz, 2-H), 6.39 (1H, d, *J* = 2.0 Hz, 8-H), 3.95 (1H, d, *J* = 11.0 Hz, 6-Hb), 3.74 (1H, d, *J* = 11.0 Hz, 6-Ha), 2.52 (1H, d, *J* = 16.0 Hz, 7-Ha), 2.51 (1H, d, *J* = 16.0 Hz, 7-Hb). ¹³C NMR (100 MHz, DMSO-*d*₆): δ_C 157.7 (C-4a), 154.8 (C-3), 145.9 (C-9), 144.2 (C-11a), 132.6 (C-1), 127.6 (C-7a), 123.3 (C-11), 113.7 (C-4), 113.3 (C-10), 111.7 (C-6a), 107.8 (C-2), 103.5 (C-8), 77.6 (C-12), 67.5 (C-6), 55.9 (OCH₃), 55.8 (OCH₃) and 39.4 (C-7).

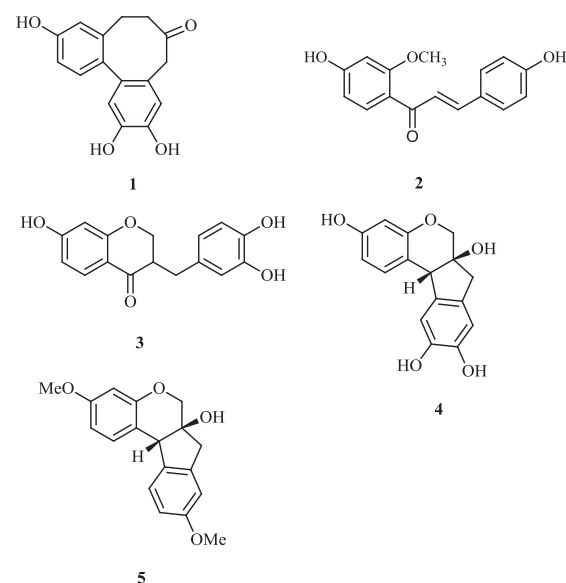


Figure 1. Chemical structure of five compounds from *Caesalpineia sappan* L

3. Results and Discussion

Phytochemical investigation of an ethanol extract of *Caesalpineasappan* L heartwoods led to the isolation of one new compound named 3,10-di-O-methylbrazilin (5) together with four known compounds, protosappanin A (1), 3-deoxysappanchalcone (2), 3-deoxysappanone B (3), and brazilin (4).

The structures of these constituents were elucidated by spectroscopic techniques including 1D and 2D NMR and mass spectrometry.

Compound 5 was obtained as a pale yellow. Two splitting patterns of 1,2,4-trisubstituted aromatic ring were also inferred from the presence of δ_{H} 6.95 (1H, d), 6.41 (1H, dd) and 6.67 (1H, d) and another one is 6.55 (1H, dd), 6.78 (1H, d) and 6.39 (1H, d). The splitting patterns of other proton are likely pattern of brazilin. The HMBC data from ^1H NMR show a significant signal of methoxy group at δ_{C} 154.8 (C-3) and δ_{C} 145.9 (C-9) are adjacent to δ_{C} 132.6 (C-1), δ_{C} 157.7 (C-4a) and δ_{C} 123.3 (C-11), δ_{C} 127.6 (C-7a) respectively. Consequently the structure of 5 was elucidated to (6aS,11bR)-3,9-dimethoxy-6,6a,7,11b-tetrahydroindeno[2,1-c]chromen-6a-ol and this compound has been named 3,10-di-O-methylbrazilin.

Table 1: Anti-cancer activity of compounds 1-4 from *Caesalpineasappan* L against KB-Oral cavity cancer and NCI-H187-Small cell lung cancer

Compounds	Concentration $\mu\text{g/ml}$	
	KB-Oral	NCI-H187
1	11.42	17.00
2	8.60	12.70
3	3.74	9.73
4	5.42	4.20
5	NT	NT
Doxorubicin	0.147	0.041

NT = not tested.

4. Conclusions

Chemical investigation of an acetone extract of *Caesalpineasappan* L heartwoods has resulted in the separation of one new compound (5) together with four known compounds.

3-Deoxysappanone B exhibited the highest anticancer activity against KB-Oral cavity cancer with IC_{50} 3.74 $\mu\text{g/ml}$ whereas brazilin exhibited highest anticancer activity against NCI-H187-small cell lung cancer with IC_{50} 4.20 $\mu\text{g/ml}$.

Acknowledgements

We are grateful to Professor Sittichai Koontongkaew, faculty of Dentistry, Thammasat University, for supported with anti-cancer testing.

References

- [1] O. Yodsauae, S. Cheenpracha and C. Karalai, C. Ponglimanont, S. Chantrapromma, H.K. Fun and A. Kanjana-Opas, *Phytochemistry* **69** (2008) 1242–1249.
- [2] C.R. Pawar, A.D. Landge and S.J. Surana, *J. Of Pharmacy Research* **2** (2008) 131–138.
- [3] X. Yan, W. Wang, D. Xing, Y. Zhao and L. D, *J. Chromatogr. A* **1077** (2005) 44–48.
- [4] S. Badami, S. Moorkoth and B. Suresh, *Nat pro Radianc* **2** (2004) 75–82.
- [5] V.L. Narajan Reddy, V. Ravikanth, V.V.N.S. Jansi Lakshmi, U. Suryanayan Murty and Y. Venkateswarlu, *Fitoterapia* **74** (2003) 600–602.
- [6] Y.Z. Wang, S.Q. Sun and Y.B. Zhou, *Journal of Ethnopharmacology* **136** (2011) 271–278.
- [7] S. S. Badami, S. Moorkoth, S. Rammanoharsingh Rai, E. Kannan and S. Bhojraj, *Biol. Pharm. Bull.* **26** (2003) 1534–1537.
- [8] I. Batubara, T. Mitsunaga and H. Ohashi, *J Wood Sci* **56** (2010) 77–81.
- [9] J. O'Brein, I. Wilson, T. Orton and F. Pognan, *Eur. J. Biochem.* **267** (2000) 5421–5426.
- [10] M. Nakai, S. Nagumo, S.M. Lee, I. Eguchi and K.I. Kaeai, *Chem. Pharm. Bull.* **34** (1986) 1–6.
- [11] M. Namikichi, H. Nagata, M. Nuo, T. Ozawa and T. Saitoh, *Chem. Pharm. Bull.* **35** (1987) 3568–3575.
- [12] L.C. Fu, X.A. Huang, Z.Y. Lai, Y.J. Hi, H.J. Liu and X.A. Cai, *Molecules* **13** (2008) 1923–1930.
- [13] D.K. Sim, N.I. Baek, S.R. Oh, K.Y. Jung, I.S. Lee and H.K. Lee, *Phytochemistry* **46** (1997) 177–178.

SIMPLE AND ENVIRONMENTALLY FRIENDLY SYNTHESIS OF BIS(HETEROARYL)ALKANES VIA BISARYLATION OF ALDEHYDES

Surisa Tuengpanya¹, Jaray Jaratjaroonphong^{1*}

¹Department of Chemistry and Center for Innovation in Chemistry, Faculty of Science, Burapha University, Bangsaen, Chonburi, 20131 Thailand

*Jaray Jaratjaroonphong; E-Mail: jaray@buu.ac.th, Tel. +66 38103053, Fax. +66 38393494

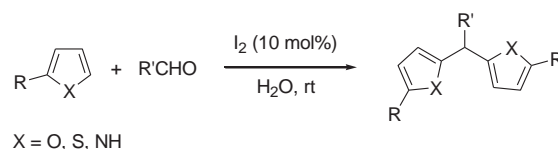
Abstract: An efficient synthesis of bis(heteroaryl)alkanes has been developed *via* bisarylation of heteroarenes with aldehydes using less expensive, readily available, and environmentally friendly iodine catalyst in water under ‘open-flask’ and mild conditions. In the presence of 10 mol% of iodine in water at room temperature affords the corresponding bis(heteroaryl)alkanes, selectively, in moderate to excellent yields.

1. Introduction

The synthesis of bis(heteroaryl)alkanes has attracted considerable attention from organic chemists and many such compounds have found widespread applications in synthetic, medicinal, and industrial chemistry.¹⁻⁹ Methods for the synthesis of bis(heteroaryl)alkanes have been developed. The available methods for the construction of bis(heteroaryl)alkanes frameworks are based on the bisarylation of electron-rich arenes with aldehydes and their imines¹⁰ in the presence of Lewis acids such as AuCl₃/AgOTf,¹¹ [Ir(-COD)Cl]₂-SnCl₄,¹² FeCl₃,¹³ Cu(OTf)₂/(±)-BI-NAP,^{14,15} ZnBr₂/SiO₂,¹⁶ PMHS-B(C₆F₅)₃,¹⁷ Yb(OTf)₃,¹⁸ Gd(OTf)₃,¹⁹ Guanidinium ionic liquid,²⁰ and FeCl₃·6H₂O.²¹ However, most of methods reported are associated with one or more disadvantages such as multi-steps process, high catalyst loading, high temperature, long reaction time and environmental unfriendliness. Furthermore, the aldehydes appear to limit to only nonenolizable aldehydes. The investigate for cheap, environmentally friendly catalysts, and mild reaction conditions is still a major challenge.²²

During the last decades, molecular iodine has received significant attention in organic synthesis and pharmaceutical due to its inexpensive, non toxic and environmental friendly characteristics.^{23,24} Iodine has a high tolerance to air as well as moisture and can be easily removed from the reaction system. Moreover, the mild Lewis acidity associated with iodine has led to its use in various organic transformation in catalytic to stoichiometric amounts.

In continuation of our interest on the use of molecular iodine for various transformation,^{25,26} herein, we wish to report a simple and environmentally friendly synthesis of bis(heteroaryl)alkanes *via* bisarylation of heteroarenes with aldehydes using iodine as catalyst under “open-flask” and aqueous conditions at room temperature (Scheme 1).



Scheme 1. Bisarylation of heteroarenes with aldehydes to produce bis(heteroaryl)alkanes

2. Materials and Methods

2.1 General methods

The high resolution 400 MHz ¹H NMR, together with 100 MHz ¹³C NMR spectra were performed on Bruker DPX-400 spectrometers at chemistry department, faculty of science, Burapha university and all spectra were measured in CDCl₃ solvent. The IR spectra were recorded on a Perkin Elmer System 2000 FT-IR. High resolution mass spectra were recorded on Finnigan MAT 95. Radial chromatography on a Chromatotron was performed using Merck silica gel 60 PF₂₅₄ with CaSO₄ 1/2 H₂O and was activated by heating in an oven at 80 °C for 45 min. Thin layer chromatography (TLC) was performed with Merck silica gel 60 PF₂₅₄ aluminium plate.

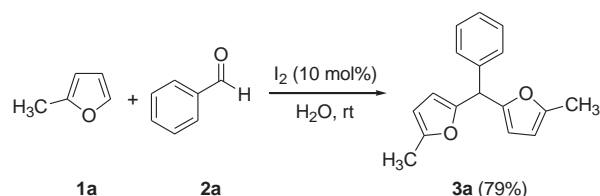
2.2 General procedure for synthesis bis(heteroaryl)-alkanes

To a water solution (1 mL) of arenes (2 mmol) and aldehydes (1 mmol) in a test-tube open to air at room temperature was added molecular iodine as catalyst (0.1 mmol, 10 mol%). The reaction was stirred until completion (TLC analysis). The reaction mixture was quenched with aqueous Na₂S₂O₃ (10 mL) and extracted with CH₂Cl₂ (2 x 10 mL). The combined organic layer was washed with brine (10 mL), dried over anhydrous Na₂SO₄, concentrated and purified by radial chromatography (hexanes/EtOAc as eluent) to give **3**.

3. Results and Discussions

We first examined the reaction of 2-methylfuran (**1a**) with benzaldehyde (**2a**) using iodine as the catalyst under open test-tube at room temperature. Additionally, the reaction was performed in water as a reaction medium due to its many advantages from economical, environmental, and safety standpoints.²⁷ Gratifyingly, treatment of 2-methylfuran (2 equiv)

with benzaldehyde (1 equiv) in the presence of 10 mol % of iodine in H₂O and stirring the reaction for 72 h afforded the bis(5-methylfur-2-yl)phenylmethane **3a**,²⁸ selectively, in good yields (Scheme 2) and this conditions was chosen as standard condition for further studied. As anticipated, no any conversion to product was obtained in the absence of iodine catalyst even after 72 h.



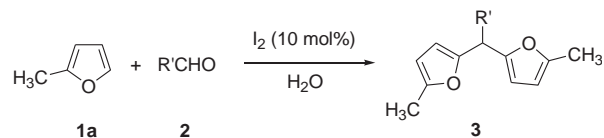
Scheme 2. Model reaction for the synthesis of bis(heteroaryl)alkanes

Following the optimization of the reaction conditions, we examined the bisarylation of 2-methylfuran with different aldehydes including both aliphatic and aromatic aldehydes (Table 1). As the results shown in Table 1, aromatic aldehyde having an electron-withdrawing substituent on the aromatic ring (Table 1, entries 2-4) gave the desired products **3b-d** in moderate yields. The reaction of aromatic aldehyde having an electron donating substituents on the aromatic ring (entry 5) also reacted smoothly to provide compound **3e** in moderate yield. It should be noted that under our experimental condition, the reaction of aliphatic aldehydes were also successful. The corresponding bis(5-dimethylfur-2-yl)alkanes **3f-h** were obtained in good to excellent yields (entries 6-8). It could also be concluded that the reaction of aromatic aldehydes required longer reaction time and gave lower yields of the products than those of aliphatic aldehydes.

We next explored the iodine catalyzed bisarylation of various heteroarenes with either aromatic or aliphatic aldehydes for the synthesis of the corresponding bis(heteroaryl)alkanes. The results presented in Table 2 show that all the reactions gave selective formation of bis(heteroaryl)alkane derivatives. The reaction of 2-ethylfuran with aliphatic aldehyde, 3-phenylpropanal, gave the desired product **3i** in excellent yield (Table 2, entry 3). Remarkably, to our great satisfaction, under iodine catalysis in water, even 2-methylthiophene possessing less reactivity reacted smoothly with both benzaldehyde and 3-phenylpropanal to give **3j** and **3k**, respectively, in fair yields (entries 4 and 5), although 5 equivalent of 2-methylthiophene was required. By lowering the catalyst loading to 2.5 mol% (entry 6), the reaction of pyrrole with 4-nitrobenzaldehyde containing electron-withdrawing groups attached to the benzene ring (NO₂) gave the corresponding bis(pyrrolyl)alkanes **3l**

in 60% yields. On the other hand, the reaction of pyrrole with 3-phenylpropanal gave **3m** as the product in lower yield (entry 7).

Table 1 I₂-catalyzed reaction of 2-methylfuran (**1a**) with various aldehydes^a



Entry	R'CHO	Products	Yield ^b (%)
1	C ₆ H ₅ CHO	3a	79 ^c
2	4-F-C ₆ H ₄ CHO	3b	45 ^c
3	4-Br-C ₆ H ₄ CHO	3c	53 ^c
4	4-O ₂ N-C ₆ H ₄ CHO	3d	31 ^d
5	4-CH ₃ O-C ₆ H ₄ CHO	3e	49
6	PhCH ₂ CH ₂ CHO	3f	99
7	(CH ₃) ₂ CHCH ₂ CHO	3g	68
8	(CH ₃) ₂ CHCHO	3h	79

^a Reaction conditions: **1a** (2 mmol), **2** (1 mmol), I₂ (10 mol %), water (1 mL), room temperature.

^b Isolated yield.

^c The reaction was carried out for 72 h.

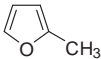
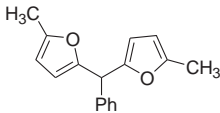
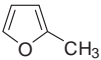
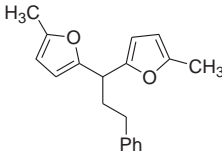
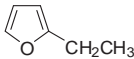
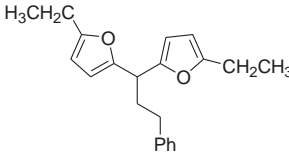
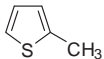
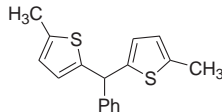
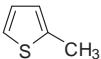
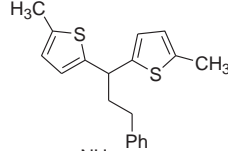
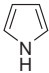
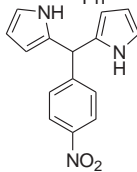
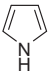
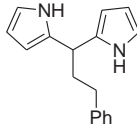
^d The reaction mixture solidified after stirring for 38 h.

Based on the above experimental results, we proposed a possible reaction mechanism for this molecular iodine-catalyzed bisarylation, as shown in Scheme 3.^{29,30} Initially, the carbonyl group of the aldehyde substrate was activated with molecular iodine which is a mild Lewis acidity to give intermediate **I**, and is followed by heteroarenes attack to **I** to give **II**. Then, dehydration and deiodination of **II** afforded intermediate **III**. Finally, addition of the second molecule of heteroarene to **III** gave the bis(heteroaryl)alkanes **IV** as the desired product and molecular iodine can catalyze the reaction in a catalytic manner.

4. Conclusions

In conclusion, we have shown that iodine can be used as an efficient catalyst for the synthesis of bis(heteroaryl)alkanes *via* bisarylation between heteroarenes with a wide variety of aldehydes in water under "open-flask" and mild conditions. The reaction of heteroarenes with aromatic and aliphatic aldehydes provides the corresponding bis(heteroaryl)alkane derivatives in moderate to excellent yields. The use of mild reaction conditions, commercially available as well as inexpensive catalyst, low catalytic loading, eco-friendly method and single step synthesis are the advantages of the present procedure. Further investigations on the scope and limitations of this reaction are in progress.

Table 2 I₂-catalyzed reaction of various arenes with aliphatic and aromatic aldehydes.^a

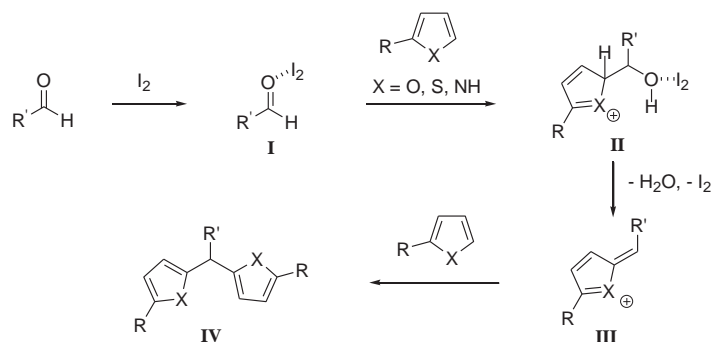
		Ar-H		+	R'CHO	$\xrightarrow[\text{H}_2\text{O, rt, air}]{\text{I}_2 (10 \text{ mol}\%)}$	$\text{Ar}-\text{C}(\text{R}')-\text{Ar}$		
		1	2				3		
Entry	Ar-H	R'CHO	Time (h)	Products		Yield (%) ^b			
1	 1a	C ₆ H ₅ CHO	72		3a	79			
2	 1a	C ₆ H ₅ CH ₂ CH ₂ CHO	24		3f	99			
3	 1b	C ₆ H ₅ CH ₂ CH ₂ CHO	5		3i	98			
4	 1c	C ₆ H ₅ CHO	48		3j	23 ^c			
5	 1c	C ₆ H ₅ CH ₂ CH ₂ CHO	3		3k	30			
6	 1c	4-O ₂ NC ₆ H ₄ CHO	4		3l	60 ^e			
7	 1c	C ₆ H ₅ CH ₂ CH ₂ CHO	2		3m	22			

^a Reaction conditions: **1a** (2 mmol), **2** (1 mmol), I₂ (10 mol %), water (1 mL), room temperature.

^b Isolated yield

^c Reaction conditions: **1b** (5 mmol)

^e The reaction was carried out at using I₂ (2.5 mol%).



Scheme 3. The possible mechanism for the reaction of heteroarenes with aldehydes.

Acknowledgements

We thank the Thailand Research Fund for financial support MRG5280024 to J.J. Financial support from the Center of Excellence for Innovation in Chemistry (PERCH-CIC), Office of the Higher Education Commission, Ministry of Education, a Grant from the Faculty of Science, Burapha University, Thailand and Burapha annual Grant (47419) are also gratefully acknowledged.

References

- [1] V. Nair, S. Thomas, S. C. Mathew and K. G. Abhilash, *Tetrahedron* **62** (2006) 6731–6747.
- [2] C. T. Walsh, S. Garneau-Tsodikova and A. R. Howard-Jones, *Nat. Prod. Rep.* **23** (2006) 517–531.
- [3] M. S. Shchepinov and V. A. Korshun, *Chem. Soc. Rev.* **32** (2003) 170–180.
- [4] A. V. Butin, T. A. Stroganova and V. G. Kul'nevich, *Chem. Heterocycl. Compd.* **35** (1999) 757–787.
- [5] V. Nair, S. Thomas, S. C. Mathew, N. Vidya and N. P. Rath, *Tetrahedron* **61** (2005) 9533–9540.
- [6] P. S. Naidu and P. J. Bhuyan, *Tetrahedron Lett.* **53** (2012) 426–428.
- [7] M. K. Parai, G. Panda, V. Chaturvedi, Y. K. Manju and S. Sinha, *Bioorg. Med. Chem. Lett.* **18** (2008) 289–292.
- [8] A. R. Katritzky, L. Xie and W.-Q. Fan, *J. Org. Chem.* **58** (1993) 4376–4381.
- [9] E. Thiery, D. Harakat, J. L. Bras and J. Muzart, *Organometallics* **27** (2008) 3996–4004.
- [10] Y. Leng, F. Chen, L. Zuo and W. Duan, *Tetrahedron Lett.* **51** (2010) 2370–2373.
- [11] V. Nair, K. G. Abhilash and N. Vidya, *Org. Lett.* **7** (2005) 5857–5859.
- [12] S. Podder, J. Choudhury, U. K. Roy and S. Roy, *J. Org. Chem.* **72** (2007) 3100–3103.
- [13] Z. Wang, X. Sun and J. Wu, *Tetrahedron* **64** (2008) 5013–5018.
- [14] J. Esquivias, R. Gómez-Arrayás, J. C. Carretero, *Angew. Chem. Int. Ed.* **45** (2006) 629–633.
- [15] N. Alonso, J. Esquivias, R. Gómez-Arrayás, J. C. Carretero, *J. Org. Chem.* **73** (2008) 6401–6404.
- [16] M. Kodomari, M. Nagamatsu, M. Akaike and T. Aoyama, *Tetrahedron Lett.* **49** (2008) 2537–2540.
- [17] S. Chandrasekhar, S. Khatun, G. Rajesh and C. R. Reddy, *Tetrahedron Lett.* **50** (2009) 6693–6697.
- [18] S. Genovese, F. Epifana, C. Pelucchini and M. Curini, *Eur. J. Org. Chem.* (2009) 1132–1135.
- [19] B. Temelli and C. Unaleroglu, *Tetrahedron* **62** (2006) 10130–10135.
- [20] K. Rad-Moghadam and M. Sharifi-Kiasaraie, *Tetrahedron* **65** (2000) 8816–8820.
- [21] P. Thirupathi and S. S. Kim, *J. Org. Chem.* **75** (2010) 5240–5249.
- [22] Z. Li, Z. Duan, J. Kang, H. Wang, L. Yu and Y. Wu, *Tetrahedron* **64** (2008) 1924–1930.
- [23] H. Togo and S. Iida, *Synlett* **14** (2006) 2159–2175.
- [24] M. Jereb, D. Vrazic and M. Zupan, *Tetrahedron* **67** (2011) 1355–1387.
- [25] J. Jaratjaroonpong, S. Sathalalai, P. Techasavapak and V. Reutrakul, *Tetrahedron Lett.* **50** (2009) 6012–6015.
- [26] J. Jaratjaroonpong, S. Krajangsri, and V. Reutrakul, *Tetrahedron Lett.* **53** (2012) 2476–2479.
- [27] C.-J. Li, *Chem. Rev.* **105** (2005) 3095–3165.
- [28] Spectral data for **3a**: ^1H NMR (400 MHz, CDCl_3): δ 7.35–7.29 (5H, brn), 5.92 (4H, brd, $J = 3.9$ Hz), 5.38 (1H, s), 2.29 (6H, s); ^{13}C NMR (100 MHz, CDCl_3): δ 152.82, 151.4, 140.0, 128.4, 128.4, 126.9, 108.1, 106.3, 45.1, 13.6; IR (Nujol): 1603, 15601, 1494, 1452, 1218, 1022 cm^{-1} ; HRMS (EI) calcd for $\text{C}_{17}\text{H}_{16}\text{O}_2$ 253.1229, found: 253.1223; Spectral data for **3f**: ^1H NMR (400 MHz, CDCl_3): δ 7.36–7.25 (5H, brn), 6.02 (2H, s), 5.95 (2H, s), 4.05 (1H, t, $J = 7.2$ Hz), 2.68 (6H, q, $J = 6.6$ Hz), 2.35 (2H, q, $J = 7.3$ Hz), 1.28 (6H, tt, $J = 7.5$ Hz, 7.5 Hz); ^{13}C NMR (100 MHz, CDCl_3): δ 156.5, 153.5, 141.9, 128.5, 128.3, 125.8, 106.1, 104.2, 38.4, 34.7, 33.5, 21.4, 12.1; IR (Nujol): 1664, 1604, 1561, 1497, 1455, 1208, 1183, 1012, 775, 699, 749 cm^{-1} ; HRMS (EI) calcd for $\text{C}_{21}\text{H}_{24}\text{O}_2$ 331.1674, found: 331.1669.
- [29] S.-J. Ji, S.-Y. Wang, Y. Zhang and T.-P. Loh, *Tetrahedron* **60** (2004) 2051–2055.
- [30] G. Sun and Z. Wang, *Tetrahedron Lett.* **49** (2008) 4929–4932.

CONTROLLED REACTIONS TOWARD CEPHALOSTATINS

Mansour Nawasreh^{1*}, Helmut Duddeck², Ekkehard Winterfeldt²

¹Applied Sciences Dept., FET, Al-Balqa Applied Univ., Amman, Jordan.

²Institut fuer Organische Chemie, Leibniz Hannover University, Hannover, Germany.

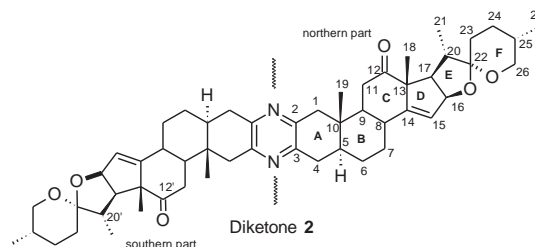
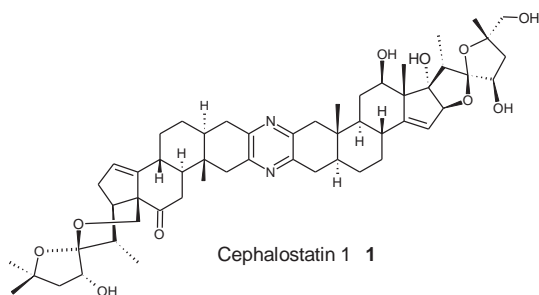
*Author for correspondence E-mail: Nawasreh@bau.edu.jo, Tel: +962 6 4790333 ext. 274, Fax: +962 6 4790350

Abstract: Due to the potent tumor inhibitory effects exhibited by the cephalostatins, a family of 19 bis-steroidal pyrazines (e.g. cephalostatin **1**) isolated from the marine algae *Cephalodiscus gilchristi*, our research group has engaged in the chemistry of these compounds since the mid 1990s. We have developed methods and devise synthetic strategies to convert the symmetrical bis-steroidal diketone into some more structurally-related analogues or to the natural products themselves. These strategies have been based on convergence, brevity, and flexibility. In our work, we have focused on the $\Delta^{14,15}$ bond, the keto group at C-12 and the ketal group at C-22.

Here, we report an unusual gas-free chlorination method of $\Delta^{14,15}$ bond through which the resulted product underwent selective reduction of the carbonyl group in the chloro-free part. Furthermore, the resulted products were dechlorinated to approve the double-functional protection role played by the chlorine atoms. Also, we mention here a metallic epoxidation of this double bond followed by selective reduction of both epoxide and carbonyl groups. Chemistry of the spiroketal moiety has also been explored. In this context, selective F-ring opening at one terminal of certain bis-steroidal system using catechol-borane complex was performed. However, the F-ring in the other terminal of the same system was opened selectively using another borane-complex.

1. Introduction

Cephalostatin **1** was first reported in 1988 as a potent growth inhibitory marine natural product.[1] The average GI₅₀ of **1** against the NCI-60, a collection of 60 human cancer cell lines, is 1.8 nM. [2] In addition to other 18 compounds, cephalostatin was isolated from the marine worm *Cephalodiscus gilchristi* by Pettit's group[1]. It has attracted few groups either toward the synthesis of analogues with potential anti-cancer activity as Winterfeldt's group [3] or toward the total synthesis as Fuchs's and Shair's groups[4,5]. Fuchs and coworkers reported the first total synthesis of cephalostatin **1** in 1998[4]. However, Shair and his coworkers reported the second total synthesis in 2010[5].



Their methods depend on asymmetrical coupling between the two proper steroids as the last step to generate the desired final target. Our strategy, however, bases on desymmetrizing a gram-scaled symmetrical diketone **2** followed by controlled interconversion methods [6]. We focused here on transformations of $\Delta^{14,15}$ bond, the keto group at C-12 and the ketal group at C-22.

2. Materials and Methods

We report here an unusual chlorination method of the $\Delta^{14,15}$ bond in the symmetrical diketone **2** using the mild oxidizing agent diacetoxy iodosobenzene in alkaline methanol/dichloromethane solution at 0 °C which led to chlorinated derivatives in a statistical ratio. Moreover, a new epoxidation method of this double bond using lithium metal in THF is also reported. Also, we mention here a selective F-ring opening of certain analogue using different borane complexes.

3. Results and Discussion

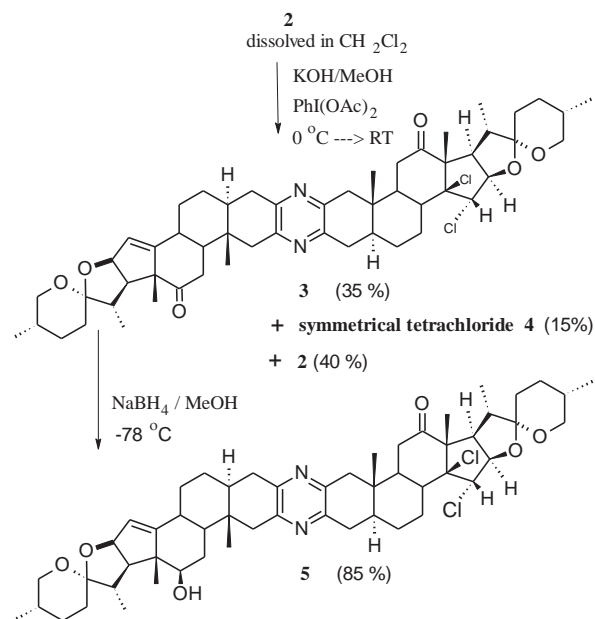
3.1 Novel Chlorination method of $\Delta^{14,15}$ bond

Treating the diketone **2** dissolved in undistilled dichloromethane with KOH/MeOH solution followed by addition of diacetoxy iodosobenzene at a relatively low temperature (0-10 °C), a method used to prepare 11 α -methoxy derivative [6], led to a strange less polar major product. The NMR spectrum of this major product showed that one of the 15-H protons disappeared and a new singlet resonating at δ 4.65 and a doublet at δ 4.59 (J = 8.1 Hz) appeared. The signal at δ 4.65 corresponding to 15-H showed no coupling with the neighboring proton 16-H. However, the main different features in ¹³C-NMR spectrum of this product compared to **2** is the appearance of the two carbonyl carbons at δ 210.7 and 209.1, in addition to a highly deshielded sp³-hybride quaternary carbon resonated at δ 90.0 ppm. The mass spectrum shows an increasing of 71 units compared to the starting material **2**. Concluding the structure was a major task. Many trials to get this product in a crystalline form failed. However, we were satisfied to get crystals of the

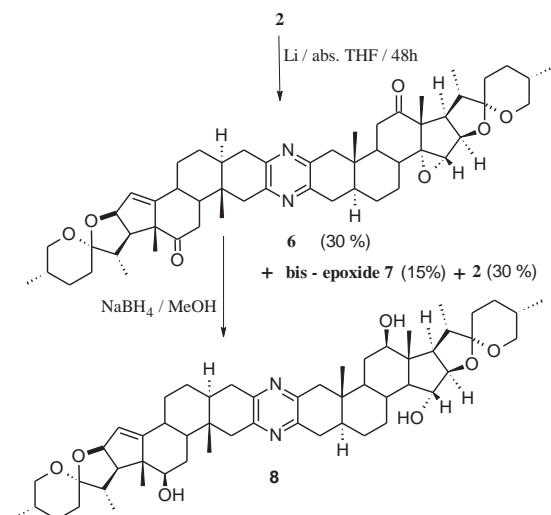
product resulting from the reduction of our candidate with NaBH_4 . The crystallographic analysis of this product showed very surprising results. It showed that, two chlorine atoms were added to one $\Delta^{14,15}$ bonds giving a *trans* 14 α ,15 β -dichloro derivative **3** (Scheme 1). Since the only source of chlorine atoms was dichloromethane, such chlorination reaction can be rationalized basing on an unusual reaction between the dichloromethane and diacetoxyl iodobenzene in basic methanol solution. This reaction was suggested firstly to be a substitution of chloro groups in the dichloromethane with methoxy groups leading to the generation of Cl^- ions which in turn substitute the acetate groups in $\text{PhI}(\text{OAc})_2$ leading to the formation of PhICl_2 . Even the addition mechanism is not yet clear, but one may suggest a decomposition of PhICl_2 under the reaction conditions to iodobenzene in addition to Cl_2 which attacks the double bond to give compound **3** and **4** in a statistical ratio. Compound **4** failed to undergo Wittig Reaction, oxime formation and reduction with sodium borohydride. These results were very useful in devising regioselective transformations of **3**. For example, treatment of **3** with sodium borohydride led to **5** as a single product in which only the carbonyl group in the chloro-free half was reduced. Moreover, we were succeeded to dechlorinate compound **3** using a refluxed Zinc powder in $\text{HOAc} : \text{CH}_2\text{Cl}_2$ (1:1) for one hour to get the starting material in 55 % yield (unmodified yield). These results were very important, since the two chloro groups work as a double-functional protecting group for both the double bond and the neighboring carbonyl groups. This enabled us to run many reactions on the unprotected-half. In addition, the chlorination method itself is a gas-free and environmental friendly process.

3.2 Metallic Epoxidation of $\Delta^{14,15}$ bond

Another method which is reported here is a new epoxidation method of the double bond using lithium metal. Compound **2** underwent a slow regioselective epoxidation of the $\Delta^{14,15}$ bond using lithium granules suspended in absolute THF to give α -epoxy derivative **6** and bis-epoxy derivative **7** in statistical ratio (Scheme 2). This unusual epoxidation method can be explained basing on the role played by the traces of H_2O_2 in THF catalyzed by Li. Treating compound **6** with NaBH_4 in methanol led to the triol **8** with three new stereogenic centers. Modification of such epoxidation reaction is under study.



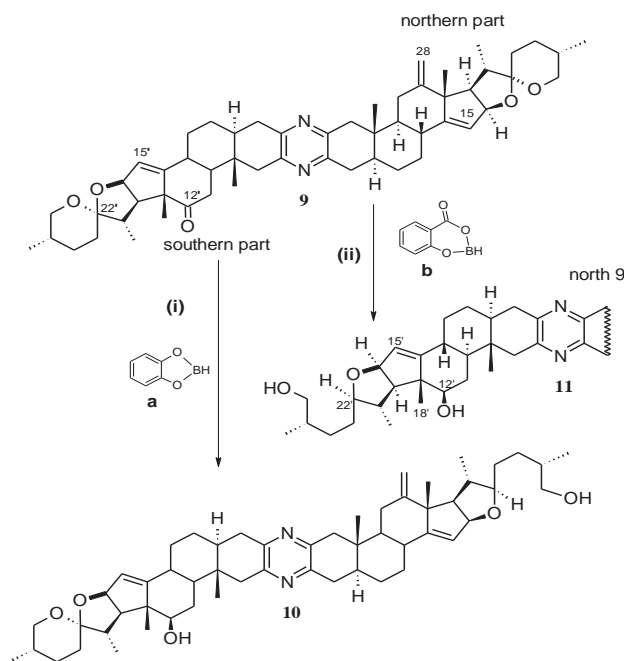
Scheme 1



Scheme 2

3.3 Selective F-Ring opening

Previously, we have reported selective F-ring opening of **9**, a Wittig-product of **2**, using the catechol-borane complex **a** to give **10**, in which the opening was from the side of the exocyclic double bond (northern part) [7]. However, we provide evidences that by using salicylic acid-borane complex **b**, the opening of the same substrate was from the keto-side (southern part) yielding compound **11** as major product[8]. This is briefly illustrated in Scheme 3. The proposed rationalization of this selectivity is based on complex space-demanded geometry and the donor-acceptor behavior between the spiroketal and the complex which is affected by the C-12 functionality.



(i) 16 eq **a**, abs THF, 0-7 °C, two weeks. (ii) 10 eq **b**, abs THF, 0-2 °C, four weeks.

Scheme 3

4. Conclusion

This new chlorination method is of great importance since it can be used as a double functional protecting method to both $\Delta^{14,15}$ bond and the neighboring carbonyl group. Also, functionalizing $\Delta^{14,15}$ bond with epoxy group is important because of the biological importance of highly oxygenated derivative which can be obtained through this route.

The opening of the terminal F-Ring in **9** is governed by both the complex geometry and the donor-acceptor behavior between the spiroketal and the complex which is affected by the C-12 functionality. The gained selectivity from the previous transformations encouraged us to think in the future with certain strategies toward the synthesis of asymmetric cephalostatins, for example **1**, starting from the symmetrical diketone **2**.

Acknowledgment

The authors would like to acknowledge Professor Dieter Fenske at Institute of Inorganic Chemistry, Karlsruhe University for crystallographic study of **3** and Professor Andreas Kirschning for helping in mechanistic suggestion of chlorination reaction. Also, the corresponding author acknowledges the DFG for the financial support.

References

- [1] a) G. R. Pettit, M. Inoue, Y. Kamano, C. Dufresne, M. Christie, M. Niven and D. L. Herald. *J. Chem. Soc., Chem. Comm.* **1988**, 865-867. b) G.R. Pettit, J. Xu, Y. Ichihara, M. Williams and M. Boyd, *Can. J. Chem.* **1994**, 72, 2260. c) G. R. Pettit, J.P. Xu, J.M. Schmidt,

M. R. Boyd, *Bioorg. and Med. Chem. Lett.* **1995**, 5 (17), 2027.

- [2] NCI-60 data are available on the web at <http://dtp.nci.nih.gov>. Cephalostatin 1 is NSC-363979.
- [3] A. Kramer, U. Ullmann, E. Winterfeldt, *J. Chem. Soc. Perk. Trans. 1*, **1993**, 2865.
- [4] T. G. LaCour, C. Guo, S. Bhandaru,; M. R. Boyd, P. L. Fuchs. *J. Am. Chem. Soc.* **1998**, 120, 692.
- [5] K. C. Fortner; D. Kato; Y. Tanaka; M. D. Shair. *JACS*, **2010**, 132, 275-280.
- [6] M. Nawasreh, E. Winterfeldt. *Curr. Org. Chem.* **2003**, 7 (7), 649-58.
- [7] M. Nawasreh. *Bioorg. and Med. Chem.* **2008**, 16, 255-265.
- [8] M. M. Nawasreh. *Pure and Appl. Chem.* **2011**, 83 (3) 699-707.

TOTAL PHENOLIC CONTENT, ANTIOXIDANT AND ANTITYROSINASE ACTIVITY OF *ARECA CATECHU* LINN. FRUITS ENDOCARP

Wanrudee Hiranrat^{*}, Asadhawut Hiranrat, Chatchadaporn Chanachol

Natural Product Research Laboratory, Department of Chemistry, Faculty of Science, Thaksin University, Phatthalung 93110, Thailand

^{*}E-mail: Kaewnok@hotmail.com

Abstract: This study was initiated to investigate the antioxidant activity, tyrosinase inhibitory effect and total phenolic content of the ethanol and aqueous ethanol (1:1) extracts from the endocarp of *Areca catechu* Linn. fruits. The total phenolic content was determined using a Folin-Ciocalteu colorimetric method, and antioxidant activity was measured according to the DPPH radical scavenging assay using ascorbic acid as a standard. The tyrosinase inhibitory activity was performed by the dopachrome method, using kojic acid as a reference compound. The ethanol extract (613 ± 1.79 mg GAE/g extract) showed higher phenolic content than the aqueous ethanol extract. The ethanol extract showed interestingly antioxidant activity with the IC_{50} value of 22.87 ± 1.25 μ g/mL (a standard ascorbic acid, IC_{50} value of 20.64 ± 1.09 μ g/mL). The ethanol extract exhibited strong antityrosinase activity with the IC_{50} value of 0.04 μ g/mL (kojic acid, IC_{50} 0.02 μ g/mL). It showed better inhibitory activity than the aqueous ethanol extract. These results suggested that the endocarp of *Areca catechu* fruits can potentially be used as a readily accessible source of natural antioxidants and tyrosinase protection system of the human body against oxidative damage and others complications.

1. Introduction

It has been reported that reactive oxygen radicals will lead to cellular damage and promote the pathological progression of atherosclerosis, carcinogenesis and diabetes [1]. On the other hand, the intake of antioxidant-containing food has been suggested as a strategy to reduce the incidence of disease due to oxidative damage and to exert a beneficial effect on human health [2]. Many bioactive substances found in plant constituents and crude extracts from fruits and vegetables have been recognized to possess beneficial effects against free radicals in biological systems as natural antioxidants [3]. These useful effects of extracts from fruits and vegetables can be attributed to many phenolic compounds with high antioxidant activity [4-7].

Hyper-pigmentation of the skin is a common problem that is prevalent in middle aged and elderly people. It is caused by over production of melanin. Tyrosinase, also known as polyphenol oxidase (PPO), is a copper containing enzyme [8] and well known to be the key enzyme in melanin production [9]. Alterations in melanin production might be responsible for a part of the histopathological features unique to malignant melanoma [10]. Therefore tyrosinase inhibitors may be useful for the treatment of skin cancer. Recently more attention is being paid to the use of natural plant extracts in the cosmetic industry as tyrosinase inhibitors [6]. Nowadays, motivation of people towards herbs is increasing due to the concern about the side effects of synthetic chemical drugs. Many of herbal and some common

medicinal plants are good sources of antioxidant and antityrosinase compounds.

Areca catechu Linn., commonly known as betel nut, is a slender palms from Arecaceae family which widely distributed in the Southeast Asia [11]. This plant has been reported to contain alkaloids, tannins, polyphenols, sugar and lipids [12] demonstrating broad ranges of pharmacological activities including the antioxidant property of the agro-industrial fruit waste [13], anti-inflammatory, antioxidant and antinociceptive properties [11], antifungal [12], antidepressant [14] and inhibited monoamine oxidase type A isolated from the rat brain [15]. In the previous study most reported for pharmacological activities of fruits pericarp, but no report on bioactivities from its endocarp. The objective of this work was to determine the total phenolic contents, antioxidant and antityrosinase activities when used the different solvents for preparation of extracts.

2. Materials and Methods

2.1 Chemicals and reagents

The solvents used in the present work were purchased from Merck (Germany). Folin-Ciocalteu reagent, sodium carbonate and 1,1-diphenyl-2-picryl-hydrazyl radical (DPPH radical) were also ordered from Merck (Germany). Gallic acid, kojic acid and L-DOPA were purchased from Sigma-Aldrich Chemicals. (Germany) and Mushroom tyrosinase were purchased from Fluka.

2.2 Plant materials

The endocarp of *A. catechu* was collected from Nakhon Sri Thammarat province, Thailand. It was then dried by a hot air oven at 60°C, and then ground into fine powder with a blender.

2.3 Sample preparation

The dried powder was separately macerated with ethanol and 50% ethanol for 3 days at room temperature. The filtrate was collected through a filter paper and the plant material was re-soaked for twice. The combined filtrate was evaporated to dryness under vacuum. The final crude extracts of fruits endocarp were named as EE (ethanol extract) and AEE (aqueous ethanol extract). Samples were kept in the sealed glass vials and stored in a refrigerator prior to analysis.

2.4 Determination of total phenolic contents

Total phenolics were measured by a modified Folin-Ciocalteu colorimetric method [16]. Briefly, a 0.5 mL sample of properly diluted extract was added to a tube containing 7.5 mL of deionised water followed by adding of 0.2 mL of Folin-Ciocalteu reagent and the tube was stirred and put it at room temperature. After 10 min, 0.6 mL of sodium carbonate (10% w/v) was added to the mixture. After

incubation at 40°C for 20 min, the absorbance at 755 nm was measured and compared to a gallic acid calibration curve. All experiments were measured in triplicate. The results were expressed as milligram of gallic acid equivalents (GAE) per gram extract.

2.5 Determination of DPPH radical scavenging capacity

The DPPH radical scavenging activity of extracts was analysed by some modified method of Chu [17], using ascorbic acid as standard. Initially, 0.2 mL of sample (dissolved in 95% ethanol) was mixed with 4 mL of 0.004% w/v DPPH in 95% ethanol. The reaction mixture was incubated at 28°C in a dark room for 30 min. The control contained all reagents except the extract while 95% ethanol was used as a blank. The scavenging activity against DPPH radical was determined by measuring the absorbance at 517 nm with spectrophotometer. All experiments were measured in triplicate. The inhibition of DPPH radical was calculated as a percentage of radical scavenging following equation.

$$\% \text{ Radical scavenging} = [(A_{\text{control}} - A_{\text{sample}}) / A_{\text{control}}] \times 100$$

Where A_{control} is the absorbance of the control and A_{sample} is the absorbance of the sample or ascorbic acid.

The results were expressed as the concentration of the extracts or ascorbic acid which scavenged DPPH radicals by 50% (IC_{50}). The IC_{50} of extracts and ascorbic acid were also assayed for comparison.

2.6 Inhibition of tyrosinase activity

The tyrosinase inhibitory activity was performed by the dopachrome method, using kojic acid as a reference compound and L-DOPA as a substrate. Briefly, a 50 μ L of mushroom tyrosinase solution (50 units/mL), 150 μ L of phosphate buffer pH 6.8 and 50 μ L of sample (dissolved in 20% ethanol) were mixed in a micro-well plate. After the mixture was incubated at 25°C for 10 min, 50 μ L of 4.25 M L-DOPA (dissolved in 0.1 M Phosphate buffer, pH 6.8) was added to the mixture solution. The absorbance at 475 nm was measured after standing for 20 min with a microplate reader. Phosphate buffer pH 6.8 and sample was used as a blank, while phosphate buffer pH 6.8, tyrosinase solution and 20% ethanol was used as a control. Kojic acid was used as a standard tyrosinase inhibitor. Percentage of antityrosinase activity was calculated as following formula.

$$\% \text{ Tyrosinase inhibition} = [(A_{\text{control}} - A_{\text{sample}}) / A_{\text{control}}] \times 100$$

Where A_{control} is the absorbance of the control and A_{sample} is the absorbance of the sample or kojic acid.

3. Results and Discussion

3.1 Extraction yield and total phenolic contents

The yields of crude extracts and the contents of total phenolics were shown in Table 1. The fruits endocarp extracts using ethanol and 50% ethanol yielded crude extracts of 5.23% and 4.83% dry weight, respectively. The total phenolic concentrations were measured by modified Folin-Ciocalteu colorimetric method. The results found that the phenolic contents of 613 \pm 1.79 mg GAE were detected for a gram of the extract EE while AEE has been reported to show 590 \pm 3.25 mg GAE. In general, these results suggested that the higher levels of phenolic component exhibited better antioxidant activity. Because phenolic compounds played an important role as antioxidants due to the presence of

hydroxyl substituents and their aromatic structure which enable them to scavenge free radicals [17].

Table 1: Extraction yield, total phenolic contents, antioxidant and antityrosinase activities of EE and AEE

	EE	AEE
% yield of extracts	5.23	4.83
Total phenolic contents (mg GAE/g extract)	613 \pm 1.79	590 \pm 3.25
Antioxidant activity (IC_{50} , μ g/mL)	22.87 \pm 1.25	24.34 \pm 0.87
Antityrosinase activity (IC_{50} , μ g/mL)	0.04	0.08

IC_{50} of ascorbic acid and kojic acid = 20.64 \pm 1.09 μ g/mL and 0.02 μ g/mL, respectively

3.2 DPPH radical scavenging effect

In DPPH radical scavenging assay, antioxidants reacted with DPPH radical (purple colour) producing yellow 1,1-diphenyl-2-picryl-hydrazine. The degree of discoloration indicated the radical scavenging activity of the antioxidants [19]. Table 1 showed the IC_{50} values of extracts from fruits endocarp with ascorbic acid as the positive control on the DPPH radical scavenging activity. It was found that the extract EE possessed scavenging activity on the DPPH radical (IC_{50} 22.87 \pm 1.25 μ g/mL) higher than the extract AEE (IC_{50} 24.34 \pm 0.87 μ g/mL). These extracts showed interestingly antioxidant activity compared with ascorbic acid (IC_{50} 20.64 \pm 1.09 μ g/mL). From the results, the active antioxidant components of *A. catechu* fruits endocarp are well extracted both of ethanol and aqueous ethanol. Antioxidant activity was positively correlated with their contents of total phenolics.

3.3 Tyrosinase inhibitory activity

Ethanol and aqueous ethanolic extracts of *A. catechu* were tested for tyrosinase activity using dopachrome method with kojic acid as a reference compound. Results showed that the IC_{50} values for EE and AEE extracts were 0.04 and 0.08 μ g/mL, respectively. However, the inhibitory activity of these extracts was weaker than a reference inhibitor, kojic acid (IC_{50} = 0.02 μ g/mL)

4. Conclusions

The evaluation of total phenolic contents, antioxidant and tyrosinase activities of ethanolic and aqueous ethanolic extracts of *A. catechu* endocarp were described. The ethanolic extract was found to show antioxidative effect, antityrosinase inhibitory effect and total phenolic concentrations better than aqueous ethanolic extract. These results suggest that *A. catechu* fruits endocarp extract exhibited strong antioxidant activity compared with ascorbic acid. In addition, *A. catechu* fruits endocarp extract had significant antityrosinase activity, although, its activity was lower than kojic acid, reference compound. Interestingly, *A. catechu* endocarp extracts may be developed as a natural source of antioxidants and also has being to apply as a natural skin-whitening agent in cosmetic products. Further work on isolation and identification of active compounds and their efficacy needs to be done.

Acknowledgements

The authors are great to thank the Department of Chemistry, Faculty of Science, Thaksin University for partly financial support.

References

- [1] B.S. Wang, L.W. Chang, W.J. Yen and P.D. Duh, *Food Chem. Toxicol.* **102** (2007) 785-790.
- [2] Y.J. Ming and C.C. Cheng, *Food Microbiology.* **27** (2010) 586-591.
- [3] K.N. Prasad, B. Yang, J. Shi, C. Yu, M. Zhao, S. Xue and Y. Jiang, *J. Pharm. Biomed. Anal.* **51** (2010) 471-477.
- [4] L.W. Chang, L.J. Juang, B.S. Wang, M.Y. Wang, H.M. Tai, W.J. Hung, Y.J. Chen and M.H. Huang, *Food Chem. Toxicol.* **49** (2011) 785-790.
- [5] P. Seephonkai, S. Samchai, A. Thongsom, S. Sunaart, B. Kiemsanmuang and K. Chakuton, *Chinese J. Med.* **9** (2011) 0441-0445.
- [6] N. Rangkadilok, S. Sitthimonchai, L. Worasuttayangkurn, C. Mahidol, M. Ruchirawat and J. Satayavivad, *Food Chem. Toxicol.* **45** (2007) 328-336.
- [7] A.M. Anagnostopoulou, P. Kefalas, V. P. Papageorgiou, A.N. Assimopoulou and D. Boskou, *Food Chemistry.* **94** (2006) 19-25.
- [8] V.L. Singleton, R. Orthofer and R.M. Lamuela-Raventos, *Methods Enzymol.* **299** (1999) 153-178.
- [9] M.B. Mapunya, A.A. Hussein, B. Roariguez and N. Lah, *Phytomedicine.* **18** (2011) 1006-1012.
- [10] M.Y. Lin, and C.L. Yen, *J. Agric. Food Chem.* **47** (1999) 1460-1466.
- [11] A.M. Bhandare, A.D. Kshirsagar, N.S. Vyawahare, A.A. Hadambar and V.S. Thorve, *Food Chem. Toxicol.* **48** (2010) 3412-3417.
- [12] P. Yenjit, M. Issarakraisila, W. Intana and K. Chantrapromma, *Postharvest Biol. Technol.* **55** (2010) 129-132.
- [13] M. Kumar, U.R. Moon and A. Mitra, *Industrial Crops and Products.* **40** (2012) 204-209.
- [14] A. Dar, S. Khatoon, G. Rahman and A.U. Rahman, *Phytomedicine.* **4** (1997) 41-45.
- [15] A. Dar and S. Khatoon, *Pharmacol. Biochem. Behav.* **65** (2000) 1-6.
- [16] S. Shukla, A. Mehta, V.K. Bajpai and S. Shukla, *Food Chem. Toxicol.* **47** (2009) 2338-2343.
- [17] Y.H. Chu, C.L. Chang and H.F. Hsu, *J. Sci. Food Agr.* **80** (2000) 561-566.

Physical and Computational Chemistry

MOLECULAR MODELING INVESTIGATIONS OF EUGENOL-CYCLODESTRINS INCLUSION COMPLEXES

Wichuta Roekmongkol¹, Jaruwan Wisarnmetinee¹, Luckhana Lawtrakul^{1,*}

¹ School of Bio-Chemical Engineering and Technology, Sirindhorn International Institute of Technology, Thammasat University, Pathum Thani, 12121, Thailand

* Author for correspondence; E-Mail: luckhana@siit.tu.ac.th, Tel. +66 (0) 2986 9009 ext 1809

Abstract: Autodock was used to dock eugenol into the cavity of β -cyclodextrin (β CD) and five of its derivatives, namely Heptakis-2,6-di-O-methyl- β CD (DM β CD), Heptakis-2,3,6-tri-O-methyl- β CD (TM β CD), 2-O(S)-2-Hydroxypropyl- β CD (2S-HP β CD) and 6-O(R)-2-Hydroxypropyl- β CD (6R-HP β CD). The total interaction energies of the eugenol- β CD inclusion complexes were optimized using PM3 calculations. The results show that EG with β CDs formed 1:1 host-guest inclusion complexes. The models confirm that when eugenol- β CD is formed in three different conformations with the phenyl ring of eugenol molecule stays inside the cavity whereas first, the hydroxyl group lines toward the primary rim and the methoxyl group lines toward the secondary rim, second, both hydroxyl group and methoxyl group line toward the primary rim and third, both hydroxyl group and methoxyl group line toward the secondary rim of β CD.

1. Introduction

Eugenol (EG) is a phenolic compound extracted from clove oil and other essential oils. Eugenol (Fig. 1), a pale yellow liquid with strong aromatic odor of clove, is widely used as a fragrant and favouring agent. In addition, EG is antioxidant and anti-microbial spoilage in foods. However, the major disadvantages of EG are light sensitivity, volatility and poor water solubility so it is hard to keep, protect and corporate well in aqueous solution.

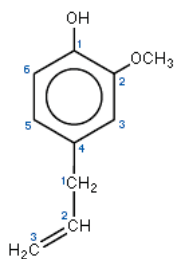


Figure 1. Molecular structure of eugenol [2-methoxy-4-(2-propen-1-yl) phenol]

β -cyclodextrin (β CD) is a cyclic oligosaccharide connecting 7 glucopyranose subunits via α -1,4 linkage as shown in the Fig. 2.

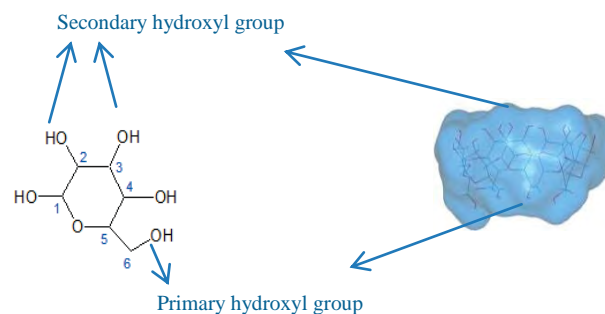
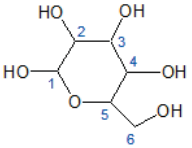
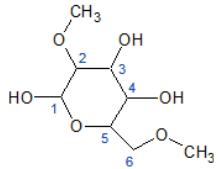
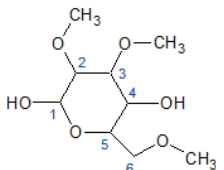
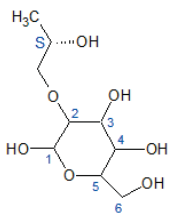
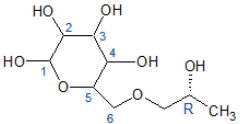


Figure 2. Schematic representations of glucose unit and truncated cone shape of β CD

β CD has a shallow truncated cone shape with secondary hydroxyl group at wider rim and primary hydroxyl group at narrow rim. It forms hydrophilic outer surface and a hydrophobic center cavity. β CD is considered as non-toxic by Food and Drug Administration (FDA). There are many derivatives of β CD, the difference is the substituent replacing H atom of the hydroxyl groups at the position C2, C3 and C6. The properties of β CDs lead to molecular formation by encapsulating the hydrophobic guest molecule inside hydrophobic cavity. There are several derivatives of β CD considered to be applicable for EG- β CD encapsulation [1-4]. However, there is no detailed information about the preferred conformations and the inclusion complex interactions to elucidate the comprehensive encapsulation mechanism which is essential towards the development of an effective process for complex production in large scale. The aim of the study was to establish the molecular model to investigate the behavior and energy of inclusion complex formation of EG and five β CD derivatives which are Heptakis-2,6-di-O-methyl- β CD (DM β CD), Heptakis-2,3,6-tri-O-methyl- β CD (TM β CD), 2-O(S)-2-Hydroxypropyl- β CD (2S-HP β CD) and 6-O(R)-2-Hydroxypropyl- β CD (6R-HP β CD).

Molecular docking was used to provide the probability of different conformations within each individual complex. A dynamic equilibrium exists between EG, β CD and the complex, as there are no covalent bonds established. The interaction energies depend on how well the host-guest complex fits together and on specific molecular interactions.

Table 1: Chemical structures of glucose unit of β CDs

Compounds	Abbreviation	Glucose unit
β -Cyclodextrin	β CD	
Heptakis(2,6-di-O-methyl)- β -cyclodextrin	DM β CD	
Heptakis (2,3,6-tri-O-methyl)- β -cyclodextrin	TM β CD	
2-O((S)-2-Hydroxypropyl)- β -cyclodextrin	2S-HP β CD	
6-O((R)-2-Hydroxypropyl)- β -cyclodextrin	6R-HP β CD	

2. Method of calculations

2.1 Structure optimization of EG and β CD derivatives

The molecular structure of EG was constructed by WebLab ViewerPro and optimized at HF/3-21G level [5] with GAUSSIAN03 program [6]. The crystal structures of β CD and its five derivatives were obtained from Cambridge Crystallographic Data Files (CCDF) with the codes of POBRON [7] for β CD, BOYF0K04 [8] for DM β CD, HEZWAK [9] for TM β CD, KOYYUS [10] for 2S-HP β CD and LEDROB [11] for 6R-HP β CD. The differences of OH group substitution at C2, C3 and C6 are shown in Table 1. To all β CD derivatives, hydrogen atoms were added and subsequently fully optimized at PM3 level [13] by using GAUSSIAN03 program package.

2.2 Molecular docking simulation

The inclusion complexes between each β CD derivatives and EG were studied with molecular docking simulations by Autodock 4.2 program [14]. The structure of each host was fixed and let flexible

movement of EG. A grid map of 0.375 Å of grid spacing and grid size of 30 Å × 30 Å × 30 Å to cover the inclusion complex structure and other parameters were remain default. A hundred Lamarckian Genetic Algorithm runs were performed.

2.3 Inclusion complexes optimization

Every conformations of the inclusion complex were optimized at Semi-empirical PM3 level to obtain the geometry and energy information of the complex structure. Among these several conformations of the inclusion complex found from each β CD derivative, the lowest binding energy with highest frequency cluster was selected as representative. Each representative was then optimized again at HF/2-31G level in order to have higher accuracy.

2.4 Basis Set Superposition Error correction

Basis Set Superposition Error (BSSE) correction was performed at DFT, B3LYP/6-31G in order to eliminate the error that might occur from the different orientation between monomer and dimer forcefield of β CD and EG. The binding energy without BSSE correction is shown in equation (1) and the counterpoise correction binding energy with BSSE is shown in equation (2).

$$\Delta E = E_{\text{complex}} - (E_{\text{CD}} + E_{\text{EG}}) \quad (1)$$

$$\Delta E^{\text{CP}} = E_{\text{complex}} - (E_{\text{CD}}^{\text{EG/CD}} + E_{\text{EG}}^{\text{EG/CD}}) \quad (2)$$

ΔE is the binding energy of inclusion complex.

E_{complex} is energy of inclusion complex structure.

E_{CD} is energy of cyclodextrin in monomer forcefield.

E_{EG} is energy of eugenol in monomer forcefield.

ΔE^{CP} is the counter poise binding energy of inclusion complex.

$E_{\text{CD}}^{\text{EG/CD}}$ is energy of cyclodextrin in dimer forcefield.

$E_{\text{EG}}^{\text{EG/CD}}$ is energy of eugenol in dimer forcefield.

3. Results and Discussion

AutoDock 4.2 program was used in order to predict the preferred orientations of EG molecule to β CD when bound to each other in inclusion complex formation. According to the simulations, all β CD molecules are able to form 1:1 inclusion complex with EG which could be indicated from the negative values of energy in the range of -15.90 to -20.88 kJ/mol. Individual host-guest inclusion complex was investigated to determine all atomic positions with a hundred of simulations to ensure all possibilities of EG's molecular conformation in the inclusion complex.

The results of each host-guest complex could be clustered in different groups based on the root mean square deviation in a position of atoms in the inclusion

complex. Molecules in the same cluster must have the variation in position less than 2 Å. Table 2 shows different clusters of each β CD molecule's conformations in the complex. Table 2 also shows the free energy of binding involved in the interaction between individual β CDs and the EG in the complex determined by AutoDock simulations. The results from AutoDock show all possible geometry of inclusion complex which came up with negative binding energy telling the attractive force interaction between EG and CD.

Table 2: Binding energy (kJ/mol) of EG and β CDs inclusion complexes from molecular docking

Compounds	Cluster	Number in cluster	Lowest binding energy	mean binding energy
β CD	1	87	-17.66	-17.07
	2	8	-16.28	-16.11
	3	5	-15.90	-15.77
DM β CD	1	22	-19.12	-19.00
	2	17	-18.95	-18.70
	3	32	-18.95	-18.70
	4	3	-18.91	-18.66
	5	13	-18.62	-18.20
	6	5	-18.49	-18.24
	7	7	-18.07	-17.82
	8	1	-17.78	-17.78
TM β CD	1	93	-20.88	-20.42
	2	4	-20.00	-19.79
	3	3	-19.71	-19.04
2S-HP β CD	1	23	-20.46	-19.87
	2	47	-20.46	-20.17
	3	26	-20.04	-19.83
	4	2	-19.62	-19.37
	5	2	-18.79	-18.70
6R-HP β CD	1	35	-19.75	-19.08
	2	10	-19.46	-18.95
	3	27	-19.12	-18.70
	4	1	-18.91	-18.91
	5	23	-18.74	-18.49
	6	4	-18.28	-18.07
6S-HP β CD	1	17	-20.29	-20.04
	2	9	-20.13	-20.04
	3	26	-20.00	-19.75
	4	24	-19.71	-19.41
	5	22	-19.33	-19.12
	6	1	-19.16	-19.16
	7	1	-18.49	-18.49

The further analysis of freely motions both of host and guest molecules has been done by using semi-empirical PM3 method since in molecular docking only EG is flexible. After the lowest free energy of binding conformation of each cluster was selected for further fully optimization at HF/2-31G and BSSE was performed, the binding energies of the inclusion

complexes with and without BSSE correction were calculated and shown in Table 3.

Table 3: Binding energy in kJ/mol for inclusion complexes at B3LYP/6-31G level

Compounds	ΔE	BSSE	ΔE^{cp}
β CD	-49.86	52.01	2.18
DM β CD	-74.19	49.96	-24.23
TM β CD	-79.25	65.90	-13.35
2S-HP β CD	-148.66	80.67	-67.99
6R-HP β CD	-84.63	68.41	-16.19

The order of interaction capacities is 2S-HP β CD >> 6R-HP β CD > TM β CD > DM β CD >> β CD and the order with BSSE is 2S-HP β CD >> DM β CD > 6R-HP β CD > TM β CD >> β CD. So 2S-HP β CD is the best derivative for inclusion complex formation with EG and β CD is the worst whereas the 3 derivatives in the middle are varied in the range of about 10 kJ.

The substitution of hydroxyl group with methoxyl group in M β CD and with hydroxypropyl group in HP β CD help to extend the length of β CD's cavity at the rims so the derivative structures are better entrapping EG inside. Some derivatives of M β CD gives better results than HP β CD and vice versa. For HP β CD, the substitution at the primary rim (6R-HP β CD) gives better result than the substitution at the secondary rim (2S-HP β CD).

The conformation of inclusion complex structures of EG with each CD derivative are different. Some derivatives can obligate all part of EG while some cannot, as shown in Fig. 3-7. β CDs are presented in surface and EG compound is presented in stick models (hydrogen atoms are omitted for clarity).

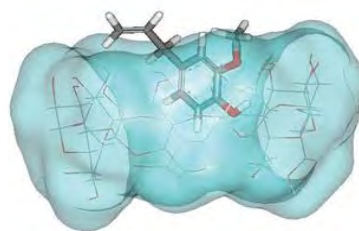


Figure 3. The conformation of EG- β CD

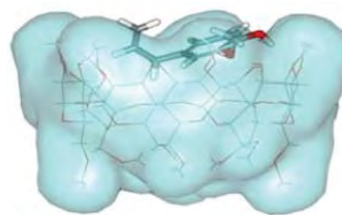


Figure 4. The conformation of EG-DM β CD

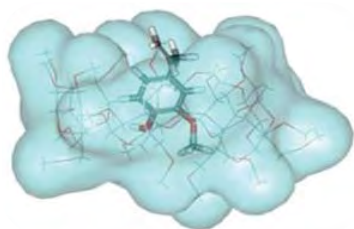


Figure 5. The conformation of EG-TMβCD

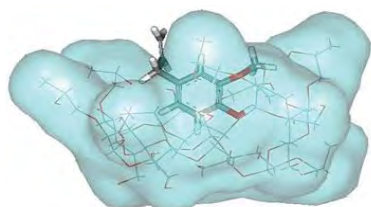


Figure 6. The conformation of EG-2S-HPβCD

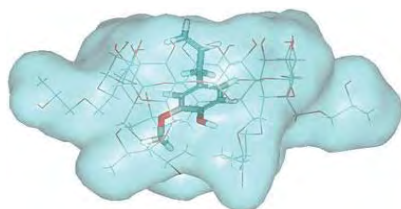


Figure 7. The conformation of EG-6R-HPβCD

Most of the inclusion complex structures indicate the phenyl group of EG is wrapped in CD cavity with hydrophobic interaction and leave the allyl group extend at the rims of the truncated cone. The interactions, including hydrogen bonds, occur between the hydroxyl group of C1 of EG and hydroxyl group of CD, some at primary hydroxyl group while others occur at secondary hydroxyl group.

4. Conclusions

The study of EG with βCD and its five derivatives inclusion complex indicate that the possibility of interaction in 1:1 molar ratio and energetically favorable. By wrapping phenyl group of EG inside CD cavity and interaction between hydroxyl groups of EG and CD provide the stability of inclusion complexes. The major interactions are hydrophobic interaction and hydrogen bonds. The best derivative for EG-CD inclusion complex among 5 CD derivatives is 2S-HPβCD with the binding energy of -16.19 kJ/mol.

References

- [1] O. Nuchuchua, S. Saesoo, I. Sramala, S. Puttipipat khachorn, A. Soottitantawat, U. Ruktanonchai, *Food Research International* **42** (2009) 1178-1185.
- [2] H.-S. Pilar, L.-M. Santiago, L.-A. Carmen, N.-D. Estrella, *Food and Nutrition Sciences* **3** (2012) 716-723.

- [3] Y. Yan, X. S. Le, *Inclusion Phenomena and Macrocyclic Chemistry* **52** (2005) 27-33.
- [4] H. Zhan, Z.-T. Jiang, Y. Wang, R. Li, T.-S. Dong, *European Food Research and Technology* **227** (2008) 1507-1513.
- [5] N. Levine, *Quantum Chemistry*, Englewood Cliffs, New Jersey: Prentice Hall (1991), pp. 455-544.
- [6] M. J. Frisch, et al., Gaussian, Inc., Wallingford CT (2004).
- [7] T. Steiner, G. Koellner, *J. Am. Chem. Soc.* **116** (1994) 5122.
- [8] T. Aree, H. Hoier, B. Schulz, G. Reck, W. Saenger, *Angew. Chem. Int. Ed. Engl.* **39** (2000) 897.
- [9] M. R. Caira, V. J. Griffith, L. R. Nassimbeni, B. van Oudtshoorn, *J. Chem. Soc., Perkin Trans. 2* (1994) 2071.
- [10] K. Harata, C. T. Rao, J. Pitha, K. Fukunaga, K. Uekama, *Carbohydr. Res.* **222** (1991), 37.
- [11] K. Harata, C. T. Rao, J. Pitha, *Carbohydr. Res.* **247** (1993) 83.
- [12] J. Stewart, *J. Comput. Chem.* **10** (1989) 209.
- [13] G.M Morris, R. Huey, W. Lindstrom, M. F. Sanner, R. K. Belew, D. S. Goodsell, A. J. Olson, *Comput. Chem.* **30** (2009) 2785-279.

THEORETICAL STUDY OF SANTALOL WITH β -CYCLODEXTRIN INCLUSION COMPLEXES

Pattaraporn Theawthua, Suchinda Poocharoen, Luckhana Lawtrakul*

School of Bio-Chemical Engineering and Technology, Sirindhorn International Institute of Technology, Thammasat University, Pathum Thani 12121, Thailand

* Author for correspondence; E-Mail: luckhana@siit.tu.ac.th, Tel. 66 (0) 2986 9009 ext 1809

Abstract: The inclusion interactions of α -santalol and β -santalol with β -cyclodextrin (β CD) have been investigated by molecular docking and quantum chemistry calculations. The results show that β CD with α -santalol and β -santalol formed 1:1 host-guest inclusion complexes. α -santalol provided only one preferable conformation while β -santalol provided two possible inclusion complex formations. The inclusion complex conformations and their interactions were comprehensively investigated.

1. Introduction

A major component of sandalwood oil (*Santalum album* L., sandalwood) is α -santalol (45-55%) and another less abundant component is β -santalol (18-24%), depending on the species and original of the plantation [1]. Different diastereomers as well as enantiomers may have different odour notes or even completely different types of odour. Therefore, the complete separations of the diastereomers and enantiomers methods are developed by using cyclodextrin as chiral selector for GC separation of volatile optically active components in the essential oil.

β -Cyclodextrin (β CD) is a non-reducing cyclic oligosaccharide consisting of 7 α -1,4-linked D-glucose units. It has a toroid structure with a non-polar (hydrophobic) cavity and hydrophilic exterior. It can interact with guest molecules through hydrophobic and van der Waals interactions which enables it to form inclusion complexes. β CD is the most accessible with reasonable price, and generally the most useful among the group of cyclodextrins.

Several groups reported the use of cyclodextrin inclusion complex with the components in sandalwood oil but the inclusion complex compositions were unidentified. Moreover, there are no report about preferred conformations and inclusion complex interactions, which are important to elucidate the encapsulation mechanism. The purpose of this study is to establish the molecular models which determine the possibility of forming inclusion complex of β CD with α -santalol and β -santalol. The inclusion complex conformations and their interactions were comprehensively investigated in order to estimate the stability within the complexes and elucidate preferable conformations.

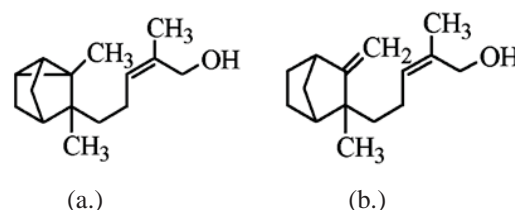


Figure 1. Chemical structures of (a.) α -santalol: 5-(2,3-dimethyltricyclo[2.2.1.0^{2,6}]hept-3-yl)-2-methylpent-2-en-1-ol, and (b.) β -santalol: (2Z)-2-methyl-5-[2-methyl-3-methylene-bicyclo[2.2.1]hept-2-yl]pent-2-en-1-ol

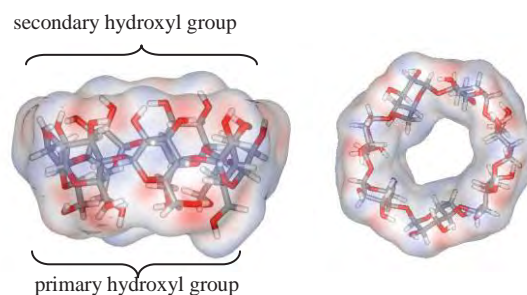


Figure 2. Chemical structure of β CD side view and top view

2. Method of calculation

2.1 Structure optimization of CD and santalol

The initial molecular structure of β CD was obtained from Cambridge Crystallographic Data Files [2] and santalol molecules were obtained from EMBL-EBI European Bioinformatics Institute [3]. Santalol molecules were optimized at HF/6-31G level while β CD was optimized at PM3 level with GAUSSIAN03 program.

2.2 Molecular docking simulation

In order to study the inclusion complex of santalols with β CD, molecular docking simulation was investigated using Autodock 4.2 program. In the step of ligand preparing, Gasteiger charges were added for santalol molecules. Grid size of 40Å×40Å×40Å and a grid map with 0.375 Å of grid space were set for

inclusion complex while other docking parameters were set as default. A hundred Lamarckian Genetic Algorithm runs were performed. The models of each cluster assigned by molecular docking calculations were further optimized using semi-empirical PM3 method. The optimized conformations of each inclusion complex cluster were analysed.

3. Results and Discussion

The binding energies of β CD with α -santalol and β -santalol obtained from molecular docking calculations are shown in Table 1. From 100 running of β CD/ α -santalol inclusion, 7 clusters were found and the lowest binding energy is $-21.80 \text{ kJ}\cdot\text{mol}^{-1}$ with 30 members. For β CD/ β -santalol, 5 clusters were found and the lowest binding energy is $-23.18 \text{ kJ}\cdot\text{mol}^{-1}$ with 37 members.

Table 1: Molecular docking calculations

Guest	Number of rotatable bonds	Cluster	Number in cluster	Energy($\text{kJ}\cdot\text{mol}^{-1}$)	
				Lowest	Mean
α -santalol	5	1	30	-21.80	-20.75
		2	40	-21.76	-21.21
		3	10	-21.46	-21.17
		4	6	-21.46	-20.92
		5	4	-21.26	-20.42
		6	8	-21.17	-20.67
		7	2	-19.50	-19.41
β -santalol	5	1	37	-23.18	-22.18
		2	32	-22.80	-22.26
		3	16	-22.47	-21.88
		4	4	-21.92	-21.55
		5	11	-21.26	-20.88

Table 2: PM3 interaction energy ($\text{kJ}\cdot\text{mol}^{-1}$)

Guest	Cluster	E_{complex}	ΔE	Inclusion complex conformation
α -santalol	1	-6269.21	-58.95	α -santalol-I
	2	-6293.10	-82.84	α -santalol-I
	3	-6293.10	-82.84	α -santalol-I
	4	-6300.02	-89.76	α -santalol-I
	5	-6300.02	-89.76	α -santalol-I
	6	-6300.02	-89.76	α -santalol-I
	7	-6300.02	-89.76	α -santalol-I
β -santalol	1	-6337.81	-83.22	β -santalol-I
	2	-6333.14	-78.55	β -santalol-I
	3	-6344.18	-89.60	β -santalol-II
	4	-6339.19	-84.60	β -santalol-I
	5	-6337.81	-83.22	β -santalol-I

$$E_{\beta\text{CD}} = -6080.16 \text{ kJ}\cdot\text{mol}^{-1}$$

$$E_{\alpha\text{-santalol}} = -130.10 \text{ kJ}\cdot\text{mol}^{-1}$$

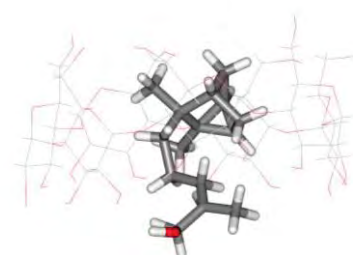
$$E_{\beta\text{-santalol}} = -174.42 \text{ kJ}\cdot\text{mol}^{-1}$$

Guest conformations in the complex of each category were further optimized using PM3 calculations to determine the interaction energies of the complexes. The interaction energy (ΔE) of the inclusion complex was calculated by the difference between total energy of the inclusion

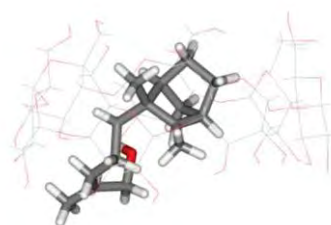
complex (E_{complex}) and the sum of their individual components in their optimization energies, as in the following equation.

$$\Delta E = E_{\text{complex}} - (E_{\text{guest}} + E_{\beta\text{CD}})$$

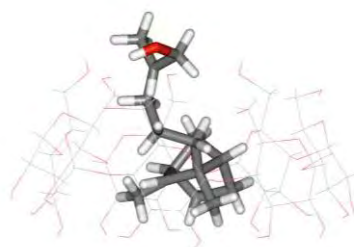
The interaction energies of all inclusion complex conformations are presented in Table 2.



(a.) α -santalol-I



(b.) β -santalol-I



(c.) β -santalol-II

Figure 3. Inclusion complex conformations

The PM3 fully optimized inclusion complex conformations of β CD/ α -santalol show the same conformation with the interaction energy varies from -58.95 to $-89.76 \text{ kJ mol}^{-1}$. The β CD/ α -santalol complex conformation was shown in Fig. 3(a). The cyclic rings of α -santalol stay inside the cavity of β CD and the hydroxyl group of α -santalol is closed to the secondary hydroxyl rim of β CD.

Two different conformations of β CD/ β -santalol inclusion complexes were found as shown in Fig. 3(b) and 3(c). β -santalol-I conformation has the interaction energy from -78.55 to $-84.60 \text{ kJ}\cdot\text{mol}^{-1}$. The cyclic rings of β -santalol stay inside the cavity of β CD and the hydroxyl group of β -santalol is closed to the secondary hydroxyl rim of β CD. This conformation is similar to the conformation of α -santalol-I.

The second conformation, β -santalol-II, has the lowest interaction energy $-89.60 \text{ kJ}\cdot\text{mol}^{-1}$. In this conformation the cyclic rings of β -santalol molecule stay inside the β CD cavity the hydroxyl group of β -santalol is closed to the primary hydroxyl rim of β CD, as shown in Fig. 3(c).

The binding energies indicated that both santalol molecules can possibly form 1:1 inclusion complex with β CD. In addition, binding energy of inclusion complex depends on the interaction between host and guest molecules which relate to the structure of host and guest. Therefore, although the two santalol structures are isomers, each molecule can form different structures of inclusion complexes with β CD with different binding energy.

4. Conclusions

Molecular modelling simulations show that two major components of the essential oil from sandalwood, α -santalol and β -santalol, are able to form the inclusion complexes with β CD. α -Santalol can form only single conformation of β CD inclusion complex while β -santalol could offer two possible complex conformations with β CD. In general, β CD usually allows the hydrophobic part of the guest molecule to enter the cavity which is also hydrophobic. The results from this work provide better understanding of the inclusion complex formation between α -santalol and β -santalol with β CD.

Acknowledgements

The authors are grateful to Thammasat University Research Fund (2012) for financial support.

References

- [1] K. Bauer, D.Garbe, H.Surburg in *Common Fragrance and Flavor Materials*, WILEY-VCH Verlag GmbH & Co. KGaA, Weinheim (2001), pp.218-219.
- [2] T. Steiner, G. Koellner, *J. Am. Chem. Soc.* **116** (1994) 5122-5128.
- [3] EMBL-EBI European Bioinformatics Institute. <http://www.ebi.ac.uk/chebi/init.do> (Retrieved August, 2012).
- [4] V.S. Venkatesh Gowda, *Global Emerging Trends on sustainable production of natural Sandalwood*. Proceedings of the Art and Joy of Wood conference, Bangalore, India (2011).
- [5] G.A. Burdock, I.G. Carabin, *Food Chem. Toxicol.* **46** (2008) 421-432.
- [6] M.J.R. Howes, M.S.J. Simonds, G.C. Kite, *J. Chromatogr. A.* **1028** (2004) 307-312.
- [7] D. Sciarrone, R. Costa, C. Ragonesea, P.Q. Tranchida, L. Tedone, L. Santi, P. Dugo, G. Dugo, L. Mondello, *J. Chromatogr. A.* **1218** (2011) 137-142.
- [8] J. Szejtli, *Pure Appl. Chem.* **Vol. 76, No. 10** (2004) 1825-1845.
- [9] E.M.M. Del Valle, *Process Biochem* **Vol.39, Issue.9** (2004) 1033-1046
- [10] H.M.C. Marques, *Flavour Frag. J.* **Vol. 25, Issue.5** (2010).
- [11] E.A. Castro, D.A.J. Barbiric, *J. Argent. Chem. Soc.* **90** (2002) 1-44.
- [12] B. Norasiha, *Inclusion complex formation between natural dyes extracted from Pitaya fruit skin and β -cyclodextrin: Kinetic and Thermodynamic study*, M.S. Thesis, University Malaysia Pahang, (2011).
- [13] W.A. König, D.H. Hochmuth, *Enantioselective J. Chromatogr. Sci.* **Vol. 42** (2004) 423-439.
- [14] Gaussian 03, Revision C.02, M. J. Frisch, et al., Gaussian, Inc., Wallingford CT (2004).
- [15] G.M Morris, R. Huey, W. Lindstrom, M. F. Sanner, R. K. Belew, D.S. Goodsell, A. J. Olson *J. Compute. Chem.* **30** (2009) 2785-2791.

MOLECULAR MODELING INVESTIGATION OF INHIBITORS BINDING TO HIV-1 REVERSE TRANSCRIPTASE

Ranita Kamolvarin, Manassanan Pisudchaikul, Sitanun Jariyapaktikorn, Luckhana Lawtrakul*

School of Bio-Chemical Engineering and Technology, Sirindhorn International Institute of Technology, Thammasat University, Pathum Thani 12121, Thailand

* Author for correspondence; E-Mail: luckhana@siit.tu.ac.th, Tel. +66 2 9869009 ext 1809, Fax. +66 2 9869112

Abstract: Molecular modeling studies were performed with known crystal structure of HIV-1 reverse transcriptase (RT) with three different inhibitors in order to evaluate the predictive abilities of the calculation models. The crystal structures of HIV-1 RT obtained from the Protein Data Bank (PDB) and water molecules were then removed and hydrogen atoms were added. Autodock 4.2 program was used to dock three inhibitors into the binding areas of HIV-1 RT. The models with the lowest energy and highest occurring frequency were selected to further investigated in details. The result models show the reliable predictive abilities which can be used to predict the binding mode and conformation in an active site of non-available crystallographic structural data in (PDB).

1. Introduction

HIV-1 is one of the most harmful diseases in the world. Many drug companies are trying to improve the anti-HIV-1 drugs since HIV-1 can mutate themselves which cause resistance to a certain drug [1]. The way to inhibit the reproduction of HIV-1 is to inhibit at a certain step of HIV-1 life cycle [2]. Earlier studies show many combinations of drugs that are used to treat HIV-1 infected patients [3]. Three inhibitors chosen in this study are rilpivirine (RPV), tenofovir (TFO), and emtricitabine (ETV), which are non-nucleoside reverse transcriptase inhibitor (NNRTI), nucleotide reverse transcriptase inhibitor (NtRTI), and nucleoside reverse transcriptase inhibitor (NRTI) respectively. The combination of the three drugs inhibits the function of viral enzyme (by NRTI and NtRTI), polymerase, located on reverse transcriptase (RT) and also interrupt the structure of RT which helps in binding of RT to dNTP substrates (by NNRTI) [3-6]. The molecular modeling is used to obtain the predictive, possible, and appropriate position that the three drugs able to bind to the reverse transcriptase molecule. These molecular modeling approaches are using to construct the structure of emtricitabine/rilpivirine/tenofovir in combination with HIV-1 RT. The constructed model will be the first predictive structure which can be useful in the future drug design and development.

2. Materials and Methods

Crystal structures of HIV-1 RT with inhibitors were obtained from the Protein Data Bank (2ZD1, 2NO6, 1T03, and 1T05). Water molecules were then

removed and hydrogen atoms were added. The inhibitor molecules were modified (change some part of crystal structure) and energy minimization by GAUSSIAN03 program at HF/6-31G level. AutoDock4.2 program was used to investigate inhibitors binding to HIV-1 RT. In this study, we survey two molecular docking calculations, fixed and flexible RT. Firstly; the structure of RT was fixed and let flexible movement of inhibitors. A grid map of 0.375 Å of grid spacing and grid size of 60 Å x 60 Å x 60 Å to cover the binding pocket and other parameters were remain default. A hundred Lamarckian Genetics Algorithm runs were performed. Secondly; some amino acid residues of the binding pocket and its inhibitor are allowed to move freely in flexible molecular docking. Among several clusters of complex conformations found from each inhibitors, the lowest binding energy and highest frequency cluster was selected as the representative.

3. Results and Discussion

3.1 Binding mode prediction of HIV-1RT/inhibitors by fixed docking

AutoDock 4.2 program was used in order to predict the preferred orientations of inhibitor molecule to HIV-1 RT binding pocket. The NNRTI binding pocket of rilpivirine (RPV, 2ZD1) composes with amino acid residues Leu100, Lys101, Lys103, Val179, and Tyr181. NtRTI binding pocket for tenofovir (TFO) composes with amino acid residues Asp110, Asp185, and Lys219 for TFO (1T03) and Lys65, Arg72, Asp110, and Lys219 for TFO (1T05). NRTI binding pocket for emtricitabine (ETV) composes with amino acid residues Lys65, Arg72, Asp110, and Lys219. According to the simulations, all inhibitor molecules are able to bind with RT at its binding pocket which could be indicated from the negative values of energy in the range of -2.11 to -6.08 kcal/mol (Table 1). Table 1: Binding energy (kcal/mol) of RT/inhibitor from fixed molecular docking

Inhibitors	Number of clusters	Lowest binding energy	mean binding energy
rilpivirine (RPV)	1	-12.87	-12.8
tenofovir - (TFO-1T03)	16	-4.55	-3.54
tenofovir -(TFO-1T05)	67	-6.08	-3.65
emtricitabine (ETV)	12	-5.26	-4.65

Individual HIV-1 RT/inhibitor was investigated to determine all atomic positions with a hundred of simulations to ensure all possibilities of inhibitor molecular conformation in the binding pocket.

The results of each HIV-1 RT/inhibitor could be clustered in different groups based on the root mean square deviation in a position of atoms in the inclusion complex. Molecules in the same cluster must have the variation in position less than 2 Å. Table 1 shows different clusters of each inhibitor molecule's conformations in the complex. Table 1 also shows the free energy of binding involved in the interaction between individual inhibitor and their binding pocket determined by fixed molecular docking simulations. The binding energy for each RT/inhibitor complex is negative which indicates that the predicted structure is stable and possible to occur. The selected binding models of RT/inhibitors are presented in Figure 1-4.

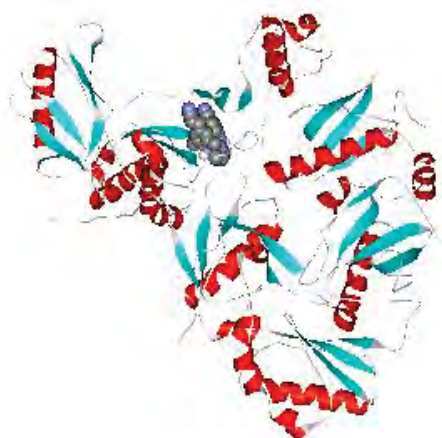


Figure 1. The predictive conformation of RT/RPV



Figure 2. The predictive conformation of RT/TFO (1T03)



Figure 3. The predictive conformation of RT/TFO (1T05)



Figure 4. The predictive conformation of RT/ETV

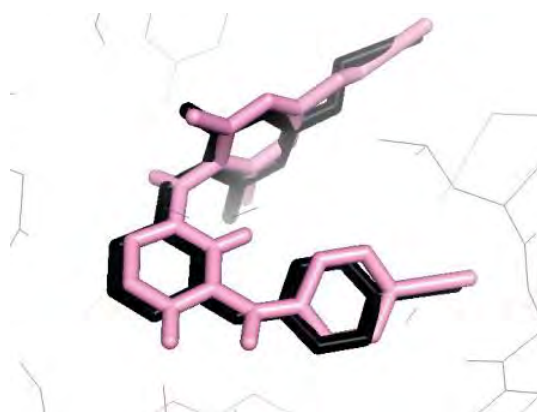


Figure 1: Superimposed structure of RPV. The black and pink models represent reference structure from PDB and predictive structure, respectively.

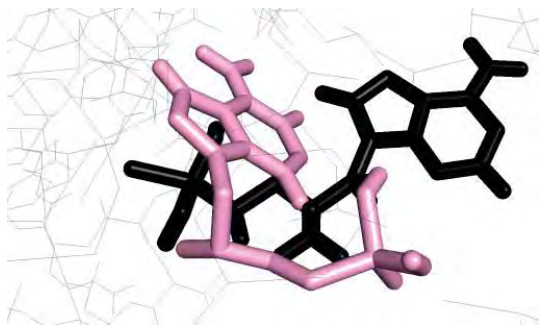


Figure 2: Superimposed structure of TFO (1T03). The black and pink models represent reference structure from PDB and predictive structure, respectively.

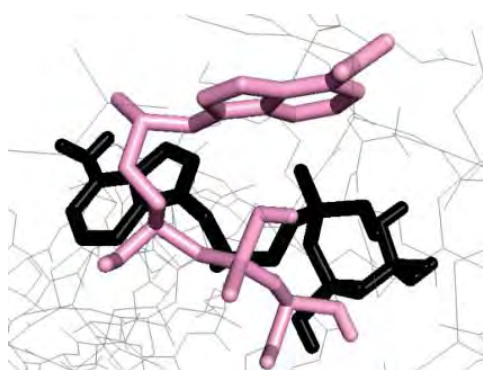


Figure 3: Superimposed structure of TFO (1T05). The black and pink models represent reference structure from PDB and predictive structure, respectively.

Table 1: Superposition results of predictive models with PDB x-ray data

Inhibitors	PDB code	RMSD (Å)
RPV	2ZD1	3.42
TFO(1T03)	1T03	2.27
TFO(1T05)	1T05	3.10

The structures of the predictive RT/RPV and RT/TFO conformations are superimposed with the x-ray structures to check the reliability of the calculation models. The root mean square deviation (RMSD) values are shown in Table 2 and the structures are shown in Figures 5-7. This comparison for ETV does not perform because the x-ray structure of RT/ETV is not available.

3.2 Binding mode prediction of HIV-1RT/inhibitors by flexible docking

Some amino acid residues of the inhibitor binding pocket and its inhibitor are allowed to move freely in flexible molecular docking (Table 3). The binding energies from flexible docking calculations are presented in Table 4. Flexible molecular docking calculations given many predictive models as indicate by their number of clusters.

Most of the models of RT/RPV and RT/TFO provide the positive binding energy values which indicated unfavorable complexes. Only the conformations with negative binding energy values are selected for further detail analyses. Table 5 shows the RMSD values from superposition of our predictive models with x-ray structures and the conformations are shown in Figures 8-10. Flexible docking of RT/ETV prediction models give the negative binding energy for all 58 clusters, the values are in the range of -0.02 kcal/mol to -3.62 kcal/mol.

Table 3: Amino acid residues which are allowed to move in flexible docking

Inhibitors			
RPV	TFO(1T03)	TFO(1T05)	ETV
Leu100	Asp110	Lys65	Lys65
Lys101	Asp185	Arg72	Arg72
Lys103	Lys219	Asp110	Asp110
Val179		Lys219	Lys219
Tyr181			

Table 4: Binding energy (kcal/mol) of RT/inhibitor from flexible molecular docking

Inhibitors	Number of Clusters	Lowest binding energy
rilpivirine (RPV)	80	-5.19
Tenofovir TFO (1T03)	28	-1.84
tenofovir TFO (1T05)	82	-2.27
emtricitabine (ETV)	58	-3.62

Table 5: Superposition results of predictive models from flexible docking with x-ray data

Inhibitors	Cluster	Binding energy (kcal/mol)	RMSD
RPV	1	-5.19	3.56
	1	-1.84	1.31
	2	-1.70	2.47
	3	-1.45	1.74
TFO(1T03)	4	-1.31	1.70
	1	-2.27	2.07
	2	-1.22	3.02
	3	-0.85	1.89
TFO(1T05)	4	-0.80	1.63

According to the results from both fixed and flexible amino acid residues, it is observed that the amount of possible clusters for fixed amino acid residues is a lot less than clusters for flexible amino acid residues because the fixed structures have more movement limitations than the flexible structures. The lowest binding energy for each cluster in fixed amino acid residues is also lower than the lowest binding energy for flexible amino acid residues. However, molecular modeling results show possible structure appear in both conditions and the flexible condition will give the value more closer to the reality because,

naturally, molecules can move freely to adjust to the most stable conformation. The RMSD value for each structure of inhibitor is also acceptable and shows that the molecular modeling result from the experiment is reliable when compare to the structure from PDB.

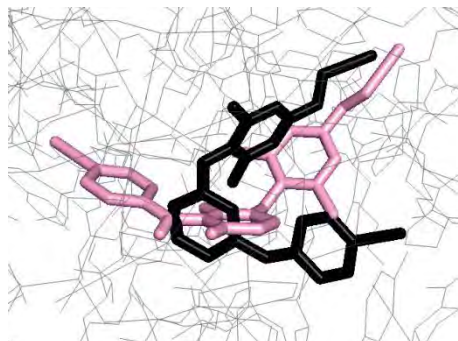


Figure 8: Superimposed structure of RPV. The black and pink models (flexible docking) represent reference structure from PDB and predictive structure, respectively.

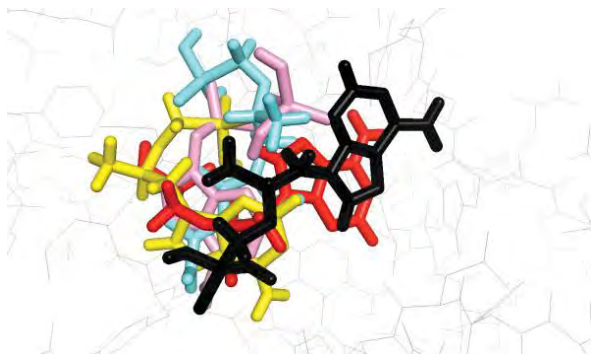


Figure 9: Superimposed structure of TFO (1T03). The black, pink, yellow, blue, and red models represent reference structure from PDB, cluster 1, 2, 3, and 4 from flexible docking respectively.

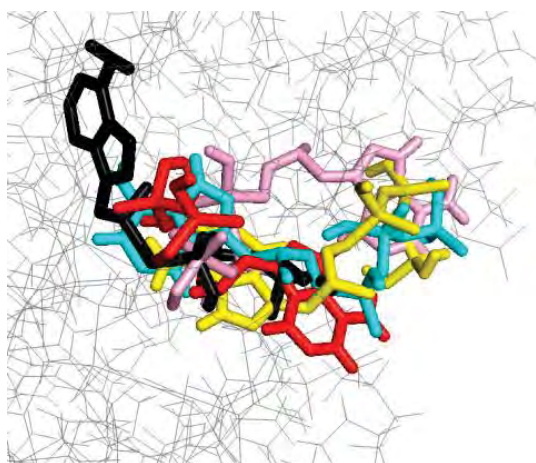


Figure 4: Superimposed structure of TFO (1T05). The black, pink, yellow, blue, and red models represent reference structure from PDB, cluster 1, 2, 3, and 4 from flexible docking respectively.

4. Conclusions

Molecular docking simulations are used to predict the interaction of three inhibitors, which are RPV, TFO, and ETV to HIV-1 RT. The representative models were selected from a hundred conformations by consider the lowest binding energy with highest occurring frequency. The results from flexible ligand and fix protein molecular docking models provide reliable predictive ability same as flexible ligand and some side chain of amino acid residues compare to the experimental data. The result models show the reliable predictive abilities which can be used to predict the binding mode and conformation in an active site of non-available crystallographic structural data in PDB.

Acknowledgements

The authors are grateful to Thammasat University Research Fund (2012) for financial support.

References

- [1] D. W. Rodgers, S.J.Gamblin, B. A. Harris, S. Ray, J. S. Culp, B. Hellmig, D. J. Woolf, C. Debouck and S.C. Harrison, *Proc. Natl. Acad. Sci. USA*. **92**(4) (1995) 1222-1226.
- [2] L. Lawtrakul, A. Beyer, S. Hannongbua and P. Wolschann, *Monatshefte für Chemie/ Chemical Monthly*, **Vol. 135** (2004) pp. 1033-1046.
- [3] N. Sluis-Cremer, D. Arion and M. A. Parniak, *Cell. Mol. Life. Sci.* **57**(10) (2000) 1408-1422.
- [4] S. Tuske, S.G.SSarafianos, A. D. Clark Jr, J. Ding, L. K. Naeger, K. L. White, M. D. Miller, C. S. Gibbs, P. L. Boyer, P. Clark, G. Wang, B. L. Gaffney, R. A. Jones, D. M. Jerina, S. H. Hughes, and E. Arnold, *Nat. Struct. Mol. Biol.* **11**(5) (2004) 469-474.
- [5] <http://pharmacologycorner.com/animation-nrti-mechanism-of-action/>. (Retrieved October 29, 2012)
- [6] E. D.Clerc, *Int. J. Antimicrob. Agents*. **33**(4) (2009) 307-320.
- [7] <http://www.aidsmap.com/How-NRTIs-and-NtRTIs-work/page/1729427/>. (Retireved November 1, 2012).
- [8] S. G. Sarafianos, B.Marchand, K. Dan, D. M. Himmel, M. A. Parniak, S. H. Hughes and E. Arnold, *J. Mol. Biol.* **385**(3) (2008) 693-713.

IN SILICO DRUG DESIGN AND MOLECULAR DOCKING STUDY OF THALIDOMIDE DERIVATIVES AS TUBULIN-POLYMERIZATION INHIBITORS

Suchaya Pongsai*, Chollatorn Duangoe

Department of Chemistry and Center of Excellence for Innovation in Chemistry, Faculty of Science, Burapha University, Chonburi, 20131 Thailand. * E-mail: busakorn@buu.ac.th, Tel. +66 38 103067, Fax. +66 38 393494

Abstract: In this work, the ADMET prediction and molecular docking study have been applied for molecular drug design of thalidomide derivatives as the tubulin-polymerization inhibitors. The experimental structure of α,β -tubulin receptor was taken from PDB code 1SA0. Various kind of functional groups have been substituted to the side chains of ligand template (5HPP-33). For computational prediction of the activity and toxicity, the 'ADMET Descriptors' were used to evaluate the druglike properties of new thalidomide analogues. The interaction energies of α,β -tubulin with each ligand analogue have been investigated by using the 'Receptor-Ligand Interaction' protocol with CDOCKER algorithm and CHARMM forcefield in DS2.5 program. The binding sites and interaction energies of the true drugs (5HPP-33 and 5HFPP-33) and the thalidomide derivatives with α,β -tubulin receptor have been investigated. From the molecular docking results, it is found that the binding site 1 provided the lowest interaction energy (-42.08 kcal/mol) between 5HPP-33 and α,β -tubulin, whereas the binding site 3 provided the lowest interaction energy (-36.47 kcal/mol) between 5HFPP-33 and α,β -tubulin. From the present study, it can be predicted that the thalidomide derivatives, which are possibly reactive as the tubulin-polymerization inhibitors rather than 5HPP-33 and 5HFPP-33, are the ligands 84 and 87, respectively.

Keywords: ADMET; Molecular docking; Thalidomide derivatives; Tubulin inhibitors

1. Introduction

According to the structural development studies of thalidomide analogues based on tubulin polymerization-inhibitory activity, the potent inhibiting agents, such as 5HPP-33 and 5HFPP-33 were obtained (Fig. 1), comparable with rhizoxin or colchicines [1,2]. Some reported that 5HPP-33 is not tubulin polymerization inhibitor [3], but the recently experimental work concluded that 5HPP-33 exhibits this activity [2,4]. Experimentally, the crucial work of new tubulin polymerization inhibitor derived from thalidomides was implicated for anti-myeloma therapy [5]. Although the direct binding of novel polymerization inhibitors with α,β -tubulin heterodimer protein was observed experimentally, however, the binding site(s) remains unclear.

In the present work, we expected to identify the binding site(s) of 5HPP-33, and 5HFPP-33, with α,β -tubulin heterodimer, and to design new thalidomide derivatives based on 5HPP-33 (parent template), in order to be the candidates of new potent anticancer drugs for the microtubule-inhibiting target in

chemotherapy [6-8]. Along with the ADMET prediction, the molecular docking has been performed for the receptor-ligand interactions. In conclusion, the possibly reactive drugs were proposed as the tubulin-polymerization inhibitors.

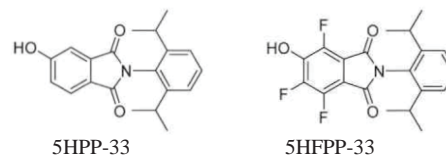


Figure 1. Structure of 5HPP-33 and 5HFPP-33

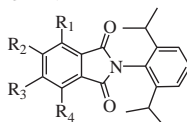
2. Computational Methods

The molecular docking method has been employed to construct binding models for a set of structurally diverse active sites, using α,β -tubulin heterodimer from PDB code 1SA0. Discovery Studio program (Accelrys, San Diego, CA) was used to evaluate the drug-target interactions. The drug templates (5HPP-33 and 5HFPP-33) were created by Chem Draw7.0 and different substituents (R_1 , R_2 , R_3 , R_4) were modified to provide a variety of new modeling thalidomide derivatives (Table 1). The three-dimensional structures of all ligands were performed for the energy minimization via Ligand Minimization protocol, in DS2.5 program [9].

Computational prediction of the activity and toxicity of new thalidomide derivatives were taken into account to evaluate the druglike properties, including real drugs: 5HPP-33 and 5HFPP-33, by using the ADMET Descriptors protocol in DS2.5 program. The Absorption, Distribution, Metabolism, Excretion, and Toxicity (ADMET) were reported. Only the available ligands with acceptable druglike properties (see Table 2) were considered to perform the molecular docking study [10].

In molecular docking simulations, the CDOCKER protocol with CHARMM forcefield has been carried out to evaluate the ligand-receptor interactions between α,β -tubulin heterodimer (receptor) and ligand (drug) in 38 binding sites, generated at random (Fig. 2). The docked ligand poses (of the most stable conformations) with lowest interaction energies were collected. The interaction energies and mechanisms were interpreted. Intermolecular hydrogen bonds were detected. Overlay similarity between each docked ligand and real drugs (5HPP-33 and 5HFPP-33) was reported, with 50% steric and 50% electrostatic contributions.

Table 1. Four different substituents (R_1 , R_2 , R_3 , R_4) of new modeling thalidomide derivatives based on 5HPP-33 template.



Ligand	R_1	R_2	R_3	R_4	Ligand	R_1	R_2	R_3	R_4	Ligand	R_1	R_2	R_3	R_4	Ligand	R_1	R_2	R_3	R_4
1	H	H	H	H	27	COH	H	H	F	53	H	CONH ₂	F	F	79	F	CH ₂ NH ₂	OCH ₃	NH ₂
2	OCH ₃	H	H	H	28	CH(NOH)	H	H	F	54	H	CH ₂ OH	F	F	80	F	COOH	OCH ₃	F
3	H	OCH ₃	H	H	29	CH ₂ NH ₂	H	H	F	55	H	COH	F	F	81	F	CONH ₂	OCH ₃	F
4	H	H	OCH ₃	H	30	COOH	H	F	F	56	H	CH(NOH)	F	F	82	F	CH ₂ OH	OCH ₃	F
5	H	H	H	OCH ₃	31	CONH ₂	H	F	F	57	H	CH ₂ NH ₂	F	F	83	F	COH	OCH ₃	F
6	H	F	F	F	32	CH ₂ OH	H	F	F	58	H	COOH	H	F	84	F	CH(NOH)	OCH ₃	F
7	H	H	F	F	33	COH	H	F	F	59	H	CONH ₂	H	F	85	F	CH ₂ NH ₂	OCH ₃	F
8	H	H	H	F	34	CH(NOH)	H	F	F	60	H	CH ₂ OH	H	F	86	NH ₂	COOH	F	F
9	OCH ₃	F	F	F	35	CH ₂ NH ₂	H	F	F	61	H	COH	H	F	87	NH ₂	CONH ₂	F	F
10	OCH ₃	F	OCH ₃	F	36	H	SOO(OH)	H	H	62	H	CH(NOH)	H	F	88	NH ₂	CH ₂ OH	F	F
11	OCH ₃	F	F	OH	37	H	POOHNH ₂	H	H	63	H	CH ₂ NH ₂	H	F	89	NH ₂	COH	F	F
12	COOH	H	H	H	38	H	CO(NHCN)	H	H	64	F	COOH	H	F	90	NH ₂	CH(NOH)	F	F
13	CONH ₂	H	H	H	39	H	POOHOEt	H	H	65	F	CONH ₂	H	F	91	NH ₂	CH ₂ NH ₂	F	F
14	CH ₂ OH	H	H	H	40	H	COOH	H	H	66	F	CH ₂ OH	H	F	92	NH ₂	COOH	H	F
15	COH	H	H	H	41	H	CONH ₂	H	H	67	F	COH	H	F	93	NH ₂	CONH ₂	H	F
16	CH(NOH)	H	H	H	42	H	CH ₂ OH	H	H	68	F	CH(NOH)	H	F	94	NH ₂	CH ₂ OH	H	F
17	CH ₂ NH ₂	H	H	H	43	H	COH	H	H	69	F	CH ₂ NH ₂	H	F	95	NH ₂	COH	H	F
18	COOH	F	F	F	44	H	CH(NOH)	H	H	70	F	SOO(OH)	OCH ₃	NH ₂	96	NH ₂	CH(NOH)	H	F
19	CONH ₂	F	F	F	45	H	CH ₂ NH ₂	H	H	71	F	POOHNH ₂	OCH ₃	NH ₂	97	NH ₂	CH ₂ NH ₂	H	F
20	CH ₂ OH	F	F	F	46	F	COOH	F	F	72	F	CO(NHCN)	OCH ₃	NH ₂	98	F	COOH	NH ₂	F
21	COH	F	F	F	47	F	CONH ₂	F	F	73	F	POOHOEt	OCH ₃	NH ₂	99	F	CONH ₂	NH ₂	F
22	CH(NOH)	F	F	F	48	F	CH ₂ OH	F	F	74	F	COOH	OCH ₃	NH ₂	100	F	CH ₂ OH	NH ₂	F
23	CH ₂ NH ₂	F	F	F	49	F	COH	F	F	75	F	CONH ₂	OCH ₃	NH ₂	101	F	COH	NH ₂	F
24	COOH	H	H	F	50	F	CH(NOH)	F	F	76	F	CH ₂ OH	OCH ₃	NH ₂	102	F	CH(NOH)	NH ₂	F
25	CONH ₂	H	H	F	51	F	CH ₂ NH ₂	F	F	77	F	COH	OCH ₃	NH ₂	103	F	CH ₂ NH ₂	NH ₂	F
26	CH ₂ OH	H	H	F	52	H	COOH	F	F	78	F	CH(NOH)	OCH ₃	NH ₂					

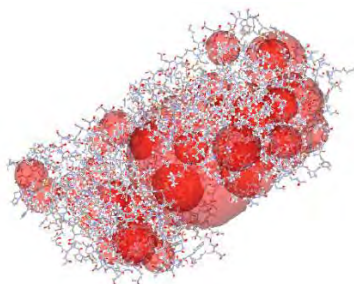


Figure 2. (a) all possibly generated 38-binding sites (spheres) in α,β -tubulin heterodimer.

3. Results and Discussion

3.1 ADMET Prediction for Available Ligands of Modeling Thalidomide Derivatives

The ADMET prediction was used to evaluate the important physicochemical properties of new 103 ligands (modeling thalidomide derivatives), including the drugs 5HPP-33 and 5HFPP-33 have been accepted. Only 8 ligands, which possess the druglike properties, have been acceptable by considering the druglikeness criteria, previously described in details [10]. The most important criteria is that the toxicity must not be greater than 0.5. The values of predicted physicochemical properties of 8 available ligands: 84, 23, 25, 90, 85, 87, 10 and 22, are listed in Table 3. These ligands will be considered to perform the molecular docking study.

Table 2. The criteria of druglikeness considered in this work [9].

Value	Description
Tox_P \leq 0.5	unlikely to cause dose-dependent liver injuries
CYP_P \leq 0.5	unlikely to inhibit Cyp2D6 enzyme
0 \leq BBB \leq 3	inside 99% confidence ellipse)
0 \leq PPB \leq 2	acceptable plasma protein binding)
0 \leq Abs \leq 2	acceptable human intestinal absorption
1 \leq Sol \leq 4	acceptable aqueous solubility

Table 3. The available ligands with acceptable druglike properties by ADMET prediction.

Ligand	Tox_P	CYP_P	BBB	Abs	Sol	PPB	AlogP	PSA
84	0.46	0.33	1	0	1	2	5.24	67.70
23	0.46	0.32	0	1	1	2	5.82	55.30
25	0.48	0.33	1	0	1	2	5.17	64.50
90	0.48	0.31	2	0	1	1	4.51	85.30
85	0.49	0.33	1	0	1	2	5.60	64.20
87	0.49	0.33	1	0	1	1	4.95	73.40
10	0.50	0.33	0	1	1	2	6.05	46.90
22	0.50	0.33	1	0	1	2	5.46	58.80
5HPP-33	0.85	0.48	1	0	1	2	5.20	58.77
5HFPP-33	0.50	0.28	1	1	1	2	5.82	58.77

Note: **Tox_P** (Hepatotoxicity Propability); **E_{int}** (Interaction Energy, in kcal/mol); **O.S.** (Overlay similarity); **H** (Number of H-bond); **BBB** (Blood-Brain Barrier Level); **Abs** (Human Intestinal Absorption Level); **Sol** (Aqueous Solubility Level); **CYP_P** (CYP2D6 Binding Probability); **PPB** (Plasma Protein Binding Level); **AlogP** (AlogP98); **PSA** (Polar Surface Area)

3.2 Molecular Docking Study of α,β -Tubulin with 5HPP-33, 5HFPP-33, and Thalidomide Derivatives

The interactions between α,β -tubulin heterodimer (receptor) and individual ligand in 38 binding sites have been simulated. The molecular docking results showed that 5HPP-33 is attracted in binding sites 1, 2, 3, 12, 13, 19 and 20 (Fig. 3); 5HFPP-33 in sites 1, 2, 3 and 13; other ligands in only sites 1, 2 and 3. Explicitly, the binding sites 1 and 3 provide the lowest interaction energies between receptor and drugs. In ref. 2, the SPR experiments observed direct interaction of 5HPP-33 with α,β -tubulin heterodimer, but no binding competition was observed. In this study, it is indicated that the preferable binding sites of 5HPP-33 with α,β -tubulin is located nearby colchicines-binding site.

From the calculated results, the binding site 1 provided the lowest interaction energy (-42.08 kcal/mol) between α,β -tubulin and 5HPP-33, whereas the binding site 3 provided the lowest interaction energy (-36.47 kcal/mol) between α,β -tubulin and 5HFPP-33. The calculated interaction energies for the docked ligands are within a range between -52.20 and -37.63 kcal/mol in binding site 1 (Table 4); and between -44.33 and -37.97 kcal/mol in binding site 3 (Table 5).

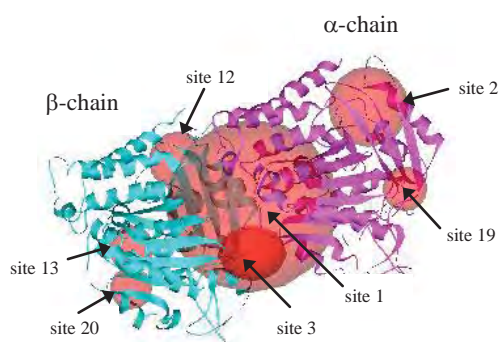


Figure 3. Binding sites 1, 2, 3, 12, 13, 19 and 20.

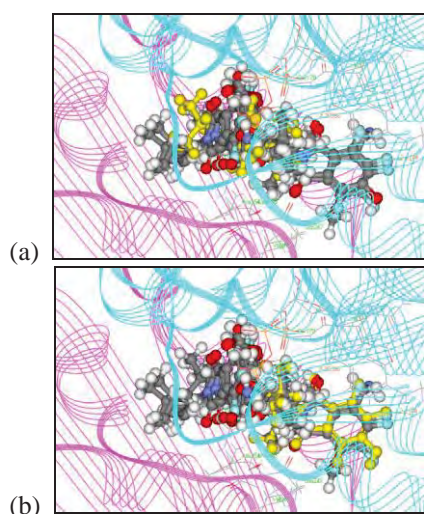


Figure 4. (a) Ligands 22, 23, 84, 85, 87 and 90 located in binding site 1, as 5HPP-33 (yellow). (b) Ligands 10 and 25 located in binding site 3, as 5HFPP-33 (yellow).

Table 4. The receptor-ligand interaction energies (kcal/mol) and hydrogen bonding in binding site 1, compared with 5HPP-33 and 5HFPP-33.

Ligand	E_{int}	H-bond
84	-52.20	CH ₃ O-HN:Gly α 144, 2F-HN:Lys β 254, CH ₂ OH-OP:GTP α 600
87	-50.99	H ₂ N-HN:Lys β 254, H ₂ N-HN:Lys β 254, NH-OP:GTP α 600, NH-O=P:GTP α 600
85	-45.57	CH ₃ O-HN:Lys β 254, CH ₃ O-HN:Lys β 254
90	-43.77	CH ₃ O-HN:Lys β 254, CH ₃ O-HN:Lys β 254
23	-42.00	HC=O-HN:Lys β 254
22	-40.74	HO-HN:Lys β 254
10	-37.66	2F-HN:Tyra224, 2C=O-HO:Tyra224
25	-37.63	2F-HN:Tyra224
5HPP-33	-42.08	HO-HN:Asn β 249, HO-HN:Lys β 254, HO-HN:Lys β 254, OH-O=P:GTP α 600
5HFPP-33	-35.90	2F-HN:Tyra224, 2C=O-HO:Tyra224

The docked ligands: 22, 23, 84, 85, 87 and 90, are locating in binding site 1, as the same as 5HPP-33, whereas ligands 10 and 25 are in binding site 3, as 5HFPP-33 (Fig. 4). The receptor-ligand interaction energies (E_{int}) and the intermolecular hydrogen bonding (H-bond) between amino acid residue(s) and docked ligand are reported in Tables 4 and 5. It is found that ligands 84 and 87, respectively, are the significantly lowest-energy conformations in binding site 1, with respect to 5HPP-33. Although in binding site 3, ligands 84 and 87 are still the significantly lowest-energy conformations, compared to 5HPP-33 and 5HFPP-33. Hence, the binding site 1 (in α,β -tubulin heterodimer) is supposed to be preferable location for ligands 84 and 87.

Table 5. The receptor-ligand interaction energies (kcal/mol) and hydrogen bonding in binding site 3, compared with 5HPP-33 and 5HFPP-33.

Ligand	E_{int}	H-bond
84	-44.33	2F-HO:Thra73, CH ₃ O-HN:Arg β 2, CH ₃ O-HN:Arg β 2, 1C=O-HN:Asn β 50, CH ₂ OH-O=C:Ala β 250
87	-42.59	H ₂ N-HN:Arg β 2, H ₂ N-HN:Arg β 2, NH-O=C:Ala β 250
85	-42.04	2F-HN:Thra73, CH=O-HN:Arg β 2, 1F-HN:Arg β 2
90	-41.56	1C=O-HO:Thra73, HO-HN:Arg β 2, 1F-HN:Arg β 2, OH-O=C:Asp β 251, NH-OH:Thra73
25	-38.92	C=O-HO:Thra73, NH-O=C:Asp β 251
22	-38.89	HO-HN:Arg β 2, OH-O=C:Ala β 250
23	-38.38	C=O-HO:Thra73, HC=O-HN:Asn β 50
10	-37.97	2C=O-HN:Arg β 48
5HPP-33	-35.39	2C=O-HN:Thra73, OH-OH:Asp β 251
5HFPP-33	-36.47	2C=O-HN:Thra73, OH-O=C:Glu β 47

Table 6. Overlay similarity values of docked ligands to 5HPP-33 and 5HFPP-33, in binding sites 1 and 3.

Site	Ligand	O.S. to 5HPP-33	O.S. to 5HFPP-33
1	10	0.69	0.95
	22	0.69	0.93
	23	0.64	0.91
	25	0.73	0.93
	84	0.76	0.84
	85	0.72	0.87
	87	0.77	0.83
	90	0.79	0.91
3	10	0.74	0.93
	22	0.73	0.94
	23	0.78	0.94
	25	0.76	0.95
	84	0.79	0.87
	85	0.79	0.90
	87	0.79	0.88
	90	0.81	0.88

The results indicated that, in binding site 1, 5HPP-33 provides three H-bonds to Asn β 249, Lys β 254 and GTP α 600; ligand 84 forms H-bond to Gly α 144, Lys β 254 and GTP α 600; ligand 87 forms H-bond to Lys β 254 and GTP α 600. In binding site 3, 5-HFPP-33 provides two H-bonds to Thr α 73 and Glu β 47; ligand 84 forms H-bond to Thr α 73, Arg β 2, Asn β 50 and Ala β 250; ligand 87 forms H-bond to Arg β 2 and Ala β 250. However, the number of intermolecular H-bond is not relatively proportional to the strength of receptor-ligand interaction [9-11].

Overlay similarity (O.S.) between docked ligand and 5HPP-33 (or 5-HFPP-33) are represented in Table 6. In binding site 1 and 3, the O.S. values for the docked ligands with respect to docked 5HPP-33 are 0.64-0.79 and 0.73-0.81, respectively, and to docked 5HFPP-33 are 0.83-0.95 and 0.87-0.95, respectively. The orientations of ligands 84 and 87 are in good agreement with 5HPP-33 and 5HFPP-33 (> 75% and 80%, respectively).

4. Conclusions

The molecular docking study suggested that the lowest interaction energy between α,β -tubulin and 5HPP-33 is at binding site 1, whereas 5HFPP-33 is at binding site 3 (Fig. 4). According to the druglike and energetic properties, the present study can predict for two of the tubulin-inhibiting agents, which are ligands 84 and 87, as illustrated in Fig. 5. Theoretically, these new thalidomide analogues provide significantly less toxicity and higher stability comparable with 5HPP-33 in binding site 1, and with 5HFPP-33 in binding site 3.

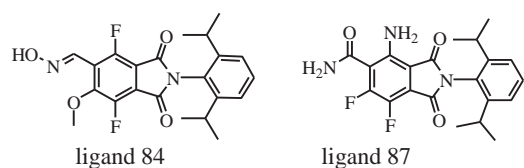


Figure 5. Structures of ligands 84 and 87, the new predicted thalidomide derivatives based on tubulin polymerization-inhibitory activity.

Acknowledgements

Financial support from the Center of Excellence for Innovation in Chemistry (PERCH-CIC), Office of the Higher Education Commission, Ministry of Education is gratefully acknowledged.

References

- [1] Y. Hashimoto, Structural Development of Biological Response Modifiers Based on Thalidomide, *Bioorg. & Med. Chem.* **10** (2002), 461-479.
- [2] H. Aoyama, T. Noguchi, T. Misawa, T. Nakamura, H. Miyachi, Y. Hashimoto and H. Kobayashi, Development of tubulin-polymerization inhibitors based on the thalidomide skeleton. *Chem. Pharm. Bull.* **55** (2007), 944-949.
- [3] S. Inatsuki, T. Noguchi, H. Miyachi, S. Oda, T. Iguchi, M. Kizaki, Y. Hashimoto and H. Kobayashi, Tubulin-polymerization inhibitors derived from thalidomide. *Bioorg. & Med. Chem. Lett.* **15** (2005), 321-325.
- [4] P.K. Li, B. Pandit, D.L. Sackett, Z. Hu, J. Zink, J. Zhi, D. Freeman, R.W. Robey, K. Werbovetz, A. Lewis and C. Li, A thalidomide analogue with in vitro antiproliferative, antimitotic, and microtubule-stabilizing activities. *Mol. Cancer. Ther.* **5** (2006), 450-456.
- [5] M. Kizaki, and Y. Hashimoto, New Tubulin Polymerization Inhibitor Derived from Thalidomide: Implications for Anti-Myeloma Therapy, *Curr. Med. Chem.* **15** (2008), 754-765.
- [6] M. Botta, S. Forli, M. Magnani, F. Manetti, *Molecular Modeling Approaches to Study the Binding Mode on Tubulin of Microtubule Destabilizing and Stabilizing Agents*, Springer-Verlag Berlin Heidelberg, New York (2008).
- [7] T.L. Nguyen, C. McGrath, A.R. Hermone, J.C. Burnett, D.W. Zaharevitz, B.W. Day, P. Wipf, E. Hamel, and R. Gussio, A common pharmacophore for a diverse set of colchicine site inhibitors using a structure-based approach, *J Med Chem.* **50** (2005), 6107-6116.
- [8] O.N. Zefirova, A.G. Diikov, N.V. Zyk, and N.S. Zefirov, Ligands of the colchicine site of tubulin: a common pharmacophore and new structural classes, *Russian Chemical Bulletin*, International Edition, **56**(2007), 680-688.
- [9] P. Sudprasert, Design of microtubule inhibitors as anticancer drugs, Master's Thesis, Burapha University (2011).
- [10] P. Sudprasert, and S. Pongsai, Design of DAMA-colchicine and Arylthioindole Derivatives as Tubulin Inhibitors by Molecular Docking and ADMET Study, *International Annual Symposium on Computational Science and Engineering Conf. Proc. (ANSCSE15)*, Bangkok, Thailand (2011), pp.17-22.
- [11] P. Sudprasert, and S. Pongsai, Molecular Docking of DAMA-colchicine, Arylthioindoles, and Methylchalcone Derivatives with Tubulin Heterodimers, *The 2nd CMU Graduate Research Conf. Proc.*, Chiang Mai, Thailand (2011), pp. 298-307.

BIOSORPTION OF CADMIUM IONS IN AQUEOUS SOLUTION USING BIOSORBENT DERIVED FROM CLAM SHELL POWDER

Nuttaporn Janprapa¹, Benchang Sangchakr¹ and Chinapong Kritayakornupong^{1,*}

¹Department of Chemistry, Faculty of Science, King Mongkut's University of Technology Thonburi, Bangkok, 10140, Thailand

* Author for correspondence; Chinapong.kri@kmutt.ac.th

Abstract: The feasibility of employing clam shell powder to remove the Cd²⁺ ion from aqueous solution was investigated. Parameters that influence the adsorption process such as adsorbent dose, contact time and temperature were studied in batch experiments. By using the treated clam shell powder, the experimental equilibrium adsorption data fitted well to the Langmuir isotherm model. The maximum monolayer adsorption capacity was found to be 10.57 mg g⁻¹ at 303 K. The results reveal that clam shell powder is a biosorbent for removing cadmium ion from aqueous solution and a low cost material that shows potential application in wastewater technology for remediation of heavy metal.

1. Introduction

Both cadmium and soluble cadmium salts are poisonous and deleterious to human beings and animals. The half life of cadmium lasts 20–40 years in body [1] and can harm body's immune system and reproductive system [2]. Several processing techniques are available to reduce the concentrations of heavy metals in wastewater, including precipitation, flotation, ion-exchange, solvent extraction, adsorption, membrane process and electrolytic methods [3].

Adsorption onto activated carbon is a well-known method for removing toxic metal ions, but the high cost of activated carbon restricts its use in developing countries, with small factories in particular often being unable to support expensive wastewater treatment methods. Therefore, numerous approaches have been studied for the development of low cost adsorbents.

Biosorption, the uptake of heavy metals by biomaterials, can be both highly efficient and cost effective. A low cost biosorbent is defined as one which is abundant in nature [4]. Clams abound on the East Coast of Thailand and it is difficult to treat and dispose of a huge amount of waste clam shells. Another potential approach is the use of waste clam shell as the adsorbent. The aim of this study is to evaluate the possibility of utilizing clam shell powder as a cheap adsorbent for removal of cadmium (II) ion from aqueous solution. The adsorption isotherm of cadmium (II) ion was also elucidated.

2. Materials and Methods

2.1 Preparation of Adsorbent

First step, pretreated clam shells by cleansing with deionized water twice to remove sand, dirt and any particles. Second step, removed proteins in shells

with 2 M KOH until it became white and then heated it in oven at 100°C until it was dried. The raw adsorbent was then crushed and sieved to yield particle size in the range of < 450 µm before scouring with 30% H₂O₂ and washings with deionized water until the washings were of approximately pH 7 and dried in the oven at 100 °C.

2.2 Adsorption Procedure

The adsorption studies of cadmium (II) ion were done using batch experiments. In each adsorption experiment, 0.1000, 0.2005, 0.3003 and 0.4004 g of clam shell powder was mixed with a 50 mL of aqueous cadmium (II) ion solution of concentration 50 mg/L in a 250 mL Erlenmeyer flask. The test solution was shaken at 150 rpm on the shaker bath, which was controlled at 30–45 °C. After shaking for a predetermined time interval, the adsorbent was removed by centrifugation and the residual cadmium (II) ion in the clear supernatant solution was determined by Atomic Absorption Spectrophotometer (AAS) at the wavelength 228.80 nanometer. The adsorption capacity of clam shell powder was calculated and presented in terms of percentage of cadmium (II) ion removal (% removal), which represented as the ratio between the amount of cadmium (II) ion adsorbed onto clam shell powder and the starting amount of cadmium (II) ion. Each experiment was made in triplicate.

3. Results and Discussion

3.1 Effect of Contact Time

Figure 1. shows the effect of contact time on the adsorption of cadmium (II) ion onto clam shell powder at the cadmium (II) ion concentrations of 50 mg/L. The curves were single, smooth and continuous, which indicated the monolayer formation of cadmium (II) ion adsorbed onto the outer clam shell powder surface. As seen in Figure 1., the adsorption of cadmium (II) ion occurred rapidly in the first time duration of the experiments, but it gradually decreased with time until it reached saturation. The rapid adsorption at the initial contact time resulted from the abundant availability of the highly negatively charged active sites on clam shell powder for adsorption of cadmium (II) ion in the solution, leading rapid attachment of cadmium (II) ion to the surface of the

adsorbent. Later slow rate is probably due to the electrostatic repulsion between the adsorbed positively charged adsorbate species onto the surface of clam shell powder and the available cationic adsorbate species in the solution as well as the slow pore diffusion of the adsorbate ions into the bulk of the adsorbent. Furthermore, the presence of less available adsorption sites of clam shell powder may cause the slow rate of cadmium (II) ion adsorption.

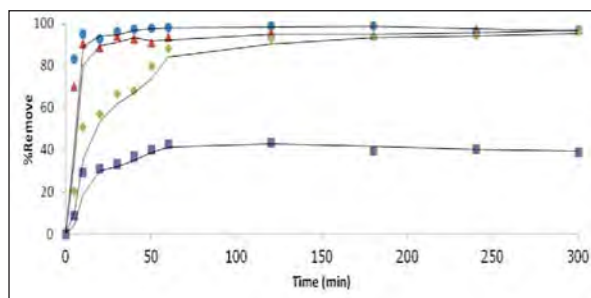


Figure 1. Effect of contact time on adsorption of cadmium (II) ion onto clam shell powder (conditions: adsorbent dose: ■ = 0.1000, ◆ = 0.2005, ▲ = 0.3003 and ● = 0.4004 g, temperature: 30°C, agitation speed: 150 rpm).

3.2 Effect of Adsorbent Dosage

The effect of clam shell powder dosage on the cadmium (II) ion adsorption capacity is shown in Figure 2. As seen in Figure 2, the efficiency of clam shell powder removal was increased with increasing the adsorbent dosage. At the initial cadmium (II) ion concentration of 50 mg/L, the percent removal of cadmium (II) ion were 43.11%, 92.61%, 95.73% and 98.85% for clam shell powder dosage of 0.1000 g, 0.2005 g, 0.3003 g and 0.4004 g, respectively.

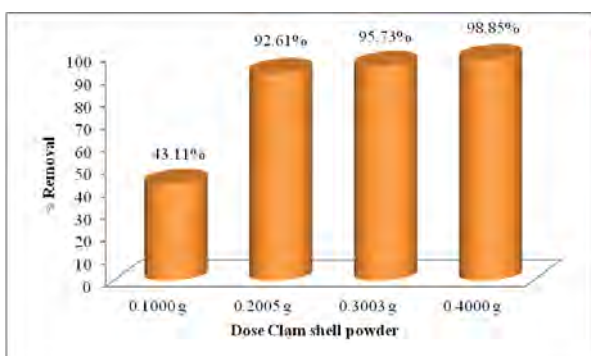


Figure2. Effect of clam shell powder dosage on adsorption of cadmium (II) ion onto clam shell powder (conditions: adsorbent dose: 0.1000, 0.2005, 0.3003 and 0.4004 g, temperature: 30°C, agitation speed: 150 rpm).

3.3 Adsorption Isotherms

Adsorption isotherm is the relationship between concentration and adsorption capacity at each specific temperature. In this study, the Langmuir and

Freundlich isotherm models were used to describe the isotherms of the adsorption of cadmium (II) ion onto clam shell powder [5,6]. The Langmuir equation can be written as follows:

$$C_e/q_e = (1/bQ^0) + (C_e/Q^0)$$

where C_e is the equilibrium concentration of cadmium(II) ion (mgL^{-1}), q_e is the amount cadmium (II) ion adsorbed onto adsorbent at equilibrium (mgg^{-1}), Q^0 is maximum amount of cadmium (II) ion adsorbed onto adsorbent (mgg^{-1}) and b is the Langmuir constants (Lmg^{-1}). Q^0 and b can be determined from the slope and intercept of the linear plot in Figure 3. The correlation coefficient (R^2), Q^0 and b are tabulated in Table 1.

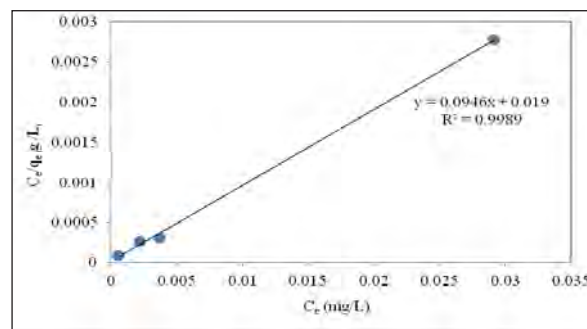


Figure 3. The Langmuir plot of the adsorption of cadmium (II) ion onto clam shell powder (conditions: adsorbent dose: 0.1000, 0.2005, 0.3003 and 0.4004 g, contact time:120 min, temperature: 30°C, agitation speed: 150 rpm).

The Freundlich equation is given as follows:

$$\log q_e = \log K_F + (1/n)\log C_e$$

where q_e is the amount adsorbed of cadmium (II) ion adsorbed onto adsorbent at equilibrium (mgg^{-1}), C_e is the equilibrium concentration of cadmium (II) ion (mgL^{-1}), and K_F is the Freundlich constants(mgg^{-1}) and $1/n$ is an empirical constant. K_F and $1/n$ can be obtained from intercept and the slope of the linear plot in Figure 4. The correlation coefficients (R^2), K_F and $1/n$ are tabulated in Table 1.

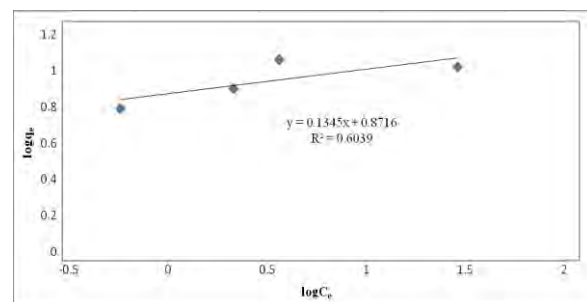


Figure4. The Freundlich plot of the adsorption of cadmium (II) ion onto clam shell powder (conditions: adsorbent dose: 0.1000, 0.2005, 0.3003 and 0.4004 g, contact time: 120 min, temperature: 30 °C, agitation speed: 150 rpm).

From the values of correlation coefficients (R^2) for Langmuir and Freundlich adsorption isotherms (Table 1), the cadmium (II) ion adsorption onto clam shell powder could be better described by Langmuir isotherm than Freundlich isotherm. Therefore, it could imply that the adsorption process of cadmium (II) ion by clam shell powder probably took place on the homogeneous adsorption surfaces under the experimental condition.

Table 1. Linearised isotherm parameters for the Langmuir and Freundlich plots of the adsorption of cadmium (II) ion onto clam shell powder at 30-45 °C

(T °C)	Langmuir Isotherm			Freundlich Isotherm		
	Q^0 (mg/g)	B (L/mg)	R^2	K_F (mg/g ⁻¹)	n	R^2
30	10.57	5.00	0.9989	7.44	7.43	0.6039
35	23.47	1.21	0.9994	10.36	2.67	0.9501
45	34.12	1.35	0.9925	7.52	-2.03	0.6907

4. Conclusion

The results of this study showed that clam shell powder can be effectively used as an efficient and inexpensive adsorbent for removal of cadmium (II) ion from aqueous solutions. The experimental data obtained from batch adsorption studies indicated that the adsorption capacity were a function of contact time, adsorbent dose and temperature. The percent removal was found to depend on the dose of adsorbent, contact time and temperature. The maximum adsorption of cadmium (II) ion was found for the adsorbent dosage of 0.4004 g. The experimental equilibrium adsorption data could be well fitted with the Langmuir isotherm model. Maximum monolayer adsorption capacity, Q^0 , obtained from the Langmuir plot was 10.57 mg/g at 30 °C. The used adsorbent can be regenerated and reused by hydrochloric acid treatment.

Acknowledgements

Computational chemistry research unit at department of chemistry, KMUTT are gratefully acknowledged for all computer resources and facilities and this work was supported by the Higher Education Research Promotion and National Research University Project of Thailand, Office of the Higher Education Commission.

Reference

- [1] Cui Yu-jing, Hung Yi-zong, and Zhu Yong-guan, *Adverse health effects of cadmium and related factors*, J. Hygiene Research. 35 (2006), pp. 656–659.
- [2] An Hong-min, Zheng Wei, Gao Yang, *Research progress in cadmium toxicity*, J. Environ. Sci. Health. 24 (2007), pp. 739–742.
- [3] H. Ting-Chu, *Assessment of adsorption of Cu^{2+} and Ni^{2+} from aqueous solution by oyster shell powder*, J. Hazard. Mater. 171 (2009), pp. 995-1000.

- [4] Prez-Marin A.B., Ballester A., Gonzalez F., Blzquez M.L., Muoz J.A., Sez J. and Meseguer Zapata V., *Study of cadmium, zinc and lead biosorption by orange wastes using the subsequent addition method*, Bioresource Technology. 99 (2008), pp. 8101-8106.
- [5] Langmuir, I. *J. Am. Chem. Soc.* 38 (1916), pp. 2221- 2295.
- [6] Freundlich, H.M.F. *Zeitschrift für, J. Phy. Chem.* 57 (1906), pp. 385-471.

STRUCTURAL AND DYNAMICAL PROPERTIES OF HYDRATED THIOSULFATE ANION IN PRE-EQUILIBRIUM: *AB INITIO* QUANTUM MECHANICAL CHARGE FIELD MOLECULAR DYNAMIC SIMULATION

Montira Trinapakul, Viwat Vchirawongkwin*

Department of Chemistry, Faculty of Science, Chulalongkorn University, Pathumwan, Bangkok, 10330 Thailand

* E-Mail: Viwat.V@chula.ac.th, Tel. +66 22187633, Fax. +66 2187598

Abstract: We applied the theoretical approach to investigate the properties of thiosulfate ($\text{S}_2\text{O}_3^{2-}$) anion, which its compounds have been widely used in a variety of industrial applications especially in agriculture and ore mine even in the photographic process and the synthesis of nanoparticles. Almost publication studies have been focused on the uses and applications of the thiosulfate. However, there is no research studying about the dynamical properties of thiosulfate anion in water as the solvent by the simulation. In this work; therefore, we studied the fundamental data of this anion. The *ab initio* quantum mechanical charge field molecular dynamics (QMCF MD) formalism was applied to simulate the system model of the thiosulfate anion in an aqueous solution to study the behavior and the interaction between thiosulfate and water molecules in the pre-equilibrium step at 298 K for 10 ps. This system consisted of one thiosulfate anion and 495 water molecules in a cubic box of 24.68 Å. We divided the pre-equilibrium steps into 2 periods and compared the results between the first 2-6 ps and last 6-10 ps. The dynamical movement data of all atoms in the system were collected during the simulation. Then, we used the data to analyze and predict the structural and dynamical properties of thiosulfate and its hydration shell in the form of RDF, CND and their molecular manner. The real movement of the water molecules in the hydration shell was presented via three-dimensional alignment.

1. Introduction

Thiosulfate ($\text{S}_2\text{O}_3^{2-}$) compounds have a number of applied uses in a variety of industries. They are used for gold leaching in ore mine industries [1-4], binding silver atoms on film or paper in photographic process [5], even studies in silver deposition [6] and silver electro-crystallization [7,8] by electrochemical reduction and synthesis of silver nanoparticles by shape transformation [9], particularly using as many kinds of fertilizers for agriculture [10-13].

Almost studies are about the usages and applications of the thiosulfate, but no attempt has been studied the dynamical properties of thiosulfate anion in aqueous solution by the computational simulation. In this work; therefore, we applied the *ab initio* quantum mechanical charge field molecular dynamics (QMCF MD) formalism to simulate the system model of the thiosulfate anion in water as solvent to study the behavior and the interaction between thiosulfate and water molecules in the pre-equilibrium steps.

2. Methods

We applied the *ab initio* quantum mechanical charge field molecular dynamics (QMCF MD) formalism [14,15], investigating the structural and dynamical properties of solute and the hydration shell. This method extends the solvent layer beyond the first hydration shell of the solute by QM to avoid the construction of potential functions between the solute and water molecules in bulk solution [16-19]. One of the advantages of the QMCF MD method is the inclusion of the point charges of the atoms in the MM region with their changing positions in core Hamiltonian. On the other hand, the Coulombic interactions between the Mulliken charges on the atoms within the QM region and the point charges of water molecules according to the water model are evaluated providing electrostatic forces described by a dynamically field of point charges, which vary according to the movements of atoms inside the QM region and water molecules in the MM region during the simulation. The QMCF MD method allows the migration of water molecules between the QM and MM region by including a smoothing function [20],

$$S(r) = \begin{cases} 1 & \text{for } r \leq r_{\text{on}} \\ \frac{(r_{\text{off}}^2 - r^2)^2 (r_{\text{off}}^2 + 2r^2 - 3r_{\text{on}}^2)}{(r_{\text{off}}^2 - r_{\text{on}}^2)^3} & \text{for } r_{\text{on}} < r \leq r_{\text{off}} \\ 0 & \text{for } r > r_{\text{off}} \end{cases}$$

where r is the distance of a given solvent molecule from the center of the simulation box, r_{off} is the radius of the QM region, and r_{on} is the inner border of the smoothing region. This function is applied to all atoms of molecules located in smoothing region to ensure a continuous transition and change of forces for these molecules according to

$$F_j^{\text{smooth}} = F_j^{\text{MM}} + (F_j^{\text{layer}} - F_j^{\text{MM}}) \times S(r)$$

where F_j^{layer} is the force acting on a particle j located in the (outer QM) smoothing zone and F_j^{MM} is the force acting on a particle j in the MM region.

The thiosulfate solution system model consisted of one thiosulfate anion and 495 water molecules in a cubic box of 24.68 Å with the periodic boundary condition, with the density of the simulation box of $0.997 \text{ g}\cdot\text{cm}^{-3}$ as the experimental value of pure water at 298 K. The simulation was performed in the NVT ensemble using a general predictor-corrector algorithm with a time step of 0.2 fs. The system temperature was

maintained at 298.16 K by the Berendsen temperature-scaling algorithm [21] with a relaxation time of 100 fs. The QM radius was set as 6.0 Å larger than the size of thiosulfate about 5 Å to surround covering thiosulfate and also hydration shell. The QM subregions, namely, the core and layer zone extended to 3.5 and 6.0 Å, respectively. The average number of water molecules located within the QM region during the simulation period is 23.1 and 24.0 molecules for the first 2-6 ps and last 6-10 ps, respectively. The QM calculation was performed by means of the Hartree-Fock method with the Dunning double- ζ plus polarization [22, 23] basis sets for hydrogen, sulfur, and oxygen atoms in the QM region. The thickness of the smoothing region was chosen as 0.2 Å with the values of r_{on} and r_{off} as 5.8 and 6.0 Å, respectively. We applied the flexible BJH-CF2 selected water model [24,25] to calculate the interactions between pairs of water in the MM region. This water model supports the fully flexible molecular geometries of water molecules transiting between the QM and MM region. In addition, the reaction field method combined with the shifted-force potential technique was applied to account for long-range electrostatic potentials and forces, with a spherical cutoff limit of 12.350 Å.

In this work, the system was equilibrated with the QMCF MD method for 50,000 steps (10 ps). The dynamical movement data of all atoms in the system were collected during the simulation. We divided the data of the pre-equilibrium steps into 2 periods: the first 2-6 ps and last 6-10 ps in order to compare the results to figure out if there is a difference between non-equilibrium and nearly equilibrium by analyzing and predicting the structural and dynamical properties of thiosulfate and its hydration shell in the form of RDF, CND and their molecular manner. The movement of the water molecules in the hydration shell was presented via three-dimensional alignment.

3. Results and Discussion

3.1 Radial Distribution Function (RDF)

The interactions of water molecules and four coordinating sites: sulfur ($S(2)$, S_s) and oxygen ($O(3)$ - $O(5)$, O_s) cause the hydration shell covering around this solute molecule. The fundamental data from each site, we can first evaluate the atomic RDFs from the QMCF MD result as shown in Figure 1 and the molecular RDFs shown in Figure 2. Although the atomic RDFs of the sulfur atom differ from those of oxygen atoms, the atomic RDFs of the sulfur atom for both periods are similar. The peaks are weak and broad, so hydration shells for sulfur site are unclear. On the other hand, other atomic RDFs of oxygen atoms and molecular RDFs for both periods represent similar interaction with the water molecules. The peaks are strong and clear representing the hydration shells. The molecular RDFs are similar to the atomic RDFs of oxygen atoms, showing that the water molecules prefer to interact with oxygen more than sulfur atom.

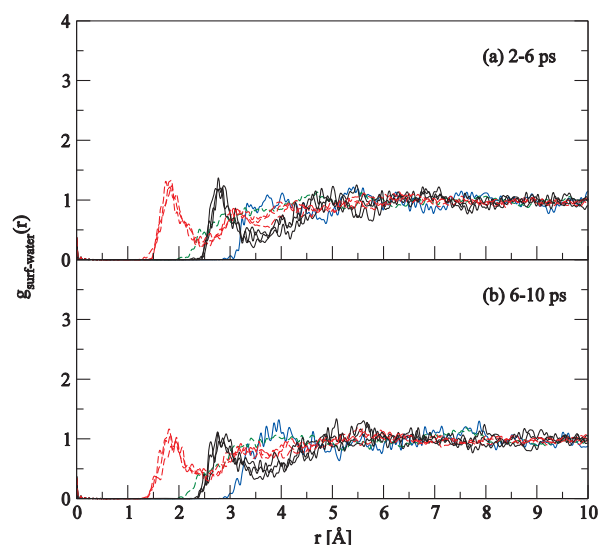


Figure 1. The atomic RDF plots of site-water for (a) 2-6 ps and (b) 6-10 ps period; solid and dashed lines refer to the RDFs for the O and H atoms of water, respectively; black solid ($O_s \cdots O_w$) and red dashed ($O_s \cdots H_w$) lines refer to the RDFs of O atoms of solute, blue solid ($S_s \cdots O_w$) and green dashed ($S_s \cdots H_w$) lines refer to the RDFs of S atom of solute.

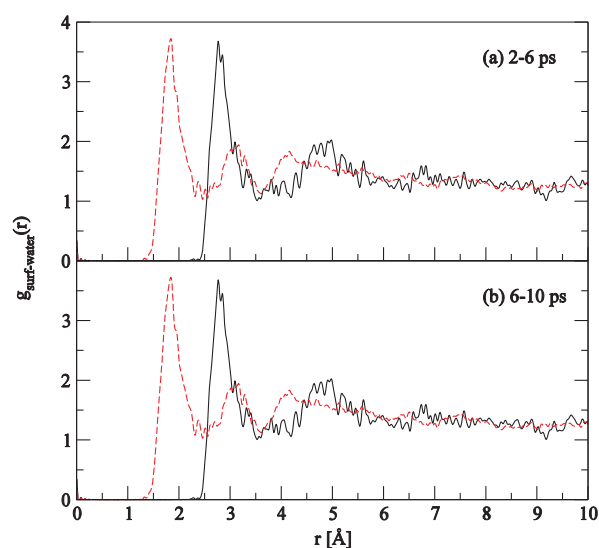


Figure 2. The molecular RDF plots of surface-water for (a) 2-6 ps and (b) 6-10 ps period; black solid (surface $\cdots O_w$) and red dashed (surface $\cdots H_w$) lines refer to the RDFs for the O and H atoms of water, respectively.

The list in Table 1 presents the distances from each coordinating site obtained from the (site) $\cdots O_{\text{water}}$ and (site) $\cdots H_{\text{water}}$ (from atomic RDFs) for the first peak and its boundary of the hydration shell (maximum and minimum of $g_{\alpha\beta}(r)$, respectively), while surface was obtained by the distance from the surface of solute molecule (from molecular RDFs) calculated by the combination of all atomic hydration spheres [26]. The distances of both maximum and minimum for each $O_s \cdots O_{\text{water}}$ are obviously longer than $O_s \cdots H_{\text{water}}$ indicating that the orientation of water molecules points H_{water} to the coordinating site via hydrogen

bonding. However, the atomic RDFs of $S_S \cdots \text{water}$ differ from $O_S \cdots \text{water}$ owing to different atoms. The distances for $S_S \cdots \text{water}$ both maximum and minimum, and $S_S \cdots O_{\text{water}}$ and $S_S \cdots H_{\text{water}}$ are longer than those of $O_S \cdots \text{water}$. From the Figure 1, the minimum of the hydration shells is above the baseline representing the exchanges of water ligand between in the hydration shell and bulk.

3.2 Coordination Number Distribution (CND)

The CND shows the diffusion of the amount of water coordinating with the solute. To evaluate the atomic CNDs for each site and molecular CNDs as shown in Figure 3, the distances for the minimum of each (site) $\cdots O_{\text{water}}$ from atomic RDFs, the hydration shell borders, were employed to define the edge for counting the number of water molecules within the hydration shell as radius from each site. The

coordination number relates to the total number of water molecules interacting with the solute throughout the simulation time. Their averaged coordination numbers (n) are also listed in Table 1 in the last column. From the molecular CND, the possible CNs in 2-6 ps period are in a range of 10 to 17, whereas in 6-10 ps period are higher flexibility of the hydration shell ranging from 11 to 21. Moreover, the atomic and molecular CNDs in 6-10 ps period are higher distributions than in 2-6 ps period. The direct summations of averaged atomic CNs for the first period (16.1) and last period (22.8) are higher than in the corresponding molecular CN, differing by 2.8 and 6.4 molecules, respectively. The different values indicate that some water molecules locate in the intersection volumes of the atomic hydration spheres, referring one water molecule can interact with more than one site.

Table 1: The Characteristic Values of the Radial Distribution Function $g_{\alpha\beta}(r)$ for Each Site of $S_2O_3^{2-}$ Ion in the Hydration Shell Determined by the QMCF MD Simulation

2-6 ps						6-10 ps					
coordinating site	$r_{\max}(O_w)$	$r_{\min}(O_w)$	$r_{\max}(H_w)$	$r_{\min}(H_w)$	n	coordinating site	$r_{\max}(O_w)$	$r_{\min}(O_w)$	$r_{\max}(H_w)$	$r_{\min}(H_w)$	n
S(2)	4.02	4.88	4.70	5.24	10.0	S(2)	4.00	5.14	3.88	5.20	13.2
O(3)	2.88	3.46	1.86	2.46	2.3	O(3)	2.76	3.86	1.84	2.70	3.7
O(4)	2.78	3.24	1.84	2.42	1.8	O(4)	2.78	3.74	1.94	2.50	3.1
O(5)	2.82	3.24	1.74	2.36	2.0	O(5)	2.76	3.64	1.80	2.60	2.8
surface	2.76	3.26	1.84	2.46	13.3	surface	2.76	3.66	1.82	2.62	16.4

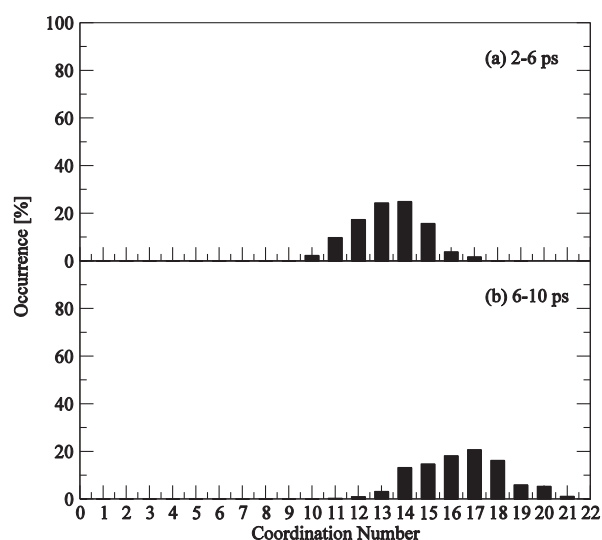


Figure 3. The molecular CNDs of the thiosulfate ion for (a) 2-6 ps and (b) 6-10 ps period.

3.3 Dynamics of the Water Molecules

The dynamical motion data of all atoms within the system were collected during the simulation. Water molecules migrated within or even come in and out of the hydration shell. The visualization of the hydration shell during the simulation period provides an insight to understand the motion of water molecules around the solute. We presented one selected water molecule moving within the molecular hydration shell

throughout the whole interested simulation time via the three-dimensional (3D) alignment [27] as shown in Figure 4.

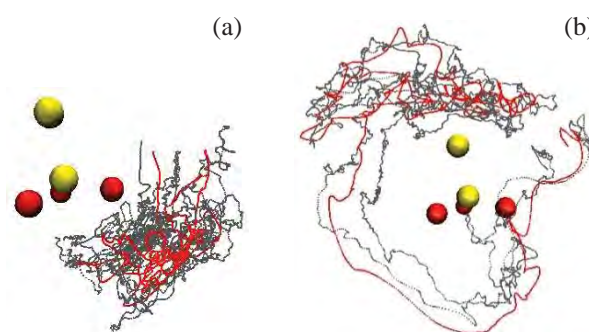


Figure 4. All superimposed trajectories for the coordinates of a selected water molecule moving in the molecular hydration shell of thiosulfate ($S_2O_3^{2-}$) ion throughout the whole interested simulation time: (a) 2-6 ps (b) 6-10 ps (only the one moving around the solute) with 3D alignment obtained from the QMCF MD simulation. The yellow spheres are sulfur atoms, red spheres are oxygen atoms of the solute, red dots are oxygen atoms of the selected water molecules, and gray dots are the hydrogen atoms of the water.

In the first 2-6 ps period, there is only one water molecule moves near oxygen as shown in Figure 4a, but other molecules move across the molecular hydration shell. However, in the last 6-10 ps period

there are many water molecules move within the molecular hydration shell along the whole simulation time. Some water molecules move near oxygen atoms but some water molecules move around the ion as shown in Figure 4b. These indicate that the two periods are different because the system in the last 6-10 ps period approaches the equilibrium closer than another period. In addition, the results agree with the RDFs that water molecules prefer to interact with oxygen. Moreover, the water molecule within the molecular hydration shell rapidly changes the coordinating site around the ion during the simulation period. This evidence proves that the total summation of all atomic CNs is overcount of some water molecules in the intersection volumes.

4. Conclusions

Studying of structural and dynamical properties of a solute in the solution by QMCF MD simulation is one of the great choices. We studied the fundamental data of the thiosulfate ion, when it is dissolved in water. The hydration shells from the atomic RDFs of sulfur for both 2-6 and 6-10 ps periods are unclear while those of oxygen atoms and molecular RDFs obviously show the hydration shells. The water molecules prefer to interact with oxygen more than the sulfur atom. The molecular RDFs indicate the orientation of a water molecule pointing a hydrogen atom to interact with the coordinating site. However, in the same time water molecules can interact with neighbouring sites presented by the dynamical visualization. The interaction between water and oxygen of the thiosulfate ion is stronger than the sulfur site, resulting to clear hydration shell of atomic RDFs of oxygen. Some water molecules locate in the intersection volumes of the atomic hydration spheres reflected by the higher direct sum of atomic CNDs (overcount) than molecular CND and dynamical visualization. The dynamical analysis by 3D alignment for the visualization of the motion of selected water molecule in the molecular hydration shell presented the difference of 2 pre-equilibrium periods.

Acknowledgements

Development and Promotion of Science and Technology Talents Project (DPST) and Department of Chemistry, Faculty of Science, Chulalongkorn University are gratefully acknowledged.

References

- [1] D.M. Muir and M.G. Aylmore In: *Thiosulfate as an alternative lixiviant to cyanide for gold ores*, Vol. 15, Elsevier, Amsterdam (2005), Chapter 22, pp. 541–560.
- [2] G. Senanayake, *Miner. Eng.* **18** (2005) 409–426.
- [3] D. Feng and J.S.J. van Deventer, *Miner. Eng.* **23** (2010) 399–406.
- [4] D. Feng and J.S.J. van Deventer, *Miner. Eng.* **24** (2011) 1022–1024.
- [5] T.H. James, in: *The theory of the photographic process*, Macmillan publishing (1977), Chapter 16.
- [6] D. Gonnissen, S. Vandeputte, A. Hubin and J. Vereecken, *Electrochim. Acta* **41** (1996) 1051–1056.
- [7] W. Simons, D. Gonnissen and A. Hubin, *J. Electroanal. Chem.* **433** (1997) 141–151.
- [8] D. Gonnissen, W. Simons and A. Hubin, *J. Electroanal. Chem.* **435** (1997) 149–155.
- [9] B. Liu, Z. Ma and K. Li, *J. Nanosci. Nanotechnol.* **11** (2011) 5001–5006.
- [10] D.M. Sullivan and J.L. Havlin, *Soil Sci. Soc. Am. J.* **56** (1992) 957–960.
- [11] R.J. Goos, *Soil Sci. Soc. Am. J.* **49** (1985) 232–235.
- [12] J. Gan, S.R. Yates, J.O. Becker and D. Wang, *Environ. Sci. Technol.* **32** (1998) 2438–2441.
- [13] J. Gan, J.O. Becker, F.F. Ernst, C. Hutchinson, J.A. Knuteson and S.R. Yates, *Pest. Manag. Sci.* **56** (2000) 264–270.
- [14] B.M. Rode, T.S. Hofer, B.R. Randolph, C.F. Schwenk, D. Xenides and V. Vchirawongkwin, *Theor. Chem. Acc.* **115** (2006) 77–85.
- [15] T.S. Hofer, A.B. Pribil, B.R. Randolph and B.M. Rode, in: J.R. Sabin and E. Brändas (Eds.), *Ab Initio Quantum Mechanical Charge Field Molecular Dynamics: A Nonparametrized First-Principle Approach to Liquids and Solutions. In Combining Quantum Mechanics and Molecular Mechanics. Some Recent Progresses in QM/MM Methods*, Academic Press, San Diego, (2010), Vol. 59, pp. 213–246.
- [16] A. Warshel, and M. Levitt, *J. Mol. Bio.* **103** (1976) 227–249.
- [17] M.J. Field, P.A. Bash and M. Karplus, *Compt. Chem.* **11** (1990) 700–733.
- [18] J. Gao, *J. Am. Chem. Soc.* **115** (1993) 2930–2935.
- [19] D. Bakowise and W. Thiel, *J. Phys. Chem.* **100** (1996) 10580–10594.
- [20] B.R. Brooks, R.E. Bruccoleri, B.D. Olafson, B.D. States, S. Swaminathan and M. Karplus, *J. Compt. Chem.* **4** (1983) 187–217.
- [21] H.J.C. Berendsen, J.P.M. Poostma, W.F. van Gunsteren, A. DiNola and J.R.J. Haak, *Chem. Phys.* **81** (1984) 3684–3690.
- [22] Jr. T.H. Dunning and P.J. Hay, in: H.F. Schaefer (Eds.), *Gaussian Basis Sets for Molecular Calculations*, Plenum Press, New York, (1977), Vol. 3, Chapter 1, pp. 1–27.
- [23] Jr. T.H. Dunning, *J. Chem. Phys.* **53** (1970) 2823–2833.
- [24] F.H. Stillinger and A. Rahman, *J. Chem. Phys.* **68** (1978) 666–670.
- [25] P. Bopp, G. Jancsó and K. Heinzinger, *Chem. Phys. Lett.* **98** (1983) 129–133.
- [26] S. Vchirawongkwin, V. Vchirawongkwin, *Comput. Theor. Chem.* **974** (2011) 26–30.
- [27] V. Vchirawongkwin, C. Pornpiganon, C. Kritayakornupong, A. Tongraar and B.M. Rode, *J. Phys. Chem. B* **116** (2012) 11498–11507.

MODEL GUANINE TETRAD INTERACTING WITH ALKALI AND ALKALI EARTH METAL IONS ($M = \text{Li}^+, \text{Na}^+, \text{K}^+, \text{Ca}^{2+}, \text{Mg}^{2+}$) BY AB INITIO QUANTUM CALCULATIONS

Phatcharanan Jongsriadisorn¹, Kaewmanee Rungkwanchit¹ and Chinapong Kritayakornupong^{1*}

¹Department of Chemistry, Faculty of Science, King Mongkut's University of Technology Thonburi, Bangkok, 10140 Thailand

*Author for correspondence; E-Mail: chinapong.kri@kmutt.ac.th

Abstract : The guanine tetrad (G4) coordinated with alkali ($\text{Li}^+, \text{Na}^+, \text{K}^+$) and alkali earth ($\text{Ca}^{2+}, \text{Mg}^{2+}$) metal ions were elucidated using the B3LYP and HF levels of theory. The optimized structure corresponding stabilities and binding energy of the tetrads were determined. It was found that the guanine tetrad with bifurcated hydrogen bond is the most stable structure, while the cation-guanine tetrad coplanar complex (G4-M) was stabilized by Hoogsteen hydrogen bond. The results were revealed that the stable sequence of G4-M is $\text{Mg}^{2+} > \text{Ca}^{2+} > \text{Li}^+ > \text{Na}^+ > \text{K}^+$. The structural properties obtained from the HF method are in good agreement with the experimental determination, while the strong hydrogen bonding was revealed by the B3LYP functional.

1. Introduction

Guanine tetrads are formed by the folding of guanine rich sequences from one, two, four-stranded nucleic acid structures occurring in telomeric regions of eukaryotic chromosomes, which lead to a DNA mutation [1-3]. The structure of guanine tetrads consist of the cyclic hydrogen-bonding of four guanine bases in a square planar. The two or more guanine tetrads can stack on top of each other to form a "Guanine quadruplexes" (see Fig. 1).

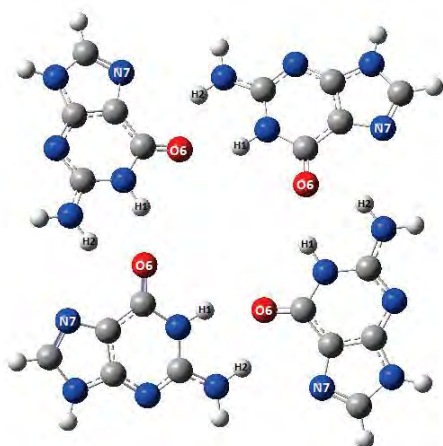


Fig. 1. Structure of a Guanine tetrad, oxygen, red; carbon, gray; nitrogen, blue; and hydrogen, white.

Guanine quadruplex plays important roles in biological regulation, design anticancer drugs and devices for nanotechnology [4]. In addition it is and inhibitor of HIV replication and telomerase [4].

It is well known that metal ions are required in the formation of guanine quadruplex and also the different types of metal ion effect the structure of the guanine quadruplex. Therefore, it is interesting to investigate their interactions with the guanine tetrad [1-6]. The cations were revealed to stabilize the guanine quadruplex structures [5-6]. Thus, in this work the metal ions $\text{Li}^+, \text{Na}^+, \text{K}^+, \text{Ca}^{2+}$ and Mg^{2+} interacting with guanine tetrad were investigated by theoretical calculations.

2. Computational Details

In this work, the calculated interactions of G4, G4-Li^+ , G4-Na^+ , G4-K^+ , G4-Ca^{2+} and G4-Mg^{2+} were studied using the Becke's three-parameter hybrid exchange functional and the Lee-Yang-Pair correlation functional (B3LYP) and also the Hartree-Fock (HF) in conjunction with the 6-31G(d) basis set for the optimized structures and the 6-311G(d,p) basis set for the binding energies. Structural properties were evaluated in terms of the average bond length of $\text{M} \cdots \text{O}_6$, $\text{O}_6 \cdots \text{H}_1, \text{N}_7 \cdots \text{H}_2$ and diagonal of $\text{O}_6 \cdots \text{O}_6$. All calculations were performed using the Gaussian 03 program [6].

Binding energy ($\Delta E_{\text{binding}}$) was defined as the energy difference between the complexes and sum of the fragments, expressed as follows;

$$\Delta E_{\text{binding}} = E(\text{G4-M}) - [E(\text{G4}) + E(\text{M})]$$

where $E(\text{G4-M})$ is total energy of the optimized cation-guanine tetrad complex, $E(\text{G4})$ is total energy of the optimized guanine tetrad and $E(\text{M})$ is the energy of the cation.

3. Results and Discussion

The optimized structures of guanine tetrads are depicted in Fig. 2. The selected bond distances and binding energies of the optimized guanine tetrads are listed in Table 1 and Table 2, respectively.

Table 1. The selected bond distances (Å) of the optimized guanine tetrads at the B3LYP/6-31G(d) and HF/6-31G(d) levels

	B3LYP				HF			
	M---O ₆	O ₆ ---H ₁	N ₇ ---H ₂	O ₆ ---O ₆ (diagonal)	M---O ₆	O ₆ ---H ₁	N ₇ ---H ₂	O ₆ ---O ₆ (diagonal)
G4-Li ⁺	2.046	1.805	1.955	3.965	2.047	1.936	2.104	3.954
G4-Na ⁺	2.288	1.870	1.935	4.564	2.316	2.002	2.056	4.633
G4-K ⁺	2.630	1.911	1.938	4.837	2.593	2.098	2.222	5.186
G4-Ca ²⁺	2.291	2.044	1.972	4.582	2.298	2.281	2.119	4.596
G4-Mg ²⁺	1.997	1.904	1.972	3.874	1.983	2.065	2.154	3.848
G4		1.933	2.608	5.818		2.034	2.581	5.988

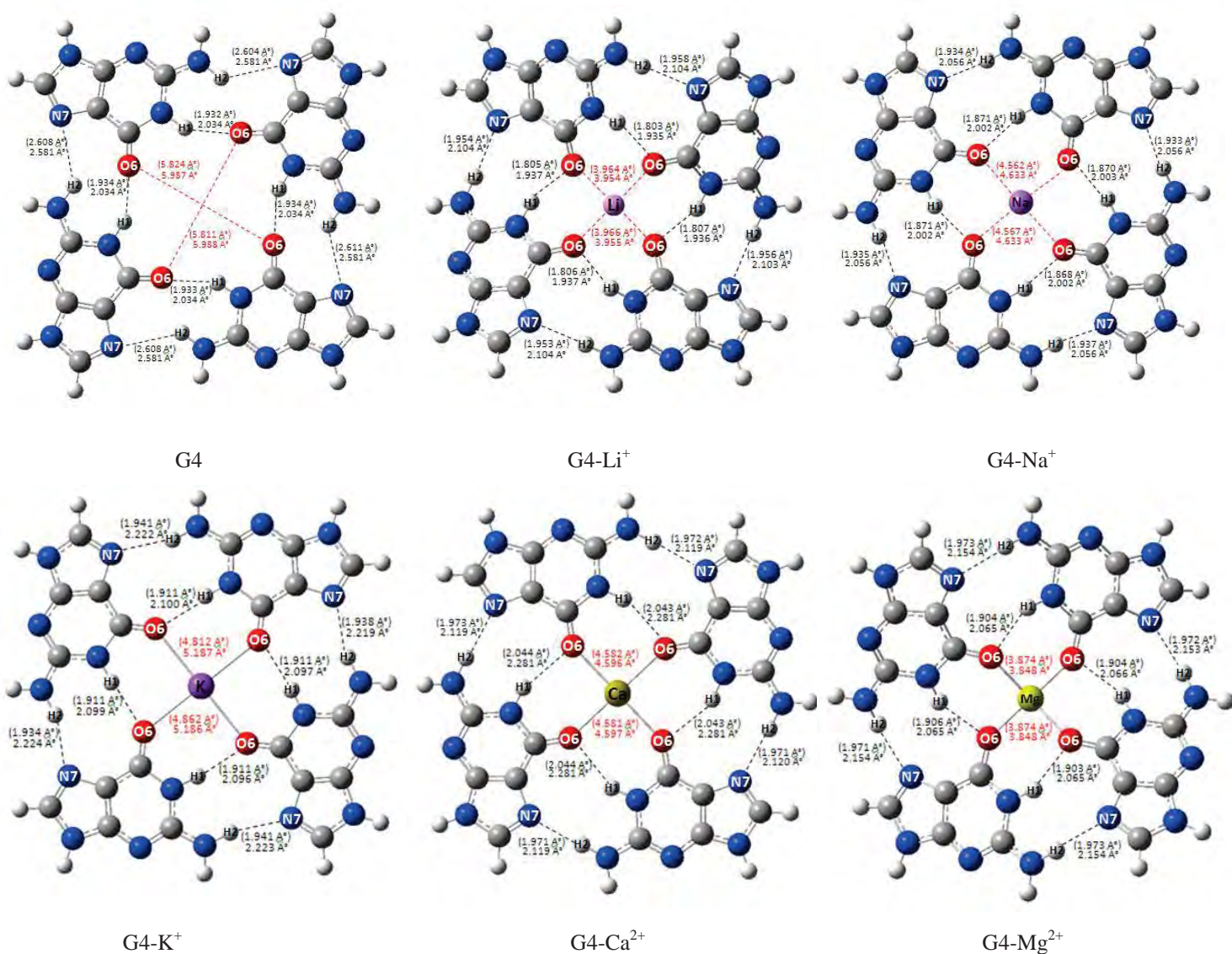


Fig. 2. The optimized structures of guanine tetrads at the HF/6-31G(d) and B3LYP/6-31G(d) levels (B3LYP data in parentheses).

According to Table 1, the M---O₆ distances at the B3LYP level of G4-Li⁺, G4-Na⁺, G4-K⁺, G4-Ca²⁺ and G4-Mg²⁺ are 2.046, 2.288, 2.630, 2.291 and 1.997 Å, respectively. The corresponding distances calculated by the HF level are equal to 2.047, 2.316, 2.593, 2.298 and 1.983 Å, respectively. Therefore, in this prediction the values of B3LYP level are close to HF level. The result obtained from experimental measurement of molecular structure of sodium ion interaction with the guanine tetrad in the crystal of a parallel-stranded guanine tetraplex (2.34±0.02 Å) agreement with the M---O₆ distance of G4-Na⁺ at the HF level [4]. The calculation has reported that the M---O₆ distance influence the stability of the structure significantly.

In the presence of cations, the G4 structure was changed and size of cations induces different structures. The distance of O₆---O₆ diagonal at the B3LYP and HF levels are evaluated to be 3.965 and 3.954 Å for G4-Li⁺, 4.564 and 4.633 Å for G4-Na⁺, 4.837 and 5.186 Å for G4-K⁺, 4.582 and 4.596 Å for G4-Ca²⁺, 3.874 and 3.848 Å for G4-Mg²⁺ as compared with G4 (5.818 and 5.988 Å), respectively. The results were indicated that the hydrogen bonds are shorted following the decrease in the size of the cations.

The distances of O₆---H₁ at the HF level are slightly influenced when Li⁺, Na⁺, K⁺ and Mg²⁺ ions were added in the cavity of G4. The difference of O₆---H₁ distances between G4 and G4-M (Li⁺, Na⁺, K⁺, Mg²⁺) are less than 0.10 Å, while this difference is more than 0.20 Å in G4-Ca²⁺. The O₆---H₁ and N₇---H₂ distances at the B3LYP level are evaluated to be 1.805 and 1.955 Å for G4-Li⁺, 1.870 and 1.935 Å for G4-Na⁺, 1.911 and 1.938 Å for G4-K⁺, 2.044 and 1.972 Å for G4-Ca²⁺, 1.904 and 1.972 Å for G4-Mg²⁺. The relative values are 1.936 and 2.104 Å, 2.002 and 2.056 Å, 2.098 and 2.222 Å, 2.281 and 2.119 Å, 2.065 and 2.154 Å at the HF level, respectively. The B3LYP and HF level results indicate that the O₆---H₁ distance is shorter than the N₇---H₂ distance in G4-Li⁺, G4-Na⁺, G4-K⁺ and G4-Mg²⁺. This effect is explained by a stronger electrostatic attraction of a cation. As shown in Fig. 2, the optimized structures exhibited that the G4-M was stabilized by Hoogsteen hydrogen bond, which no bifurcated hydrogen bond is observed by the N₇---H₂ distance, while G4 with bifurcated hydrogen bond is the most stable structure.

The O₆---H₁ and N₇---H₂ distances at the B3LYP level is shorter than HF level, which lead to the stronger hydrogen bonding. In addition the M---O₆ distance of G4-Na⁺ at the HF level is exactly predicted. The corresponding distance calculated by the B3LYP level might overestimate the stronger hydrogen bonding in the G4.

Table 2. The binding energies (kcal/mol) of the optimized G4-M complexes at the B3LYP/6-311G(d,p) and HF/6-311G(d,p) levels

Metal	B3LYP	HF
Li ⁺	-132.9 (-128.5)	-124.7 (-121.3)
Na ⁺	-110.4 (-106.5)	-102.5 (-99.7)
K ⁺	-83.0 (-80.0)	-71.8 (-69.5)
Ca ²⁺	-284.9 (-280.8)	-269.0 (-266.3)
Mg ²⁺	-365.0 (-360.5)	-356.0 (-351.7)

The values in parentheses are BSSE corrected stabilization energies.

As seen in Table 2, the binding energy results were revealed that the stable sequence is Mg²⁺> Ca²⁺>Li⁺>Na⁺> K⁺ at both HF and B3LYP levels. The binding energy is obtained from alkali earth is stronger than those derived from alkali ion. In the alkali ions, the binding energies are enhanced following the decrease in the size of the cations. The highest binding energy of -365.0 kcal/mol (-356.0 kcal/mol at the HF level) was predicted from Mg²⁺ while the lowest value was obtained from K⁺ (-83.0 kcal/mol at the B3LYP and -71.8 kcal/mol at the HF levels). Finally, a cation stabilizes the G4 structure by a neutralization of the negative charges among the oxygen atoms.

4. Conclusions

G4-M complexes were studied using the B3LYP and HF levels of theory. The optimized structures were predicted that G4 with bifurcated hydrogen bond is the most stable structure, while the G4-M was stabilized by Hoogsteen hydrogen bond. A cation stabilizes the G4 structure by a neutralization of the negative charges among the oxygen atoms, which this stable structure leads to a DNA mutation. The stable sequence in the order Mg²⁺> Ca²⁺> Li⁺> Na⁺> K⁺. The result obtained from experimental measurement of molecular structure of sodium ion interaction with the guanine tetrad in the crystal of a parallel-stranded guanine tetraplex (2.34 ± 0.02 Å) corresponding the M---O₆ distance of G4-Na⁺ at the HF level. Thus, the B3LYP result of the M---O₆ distance of G4-Na⁺ might overestimate the stronger hydrogen bonding in the G4.

Acknowledgements

Computational Chemistry Research Unit at Department of Chemistry, KMUTT is gratefully acknowledged for all computer resources and facilities and this work was also supported by the Higher Education Research Promotion and National Research University.

References

- [1] J.R. Williamson, *Proc. Natl. Acad. Sci. USA*.**90** (1993) 3124
- [2] M. Meyer, M. Brandl and J. Sühnel, *J. Phys. Chem.***105** (2001) 8223-8225.
- [3] J. Gu, J. Leszczynski and M. Bansal, *J. Phys. Chem.***311** (1999) 209-214.
- [4] W. Liu, Y. Fu, B. Zheng, S. Cheng, W. Li, T. Lau and H. Liang, *J. Phys. Chem.***115** (2011) 13051-13056.
- [5] J. Gu and J. Leszczynski, *J. Phys. Chem.***104** (2000) 6308-6313.
- [6] F.Meng, F. Wang, X. Zhao and A. F.Jalbout, *J. Mol.Struct.***854** (2008) 26-30.
- [7] M.J. Frisch, et al., Gaussian Inc., Pittsburgh PA, 2003.

INFLUENCE OF THE T-SHAPE FOUR GOLD CLUSTER ON THE INTERACTIONS AND CHARGE DENSITY REORGANIZATION IN GUANINE-CYTOSINE BASE PAIRS

Jakkapong Wicheandee¹, Chinapong Kritayakornupong^{1*}

¹ Department of Chemistry, Faculty of Science, King Mongkut's University of Technology Thonburi, Bangkok 10140, Thailand

* Author for correspondence; E-Mail: chinapong.kri@kmutt.ac.th

Abstract: Characteristic of charge transfer reactions in the T-shape four gold cluster with the guanine-cytosine (G-C) base pair on the N7 site of guanine base in deoxyribonucleic acid (DNA, d) and peptide nucleic acid (PNA, p) were theoretically elucidated by using the B3LYP/6-31G(d)∪LANL2DZ method. Different backbones such as dG-dC, dG-pC, and pG-dC complexes were selected. The result shows that the strongest interaction energy of -33.92 kcal/mol was calculated from the pG-dC complex with the O6-N4, N1-N3, and N2-O2 bond distances of 2.87, 2.94, and 2.85 Å, respectively. In contrast, the weakest interaction energy of -7.26 kcal/mol was obtained from the dG-dC model with the slightly larger H-bonding distances compared to the pG-dC model. In addition, for the T-shape four gold cluster attached to the N7 site of the guanine base in complexes, the H-bonding interaction energies were decreased by ~6 kcal/mol. Finally, the results revealed that the sum of the Mulliken charge was transferred to Au₄, which take place mainly from guanine base and partially from cytosine base and their backbones.

1. Introduction

The three hydrogen bonds of guanine-cytosine (G-C) base pair play an important role for understanding the Watson-Crick model. Recent theoretical studies have shown that the influence of the G-C base pair or individual base attachment by gold nanoparticles is an attractive subject for bioscience application [1-2]. The interaction of the G-C base pair with triangular T-shape four gold cluster was studied using quantum calculation, showing that the strongest interaction energy from four gold atoms was evaluated [2-3]. The gold atoms bonding on the N7 site of guanine base is proved to be the major groove site within the G-C base pair [4-5]. It's well known that the DNA (deoxyribonucleic acid, d) backbone has a negative charge inside a phosphate group, while a neutral charge of a peptide nucleic acid (PNA, p) is imitated for DNA backbone. Consequently, the aim of this work is to investigate T-shape four gold cluster in the G-C base pair for the different backbones between DNA and PNA (base on *trans*-(1*S*,2*S*)-2-aminocyclopentanecarboxylic acid, *SS*-ACPC) [6].

2. Methods

To theoretically calculate the structural properties, the complexes of T-shape four gold nanoparticles in the G-C base pair coordinated at the N7 site of guanine

base for DNA and PNA backbones were fully optimized at the Becke's three-parameter hybrid exchange functional and the Lee-Yang-Parr correlation functional (B3LYP) level of theory. The 6-31G(d) basis set was used for all atoms except gold atoms, while the LANL2DZ basis set was applied for gold nanoparticles. The geometrical optimizations of all complexes were performed by using the Gaussian 03 program [7]. The interaction energies of structures were corrected by the basis set super position error (BSSE). In this study, the three different backbone complexes were chosen such as the doubly anionic form of the dG-dC structure, and the singly anionic form of the dG-pC, and pG-dC structures. Moreover, the charge distributions of such models were determined by Mulliken population analysis scheme [8].

3. Results and Discussion

Table 1: Hydrogen bond lengths (angstroms) of the G-C base pairs in DNA and PNA backbones with gold cluster located near at the N7 site of the G base obtained from the B3LYP/6-31G(d)∪LANL2DZ method

Complexes	Bond Distances (Å)			
	O6-N4	N1-N3	N2-O2	N7-Au
dG-dC	2.85	2.96	2.91	-
dG-pC	2.77	2.99	3.01	-
pG-dC	2.87	2.94	2.85	-
dG(Au ₄)-dC	2.89	2.91	2.83	2.12
dG(Au ₄)-pC	2.81	2.94	2.93	2.13
pG(Au ₄)-dC	2.90	2.89	2.79	2.14

The hydrogen bond distances of G-C base pairs in different DNA and PNA backbones with and without T-shape four gold nanoparticles obtained from the B3LYP/6-31G(d)∪LANL2DZ method are presented in Table 1. For the dG-dC structure without gold cluster, the O6-N4, N1-N3, and N2-O2 distances were found to be 2.85, 2.96, and 2.91 Å, respectively. It was found that the hydrogen bond distances of the N1-N3 and N2-O2 evaluated from the dG-pC model are increased, while the decreasing O6-N4 distance was observed. The longest O6-N4 bond and shortest N1-

N3 and N2-O2 distances of 2.87, 2.94, and 2.85 Å were evaluated from the pG-dC structure, showing the specification of the backbone coordinated with the base pairs. For the T-shape four gold cluster attached at the N7 site of the G base, the O6-N4 bond of 2.89, 2.81, and 2.90 Å were obtained from the dG-dC, dG-pC, and pG-dC complexes, respectively, which are longer than the corresponding complexes without gold atoms, while the N1-N3 and N2-O2 hydrogen bonding distances are all decreased in the range 0.05-0.08 Å. For the N7-Au bond length, the values of 2.12, 2.13, and 2.14 Å are detected from the dG(Au₄)-dC, dG(Au₄)-pC, and pG(Au₄)-dC complexes, respectively. This indicates that the charged backbone plays a significant role on the N7-Au interaction.

Table 2: BSSE-Uncorrected and -Corrected interaction energies (E_{int}) of G-C base pairs in DNA and PNA backbones with coordination by gold cluster calculated from the B3LYP/6-31G(d) LANL2DZ method

Complex	E_{int} (kcal/mol)	
	B3LYP/6-31G(d) (without BSSE correction)	B3LYP/6-31G(d) (BSSE correction)
dG-dC	-12.80	-7.26
dG-pC	-30.79	-25.82
pG-dC	-39.25	-33.92
dG(Au ₄)-dC	-11.03	-5.60
dG(Au ₄)-pC	-25.97	-19.96
pG(Au ₄)-dC	-34.58	-28.21

Table 2 presents the interaction energies of the G-C base pairs with and without the T-shape four gold cluster in DNA and PNA backbones obtained from B3LYP/6-31G(d) LANL2DZ method. Difference between to the BSSE-corrected and BSSE-uncorrected interaction energies of the dG-dC, dG-pC, and pG-dC complexes with gold nanoparticles amounts to ~6 kcal/mol. For the BSSE-corrected E_{int} , the most stable interaction energy of -33.92 kcal/mol was determined from the pG-dC complex. For the interchanging of backbones (dG-pC), the hydrogen bonding interaction was decreased by 8.1 kcal/mol, whereas the value of -7.26 kcal/mol was evaluated from the dG-dC model. In addition, the interaction energies of these complexes with the T-shape four gold cluster attached at the N7 site of the G base for DNA and PNA backbones were also calculated in computing BSSE-corrected. These values of such interaction were decreased in the range of 1.66 to 5.86 kcal/mol.

As shown in Table 3, the sum of Mulliken charges of the separate base, backbone, and gold cluster of the G-C base pairs for the different backbones with and without four gold nanoparticles were calculated.

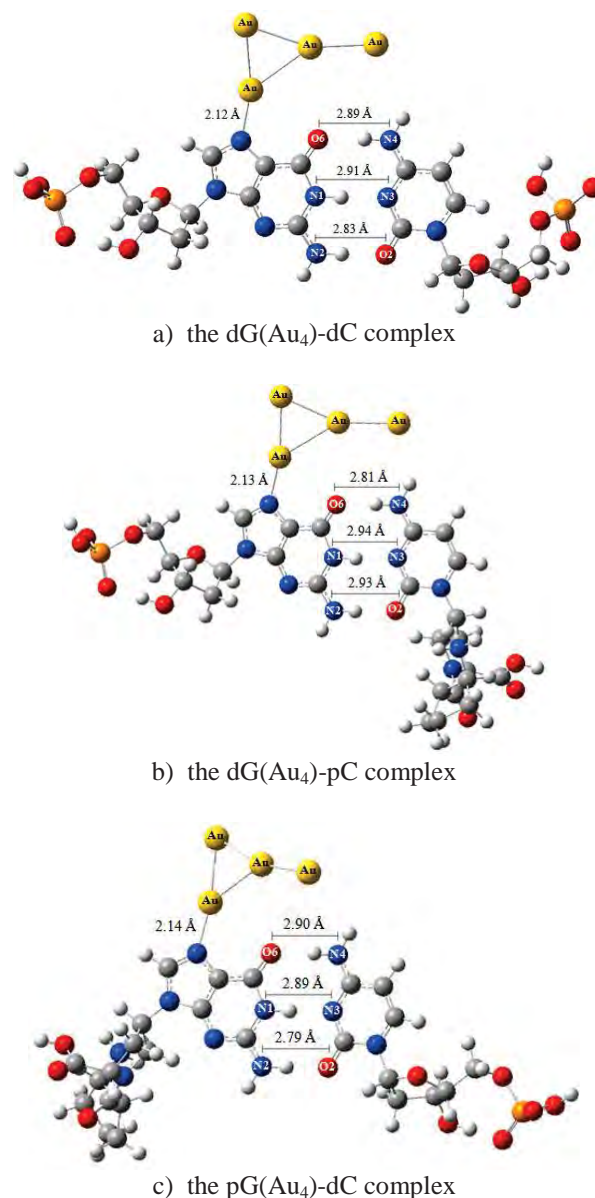


Figure 1. Optimized structures of (a) the dG(Au₄)-dC, (b) the dG(Au₄)-pC, and (c) the pG(Au₄)-dC for the T-shape four gold cluster interaction coordinated at the N7 site of the G base

Table 3: Sum of the Mulliken charges each part on the G-C base pair with different backbones complexes coordinated by gold cluster

Complex	Sum of Mulliken Charges				
	BB1	G	C	BB2	Au ₄
dG-dC	-0.731	-0.340	-0.242	-0.684	-
dG-pC	-0.684	-0.336	-0.191	0.214	-
pG-dC	0.192	-0.290	-0.255	-0.646	-
dG(Au ₄)-dC	-0.652	-0.143	-0.177	-0.685	-0.346
dG(Au ₄)-pC	-0.629	-0.117	-0.122	0.207	-0.335
pG(Au ₄)-dC	0.222	-0.077	-0.187	-0.647	-0.321

BB1 Backbone of G base.

BB2 Backbone of C base.

In the case of DNA-DNA backbones, the negative charges of -0.340, -0.242, -0.731, and -0.684 are found for the G base, C base, and their backbones, respectively. For DNA and PNA backbones attached with G and C bases, the charges on G and C bases are decreased except in these cases of C base attached by the DNA backbone. These charges in DNA backbones were less negative (-0.684 and -0.646 in the dG-pC and pG-dC structures, respectively), whereas the sum of charges on PNA backbones connected with the G and C bases resulted positive charge. For T-shape four gold nanoparticles coordination by the N7 site for the G base, the charge of gold clusters in all structure are negative, indicating that the majority of effective charges are transferred from the G base, while the charges of C base and the backbone are minor.

4. Conclusions

Our results proved that the pG-dC structure gives the highest H-bond interaction, while the weakest H-bond interaction was obtained from the dG-dC complex. The gold cluster plays an important role in the base pair interaction. It can be concluded that the migration of charge was mainly transferred from the G base to gold cluster, while the rest of the charge was contributed from the C base and their backbones.

Acknowledgements

This work was supported by the Higher Education Research Promotion and National Research University Project of Thailand, Office of the Higher Education Commission.

References

- [1] E.S. Kryachko and F. Remacle, *Nano Lett.* **5** (2005) 735-739.
- [2] A. Kumar, P.C. Mishra and S. Suhai, *J. Phys. Chem. A.* **110** (2006) 7719-7727.
- [3] A.H. Pakiari and Z. Jamshidi, *J. Phys. Chem. A.* **111** (2007) 4391-4396.
- [4] M.K. Shukla, M. Dubey, E. Zakar and J. Leszczynski, *J. Phys. Chem. C.* **113** (2009) 3960-3966.
- [5] T. Matsui, Y. Shigeta and K. Hirao, *Chem. Phys. Lett.* **423** (2006) 331-334.
- [6] C. Suparpprom, C. Srisuwannaket, P. Sangvanich and T. Vilaivan, *Tetrahedron Lett.* **46** (2005) 2833-2837.
- [7] M.J. Frisch, G. W. Trucks, H. B. Schlegel, G. E. Scuseria, M. A. Robb, J. R. Cheeseman, J. A. Montgomery, Jr., T. Vreven, N. Kudin, J. C. Burant, J. M. Millam, S. S. Iyengar, J. Tomasi, V. Barone, B. Mennucci, M. Cossi, G. Scalmani, N. Rega, G. A. Petersson, H. Nakatsuji, M. Hada, M. Ehara, K. Toyota, R. Fukuda, J. Hasegawa, M. Ishida, T. Nakajima, Y. Honda, O. Kitao, H. Nakai, M. Klene, X. Li, J. E. Knox, H. P. Hratchian, J. B. Cross, C. Adamo, J. Jaramillo, R. Gomperts, R. E. Stratmann, O. Yazyev, A. J. Austin, R. Cammi, C. Pomelli, J. W. Ochterski, P. Y. Ayala, K. Morokuma, G. A. Voth, P. Salvador, J. J. Dannenberg, V. G. Zakrzewski, S. Dapprich, A. D. Daniels, M. C. Strain, O. Farkas, D. K. Malick, A. D. Rabuck, K. Raghavachari, J. B. Foresman, J. V. Ortiz, Q. Cui, A. G. Baboul, S. Clifford, J. Cioslowski, B. B. Stefanov, G. Liu, A. Liashenko, P. Piskorz, I. Komaromi, R. L. Martin, D. J. Fox, T. Keith, M. A. Al-Laham, C. Y. Peng, A. Nanayakkara, M. Challacombe, P. M. W. Gill, B. Johnson, W. Chen, M. W. Wong, C. Gonzalez, and J. A. Pople, Gaussian Inc., Pittsburgh PA, 2003.
- [8] R. S. Mulliken, *J. Chem. Phys.* **23**, 1833 (1955).

ELECETROCHEMICAL DEPOSITION OF PLATINIUM ON GOLD NANOPARTICLES ON CARBON NANOTUBE FOR ETHANOL OXIDATION

Pitak Wongthep^{1*}, Surin Saipanya^{1,2}, Thapanee Sarakonsri^{1,2}, Laoungnuan Srisombat^{1,2}

¹ Department of Chemistry, Faculty of Science, Chiang Mai University, Chiang Mai, 50200 Thailand

² Materials Science Research Center, Faculty of Science, Chiang Mai University, 50200 Thailand

* Author for correspondence; E-Mail: pitakwo@gmail.com, Tel. +66 53943336 ext 103, Fax. +66 53892277

Abstract: Pt loaded Au metal nanoparticles on carbon nanotube (CNT) were prepared for the electrocatalytic study of ethanol oxidation. All electrochemical measurements were carried out in a three-electrode cell. A Platinum wire and Ag/AgCl were used as auxiliary and reference electrodes, respectively. Suspension of the Au nanoparticle, CNT and Nafion were mixed and dropped on glassy carbon as a working electrode. Cyclic voltammograms in H₂SO₄ solution correspond to hydrogen adsorption and hydrogen desorption. Cyclic voltammograms of ethanol electrooxidation studied in 2 M CH₃CH₂OH in 1 M H₂SO₄ show a characteristic peak with a well-known oxidation curve in the forward scan contributed to ethanol oxidation while the reverse scan is allied with the oxidation of the carbonaceous species.

1. Introduction

As a limit of power supply, there are many alternative resources to solve the problem and fuel cell can be one of the promising choices. Direct methanol fuel cell (DMFC) has also been a focus for scientist interests because of various advantages, such as light weight, rich resource and friendly environment [1-3]. Nowadays, new sources of energy are being searched and small organic molecules such as methanol, ethanol and formic acid can be used as fuel. However, the anode catalyst is easily poisoned by carbon monoxide adsorption (CO_{ads}) resulting in cell efficiency reduction. Platinum (Pt) is commonly known as electrocatalyst and stable in acid solution [4-6]. Ethanol oxidation giving CO species poisons the Pt active sites resulted in reduction of the Pt activity. Former studies reported that the provided metals (M is a precious or transition metal) generate oxygen containing species leading to CO₂ at low potentials compared to pure Pt [4]. PtRu is one of the exceptional bimetal catalysts for the methanol electrooxidation with well resistance for CO adsorption [6]. However, there are other precious metals have recently been studied to prepare binary electrocatalysts such as PtAu [8]. Moreover, CNT is a good catalyst support which has high surface area, good electrical conductivity and high stability [9].

Researchers have prepared Pt and Pt-Metal catalysts via numerous methods. To avoid those difficulties of preparation, we have tried with electrodeposition of Pt on Au nanoparticle at CNT matrix electrode in an aqueous solution [4]. The electro-

catalytic activities of the prepared Pt and Au metal catalysts were carried out by cyclic voltammetry (CV).

2. Materials and Methods

2.1 Materials and gold nanoparticles loaded CNT

H₂PtCl₆.6H₂O and HAuCl₄ were obtained from Merck. Ethanol and sulfuric acid were purchased from Lab. Scan. Water was acquired from a Millipore Milli-Q water system. Gold nanoparticles were simply prepared by reduction of hydrogen tetrachlorideaurate (II) with alkaline tetrakis(hydroxymethyl) phosphonium chloride (THPC) [7]. 1 mL of a 1 M solution of NaOH, 2 mL of THPC solution (12 µL of 80% THPC in 1 mL of water), and 200 mL of Milli-Q water were mixed in a 250 mL flask and vigorously stirred for at least 15 min. An aliquot (4 mL) of 1% aqueous HAuCl₄ was added quickly to the stirred solution, which was stirred further for 30 min. Afterward, Au-CNT were prepared by mixed 100 mg CNT with 40 mL water and 10 mL THPC Au nanoparticles. The mixture was stirred for 4 h. Then, it was washed by water and dried in the oven. CNT electrode can be prepared similar to above procedure but without THPC Au nanoparticles.

2.2 Electrochemistry

A glassy carbon electrode (BAS and 3.0 mm diameter) was polished with alumina slurries (0.005 µm). The supports such as CNT and Au-CNT dispersed in mixtures of Nafion, phosphate buffer and isopropanol were dropped onto the clean glassy carbon surface by micropipette and left the suspension to be dried for 1 hr. The obtained electrodes were denoted as CNT and Au-CNT nanocomposite modified glassy carbon electrode.

Pt was used as a precursor for electrodeposition on CNT and Au-CNT from the solution of 1 mM H₂PtCl₆.6H₂O. Voltammetric measurements were carried out with EDAQ potentiostat with a three electrode cell system. The prepared electrodes were employed as the working electrode and the obtained electrodes were denoted as Pt/CNT and Pt/Au-CNT. Ag/AgCl and Pt wire were used as reference and counter electrodes, respectively. The obtained CNT, Pt-CNT and Pt/Au-CNT electrodes were examined in 1 M H₂SO₄ solution and ethanol oxidation in 2 M CH₃CH₂OH + 1 M H₂SO₄ by CV at a scan rate of 50

mV.s^{-1} . The solutions were deaerated by N_2 gas for 20 min and maintained with N_2 atmosphere during the electrochemical experiments.

3. Results and Discussion

Figure 1 shows general shape of voltammograms for Pt and Pt/Au which are similar to their characteristic. It was found that the currents of hydrogen adsorption/desorption are observed. The hydrogen desorption peaks imply electrochemically active surface area. This indicates that Pt/Au-CNT has a different stoichiometry for hydrogen adsorption. However, the voltammograms for CNT and Pt/CNT has a thick double layer. The electro-adsorption of two different hydrogen species are the under-potential and over-potential adsorbed hydrogen (H_{UPD} and H_{OPD}). The electro-adsorption of H_{UPD} is characteristic of Pt group while the electro-adsorption of H_{OPD} takes place at all electrode materials. As shown in Figure 1 UPD H in H_2SO_4 aqueous electrolyte solution is a phenomenon characteristic of only noble metals. The prepared electrodes (Pt-CNT and Pt/Au-CNT) demonstrate the very distinguished hydrogen adsorption (H_{ads}) and desorption (H_{des}) regions in the potential region of ca. -0.30 to -0.10 V. The oxide formation and reduction on electrode has been obtained at 0.20 to 0.60 V.

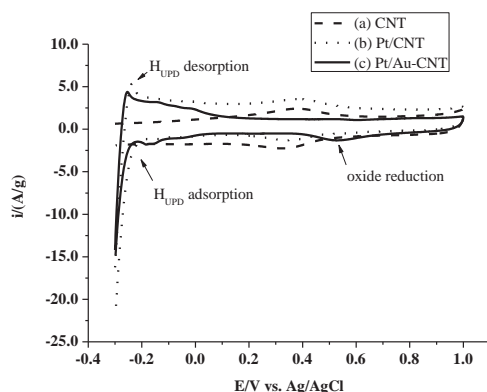


Figure 1. Cyclic voltammograms recorded in 1 M H_2SO_4 solution at (a) CNT, (b) Pt-CNT and (c) Pt/Au-CNT in the potential range -0.30 to 1.00 V at a scan rate 50 mV s^{-1} .

Cyclic voltammograms of ethanol electrooxidation of Pt-CNT and Pt/Au-CNT were measured in 2 M $\text{CH}_3\text{CH}_2\text{OH}$ in 1 M H_2SO_4 solution in Figure 2. The voltammogram of CNT shows no oxidation peak. Voltammograms of Pt-CNT and Pt/Au-CNT show a characteristic peak with outstanding oxidation peaks in the forward scan and second oxidation peaks at negative potentials in the backward scan [3,6]. The peaks at ca. 0.70 V in anodic scan is attributed to ethanol oxidation and the peak at ca. 0.50 V in the cathodic scan is related with the reaction of the electrode after deactivation giving highest peak to oxidation of unreacted ethanol and absorbed intermediates. The efficiency of the electrocatalyst

towards ethanol oxidation is normally characterized by the onset potential of ethanol oxidation and current density of the forward peak. Voltammogram of CNT shows no additional oxidation peak. The onset potential and current density of CNT are hardly determined. The onset potentials of Pt-CNT and Pt/Au-CNT are 0.50 and 0.35 V, respectively. The current densities of Pt-CNT and Pt/Au-CNT are 12.0 and 35.0 A/g, respectively. Pt/Au-CNT illustrates more enhancements in current density and lower onset potential than the others.

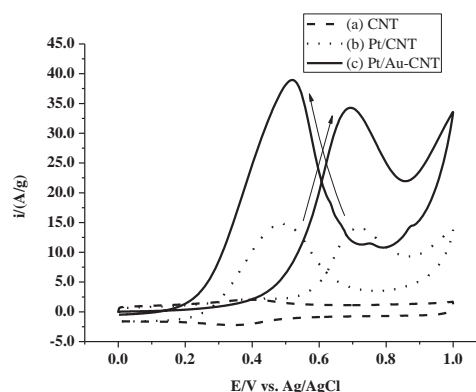


Figure 2. Cyclic voltammograms recorded in 2 M $\text{CH}_3\text{CH}_2\text{OH}$ + 1 M H_2SO_4 solution at (a) CNT, (b) Pt-CNT and (c) Pt/Au-CNT in the potential range 0 to 1.0 V at a scan rate 50 mV s^{-1} .

4. Conclusions

CNT was modified with Pt and Au nanoparticles by electrodeposition. The electro-deposited Pt nanoparticles on the surface of Au-CNT support show an excellent catalytic activity for ethanol oxidation. The electrodeposited Pt/Au catalyst demonstrates the very recognized hydrogen adsorption (H_{ads}) and desorption (H_{des}) regions in the potential region of ca. -0.30 to -0.10 V. An enhanced electrocatalytic performance for ethanol oxidation is also obtained for Pt/Au-CNT.

Acknowledgements

The authors would like to thank the National Research University Project under Thailand's Office of the Higher Education Commission for financial support, Thailand.

References

- [1] H.L.a.J. Zhang, *Electrocatalysis of Direct Methanol Fuel Cell*, Wiley-VCH, Weinheim, (2009).
- [2] J.L.a.A. Dicks, *Fuel Cell Systems Explained*, John Wiley & Sons, Ltd, New York, (2000).
- [3] G.S. Karl Kordesch, *Fuel Cells and Their Applications*, VCH, New York, (1996).
- [4] H. Liu, C. Song, L. Zhang, J. Zhang, H. Wang and D.P. Wilkinson, *J. Power Sources*. **155** (2006) 95-110.

- [5] A. Guha, W. Lu, T.A. Zawodzinski Jr and D.A. Schiraldi, Carbon, **45** (2007) 1506-1517.
- [6] D.T. Thompson, Nano Today. **2** (2007) 40-43.
- [7] D. G. Duff, A. Baiker and P. P. Edwards, Langmuir. **9** (1993) 2301.
- [8] J. Wang, G. Yin, H. Liu, R. Li, R.L. Flemming and X. Sun, J. Power Sources. **194** (2009) 668-673.
- [9] E. Antolini, Appl. Catal., B. **88** (2009) 1-24.

KEY STRUCTURAL GUIDELINES OF DIARYLPYRIMIDINES DERIVATIVES AS HIV-1 NON-NUCLEOSIDE REVERSE TRANSCRIPTASE WILD-TYPE AND K103N/Y181C USING 2D AND 3D-QSAR APPROACHES

Apinya Srisupan¹, Pharit Kamsri¹, Auradee Punkvang², Kodchakon Kun-asa¹, Patchreenart Saparpakor³, Supa Hannongbua³, Peter Wolschann^{4,5}, Supakit Prueksaaron⁶, Pornpan Pungpo^{1,*}

¹Department of Chemistry, Faculty of Science, Ubon Ratchathani University, 85 Sthollmark Rd., Warinchamrap, Ubonratchathani 34190, Thailand

²Faculty of Liberal Arts and Sciences, Division of Science, Nakhon Phanom University, Nakhon Phanom, 48000, Thailand

³Department of Chemistry, Kasetsart University, Chatuchak, Bangkok 10900, Thailand

⁴Department of Pharmaceutical Technology and Biopharmaceutics, Faculty of Life Sciences, University of Vienna, Althanstrasse 14, A-1090 Vienna, Austria

⁵Department of Drug and Natural Product Synthesis, University of Vienna, Althanstrasse 14, 1090 Vienna, Austria

⁶Large-Scale Simulation Research Laboratory, National Electronic and Computer Technology Center (NECTEC), Phatuntani 12120, Thailand

* Author for correspondence; E-Mail: pornpan_ubu@yahoo.com, Tel. +66 45353400 4124, Fax. +66 45288379

Abstract: Diarylpyrimidines (DAPYs) have been synthesized as non-nucleoside reverse transcriptase inhibitors (NNRTIs). The antiviral evaluation indicates that some of these compounds display strong activity against wild-type HIV-1 and the double mutant (K103N/Y181C) strains. Most of diarylpyrimidines derivatives exhibited moderate to excellent activities against wild type and potent K103N/Y181C HIV-1 RT. To investigate the key structural features for novel DAPYs, 2D and 3D-QSAR studies (HQSAR, CoMFA and CoMSIA) were applied on a set of 36 DAPYs of wild-type HIV-1 RT and K103N/Y181C HIV-1 RT. The results obtained from molecular docking calculation could provide the suitable molecular alignment of DAPY derivatives in the WT and K103N/Y181C HIV-1 RT binding pockets. The resulting QSAR models are satisfied based on the predictive ability values. The QSAR contour maps highlight different characteristics for different types of wild-type and mutant-type HIV-1 RT. In addition, these contour maps agree with experimental data for the binding topology. Accordingly, the integrated results can be powerful guideline for designing novel and highly effective DAPYs derivatives.

1. Introduction

Reverse transcriptase (RT) of the human immunodeficiency virus type 1 (HIV-1) is a crucial target for inhibition of HIV-1 replication. The successful treatment of HIV-1 infection with non-nucleoside reverse transcriptase inhibitors (NNRTIs) is undermined. Accordingly, the development of new highly effective drug against wild-type and drugresistance of HIV-1 remains essential [1]. Diarylpyrimidine derivatives (DAPY) have been proven to be a next generation of NNRTIs that are extremely potent against both wild-type (WT) and mutant type HIV-1 RT [2]. The antiviral and cytotoxicity evaluation indicated that these compounds displayed strong activity against wild-type HIV-1 at nanomolar concentrations [3,]. Furthermore, the inhibitors exhibited activity against the double mutant

(K103N+Y181C) strains [3-5]. In the present study, computer aided molecular design approaches based on molecular docking calculations and quantitative structure activity relationship based on two-dimensional quantitative structure-activity relationship, 2D-QSAR using hologram quantitative structure activity relationship (HQSAR) and three-dimensional quantitative structure-activity relationship, 3D-QSAR using comparative molecular field analysis, CoMFA and comparative molecular similarity indices analysis, CoMSIA, were performed on a series of DAPY derivatives to determine the different structural requirements concerning the WT and double mutant (K103N/Y181C) HIV-1 RT inhibition.

2. Materials and Methods

2.1 Structures and Biological activity of DAPY derivatives

The structures and biological activity of 36 DAPY derivatives in Table 1 were taken from literatures [3-5]. The biological activity expressed as log (1/EC50), where EC50 is the effective concentration of a compound required to achieve 50% protection of MT-4 cell infected with the wild-type and K103N/Y181C HIV-1 RT strains.

2.2 Computational details

2.2.1 Molecular docking calculations

All DAPY derivatives were constructed Gaussview 3.07 program and then, fully optimized by HF/3-21G method. The structures of wild-type and the double mutant type were taken from X-ray crystallographic data (PDB: 2ZD1 and 2ZE2), respectively. Molecular docking studies of DAPY derivatives in the wild-type and the double mutant type HIV-1 RT binding pockets were carried out using Autodock 3.05 program.

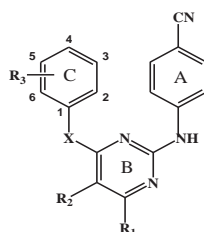
2.2.2 2D and 3D-QSAR Studies

In this work, the binding modes of DAPY derivatives in the HIV-1 RT wide type and the double mutant type binding pockets obtained from molecular docking calculations were used for molecular alignment. SYBYL 8.0 software was used to calculate the CoMFA and CoMSIA models.

2.2.3 HQSAR study

For the HQSAR study, the HQSAR module of SYBYL 8.0 was used. The PLS method was used to establish a correlation of the molecular hologram descriptors with the biological data of naphthyl DAPY inhibitors. The r^2 and q^2 values were used to evaluate the predictive ability of the HQSAR model.

Table 1. Structures and biological activity of DAPY derivatives



No	X	R1	R2	R3	Biological activity log (1/EC ₅₀) (M)	
					WT	K103N/Y181C
1	CH(OH)	H	H	2-F	7.51	8.09
2	CH(OH)	H	H	2-Cl	8.05	8.21
3	CH(OH)	H	H	2-Br	8.05	7.99
4	C=NOH	H	H	H	6.24	8.25
5	C=NOH	H	H	4-F	6.08	7.86
6	C=NOH	H	H	3-Me	7.49	8.34
7	C=NOH	H	H	3-OMe	7.60	8.06
8	C=NOH	H	H	4-OMe	7.89	7.99
9	C=NOH	H	H	4-t-Bu	6.84	8.14
10	C=NOH	H	H	3,5-diMe	7.33	8.10
11	C=NNH2	H	H	H	7.95	5.07
12	C=NNH2	H	H	2-Me	8.19	5.21
13	C=NNH2	H	H	3-Me	7.98	5.30
14	C=NNH2	H	H	4-Me	8.62	5.28
15	C=NNH2	H	H	3-F	7.64	5.12
16	C=NNH2	H	H	4-F	7.41	5.24
17	C=NNH2	H	H	3-Cl	7.71	5.28
18	C=NNH2	H	H	4-Cl	8.04	4.90
19	C=NNH2	H	H	4-OMe	8.44	5.29
20	C=NNH2	H	H	3,4-diF	7.36	5.15
21	NH	H	H	2-Me-4-CH=CH-CN	9.05	7.05
22	NH	H	H	4-CH=CH-CN	7.47	5.40
23	NMe	H	H	2-Me-4-CH=CH-CN	9.00	6.80
24	NH	H	H	2-Et-4-CH=CH-CN-6-Me	8.52	8.28
25	NH	H	H	2-iPr-4-CH=CH-CN-6-Me	8.40	7.97
26	NH	H	H	2-OMe-4-CH=CH-CN-6-Me	9.15	8.37
27	NH	H	H	2-Cl-4-CH=CH-CN-6-Me	9.10	8.39
28	NH	H	H	2-Cl-4-CH=CH-CN-6-OMe	10.00	8.70
29	O	H	H	2,6-diMe-4-CH=CH-CN	4.55	8.37
30	S	H	H	2,6-diMe-4-CH=CH-CN	5.17	7.73
31	O	Me	H	1-Cl-2-naphthyl	7.94	5.37
32	O	H	Me	1-Cl-2-naphthyl	8.42	5.12
33	O	H	H	1-Cl-2-naphthyl	8.50	4.28
34	O	Me	H	1-Br-2-naphthyl	8.07	5.34
35	O	H	Me	1-Br-2-naphthyl	8.34	5.02
36	O	H	H	1-Br-2-naphthyl	8.63	5.18

To valuate relationships between molecular descriptors and activities, the partial least square (PLS) method was applied to build QSAR models. The r^2 and q^2 values were used to evaluate the predictive ability of the CoMFA and CoMSIA models.

3. Results and Discussion

3.1 QSAR models

The statistic results of the best CoMFA, CoMSIA and HQSAR models are shown in Table 2. CoMFA, CoMSIA and HQSAR models of WT and DMT reveal the satisfied predictive ability with q^2 of 0.55, 0.61, 0.60, 0.61, 0.60 and 0.85, respectively. Satisfied correlations between experimental and predicted

biological activities of data set, based on the best model of CoMFA, CoMSIA and HQSAR, are depicted in Figure 1. The predicted biological activities of the data set derived from the best QSAR modes are closed to the experimental biological activities indicating the high degree of correlation.

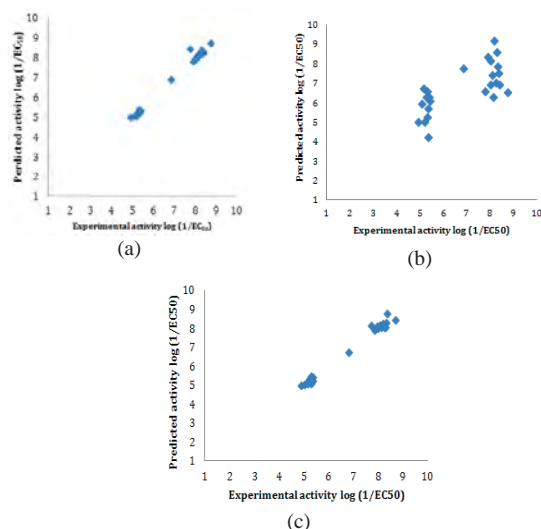


Figure 1 Plots between the experimental biological and predicted biological activities from the best CoMFA (a), CoMSIA (b) and HQSAR (c) models, respectively.

Table 2. Statistical results of WT and K103N/Y181C the best QSAR models

	Models	Statistical parameters					
		q^2	r^2	N	s	SEE	F
WT	CoMFA	0.55	0.99	6	0.68	0.04	1065
	S/E						
	CoMSIA						
	H/A						
K103N/ Y181C	HQSAR	0.60	0.97	6	0.65	0.18	-
	A/C/B/D/A						
	CoMFA	0.61	0.93	3	1.01	0.41	107
	S/E						
	CoMSIA	0.60	0.99	4	1.04	0.14	714
	H/A						
	HQSAR	0.85	0.99	6	0.66	0.16	-
	A/C/B/D/A						

q^2 , leave-one-out (LOO) cross-validated correlation coefficient; r^2 , non-cross-validated correlation coefficient; N, optimum number of components; s, standard error of prediction; SEE, standard error of estimate; F, F-test value; S, steric field; E, electrostatic field; H, hydrophobic field; A, atom; B, bond; C, connection

3.2 Interpretation of CoMFA and CoMSIA models

To visualize the structural requirements of DAPYs derivatives active against WT and K103N/Y181C HIV-1 RT, CoMFA and CoMSIA contour maps were shown in Figures 2 and 3, respectively. As the steric and electrostatic contour maps obtained from the CoMSIA models show high correspondence to those of the CoMFA models, only hydrophobic and hydrogen acceptor fields derived from the CoMSIA models were discussed. Green and yellow colors represent favorable and unfavorable steric effects, whereas blue and red contours refer to favorable positive and negative charges, respectively. Regarding hydrophobic fields, magenta and gray contour maps represent favorable and unfavorable effects, respectively, whereas orange and gray contour maps refer to favorable and unfavorable hydrogen acceptor fields, respectively.

With regard to the WT HIV-1 RT inhibition, at the position of the pyrimidine ring, B ring, green and red contours located near the R1 substituent indicate that bulky substituent with negative charge property would increase the binding affinities. Blue, magenta and gray contours near R₂ substituent showed that a positive charge substituent with hydrophobic and hydrogen donor properties at this site would be favorable. At the position of the phenyl ring, C ring, yellow, blue and gray contours close to the C5 position suggested that small substituent with positive charge and hydrogen donor properties should be favorable of activities, whereas the substituent attached to the C6 position should be hydrogen donor group and not too steric as indicated by yellow and gray contours. Orange and red contours in the vicinity of the C4 position suggested that hydrogen acceptor substituent with negative charge properties would enhance the binding affinities.

In contrast, to effectively inhibit the K103N/ Y181 HIV-1 RT, structural requirements of DAPY derivatives derived from the best CoMFA and CoMSIA models can be highlighted as following details; small and hydrophilic substituent at the R1 would increase the inhibitory activity as indicated by yellow and gray contours located near the R1 substituent. The large magenta contours close to the C2 and C3 positions suggested that hydrophobic substituent attached to the position would be beneficial for the inhibitory activity. Blue and yellow contours close to the C4 suggested that small substituents with positive charge would be favorable for the binding affinities. The substituent attached to C5 should be negative charge property as indicated by a red contour nearby, whereas the substituent attached to C6 should be bulky group with possessing negative charge property as indicated by green and red contours close the position.

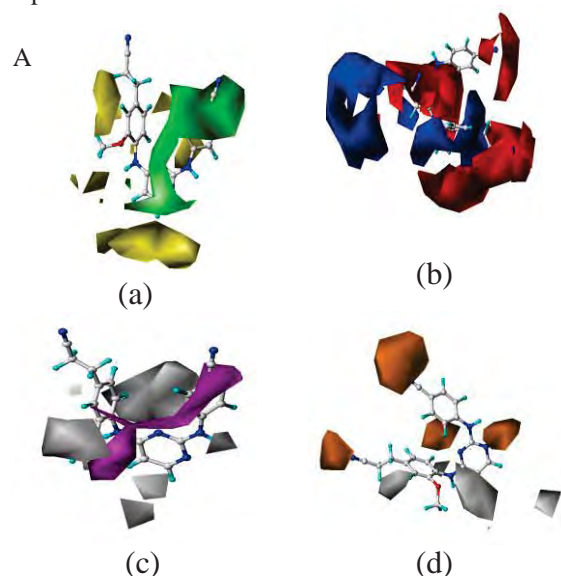


Figure 2. steric (a), electrostatic (b), hydrophobic (c), and H-acceptor (d) contour maps for the WT inhibition. Compound 28, the highest active compound, was merged in the contour maps.

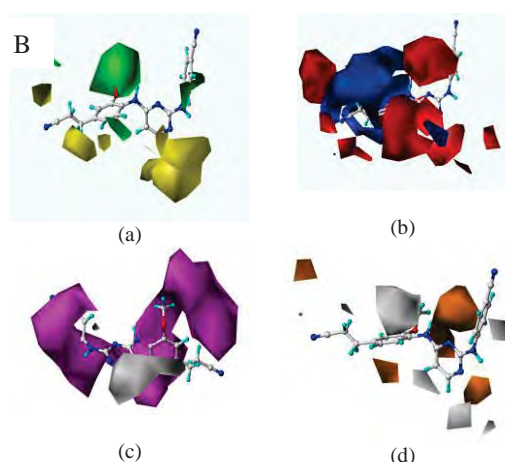


Figure 3. Steric (a), electrostatic (b), hydrophobic (c), and H-acceptor (d) contour maps for the K103N/Y181C inhibition. Compound 28, the highest active compound, was merged in the contour maps.

The contour maps highlight different characteristics for different types of wild-type and double mutant-type (Y181C/K103N) HIV-1 RT. In addition, these contour maps are in agreement with the DAPY derivatives used in the analysis listed in Table 1.

3.3 Interpretation of HQSAR models

Molecular fragments of DAPYs derivatives, which contribute directly to biological activity, can be visualized through HQSAR contribution maps. The different contributions of all atoms in DAPYs derivatives to the biological activity are discriminated by a color code. Negative contributions are represented via a red spectrum. Positive contributions are represented via a green spectrum. Figure 2 depicts the individual atomic contributions to the activity of compounds 28 and 23, the most active and the least active compounds, respectively. Atoms with positive contributions are represented at the phenyl ring C. The R₃ substituent that contains the small substituents with hydrophobic possessing negative charge properties would enhance the K103N/Y181C HIV-1 inhibition, whereas too bulky substituents induce the negative contribution having the red atoms. Hydrogen hydrogen donor substituents with negative charge properties would enhance the binding affinities for the WT HIV-1 RT inhibition as color coded in green atoms.

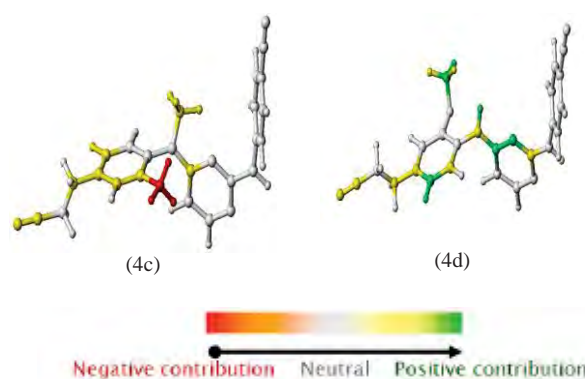
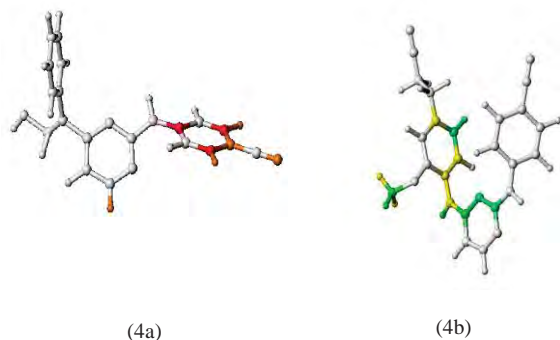


Figure 4. The HQSAR contributions of the most active compound compound 28, and less active compounds, for WT and K103N/Y181C inhibitions.

4. Conclusions

Computer aided molecular design based on molecular docking and QSAR approaches were successfully applied to discriminate structural requirements between WT and K103N/Y181C inhibitory activities of the DAPY inhibitors. In this study, the QSAR models are reasonable based on both statistical significance and predictive ability. These contour maps show good consistency with the experimental data. Accordingly, these results lead to a better understanding of important drug-receptor interactions and structural requirements in the class of DAPY compounds. The QSAR information provides a helpful guideline to design and predict the affinity of novel compounds with enhanced WT and K103N/Y181C HIV-1 RT inhibitory activities prior to synthesis.

Acknowledgements

We are grateful to the Thailand Research Fund (RTA53800010, DBG5380006). P. Kamsri is gratefully acknowledged to Royal Golden Jubilee Ph.D. program (PHD/004/2554) for the financial supports. Faculty of Science, Ubon Ratchatani University, University of Vienna, ASEA-Uninet, NECTEC are gratefully acknowledged for supporting this research.

References

- [1] D.G. Prajapati, R. Ramajayam, M.R. Yadav and R.Giridhar, *Bioorg. Med. Chem.* **17** (2009), 5744–5762
- [2] M.-P. de Béthune, *Antiviral Res.* **85** (2010), 75–90.
- [3] X.-Q. Feng, Y.-H. Liang, Z.-S. Zeng, F.-E. Chen, J. Balzarini, C. Pannecouque and E.D. Clercq, *ChemMedChem.* **4** (2009), 219 – 224.
- [4] S.-X. Gu, X.-D. Ma, F.-E. Chen, E.-D. Clercq, J. Balzarini and C. Pannecouque, *Bioorg. Med. Chem.* **19** (2011), 5117–5124.
- [5] C. Mordant, B. Schmitt, E. Pasquier, C. Demestre, L. Queguiner, C. Masungi, A. Peeters, L. Smeulders, E. Bettens, K. Hertogs, J. Heeres, P. Lewi and J. Guillemonet, *Eur. J. Med. Chem.* **42** (2007), 567–579.

INSIGHT INTO THE BINDING MODE OF THE POTENTIAL BI-SUBSTRATE InhA INHIBITORS AS ANTI-TUBERCULOSIS AGENTS: MOLECULAR DYNAMICS SIMULATIONS

Pharit Kamsri¹, Apinya Srisupan¹, Auradee Punkvang²,
Patchareenart Saparpakorn³, Supa Hannongbua³, Peter Wolschann^{4,5},
Supakit Prueksaaron⁶ and Pronpan Pungpo^{1,*}

¹ Department of Chemistry, Faculty of Science, Ubon Ratchathani University,
85 Sthollmark Rd., Warinchamrap, Ubonratchathani 34190, Thailand

² Faculty of Liberal Arts and Sciences, Division of Science, Nakhon Phanom University,
Nakhon Phanom, 48000, Thailand

³ Department of Chemistry, Kasetsart University, Chatuchak, Bangkok 10900, Thailand

⁴ Institute for Theoretical Chemistry, University of Vienna, A-190 Vienna, Austria

⁵ Department of Pharmaceutical Technology and Biopharmaceutics, Faculty of Life Sciences,
University of Vienna, Althanstrasse 14, A-1090 Vienna, Austria

⁶ Large-Scale Simulation Research Laboratory, National Electronic and Computer Technology Center (NECTEC),
Phatuntani 12120, Thailand

* Author for correspondence; E-Mail: pornpan_ubu@yahoo.com, Tel. +66 45 353400 ext 4124, Fax. +66 45 288379

Abstract: The enoyl acyl carrier protein reductase (InhA) of *M. tuberculosis* catalyzing the NADH-specific reduction of 2-*trans*-enoyl-ACP is an attractive target for designing novel anti-mycobacterial agents. The new bi-substrate inhibitors have been developed as inhibitors of InhA based on a covalent association between molecules mimicking the InhA substrate and the NADH cofactor. Several developed compounds are indeed able to inhibit the InhA activity and show promising anti-mycobacterial activities. As the molecules mimicking the InhA substrate and the NADH cofactor of the bi-substrate inhibitors, these inhibitors might be possible to bind in where the substrate and the NADH cofactor are bound in InhA, or be possible to bind in both sites at the same time. Accordingly, there are three possibilities of InhA binding sites for the binding of the bi-substrate inhibitors. However, the bi-substrate mode of action has not yet been clearly investigated. Therefore, to model the potential binding modes of the bi-substrate inhibitors in InhA binding pocket, molecular dynamics simulations were applied. Based on the obtained results, the potential binding modes of the bi-substrate inhibitors in InhA binding pocket are successfully proposed. The dynamic behaviours in term of flexibility, conformation and the inhibitor-enzyme interaction of the bi-substrate inhibitors in InhA binding pocket were elucidated. Consequently, the obtained results should suggest the structural guideline for further design of the novel inhibitors.

1. Introduction

Tuberculosis (TB) caused by *Mycobacterium tuberculosis* (*M. Tuberculosis*) are leading causes of the death in the world. In 2011, there are 8.7 million incident cases of TB, 9 million new cases, 1.4 million deaths from TB among HIV-negative people (990,000 among HIV-negative people and 430,000 HIV-associated TB deaths) [1].

Enoyl-ACP reductase (InhA) is the important enzyme of *M. tuberculosis* catalyzing the specific

reduction of the *trans* double bond of fatty acid substrate in fatty acid synthase type II (FASII) and attractive target for anti-tuberculosis drug development [2]. InhA has been identified as the primary molecular target of isoniazid, the first line drug for tuberculosis treatments. To inhibit the InhA, isoniazid is required the activation process by KatG to generate bioactive form [3]. However, the biological activity of isoniazid was reduced by mutation of KatG and InhA active pocket [4]. Accordingly, the designing and developing new more potent anti-tuberculosis drugs for the management of drug-sensitive and drug-resistant TB is imperative.

Bi-substrate inhibitors, the structure based on a covalent association between molecules mimicking the InhA substrate and the NADH cofactor were designed and developed to overcome isoniazid resistant. Several compounds showed potential activity to inhibit the InhA and promising antimycobacterial activities [5-7]. The inhibitory mechanism of these compounds was proposed as the bi-substrate InhA inhibitors that might be bound in the both of substrate and cofactor binding sites. However, the action modes of these compounds have not yet been investigated.

To study the binding modes and molecular behaviour of the bi-substrate InhA inhibitor in the InhA binding site, Molecular dynamics (MD) simulations was performed. The obtained results show that the bi-substrate InhA inhibitor possibly bounds in both substrate and cofactor binding site.

2. Materials and Methods

2.1 Bi-substrate InhA inhibitor/InhA complex

The bi-substrate InhA inhibitor/InhA complexes used in this study were obtained by molecular docking calculations using Autodock 3.05 program [8]. The bi-substrate InhA inhibitor compound 6 was taken from the literatures [5-7]. The inhibition percentage is

41% at 100 μ M. The inhibitory concentration of the bi-substrate compound 6 required for InhA inhibition (IC_{50}) is 83 μ M *M. smegmatis* and MIC with 156 μ M in *M. tuberculosis* and *M. smegmatis*.

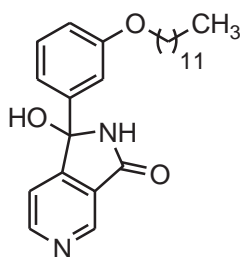


Figure 1 Chemical structure of bi-substrate InhA inhibitor compound 6

2.2 Simulation systems

Three simulation systems from the bi-substrate/InhA complex are showed in Table 1, each solvated in a water box of truncated cubic with Na^+ as counter ions to neutralize the system. The GROMOS 53a6 force field was chosen and correctly applied to represent the InhA, and SPC216 model was chosen to represent water. Because of no such standard force field for bi-substrate inhibitor and NAD^+ cofactor, hence, the force field was calculated from <http://davapc1.bioch.dundee.ac.uk/prodrg>.

Table 1: Summary of the molecular dynamics simulations performed in this study

System ID	Protein	Ligand	NAD^+	Solvent	Ion
1	InhA ^a	1	1	18,301	5
2	InhA ^a	1	-	18,324	4
3	InhA ^b	1	-	16,876	4

^a PDB code : 1BVR

^b PDB code : 2IDZ

2.3 Molecular dynamics (MD) simulations

Energy minimization with 2,000 steps using the steepest descent algorithm was performed for these systems with all bonds constrained. To relative close contacts before the full MD simulations, 200 ps position restraining with LINCS constrains was performed in the NVT ensemble at 300 K. For full MD simulations, the Particle Mesh Ewald (PME) method was used to calculate long-range electrostatics. A 10 cut-off for Lennard-Jones and a short-range Coulomb interaction were employed. 10 ns full MD simulations without position restrains were performed with coordinates and energy of simulation systems saved at 2 ps.

3. Results and Discussion

3.1 Structural stability during MD simulations

The root mean square deviations (RMSD) as a function of the simulation time of each complex with

respect to the starting structure were analyzed as shown in Figure 2. RMSDs of all atoms of InhA in three complexes, InhA/ NAD^+ /Cpd.6 (substrate binding site), InhA/Cpd.6 (substrate and cofactor binding site) and InhA/Cpd.6 (cofactor binding site), reach the plateau characteristic at 2.0 ns. These results indicate that 8 ns unrestrained simulation is enough for stabilizing the fully relaxed systems.

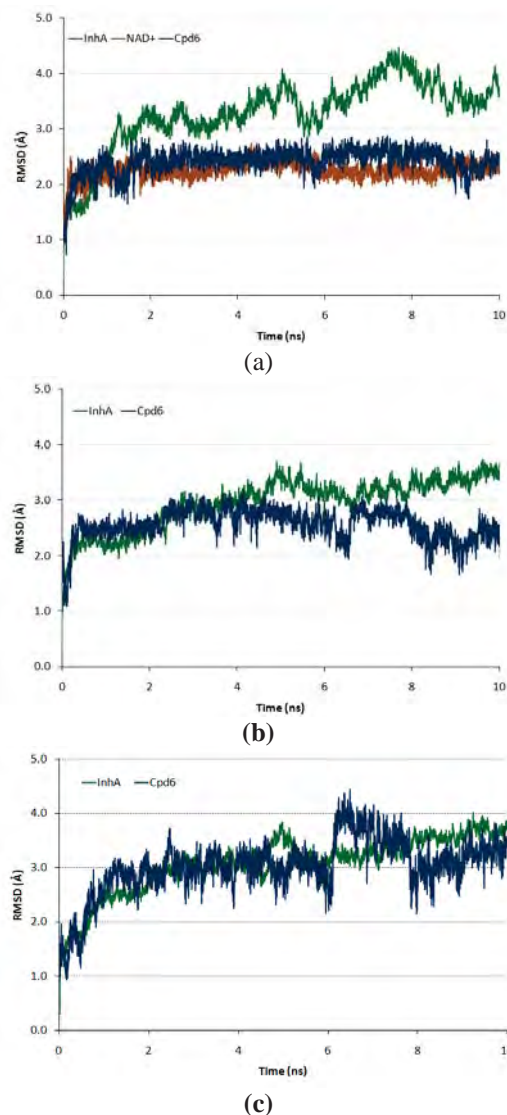


Figure 2 RMSD of all atoms of each molecule in complexes of (a) InhA/ NAD^+ /Cpd.6 (substrate binding site), (b) InhA/Cpd.6 (substrate and cofactor binding site) and (c) InhA/Cpd.6 (cofactor binding site)

3.2 Binding free energy

To gain quantitative insights into the affinity for binding of the bi-substrate InhA inhibitor in the InhA binding sites were evaluated by experimental and linear interaction energy (LIE) method from MD simulations as shown in Table 2. The experimental binding free energy was calculated by equation 1 as following;

$$\Delta G_{exp} = RT \ln[\text{Activity}] \quad \text{----- (1)}$$

Where biological activity expressed in IC_{50} , R represents the gas constant (1.988 cal/mol K), T represents the temperature (300K), respectively.

The binding free energy based on LIE method can be expressed by the following equation 2;

$$\Delta G_{bind} = \alpha[(V_{LI})_{bound} - (V_{LI})_{free}] + \beta[(V_{CL})_{bound} - (V_{CL})_{free}] \quad \text{----- (2)}$$

Where $(V_{LI})_{bound}$ = average Lennard-Jones energy for ligand/solvent interaction; $(V_{LI})_{free}$ = average Lennard-Jones energy for ligand/water interaction; $(V_{CL})_{bound}$ = average electrostatic energy for ligand/solvent interaction; $(V_{CL})_{free}$ = average electrostatic energy for ligand/water interaction; α, β = scaling factors with $\alpha = 0.22$ and $\beta = 0.18$.

Table 2: Binding free energy form experimental and LIE method of MD simulations

System	Energy (kcal/mol)
Exp.	-5.60
1	-4.15
2	-5.36
3	-2.51

Only the binding free energy of the bi-substrate InhA inhibitor bound in both substrate and cofactor binding site (-5.36 kcal/mol) shows a higher value than that of substrate binding site (-4.15 kcal/mol) and cofactor binding site (-2.51 kcal/mol), respectively. Moreover, it is notable that the calculated binding free energies of inhibitor bound in the InhA active site are in the correct order as compared with the IC_{50} values. The obtained results could be successfully used to explain the binding modes of the bi-substrate InhA inhibitor compound 6 in this study. Therefore, based on the binding free energy calculated from LIE method supported the bi-substrate InhA inhibitor bound in both substrate and cofactor binding site is the binding mode.

3.3 Structural flexibility during MD simulations

The root mean square fluctuation (RMSF) of the InhA was calculated to reveal the mobile flexibility of residues in InhA binding site. RMSF of these residues are shown in Figure 3(a). RMSF of all atoms of the bi-substrate InhA inhibitor compound 6 that directly interacts with inhibitors were also calculated as shown in Figure 3(b). In the InhA binding site, residues 20-25, 93-100, 147-150, 155-161 and 192-199 are surrounding the bi-substrate InhA inhibitor compound 6. Figure 3(a) clearly depicts the different flexibilities in the binding site of InhA whereas the bi-substrate InhA inhibitor compound 6 is bound to their active sites. All residues of the InhA binding site which bound to the bi-substrate InhA inhibitors show a small degree of flexibility, with the RMSF less than 2.5 Å. These results indicate that the residues are not flexible enough to bind with the bi-substrate inhibitors. In

addition, the dynamical flexibility of all atoms of the bi-substrate InhA inhibitor seem to be rigid with a RMSF value less than 0.8 Å.

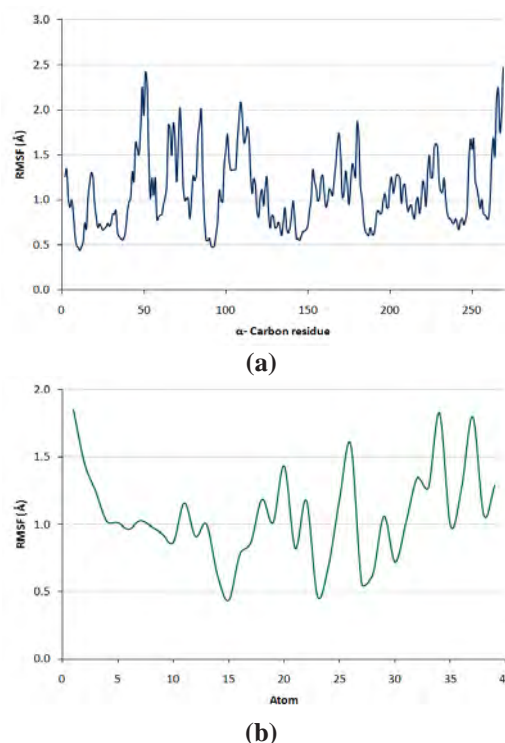


Figure 3 RMSDF of (a) α -Carbon of InhA (b) bi-substrate InhA inhibitor compound 6

3.4 Binding modes and binding interactions of the bi-substrate InhA inhibitor compound 6 with InhA complex

For a better understanding of the binding behaviors of the bi-substrate inhibitors in InhA binding pocket, MD simulations of the bi-substrate InhA inhibitor compound 6 was performed. Figure 4 shows the binding mode of the bi-substrate InhA inhibitor compound 6 obtained from MD simulations in the InhA binding pocket which is beneficial to gain insight into the binding modes of the bi-substrate InhA inhibitor compound 6. It can be seen that the position of 1-(3-Dodecyloxyphenyl)-1-hydroxy-1,2-dihydro pyrrolo [3,4-c]pyridin-3-one ring bound in the substrate binding site and only phenyl ring and -O(CH₂)₃- alkyl chain bound in cofactor binding site of the InhA. Figure 5(a) shows the binding interactions of the bi-substrate InhA inhibitor in the binding pocket. In the cofactor binding site, phenyl ring was bound electrostatic bond with Arg153. Phenyl ring and thiomethyl group of Met155 formed hydrogen-pi interaction. Moreover, hydrophobic interactions between phenyl and -O(CH₂)₃- alkyl chain with amino acid in the cofactor binding site; Ser20, Ile21, Ala22, Ile25, His93, Ser94, Met147, Adp148, Phe149, Val189, Ala190, Ala191, Gyl192, Pro193, Trp222, Ala235 and Val238 were bound.

For the substrate InhA binding site, hydrogen bond interactions between 1-hydroxy-1,2-dihydropyrrolo

[3,4-c]pyridin-3-one ring and amino acid; Tyr158 (Nar---OH, 1.80 Å), Ile94 (OH---NH backbone, 3.31 Å) and Thr196 (=O---H, 1.87 Å) were formed. Additionally, hydrophobic interactions between 1-(3-Dodecyloxy phenyl)- 1-hydroxy-1,2-dihydropyrrolo [3,4-c]pyridin-3-one and amino acid; Ile95, Gly96, Phe97, Met98, Pro99, Gln100, Pro156, Met161, Arg195 and Met199 were bound.

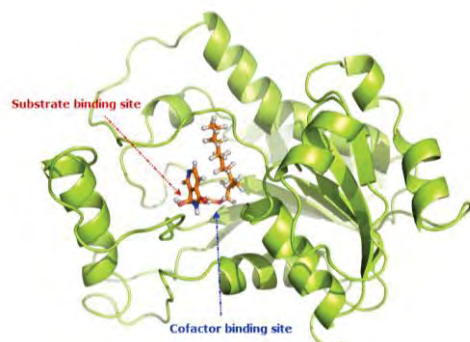


Figure 4 the binding mode of bi-substrate InhA inhibitor compound 6 obtained from MD simulations in InhA binding pocket

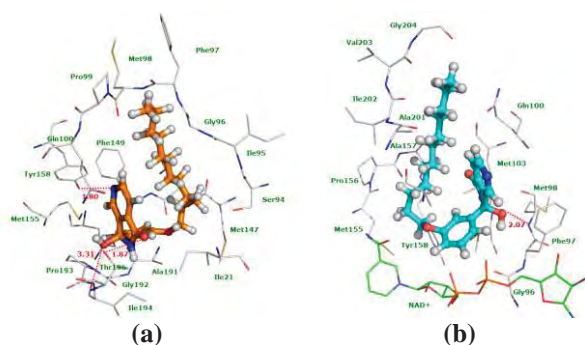


Figure 5 the binding interactions of bi-substrate InhA inhibitor compound 6 obtained from MD simulations in substrate and cofactor InhA binding pocket (a) and substrate InhA binding pocket (b)

To compare the binding mode of the obtained bi-substrate complexed with InhA system with the bi-substrate/NAD⁺/InhA system, the binding interactions of compound 6 in the substrate binding pocket was additionally described as shown in Figure 5(b). Only hydrogen bond interaction between OH of the inhibitor and NH backbone of Met98 (OH---NH, 2.07 Å) is still found, whereas crucial hydrogen bond interactions between the inhibitor and amino acid residues of Tyr158, Ile94 and Thr196 lost. The Van der Waals interaction of O of ether group of inhibitor and O carbonyl of amide group of nicotinamide (NAD⁺ cofactor) can be possibly formed. Additionally, hydrophobic interactions between bi-substrate compound 6 and amino acid surrounding the binding pocket; Gly96, Phe97, Gln100, Met103, Met155, Pro156, Ala157, Tyr158, Met161, Ala198, Ala201, Ile202, Val203 and Gly204 were bound. Based on the obtained results, it clearly indicates that the bi-substrate inhibitor complexed with InhA system

is more preferable than that of the bi-substrate/NAD⁺/InhA system,

4. Conclusions

The binding modes and molecular behavior of the bi-substrate InhA inhibitor bound in the InhA active site are successfully investigated by MD simulations. Based on the binding free energies of three systems, the bi-substrate InhA inhibitor bound in both substrate and cofactor InhA binding. Hydrogen bond interactions, hydrogen- π interaction, electrostatic interaction and hydrophobic interactions are crucial for the binding affinity of this inhibitor in the InhA binding pocket. Accordingly, based on the results obtained from MD simulations should suggest the structural guideline for further design of the novel inhibitors with the prominent mechanism to inhibit InhA leading to overcome the resistance of isoniazid.

Acknowledgements

The financial support from Royal Golden Jubilee Ph.D. program (PHD/0004/2554) to P. Kamsri is gratefully acknowledged. This work was supported by Thailand Research Fund (DBG5380006 and RTA5380010) and National Research Council of Thailand. Faculty of Science, Ubon Ratchatani University, University of Vienna, ASEA-Uninet, NECTEC are gratefully acknowledged for supporting research.

References

- [1] World Health Organization, Global Tuberculosis Report 2012, WHO. (2012)
- [2] A. Quémard, J.C. Sacchettini, A. Dessen, C. Vilcheze, R. Bittman, W.R. Jacobs Jr. and J.S. Blanchard, *Biochemistry* **34** (1995) 8235-8241.
- [3] A. Quémard, A. Dessen, M. Sugantino, W.R. Jacobs Jr., J.C. Sacchettini and J.S. Blanchard, *J. Am. Chem. Soc.* **118** (1996) 1561-1562.
- [4] X. Zhao, H. Yu, S. Yu, F. Wang, J.C. Sacchettini and R.S. Magliozzo, *Biochemistry* **45** (2006) 4131-4140.
- [5] T. Delaine, V. Bernardes-Génisson, A. Quémard, P. Constant, B. Meunier and J. Bernadou, *Eur. J. Med. Chem.* **45** (2010) 4554-4561.
- [6] C. Deraeve, I.M. Dorobantu, F. Rebbah, F.L. Quémener, P. Constant, A. Quémard, V. Bernardes-Génisson, J. Bernadou and G. Pratiel, *Bioor. Med. Chem.* **19** (2011) 6225-6232.
- [7] T. Delaine, V. Bernardes-Génisson, A. Quémard, P. Constant, F. Cosledan, B. Meunier and J. Bernadou, *Chem. Biol. Drug Des.* **79** (2012) 1001-1006.
- [8] P. Kamsri, A. Punkvang, K. Kun-asa, D. Kasemsee, P. Suprapakorn, S. Hannongbua, P. Wolschann, S. Prueksaaron and P. Pungpo, (2012) 987-989.

ELUCIDATING THE KEY STRUCTURAL FEATURES OF DIRECT InhA INHIBITORS IN A SERIES OF DIPHENYL ETHER DERIVATIVES AS ANTI-TUBERCULOSIS AGENTS: QSAR STUDIES

Namfon Koohatammakun¹, Pharit Kamsri¹, Apinya Srisupan¹, Kodchakon Kun-asa¹, Auradee Punkvang², Patchareenart Saparpakorn³, Supa Hannongbua³, Peter Wolschann^{4,5}, Supakit Prueksaaroon⁶ and Pornpan Pungpo^{1,*}

¹ Department of Chemistry, Faculty of Science, Ubon Ratchathani University, 85 Sthollmark Rd., Warinchamrap, Ubonratchathani 34190, Thailand

² Faculty of Liberal Arts and Sciences, Division of Science, Nakhon Phanom University, Nakhon Phanom, 48000, Thailand

³ Department of Chemistry, Kasetsart University, Chatuchak, Bangkok 10900, Thailand

⁴ Department of Pharmaceutical Technology and Biopharmaceutics, Faculty of Life Sciences, University of Vienna, Althanstrasse 14, A-1090 Vienna, Austria

⁵ Institute for Theoretical Chemistry, University of Vienna, A-1090 Vienna, Austria

⁶ Large-Scale Simulation Research Laboratory, National Electronic and Computer Technology Center (NECTEC), Phatuntani 12120, Thailand

* Author for correspondence; E-Mail: pornpan_ubu@yahoo.com, Tel. +66 45 353400 ext 4124, Fax. +66 45 288379

Abstract: Multi-drug resistant (MDR) and extensively drug resistant (XDR) of *M. tuberculosis* are mainly problems for tuberculosis treatment. With the aim to develop novel anti-tuberculosis drugs, various structurally different classes of direct InhA inhibitors, diphenyl ether derivatives have been recognized as one of the most successful family developed due to their excellent against mycobacterial strains. These compounds are directly inhibiting enoyl-ACP reductase (InhA) of *M. tuberculosis*. To enhance the anti-mycobacterial activity of diphenyl ether derivatives, the requirement on the structural basis of diphenyl ether derivatives prompts the research to find out. In this work, 2D and 3D QSAR approaches, HQSAR, CoMFA and CoMSIA, were applied to an extended series of 47 diphenyl ether compounds effectively inhibiting InhA. The resulting QSAR models are reasonable based on both statistical significance and predictive ability. The results obtained from the graphic interpretation highlight different characteristics for on the biological activity of these compounds indicating that the derived models are fruitful to discriminate structural requirements of direct InhA inhibitors in class of diphenyl ether derivatives. Based on our finding results, various QSAR models aid to a better understanding of structural requirements of diphenyl ether derivatives for rational design with more potent direct InhA inhibitors.

1. Introduction

Tuberculosis is the leading cause of mortality from a single infectious agent and is responsible for more than 2 million deaths worldwide every year [1]. Therefore, there is an urgent need to develop novel TB chemotherapeutic agents. The current front-line treatment strategy utilizes isoniazid (INH), a pro-drug which inhibits the synthesis of mycolic acids that are essential components required for the integrity of the bacterial cell wall [2]. INH inhibits InhA, the FabI enoyl reductase (ENR) in the fatty acid synthesis (FAS-II) pathway. However, before INH can inhibit

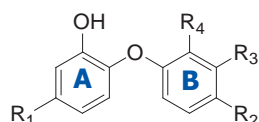
InhA, it must be activated by KatG, a catalase peroxidase enzyme. The activated form of INH then reacts with NAD⁺ to form the INH-NAD adduct. A significant number of the strains resistant to INH arise from mutations in KatG. [3]. Therefore, the development of an InhA inhibitor which can bypass this initial activation step should have activity against INH resistant strains of *Mycobacterium tuberculosis* (MTB). The diphenyl ether triclosan is a potent inhibitor of ENR's from many organisms [4]. A series of alkyl diphenyl ethers that are potent inhibitors of InhA against MTB have been developed [5-7]. Importantly, the alkyl diphenyl ethers display similar MIC values against INH-resistant strains of MTB. To obtain the structural requirements crucial for designing new and more potent InhA inhibitors in the class of alkyl diphenyl ethers involving triclosans, computer aided molecular design approaches using molecular docking calculations and quantitative structure activity relationship based on two-dimensional quantitative structure-activity relationship (2D-QSAR) using hologram quantitative structure activity relationship (HQSAR) and three-dimensional quantitative structure-activity relationship, 3D-QSAR using comparative molecular field analysis (CoMFA) and comparative molecular similarity indices analysis (CoMSIA) were applied on a series of alkyl diphenyl ethers derivatives.

2. Materials and Methods

Chemical structures and experimental biological activities against of 47 diphenyl ether derivatives were collected from the literature [8-10], presented in Table 1, where they are described to be determined under the same experimental conditions. The biological activity of these compounds for InhA inhibition were expressed in terms of IC₅₀ values. For QSAR studies, IC₅₀ values were converted as usual to the

corresponding $\log(1/IC_{50})$. 40 compounds were used as the training set and 7 compounds, (compounds 9,11,22,26,31,39,46) were taken as the test set in this study, as shown in Table 1. All chemical structures of these inhibitors were constructed using the standard tools available in GaussView 3.07 program and were then fully optimized using the HF/3-21G method. Molecular alignment was performed by molecular docking calculations using Autodock 3.05 program in the InhA binding pocket (PDB code 2X23). CoMFA, CoMSIA and HQSAR techniques using Sybyl 8.0 program were applied to the data set for the QSAR study.

Table 1 Structure and biological activity of diphenyl ether derivatives



No	R ₁	R ₂	R ₃	R ₄	Log (1/IC ₅₀)
1	Cl	Cl	H	Cl	5.96
2	Me	Cl	H	Cl	6.09
3	2H-tetrazol-5-yl	Cl	H	Cl	5.00
4	COOH	Cl	H	Cl	5.00
5	C(O)NH ₂	Cl	H	Cl	5.00
6	Ph	Cl	H	Cl	5.00
7	CH ₂ (C ₆ H ₁₁)	Cl	H	Cl	6.96
8	Ethyl	Cl	H	Cl	6.92
9*	Propyl	Cl	H	Cl	7.04
10	Butyl	Cl	H	Cl	7.26
11*	CH ₂ CH(CH ₃) ₂	Cl	H	Cl	7.02
12	(CH ₂) ₂ CH(CH ₃) ₂	Cl	H	Cl	7.20
13	CH ₂ CH(CH ₃)CH ₂ CH ₃	Cl	H	Cl	6.89
14	2-pyridyl	CN	H	Cl	5.00
15	4-pyridyl	CN	H	Cl	5.00
16	CH ₂ (2-pyridyl)	Cl	H	Cl	7.54
17	CH ₂ (3-pyridyl)	Cl	H	Cl	7.38
18	<i>o</i> -CH ₃ -Ph	Cl	H	Cl	5.88
19	<i>o</i> -CH ₃ -Ph	CN	H	Cl	5.00
20	<i>p</i> -CH ₃ -Ph	Cl	H	Cl	6.06
21	<i>p</i> -F-Ph	Cl	H	Cl	5.00
22*	CH ₂ Ph	Cl	H	Cl	7.29
23	(CH ₂) ₂ Ph	Cl	H	Cl	7.67
24	(CH ₂) ₃ Ph	Cl	H	Cl	7.30
25	hexyl	H	H	H	7.96
26*	ethyl	H	H	H	5.70
27	butyl	H	H	H	7.10
28	pentyl	H	H	H	7.77
29	octyl	H	H	H	8.30
30	hexyl	H	H	NO ₂	6.74
31*	hexyl	H	NO ₂	H	7.32
32	hexyl	NO ₂	H	H	7.05
33	hexyl	H	H	NH ₂	7.21
34	hexyl	H	NH ₂	H	5.96
35	hexyl	NH ₂	H	H	7.26
36	hexyl	H	H	H	5.81
37	hexyl	NHCOCH ₃	H	H	5.88
38	hexyl	H	H	NHCOCO ₂ H	5.63
39*	hexyl	H	NHCOCO ₂ H	H	6.24
40	hexyl	NHCOCO ₂ H	H	H	5.71
41	hexyl	H	H	N-isoxazole-5-carboxamide	5.49
42	hexyl	H	N-isoxazole-5-carboxamide	H	5.91
43	hexyl	H	H	methylpiperazine	5.88
44	hexyl	H	methylpiperazine	H	6.51

45		6.63
46*		6.79
47		6.18

* compounds served as the test set in this study

3. Results and Discussion

3.1 QSAR models

The molecular alignments for CoMFA and CoMSIA method were constructed based on the obtained molecular docking conformation. With the RMSD less than 1 Å of the obtained docking conformation compared to the X-ray structure, docking parameters used are validated to give the conformations of each compounds served as the molecular alignment in the QSAR study. The obtained CoMFA, CoMSIA and HQSAR models are statistically satisfied. The best QSAR model obtained from partial least square (PLS) method is summarized in Table 2. For 3D-QSAR, the CoMFA model employing both the steric and electrostatic descriptors, gives cross-validated correlation coefficient (q^2) of 0.615 and non-cross-validated correlation coefficient (r^2) of 0.971. For the CoMSIA model, only four descriptors (steric, electrostatic, hydrophobic, and hydrogen bond donor) can produce the satisfied QSAR model with q^2 of 0.626. The best HQSAR model with highly predictive ability value, ($q^2 = 0.728$) was generated based on the combination of the different fragment types, atom (A), bond (B), connection (C), Hydrogen atom (H) and donor and acceptor (DA).

3.2 Validation of QSAR models

Satisfied correlations between experimental and predicted biological activities of data set, based on the best models of CoMFA, CoMSIA and HQSAR, were obtained. The graphical representations of correlation between actual and predicted $\log(1/IC_{50})$ values of the training set and the test set predicted by the three QSAR models are shown in Figure 1. These results indicate that QSAR models show high predictive ability for the training set, whereas the predicted biological activities of the compounds in the test set compounds are rather poor with r^2 value of 0.04, 0.02 and 0.31 for CoMFA, CoMSIA and HQSAR models, respectively.

Table 2 Summary of statistical results of CoMFA, CoMSIA and HQSAR models

Models	Descriptors	Statistical parameters						
		q^2	r^2	N	S	SEE	F	Fraction
CoMFA	S/E	0.615	0.971	6	0.665	0.181	181.572	61.8/38.2
CoMSIA	S/E/H/D	0.626	0.975	6	0.645	0.166	217.190	14.8/21.3/30.4/33.5
Models	Descriptors	q^2	r^2	N	S	SEE	Bond length	
HQSAR	A/B/C/H/DA	0.728	0.945	6	0.503	0.245	307	

S, Steric field; E, Electrostatic field; H, Hydrophobic field; A, Atom; C, Connection; B, Bond; H, Hydrogen atom; DA, donor and acceptor ; q^2 , Cross-validated correlation coefficient; r^2 , Non-cross-validated correlation coefficient; N, Optimal number of components; s, standard error of prediction; SEE, standard error of estimate; F, F-test

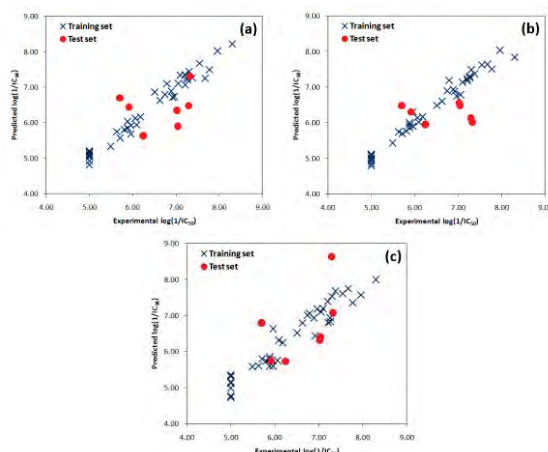


Figure 1. Plots between the experimental biological and predicted biological activities from the best CoMFA (a), CoMSIA (b) and HQSAR (c) models, respectively.

3.3 Graphical interpretation of CoMFA and CoMSIA contour maps

To gain insight into the structural requirement of diphenyl ether derivatives to design new highly potent InhA inhibitors based on our obtained QSAR results, CoMFA and CoMSIA contour maps were discussed. Figure 2 show the CoMFA steric and electrostatic field, and CoMSIA hydrophobic and hydrogen donor fields in the InhA binding pocket, respectively. From the CoMFA contour maps, steric field is represented by green and yellow contour maps. Electrostatic field is represented by blue and red contour maps. Green contours near R_1 substituent phenyl ring A and R_4 of phenyl ring B indicated that a bulky substituent at this site would be favorable. In general, bulky R_1 substituted derivatives exhibited significantly improved activities than that with small R_1 substituted compounds. Yellow contours located at R_2 and R_3 substituent suggested that the small substituents are favorable. For electrostatic contour maps, blue contours near R_1 , R_2 , R_3 and R_4 substituent indicated that electron donating group at the position is favorable to improve the biological activity.

For CoMSIA contour maps, steric and electrostatic contour maps were highly similar to the CoMFA steric and electrostatic contour maps. Therefore, only hydrophobic and hydrogen bond donor contour maps were discussed. The magenta contour near R_1 , R_2 , R_3 and R_4 position indicated that a hydrophobic

substituent at this site would be beneficial for the activity. For hydrogen bond donor contour maps, small purple contour located at the R_1 substituent indicated that the substituent R_1 with hydrogen bond acceptor property would enhance the binding affinity. Cyan contours located at the R_3 substituent and hydroxyl group indicated favorable hydrogen bond donor properties. It clearly explains why diphenyl ether derivatives possessing a hydroxyl group at the phenyl ring A show promising their biological activities.

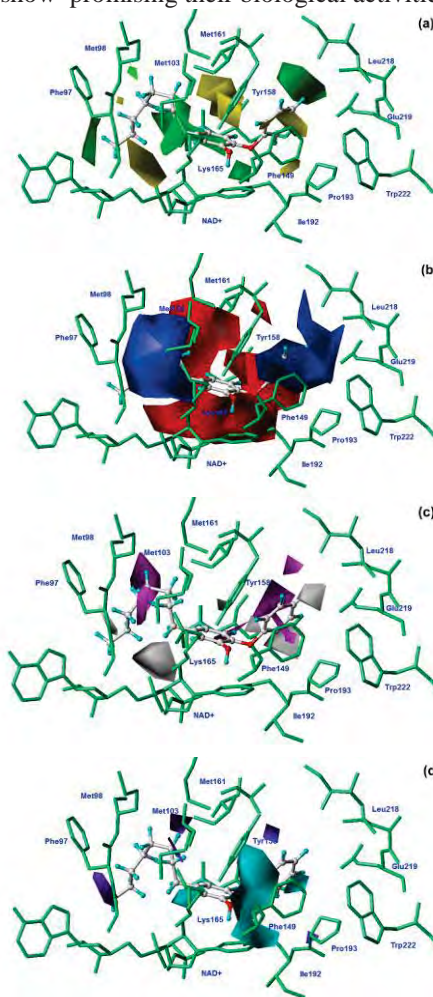


Figure 2 CoMFA and CoMSIA contour maps; (a) steric (b) electrostatic (c) hydrophobic and (d) hydrogen bond donor fields

Moreover, to get better insight into the interaction of amino acid residues surrounding the binding pocket of InhA enzyme and the inhibitors, the InhA binding pocket was included in the CoMFA and CoMSIA contour maps. At the R_1 substituent attached to the phenyl A ring, the large substituent with electron donating, hydrophobic and hydrogen bond acceptor properties are required for forming hydrophobic interaction with Gly96, Phe97, Met98, Met103, Met161, Ile202 in the binding pocket. The hydroxyl group at phenyl A ring is required for forming hydrogen bond interaction with Tyr158, Lys165 and nicotinamide ribose of NAD^+ cofactor. At the phenyl ring B, the small group with the electron donating, hydrophilic and hydrogen bond donor properties of the R_2 substituent is required for interacting with Ile215, Leu218, Glu219 and Trp222. Small substituent with electron donating and hydrophobic properties at the R_3 and R_4 substituents are required for interacting with Phe149, Pro193, Ala198 and Met199.

3.4 HQSAR contributions

Molecular fragments of diphenyl ethers which contribute directly to biological activity can be visualized through HQSAR contribution maps. The different contributions of all atoms in diphenyl ether analogs to the biological activity are discriminated by a color code. Negative contributions are represented in red spectrum. Positive contributions are represented in green spectrum. Figure 3 depicts the individual atomic contributions to the activity of the high active compounds **25** and **27**. The hydroxyl phenyl ring A shows positive contribution to the biological activity of diphenyl ether derivatives. The bulky phenyl substituent of diphenyl ether ring A of compound **25** shows the positive contribution which is corresponding well to the CoMFA steric contour.

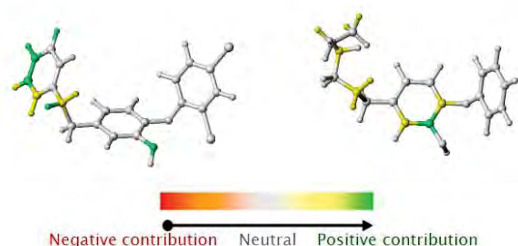


Figure 3 The HQSAR contribution map for diphenyl ether compound **25** and **27**

4. Conclusions

The QSAR studies based on molecular docking alignment were successfully applied to investigate the molecular requirement of diphenyl ether derivatives. Based on CoMFA and CoMSIA contour map guidelines, compounds with the combination of substituents of diphenyl ether derivatives should display potential InhA inhibitors. These results demonstrate that QSAR approaches are fruitful for rational design and for possible syntheses of novel and more active InhA inhibitors that might be next

generation of anti-tuberculosis agents to overcome MDR and XDR of *M. tuberculosis*.

Acknowledgements

This work was supported by National Research Council of Thailand, Thailand Research Fund (DBG5380006 and RTA5380010). P. Kamsri is grateful to Royal Golden Jubilee Ph.D. program (PHD/004/2554) for the financial support. Faculty of Science, Ubon Ratchathani University, University of Vienna, ASEA-Uninet, NECTEC are gratefully acknowledged for supporting research.

References

- [1] World Health Organization, Global Tuberculosis Report 2012, WHO. (2012)
- [2] P.J. Brennan, S.A. Rooney and F.G. Winder, *J. Med. Sci.* **3** (1970) 371-390.
- [3] Y. Zhang, B. Heym, B. Allen, D. Young, S. Cole, *Nature* **358** (1992) 591-593.
- [4] C. Baldock, J.B. Rafferty, S.E. Sedelnikova, P.J. Baker, A.R. Stuitje, A.R. Slabas, T.R. Hawkes, D.W. Rice, *Science* **274** (1996) 2107-2110.
- [5] R.J. Heath, Y.T. Yu, M.A. Shapiro, E. Olson, C.O. Rock, *J. Biol. Chem.* **273** (1998) 30316-30320.
- [6] S. Sivaraman, T. Sullivan, F. Johnson, P. Novichenok, G. Cui, C. Simmerling, and P.J. Tonge, *J. Med. Chem.* **47** (2004) 509-518.
- [7] J.S. Freundlich, J.W. Anderson, D. Sarantakis, H.M. Shieh, M. Yu, J.C. Valderramos, E. Lucumi, M. Kuo, W.R. Jacobs Jr., D.A. Fidock, G.A. Schiehsler, D.P. Jacobus and J.C. Sacchettini, *Bioorg. Med. Chem. Lett.* **15** (2005) 5247-5252.
- [8] J.S. Freundlich, F. Wang, C. Vilchèze, G. Gulten, R. Langley, G.A. Schiehsler, D.P. Jacobus, W.R. Jacobs Jr. and J.C. Sacchettini, *ChemMedChem.* **4** (2009) 241-248.
- [9] T.J. Sullivan, J.J. Truglio, M.E. Boyne, P. Novichenok, X. Zhang, C.F. Stratton, H.-J. Li, T. Kaur, A. Amin, F. Johnson, R.A. Slayden, C. Kisker and P.J. Tonge, *ACS Chem. Biol.* **1** (2006), 43-53.
- [10] C.W. Am Ende, S.E. Knudson, N. Liu, J. Childs, T.J. Sullivan, M. Boyne, H. Xu, D.L. Knudson, F. Johnson, C.A. Peloquin, R.A. Slayden and P.J. Tonge, *Bioorg. Med. Chem. Lett.* **18** (2008) 3029-3033.

COMPUTER-AIDED MOLECULAR DESIGN OF DIARYLPYRIMIDINE DERIVATIVES AS HIV-1 NNRTIS: MOLECULAR DOCKING CALCULATIONS AND QSAR STUDIES

Kodchakon Kun-asa¹, Pharit Kamsri¹, Apinya Srisupan¹, Namfon Koohatammakun¹, Auradee Punkvang², Patchareenart Saparpakorn³, Supa Hannongbua³, Peter Wolschann^{4,5}, Supakit Prueksaaron⁶ and Pornpan Pungpo^{1,*}

¹Department of Chemistry, Faculty of Science, Ubon Ratchathani University, 85 Sthollmark Rd., Warinchamrap, Ubonratchathani 34190, Thailand

²Faculty of Liberal Arts and Sciences, Division of Science, Nakhon Phanom University, Nakhon Phanom, 48000, Thailand

³Department of Chemistry, Kasetsart University, Chatuchak, Bangkok 10900, Thailand

⁴Department of Pharmaceutical Technology and Biopharmaceutics, Faculty of Life Sciences, University of Vienna, Althanstrasse 14, A-1090 Vienna, Austria

⁵Department of Drug and Natural Product Synthesis, University of Vienna, Althanstrasse 14, 1090 Vienna, Austria

⁶Large-Scale Simulation Research Laboratory, National Electronic and Computer Technology Center (NECTEC), Phatuntani 12120, Thailand

* Author for correspondence; E-Mail: pornpan_ubu@yahoo.com, Tel. +66 45353400 4124, Fax. +66 45288379

Abstract: Diarylpyrimidines (DAPYs) are one of the most commonly compounds for anti- HIV-1 RT as non-nucleoside reverse transcriptase inhibitors. Moreover, the DAPYs derivatives show potential activity in wild type and mutant types. To evaluate the binding interactions of the DAPYs to the HIV-1 RT and the key structural features relating to activities of DAPYs, molecular docking calculations and QSAR approaches based on 2D and 3D-QSAR using HQSAR, CoMFA and CoMSIA, are convenient tools to establish correlations between activities and various molecular properties. Our results indicate that hydrogen bond, interaction and hydrophobic interaction play a key role in the binding and probably also in its biological activity. Moreover, QSAR models using the data sets of wild type HIV-1RT are satisfying based on statistical parameters and predictive ability. Graphical contour interpretations in CoMFA and CoMSIA models indicate the structure requirement to improve the activities of the DAPYs derivatives. The contribution maps obtained from HQSAR model were used to explain the individual atomic contributions to the overall activity. Consequently, the obtained results suggest a structural guideline more efficiently in the rational design of novel compounds which will display a better potency against wild type HIV-1 RT.

1. Introduction

Multi-drug therapy against the human immune-deficiency virus (HIV), known as highly active anti-retroviral therapy (HAART) [1], has drastically reduced the morbidity and mortality of HIV-infected patients during the last decade and slowed down the progression of acquired immunodeficiency syndrome (AIDS). Diarylpyrimidine (DAPY) analogues represent a class of highly potent non-nucleoside reverse transcriptase inhibitors (NNRTIs), endowed with micromolar to nanomolar activity against wild-type (WT) human immunodeficiency virus type 1 (HIV-1) and clinically relevant mutant HIV-1 strains [2].

Highly effective drug against wild-type and drug-resistance of HIV-1 remains essential are required.

Diarylpyrimidine derivatives (DAPY) have been proven to be a next generation of NNRTIs that are extremely potent against both wild-type (WT) and mutant type HIV-1 RT. Naphthyl diarylpyrimidine derivatives are the novel class of DAPY inhibitors. The antiviral and cytotoxicity evaluation indicated that these compounds displayed strong activity against wild-type HIV-1 at nanomolar concentrations. Furthermore, inhibitors exhibited activity against the double mutant (K103N+Y181C) strains [3-5].

To understand the molecular requirement of a novel class of DAPY derivatives, the computer aided molecular design approaches based on molecular docking calculations, and the quantitative structure activity relationship based on 3D-QSAR (Comparative Molecular Field Analysis, CoMFA and Comparative Molecular Similarity Indices Analysis, CoMSIA), and the 2D-QSAR (using Hologram Quantitative Structure Activity Relationship, HQSAR) were performed on a series of DAPY derivatives to achieve the insight into the inhibitor-enzyme interactions and structure activity relationship of DAPY in wild-type.

2. Materials and Methods

2.1 Structures and biological activity of DAPY derivatives

The structures and biological activity of DAPY derivatives were taken from literatures [6-8] as shown in Table 1. Figure 1 shows the general structure of DAPY derivatives in this study. The biological activity was expressed as $\log(1/EC_{50})$, where EC_{50} is the effective concentration of a compound required to achieve 50% protection of MT-4 cell infected with the HIV-1 wild-type virus.